'THE CARBONYLATION OF AMMONIA TO UREA'

Thesis submitted in accordance with the requirements of the University of St. Andrews for the degree of Doctor of Philosophy by David Charles Donnell Butler

DECLARATION

I, David Charles Donnell Butler, hereby certify that this thesis, which is approximately 40,000 words in length, has been written by me, that it is the record of work carried out by me and that it has not been submitted by any previous application for a higher degree.

Date...4.11.97.....signature of candidate.

I was admitted as a research student in September, 1994 and as a candidate for the degree of Doctor of Philosophy in October, 1995; the higher study for which this is a record was carried out in the University of St. Andrews between 1994 and 1997.

Date...4.11.97..signature of candidate.

I hereby certify that the candidate has fulfilled the conditions of the Resolution and Regulations appropriate for the degree of Doctor of Philosophy in the University of St. Andrews and that the candidate is qualified to submit this thesis in application for that degree

Date..4.XI.97.....signature of supervi

UNRESTRICTED

In submitting this thesis to the University of St. Andrews, I understand that I am giving permission for it to be made available for use in accordance with the regulations of the University Library for the time being in force, subject to any copyright vested in the work not being affected thereby. I also understand that the title and abstract will be published, and that a copy of the work may be made and supplied to any bona fide library or research worker.

Date.....4.11.97...signature of candidate

ACKNOWLEDGEMENTS

I would like to express my thanks to the following people:

My internal supervisor, Professor David Cole-Hamilton for his advice and invaluable encouragement throughout the period of this work.

Thanks also to my industrial supervisor, Allin Pratt, for very helpful discussions and for providing us with the thermodynamic calculations presented here. We wish to express our gratitude to Johnson Matthey plc for full funding of this project, and for the generous loan of platinum group metal complexes.

Dr. Phil Lightfoot for his help with crystal structures contained in this thesis, and Dr. Alisdair Brown for help mounting air-sensitive crystals.

Thanks to Dr. Douglas Foster for generosity with glassware, and for knowing a bit about chemistry.

Technical staff, in particular, Peter Pogorzelec and Mrs. Melanja Smith for her help with the practicalities of NMR.

Thanks also to my colleagues in labs 334-337 and my friends Julian Osman and John Morrison for moral support.

Janice Laidlaw for being a superb friend.

Finally, thanks to my parents, Raymond and Elsie Butler for helping me through both of my degrees and for being there when I need them.

THE CARBONYLATION OF AMMONIA TO UREA

Abstract:

Present industrial production of urea involves high temperature/ high pressure conversion of NH_3 and CO_2 *via* carbamate. There would be economic interest in a low-cost method for the manufacture of urea. One possible way of achieving this is by conversion of NH_3 and CO to urea with elimination of H_2, or H_2O. Although the thermodynamics of such a process are favourable, the reaction does not occur in the absence of catalyst due to the high energy barrier of activation. From what is already known about species which can lower this energy barrier, a mechanistic strategy has been devised to screen complexes which are active for the Water Gas Shift Reaction (WGSR) under basic conditions.

$[M(CO)_6]$ (M = Cr, W), $[Fe(CO)_5]$, $K[Ru(HEDTA)Cl].2H_2O$ and $[RhH(PR_3)_3]$ (R = PEt, P^iPr) are known WGSR catalysts which *do not* catalyse the carbonylation of NH_3 to urea under conditions for which they are active for the WGSR, however, $[Ru_3(CO)_{12}]$ *is* active for this reaction with methanol or ethanol as solvent. Conditions for optimum activity are T = 160°C, CO charging pressure = 2-10 bar and $[NH_3]$ = ca. 7 mol dm^{-3}. ^1H NMR, IR and electrospray mass spectroscopy were employed for carbonyl cluster identification, and species found to be present after catalysis include $[HRu_3(CO)_{11}]^-$, $[H_3Ru_4(CO)_{12}]^-$, $[H_2Ru_4(CO)_{12}]^{2-}$, $[Ru_6C(CO)_{16}]^{2-}$, $[Ru_6(CO)_{18}]^{2-}$, $[Ru_4(CO)_{13}]^{2-}$, $[H_2Ru_3(NH)(CO)_9]$, $[H_3Ru_4(NH_2)(CO)_{12}]$, and some unidentified Ru_7 and Ru_8 monoanionic cluster species. $[HRu_3(CO)_{11}]^-$ appears to be the most abundant species present in solution, both before, during (identified by high pressure IR spectroscopy), and after catalysis. Additionally, $[HRu_3(CO)_{11}][NEt_4]$ catalyses the reaction as a starting material and so is thought to be the catalytic intermediate in the reaction with $[Ru_3(CO)_{12}]$ as precursor.

The period of catalytic activity is short. Possible reasons for this include incorporation of NH_3 into formamide (effectively reducing $[NH_3]$), and the formation of a non-catalytic species, possibly a dianion such as $[Ru_3(CO)_{11}]^{2-}$, $[Ru_6C(CO)_{16}]^{2-}$, or $[H_2Ru_4(CO)_{12}]^{2-}$.

$[RhHCl_2(P^iPr_3)_2]$ reacts with sodium amalgam in THF solution with trace H_2O to form $[RhH_2Cl(P^iPr_3)_2]$, which we have isolated. The crystal structure of a new polymorph of this complex is described. $[RhH_2Cl(P^iPr_3)_2]$ can be used as an alternative route to make $[RhH(P^iPr_3)_3]$, by the reaction with strong base in excess P^iPr_3.

$[RhCl_3.xH_2O]$ reacts with excess P^iPr_3 in THF and in the presence of H_2O under reflux to give $[RhHCl_3(P^iPr_3)_2][H\ P^iPr_3]$, the crystal structure of which is described. In solution, at room temperature, it dissociates to $[RhHCl_2(P^iPr_3)_2]$ and $[ClH\ P^iPr_3]$, and, on cooling, $[RhHCl_3(P^iPr_3)_2][H\ P^iPr_3]$ can be observed in the ^{31}P and low-field ^1H NMR spectra.

$[RhH(P^iPr_3)_3]$ and $[RhH_2Cl(P^iPr_3)_2]$ both react with NH_3 in THF solution to yield an unknown adduct thought to be $[RhH_2(NH_2)(P^iPr_3)_2]$. Reaction with NH_3 is unprecedented for any complex of Rh and has possible mechanistic significance in the carbonylation of NH_3 to urea.

ABBREVIATIONS USED IN THIS TEXT

APcI	Atmospheric Pressure Chemical Ionisation
DEPT	Distortionless Enhancement by Polarisation Transfer
diglyme	2-methoxyethylether
DPPM	*bis*-diphenylphsophinomethane
DPPE	*bis*-diphenylphsophinoethane
EDTA	ethylenediaminetetraacetic acid
ESI	Electrospray Ionisation
ESP	Electrospray
ESMS	Electrospray Mass Spectroscopy
FABMS	Fast Atom Bombardment Mass Spectrometry
GC	Gas Chromatography
GCMS	Gas Chromatography with Mass Spectroscopy detection
HPIR	High Pressure Infra Red
NMR	Nuclear Magnetic Resonance
HPLC	High Performance Liquid Chromatography
IR	Infra-Red
LC/MS	Liquid Chromatography/ Mass Spectrometry
PPh_3	triphenylphosphine
P^iPr_3	tri*iso*-propylphosphine
PEt_3	triethylphosphine
PMe_3	trimethylphospine
PEG	polyethyleneglycol
THF	Tetrahydrofuran
TIC	Total Ion Current
WGSR	Water Gas Shift Reaction

CONTENTS

CHAPTER 1

INTRODUCTION

CHAPTER 2

TECHNIQUES FOR THE ANALYSIS OF UREA

CHAPTER 3

THE CARBONYLATION OF AMMONIA TO PRODUCE UREA

For;

My mother, father, granny and brothers
and Janice

CHAPTER 1

Introduction.

1.1 Background

1.1.1 A brief history

Urea was discovered originally in human urine by H.M. Rouelle in 1773, and in 1828 it was synthesised by Friedrich Wohler[1]. Wohler found that when he attempted to synthesise ammonium cyanate by treating silver cyanate with ammonium chloride solution, he obtained instead a white crystalline material which analysed identically to urea produced from urine. He observed that urea had been produced "without benefit of kidney, bladder or dog", and this was the first recognised example of an organic compound being synthesised from exclusively inorganic starting materials, serving a cruel blow to the accepted theory of "vitalism" which had maintained that organic chemicals could only be modified by chemistry through the agency of a vital force present in living plants and animals.

In 1870, urea was produced synthetically by heating ammonium carbamate in a sealed tube. This reaction formed the basis for the current industrial process for its production.

1.1.2 Physical and chemical properties

Urea is a white crystalline solid with molecular formula $CO(NH_2)_2$ which acts as a monobasic substance to form salts with acids and bases and has a dissociation constant of 7.94×10^{-1} in aqueous solution. Its decomposition to CO_2 and NH_3 in aqueous solution at neutral pH is extremely slow with $t_{1/2}$ of several years; however, in acidic solution this process is accelerated. At its melting point (135°C), and at atmospheric pressure, urea decomposes to ammonia, biuret (I), cyanuric acid (II), ammelide, (III), and triuret (IV) (figure 1.1)

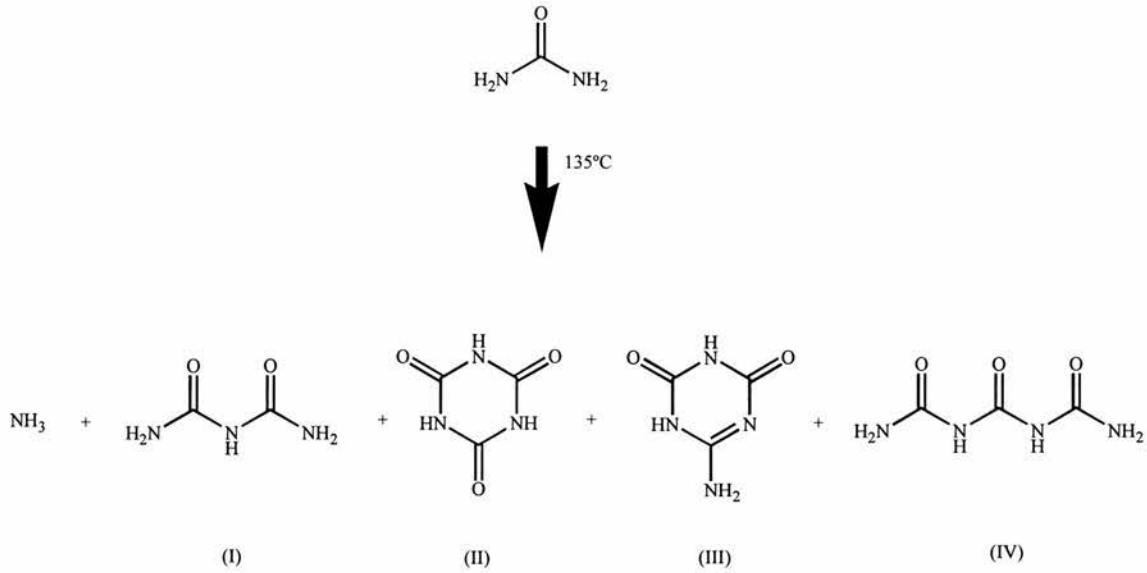

Figure 1.1. Decomposition of urea at its melting point

1.1.3 Industrial uses for urea

Commercially, urea has several important applications. Due to its high nitrogen content (46.6 %), urea is the most popular form of **nitrogen fertiliser**, and when compared to other dry fertilisers, it has captured 65 % of the world trade. Mixed with additives urea is used in solid fertilisers of various formulations, e.g., urea-ammonium phosphate (UAP), urea-ammonium phosphate (UAS), and urea-phosphate (urea and phosphoric acid). Concentrated solutions of urea and ammonium nitrate (UAN) solutions have a high nitrogen content, are easily transported and can be sprayed directly onto crops. Urea is safe to ship and handle, non-corrosive to equipment and can be used on nearly all crops. As a result of its high solubility in water, it moves readily into the soil and is easily broken down by hydrolysis firstly to ammonium carbamate, then NH_3 and CO_2 with the action of urease, an enzyme which is found in all soils in sufficient quantities to bring about rapid breakdown of urea (figure 1.2). This process normally takes 2-4 days.

The agricultural industry is by far the greatest sector for the consumption of urea. However, it is not only crops which benefit - urea is also used as a feed supplement for ruminants, in particular cattle, where it assists in the utilisation of protein.

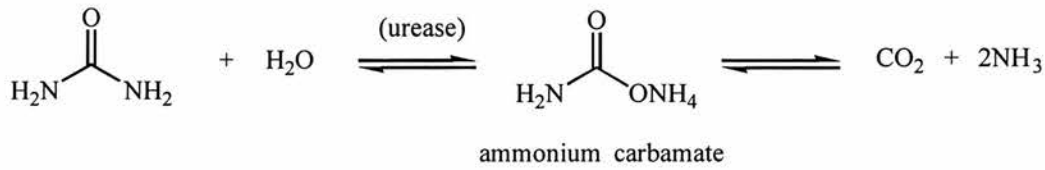

Figure 1.2 Hydrolytic action of the enzyme urease on urea

Urea is one of the raw materials for urea-formaldehyde **resins**[2] (figure 1.3), although consumption of urea for these materials has decreased in recent years due to new findings about the toxicity of formaldehyde slowly released from the resin.

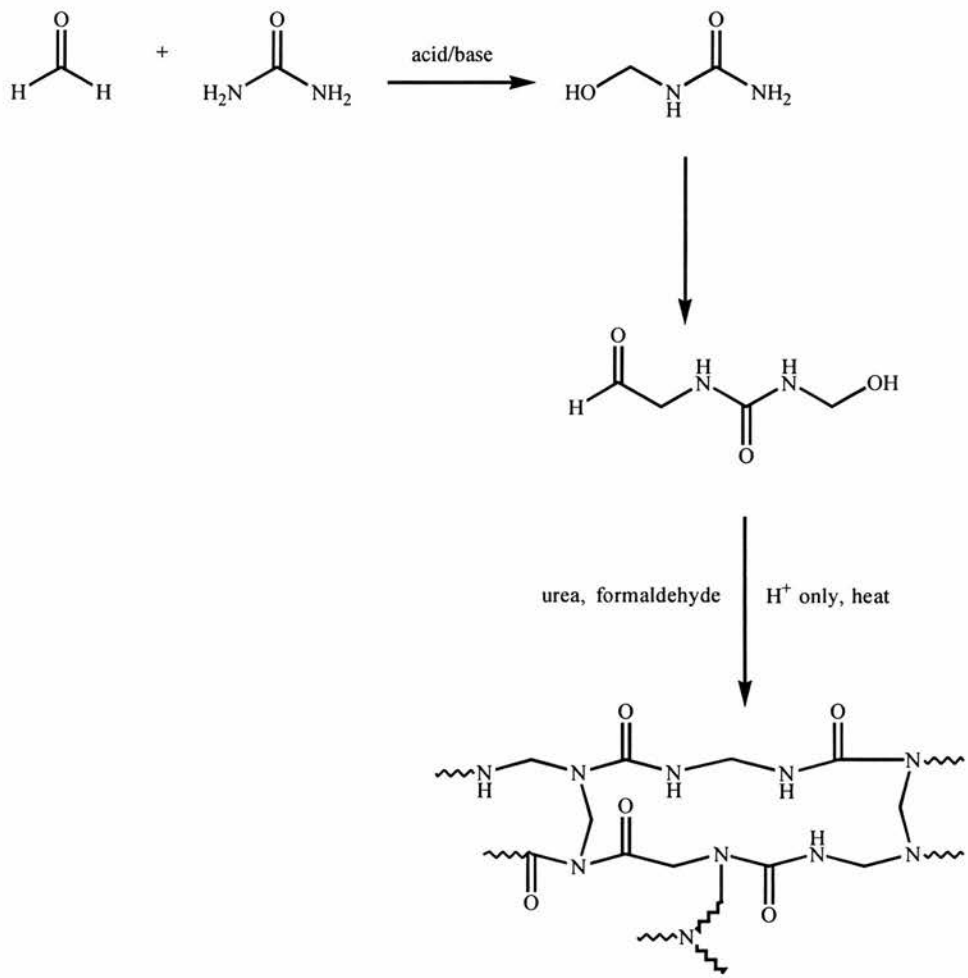

Figure 1.3 A general reaction of formaldehyde and urea to give formaldehyde resin.

Melamine, which is used primarily in the production of melamine-formaldehyde resins can be formed by the dehydration of urea (figure 1.4). Melamine-fomaldehyde resins have a much greater hardness and stain-resistance than urea-formaldehyde resins, however, both have varied uses including adhesives, laminates, moulding compounds, coatings and textile finishes.

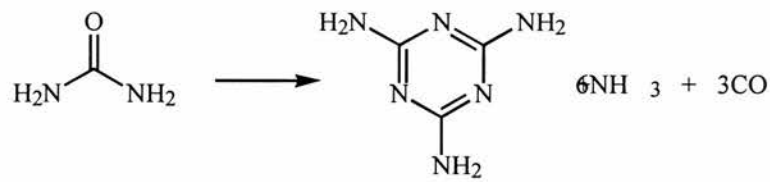

melamine

Figure 1.4 Dehydration of urea to form melamine

Urea and malonic acid react to form barbituric acid[3] providing a **pharmacaeutical** application (figure 1.5) and although it was discovered in 1878 by reaction of urea with malonic acid in the presence of phosphoryl chloride, barbiturates were not exploited as hypnotics until the early 1900's. Urea is also used in the production of various acylureas and urethanes for use as sedatives and hypnotics.

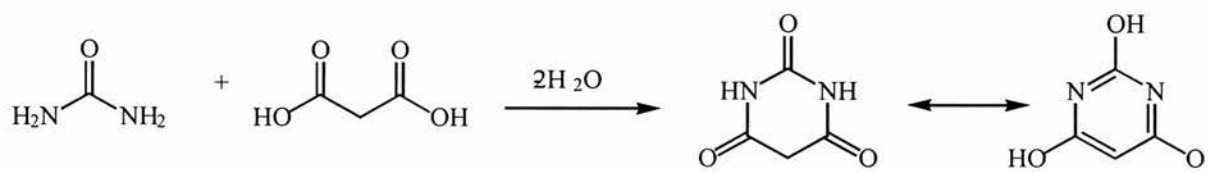

barbituric acid

Figure 1.5 Barbituric acid production by reaction of malonic acid with urea

Urea is capable of forming large interpenetrating helices as a result of hydrogen bonding which are able to hold organic molecules in channels, a property which can be applied for the separation of both optically active and non-optically active mixtures with potential for use in chromatographic phases.

An important **biomedical** application of urea is in the identification of the bacterium, *Helicobacter pylori* (implicated along with emotional stress in causing stomach ulcers). *H. pylori* is capable of converting urea to carbon dioxide and ammonia. Urea is a normal product of the biochemical pathway the cells in our body use to eliminate many nitrogen-containing compounds found in the body (e.g. proteins which contain amino acids) which would otherwise break down to form ammonia resulting in death. *H. pylori* produces a very active form of the urease enzyme which results in the formation of ammonia (by action on urea) in the local area of the ulcer. The high acidity of the stomach is therefore reduced locally by neutralisation with ammonia allowing the bacteria to flourish around the ulcer. If one ingests a very small quantity of ^{14}C labelled urea, and if *H. pylori* is present, urease will convert the urea to ammonia and carbon dioxide. If $^{14}CO_2$ is exhaled, then it is very likely that the stomach contains *H. pylori*.

1.1.4 The world market for urea

The global demand for urea is predicted to rise to around 108 million tonnes by the turn of the century (in 1994 the global demand was 81.8 million tonnes, with a total value of around $ 10 billion). China and India are currently the major importers (during 1995-96, urea demand in India grew by 13 per cent to 19.30 million tonnes, accounting for 80 per cent of the country's nitrogenous fertiliser capacity).

1.2 Current methods of preparation of urea and possible alternatives

1.2.1 Current preparative methods

Industrially, urea is produced from liquid NH_3 and gaseous CO_2 via the dehydration of ammonium carbamate[4] at high pressure and temperature (figure 1.6). The formation of ammonium carbamate and production of urea by dehydration of ammonium carbamate occur simultaneously in a one-pot synthesis typically at a pressure of 200-250 bar and a temperature of 200°C. The thermodynamics of the overall

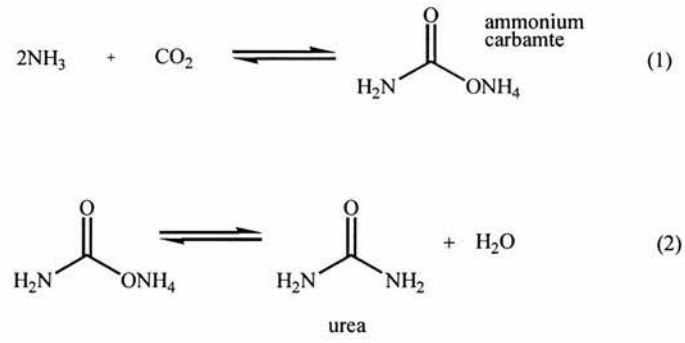

Thermodynamics
$\Delta G°_{298} = -7.22$ kJmol^{-1}
$\Delta S° = -424.13$ JK^{-1}mol^{-1}
$\Delta H° = -133.61$ kJmol^{-1}

Figure 1.6 conversion of NH_3 and CO_2 to urea

system reveal a negative free energy change. Equilibrium (1) is highly exothermic and depends greatly upon the temperature and pressure because large volume changes take place. Equilibrium (2) is endothermic (31.4 kJmol^{-1} of urea formed) and takes place mainly in the liquid phase. At room temperature, and in aqueous solution, ammonium

carbamate dissociates to ammonium carbonate ($(NH_4)_2CO_3$). At 60°C it begins to revert to carbamate solution, and at 100°C, only carbamate is present in solution. At and above 150°C, ammonium carbamate loses a mole of water and forms urea. The rate of conversion increases with increasing temperature and reaches a maximum at 185°C with a conversion of ca. 53% at equilibrium. The conversion at equilibrium can be increased by raising the temperature and pressure, and by dehydrating the ammonium carbamate in the presence of excess ammonia.

For the reaction in the absence of solvent, thermodynamic calculations[5], the results of which are summarised as graphs in figure 1.7 indicate that at a pressure of 50 bar, a maximum conversion of about 40% of ammonium carbamate to urea is achieved at a temperature of just below 400 K. When the pressure of the system is raised to 200 bar, two things happen. Firstly, the temperature range for which urea can be viably formed increases, but more importantly, a maximum conversion of nearly 60% can be reached at a temperature of ca. 475 K. In practice, most commercial urea synthesis is attained under these type of conditions. For example, in the Montedison urea process, a pressure of 197-217 atm and an overall NH_3 to CO_2 ratio of 3.5:1 is used. A 62-63% conversion to of carbamate is reported[7]. Although maximum conversion increases still with increasing pressure, the higher operating temperatures and pressures required make the process somewhat unattractive.

The water content of the aqueous urea produced by these processes can be removed by steam-heating and evaporation under reduced pressure. Crystallisation and remelting remove a lot of the biuret content, an impurity which is detrimental to the use of urea as a fertiliser (it impairs plant growth) and is only commercially tolerated in quantities of less than 2.0%.

The high temperature and pressure of this urea synthesis make its production quite costly, so there would be great industrial interest in reducing this cost by considering an alternative strategy for its manufacture. This possibility is discussed in the following section.

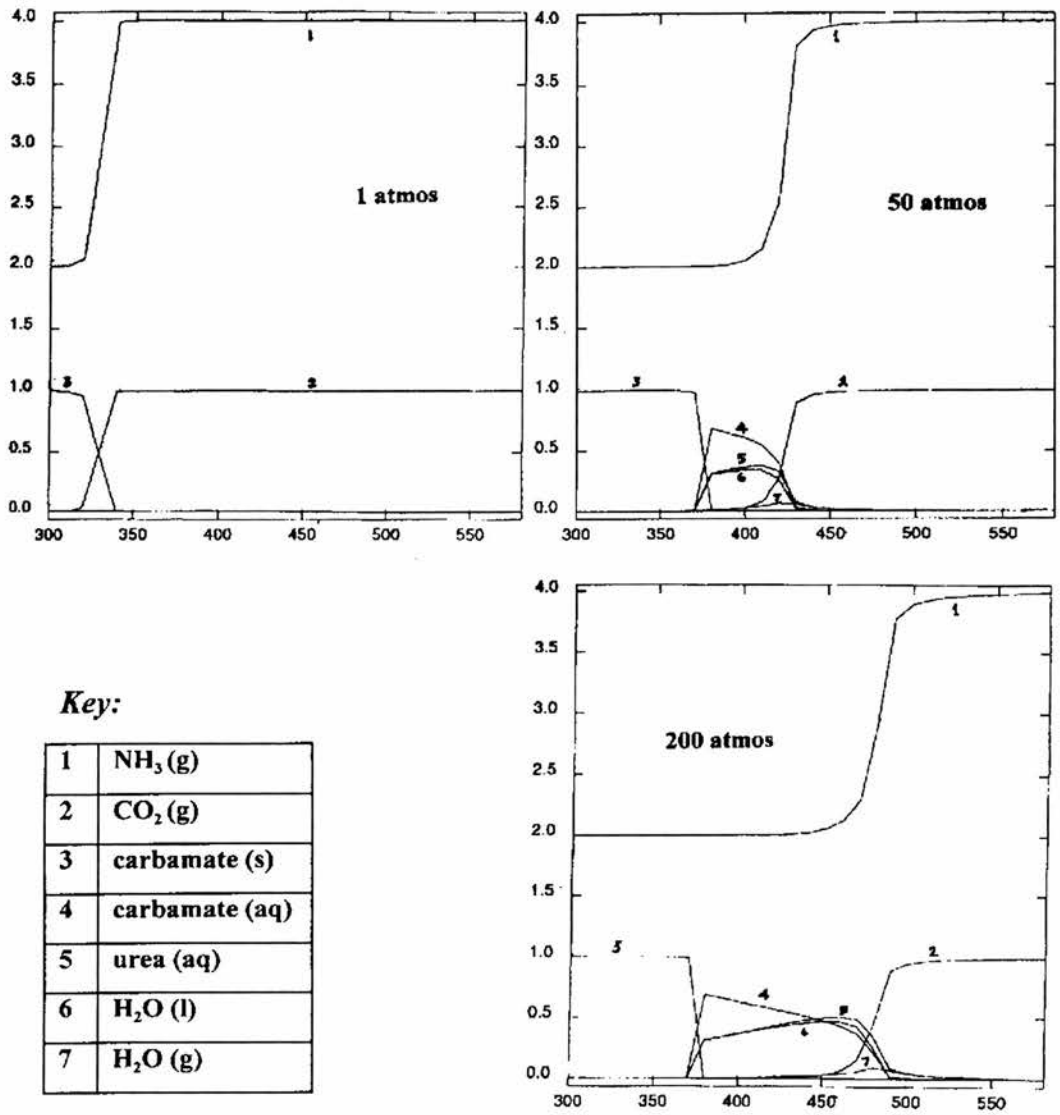

Figure 1.7 Thermodynamics of urea production (x-axis = T/ K, y-axis = No. mols of species) from CO_2 and NH_3

1.2.2 Alternative strategies for urea production

1.2.2.1 Carbonylation of ammonia in the *absence* of an oxidant

The logical way to proceed in this strategy is with the simplest system possible, combining two moles of ammonia with one mole carbon monoxide. In principal therefore, the catalytic carbonylation of NH_3 can be performed in the absence of an

oxidant where urea or a derivative thereof is produced with the elimination of hydrogen (figure 1.8). As the temperature of this reaction is increased, the mole fraction of

Thermodynamics
$\Delta G°_{298} = -27.27\ kJmol^{-1}$
$\Delta S° = -347.286\ JK^{-1}mol^{-1}$
$\Delta H° = -130.76\ kJmol^{-1}$

Figure 1.8 Reaction of NH_3 and CO to produce urea

urea in the product at equilibrium decreases. This is as a direct result of the application of the Gibbs free energy equation;

$$\Delta G° = \Delta H° - T\Delta S°$$

- The Gibbs free energy equation.

the entropic term increases with temperature positively increasing the free energy. However, the yield of the reaction may also defined by the *rate* of the process and upon the activation energy and therefore, even at high temperatures it may take a long time for equilibrium to become established. One way of reducing the free energy of activation and increase the rate of a reaction is to add a catalytic species.

1.2.2.2 Oxidative carbonylation of ammonia

Where there is a need for regeneration of a catalyst (as for urea produced stoichiometrically from CO and NH_3 resulting in the simultaneous production of a dihydride complex inactive for urea production) , the reaction can be carried out in the presence of an oxidant (e.g. oxygen in the air) where urea is produced, this time with the elimination of water (figure 1.9).

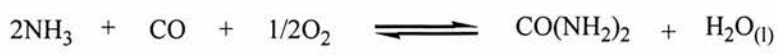

Thermodynamics
$\Delta G°_{298} = -264.39$ kJmol^{-1}
$\Delta S° = -510.629$ JK^{-1}mol^{-1}
$\Delta H° = -416.19$ kJmol^{-1}

Figure 1.9 Reaction of NH_3 and CO in the presence of oxygen to produce urea.

It is evident that the large negative free energy for this process makes it favourable in terms of products at equilibrium, however, as is the case for the reaction observed in figure 1.6, a catalyst is required in order to overcome the high activation energy for the process.

Thermodynamic calculations[5] upon the system without oxidant (hydrogen elimination) in the absence of solvent (figure 1.10) show the potential for the production of urea from CO and NH_3 under mild conditions of temperature and pressure. For all pressures above 1 bar, maximum conversions of urea can theoretically be attained at temperatures below 80°C with the equilibrium in figure 1.8 being displaced from urea at temperatures about 80°C. Little or no urea is present at temperatures above 220°C for a charge pressure of 30 bar, and this temperature decreases still further to about 150°C at a pressure of 3 bar.

These calculations allow for the reaction of CO and $2H_2$ to produce MeOH. If this reaction is not catalysed under the same conditions of temperature and pressure described above, then the yield of urea may be even higher. The computed thermodynamic model for urea production from CO and NH_3 looks favourable, and if a suitable catalyst can be used to reduce the activation energy for the reaction, then there is possibility for the real application of this system.

It is perhaps surprising then that there are relatively few reported cases of the production of urea by the catalytic (or stoichiometric) carbonylation of ammonia. Most literature for these reactions was published between 1960 and 1980 and a brief review of these examples is given in the next section.

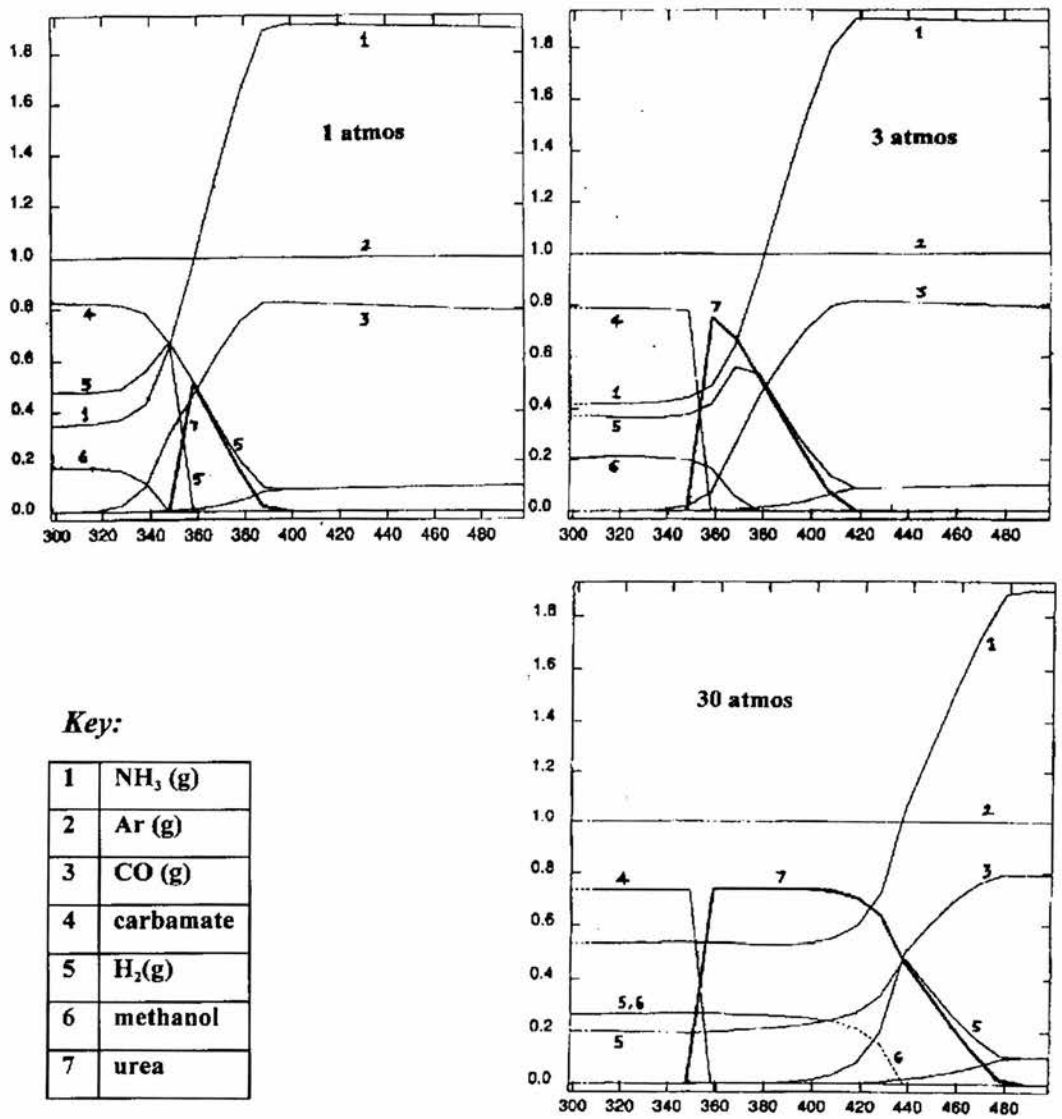

Key:

1	NH_3 (g)
2	Ar (g)
3	CO (g)
4	carbamate
5	H_2(g)
6	methanol
7	urea

Figure 1.10 Calculated thermodynamics of urea production from CO and NH_3 (x-axis = T/ K, y-axis = No. mols of species)

1.3 Review of reported alternatives to carbamate for urea production

1.3.1 $[Ru^{(III)}(EDTAH)Cl]^-$

The reaction of CO with NH_3 under aqueous conditions was performed[8-10] by Taqui Kahn and co-workers using $K[Ru(EDTAH)Cl].2H_2O$ as catalyst precursor. $[Ru^{(II)}(EDTAH)CO]^-$ was identified as the active catalytic species in the reaction mixture and under optimum conditions, the reaction was found to yield urea with a catalytic turnover of 16 moles h^{-1} per mole $[Ru(EDTAH)Cl]^-$ with a selectivity of greater than 70% at 30 atm. pressure CO at a temperature of 100°C. Side-products of this reaction included formaldehyde, formamide hexamethylenetetramine, and urea-formaldehyde resin. The operating conditions of catalysis were quite versatile, operating over wide ranges of temperature and pressure.

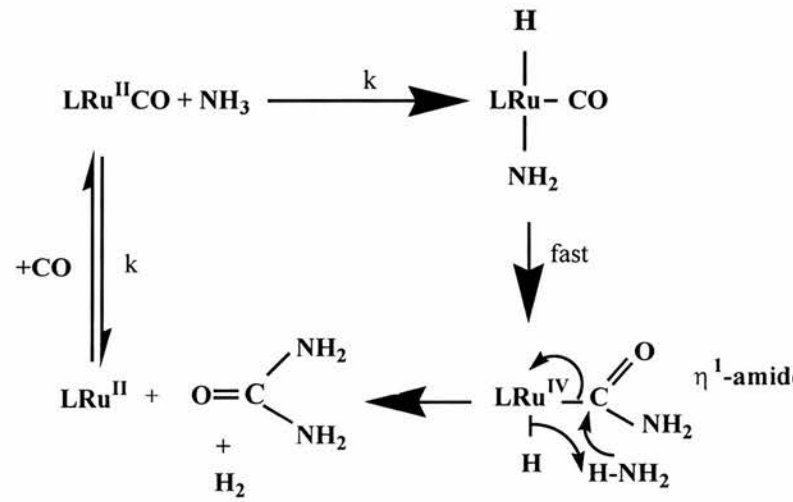

Figure 1.11 Oxidative addition of ammonia described by Taqui Khan and co-workers[8]

Oxidative addition of ammonia was suggested to be the initial stage of this catalytic cycle after generation of $[Ru(EDTAH)CO]^-$ by reaction of $[Ru(EDTAH)Cl]^-$ with CO (see figure 1.11). The resulting ruthenium (IV) complex then undergoes CO insertion into Ru-N to give the carbamoyl complex followed by a nucleophilic attack of ammonia on CO. A concerted β-hydrogen abstraction to yield urea and reductive elimination to give H_2 complete the cycle.

The carbonylation of primary and secondary amines was also achieved using this catalytic species under mild conditions of temperature and pressure to give high yields of corresponding formamides and ureas[11] in aqueous media.

1.3.2 Chalcogens (by oxidative carbonylation)

Group 16 compounds have been shown to be active[12-21] for the oxidative carbonylation of CO and NH_3 to urea by the reaction described in figure 1.9. For example, reaction of sulphur or metal sulphides with CO results in the production of COS which can then react with ammonia through a double nucleophilic attack to give urea and H_2S. The reaction is stoichiometric rather than catalytic (reoxidation of the H_2S produced to S is required to attain the full 'catalytic' cycle). High selectivities (up to 96%)[12,14] can be attained under relatively mild conditions (36-100 atmos, 10-120°C), however, there has only been one successful attempt to oxidise *in situ* the H_2S produced[19].

Similarly, there is a process described which uses selenium instead of sulphur[20], and in this case, the H_2Se produced can be air-oxidised to produce water and selenium. Primary and secondary amines have also been oxidatively carbonylated in this system to 1,3-dialkylureas and 1,1,3,3-tetraalkyl ureas respectively. Reactions are carried out in tetrahydrofuran in the presence of amorphous Se at room temperature and pressure. CO and NH_3 are blown through the suspension with recirculation for several hours. Yield of urea is reported relative to the reactive ammonia at 97 mole %.

An oxidative carbonylation has been performed *in situ* with SeO_2 as the catalyst in the presence of CO, NH_3, O_2 and a tertiary amine[21]. A likely mechanism for these reactions of double nucleophilic attack on coordinated CO has been described and is shown in figure 1.12. β-H abstraction of urea from the coordinated alkoxydiamine yields urea and chalcogen dihydride. The dihydride is stable and requires oxidation (by O_2 with production of H_2O) to complete the cycle. In the presence of amine (triethylamine for example), arylureas can be prepared in high yield from aromatic amines and CO in refluxing benzene[22,23]. Air oxidation of H_2Se again closes the cycle.

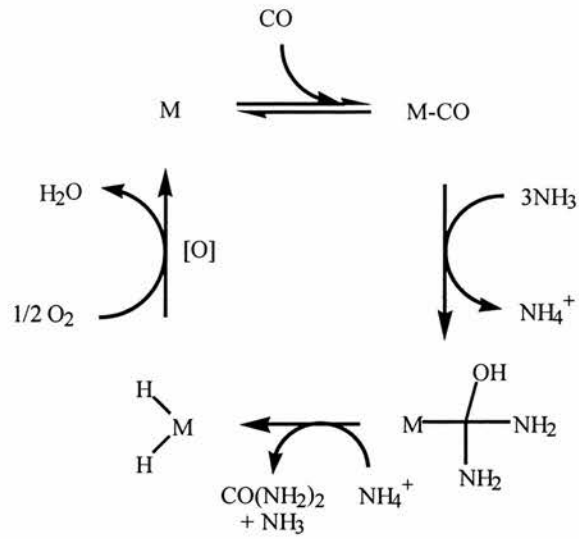

Figure 1.12 Mechanism for oxidative carbonylation of ammonia (M = S or Se)

The catalytic carbonylation of ammonia using tellurium has not been successfully performed under any conditions, however, the *non*-oxidative catalytic carbonylation of aromatic and alkyl primary amines to produce aryl and alkyl ureas, with formamides as bi-products using tellurium has been accomplished[24,25]. Typically, the reaction is performed at 140°C and p_{CO} = 30 bar. The corresponding formamide is normally the major product of the reaction, although at very low Te concentrations, the relative yield of corresponding urea can be increased. The reaction is truly catalytic in this case as the TeH_2 postulated as an intermediate in the reaction decomoposes readily to produce elemental tellurium and molecular hydrogen. It is likely that Te-CO is the intermediate which is active to nucleophilic attack on CO by NH_3 by analogy with S and Se. Although Te-CO is unstable, it has been identified by IR[26].

The elevated cost of removing toxic hydrogen sulphide or hydrogen selenide by oxidation makes the commercial use of S or Se in the production of urea undesirable. Hydrogen telluride, whilst easily disposed of, is extremely toxic and difficult to control in a high temperature high pressure process making Te an unlikely candidate for commercial interest for the production of substituted ureas.

1.3.3 Oxidative conversion of CO and NH_3 to urea using a mixed W-Ni sulphide catalyst

It has been reported that CO and NH_3 can be converted to urea in the presence of nitrobenzene as oxidant, using a mixed metal sulphide of tungsten and nickel[27]. The reaction also works for the synthesis of substituted ureas from CO and in the presence of nitrobenzene. Conversions to urea of up to ca. 30 % are attainable at a CO charging pressure of 35 bar and at a temperature of 120°C. Aniline was recovered from the reaction mixture as a co-product.

1.3.4 Carbonylation of ammonia to urea using $Cu^{(II)}$

The main process based on a soluble complex for the production of urea from CO and NH_3 is that using a copper (II) complex[28].

It is reported that, in the presence of $[CuCl(HMPA)]_2O_2$ (prepared by passing air at 30°C through a solution of CuCl and HMPA in sulpholane), CO and NH_3 react to produce urea in high yield (ca. 90 %), although the reaction is less than stoichiometric in copper.

1.3.5 Platinum group metals

There are as far as we know no examples of the *non*-oxidative catalytic production of urea from NH_3 by carbonylation in the presence of a material other than $[Ru(EDTAH)Cl]^-$, however, there are many examples of platinum group metal complexes which are active for oxidative carbonylation of primary and secondary amines to substituted ureas.

One of the most important areas of homogeneous catalysis is metal-catalysed carbonylation reactions[29-31] and carbonylation of amines other than ammonia to ureas[11,32-47] and formamides[48-53] has attracted considerable interest in recent years. Most of the carbonylations to ureas described in these references occur by an oxidative pathway with oxygen in the air reacting with a stable intermediate with elimination of H_2O as described in section 1.2.2.2.

A typical commercial method for the manufacture of ureas is by reaction of primary or secondary amines with isocyanates (figure 1.13). Ureas are of importance in the chemical industry as precursors of pigments[54] and resins[55] and can be converted to carbamates, (which are also very important, in the production of some isocyanates[56]) using a palladium catalyst[57].

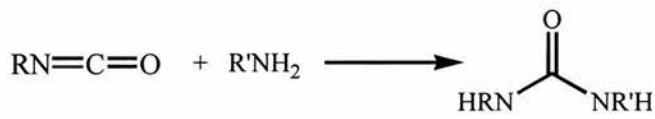

Figure 1.13 Manufacture of ureas using isocyante

The mechanisms of catalysis of substituted urea production from primary and secondary amines by platinum group metal complexes are interesting and are described below.

1.3.5.1 Oxidative carbonylation of amines other than ammonia by platinum group metal complexes

This method is by far the most widely reported in the literature for the catalytic production of ureas from complexes of platinum group metals

Recently, it has been shown that the carbonylation of amines to ureas can be facilitated by mononuclear palladium$^{(II)}$ complexes containing substituted pyridine ligands in the presence of $CuCl_2$ as cocatalyst[34]. The reactions proceed to between 0 and 100 % conversion, depending on the amine, in a period of 24 hours at a temperature of 150°C at a CO pressure of 40 bar with methanol as solvent. Diethylamine is the simplest substrate for which results are reported, and no results are presented for the carbonylation of ammonia.

Early reports[46,47] show that Cu(II)(amine) complexes can be used to catalyse the production of ureas from carbon monoxide and amines (e.g. carbonylation of piperidine, part of the mechanism of which is shown in figure 1.14). Carbon monoxide coordinated to these complexes was found to be much more susceptible to oxidation by a double nucleophilic attack of amine upon coordinated CO of $Cu^{(I)}$.

Again, this process can be made catalytic by reoxidising Cu(I) back to Cu(II) with oxygen. The mechanism is postulated to be a one-electron redox reaction whereby the formylpiperidinium radical formed is rapidly oxidised by a Cu(II) complex to form an isocyanate ion, which adds to piperidine and forms the final urea.

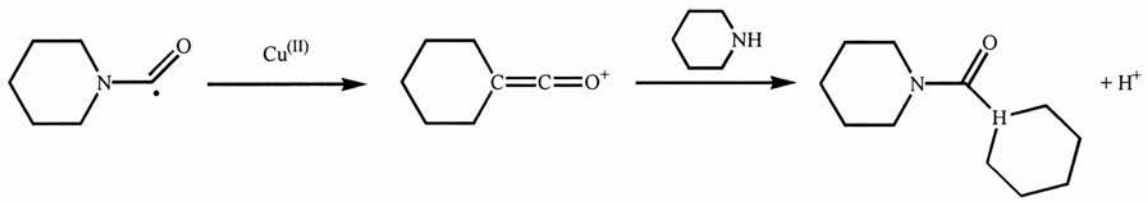

Figure 1.14 Catalysis of urea production from CO and NH_3 by $Cu^{(II)}$

Iodine has been shown to be an effective promoter for the carbonylation of primary and secondary amines to ureas using palladium acetate as catalyst in the presence of base[41]. The conversion to urea can be as great as 98 % at 95°C and 2.7 atm pressure. Again, oxygen is required to regenerate the initial active species.

The novel synthesis of ureas from formamides using a ruthenium catalyst has been reported[33]. This is interesting because formyl compounds offer an economically viable C=O unit. It was found that formamide itself could be used as a versatile carbonyl source from which, when reacted with primary amines, the corresponding 1,3-disubstituted ureas were obtained in high yields together with evolution of H_2 and NH_3. NH_3 is not reported as having been used as a source amine, however, the fact that no conversion of NH_3 produced *in situ* was reported probably indicates that this system would be inactive for urea production from NH_3. Co-ordination of formamide through the carbonyl oxygen is reported as being pertinent to the mechanism of the reaction.

Oxygen is not the only option as a reactant for oxidative carbonylation. The carbonylation of primary alkylamines to 1,3-dialkylureas was performed in the presence of $[Ru(DPPE)(CO)_3]$ using nitrobenzene as oxidant under conditions of P_{CO} = 70 bar, T = 120-160°C[35] (see figure 1.15). A five-coordinate bis(carbamoyl) complex[58] (species (I) in the cycle) was shown to react under the catalytic conditions to produce urea.

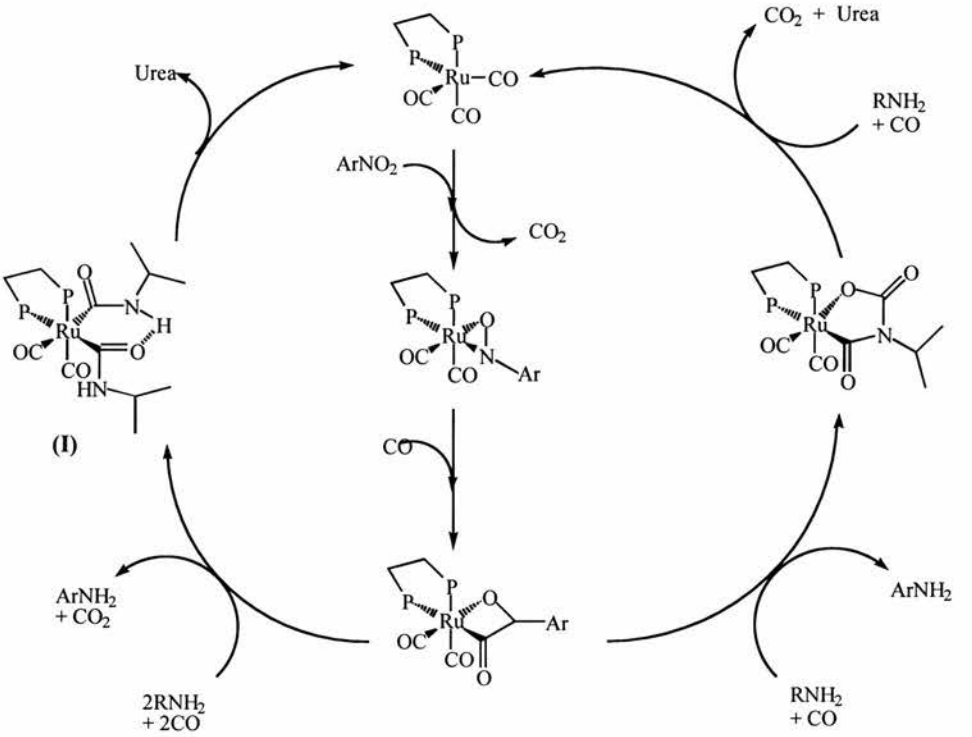

Figure 1.15 Ruthenium catalysed formation of 1,3-dialkyl ureas with $ArNO_2$ as oxidant

1.3.5.2 Reduction of NO with CO and H_2 to produce urea

NO can be reduced efficiently and in high yield with CO and H_2 using platinum group metals (Rh, Pd, Pt, Monel metal), with or without supports (Al_2O_3, charcoal) under relatively mild conditions to produce NH_4OCN[59-62] as shown in figure 1.16.

$$2NO + 2H_2 + 3CO \longrightarrow NH_4OCN + 2CO_2$$

Figure 1.16 Catalytic reduction of NO to ammonium cyanate

Surface isocyanate species are thought to play an important role in the catalysis, which could be significant from a mechanistic point of view. Urea is formed by the conversion of NH_4OCN during collection by condensation at temperatures of 80-120°C. The process is unlikely to generate an industrial interest due to the relatively high cost of NO as a raw material.

1.3.5.3 Reduction of nitro aromatic compounds to ureas using CO[63]

Using excess aniline as a reagent and solvent, nitrobenzene can be converted to diphenyl urea in high yield. Diphenyl ureas are a well-known class of commercially available herbicides. There is question over the mechanism of the[64,65] catalysis. One postulation which retains [Pd] in the same oxidation state throughout, as shown in the top cycle of figure 1.17, is that nitrobenzene is deoxygenated to form a nitrene complex which reacts with CO to give a phenyl isocyanate complex (I). This then reacts with aniline to give N,N-diarylurea. Stoichiometric amounts of aniline and nitrobenzene are used as starting materials. Another pathway shown in the bottom cycle of figure 1.17 proceeds with different stoichiometry of aniline which reacts with CO to give a carbamoyl complex. Aniline reacts with this complex to give the same phenyl isocyanate species arrived at in the first mechanism. Reaction then proceeds as before to give N,N-diaryl urea. It has been found that stepwise addition of aniline during the period of the reaction results in an increased yield of the diphenylurea[66]. At low concentrations, this supports the argument for the first pathway described.

It was found that electronic and steric effects of ligands have a great influence on diphenyl urea formation[67,68]. Most significantly, it was shown that with increased electron density on the palladium centre, the rate of the reaction was increased.

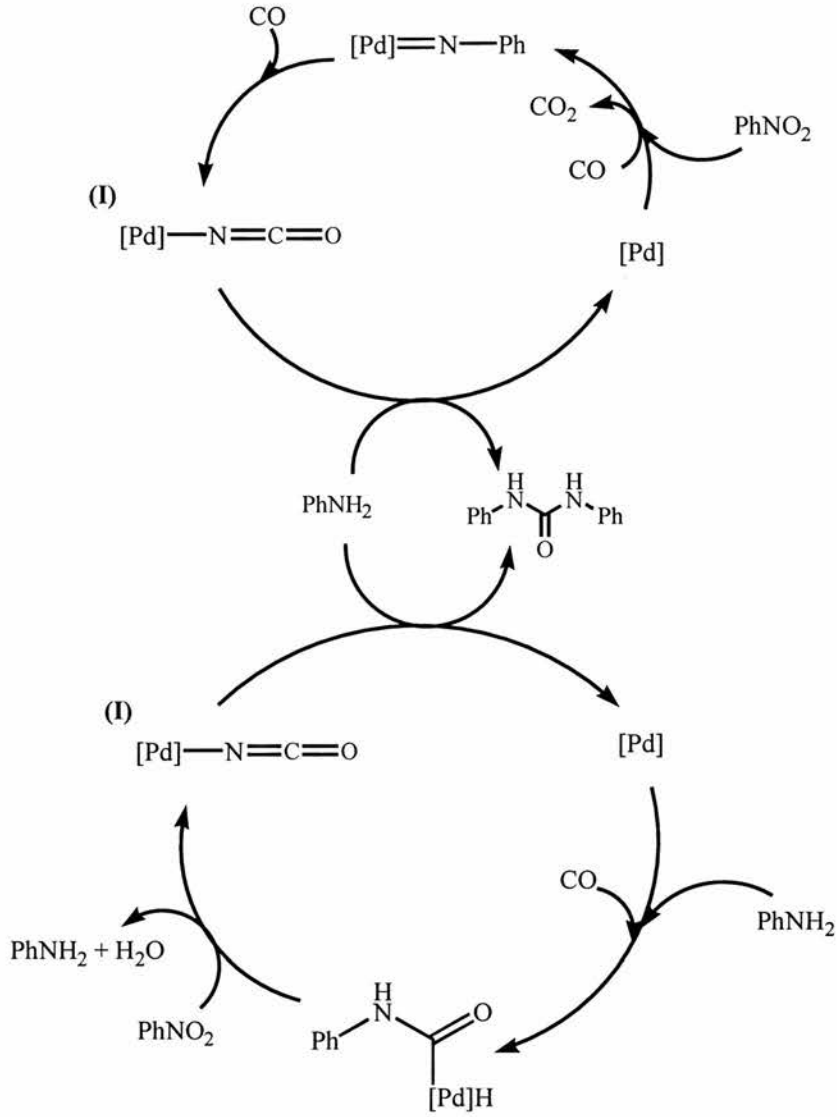

Figure 1.17 Two pathways proposed for the catalytic formation of urea from nitrobenzene and aniline.

1.3.5.4 Activation of coordinated isocyanate

We have seen in the above example that coordinated isocyanate is very likely to be an intermediate in the catalytic production of symmetrical ureas from aniline and nitrobenzene. In a recent publication on N-H bond activation of ethyl carbamate and urea, ruthenium hydride complexes were examined[69]. The initial step in the activation of ethyl carbamate is the formation of a carbamato complex followed by facile loss of

ethanol to yield an isocyanato complex as shown in figure 1.18. The reaction was found to be non-reversible affording instead $[Ru(CO)_3(PPh_3)_2]$ by reduction with ethanol.

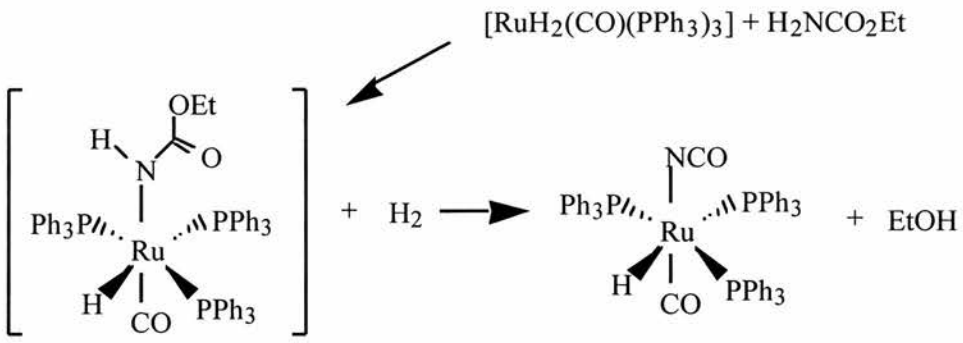

Figure 1.18 Activation of isocyanate

The mechanism involving activation of urea was thought to be similar, yielding ammonia instead of ethanol, however, the reversibility of the reaction was not commented upon (see figure 1.19). Certainly, reaction of the isocyanato complex produced by reaction with ammonia is more likely to occur than for ethanol (NH_3 is a much better nucleophile than EtOH), and it may be worth-while attempting this reaction starting with this (and other) isocyanato complexes and ammonia.

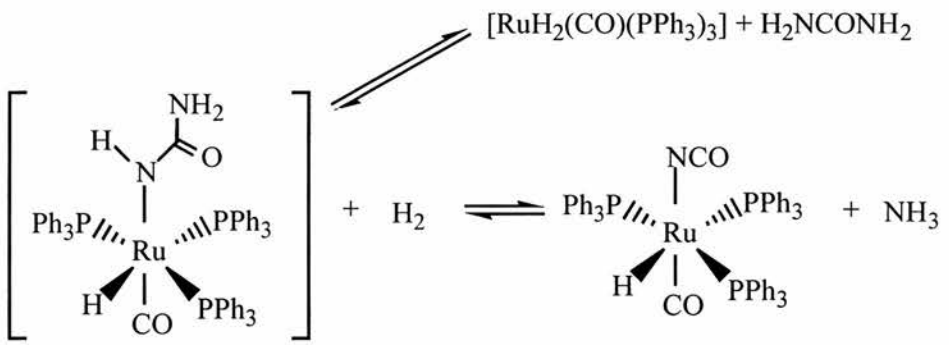

Figure 1.19 Proposed reaction of ammonia with co-ordinated isocyanate

1.3.6 Urea production activated by metal carbonyl species

1.3.6.1 Stoichiometric urea production from NH_3 and CO by reaction with iron and manganese carbonyls

Stoichiometric formation of urea has been observed for the complexes $[Fe(CO)_5]$, $[Fe_2(CO)_9]$ and $[Fe_3(CO)_{12}]$[70] by their reaction with liquid ammonia. These reactions correspond to the hydrolysis of the carbonyl compounds by alkali hydroxide (see figure 1.20).

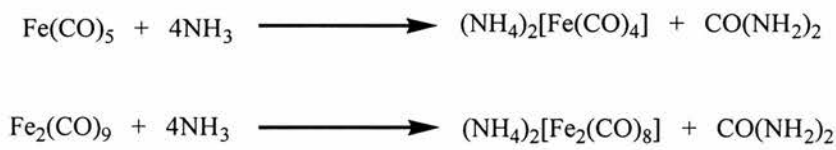

Figure 1.20 Stoichiometric reaction of $[Fe(CO)_5]$ and $[Fe_2(CO)_9]$ with ammonia to produce urea.

$[Mn_2(CO)_{10}]$[71] is also found to promote the stoichiometric production of urea from NH_3 at 20°C. Whilst nucleophilic attack of ammonia upon the carbonyl moiety to form the coordinated amide complex is generally accepted to be the first step, there is ambiguity surrounding the mechanism of formation of urea from the amide complex. A second nucleophilic attack upon the amide complex by a second molecule of ammonia followed by reductive elimination of a molecule of urea is one possibility[71] as shown in figure 1.21.

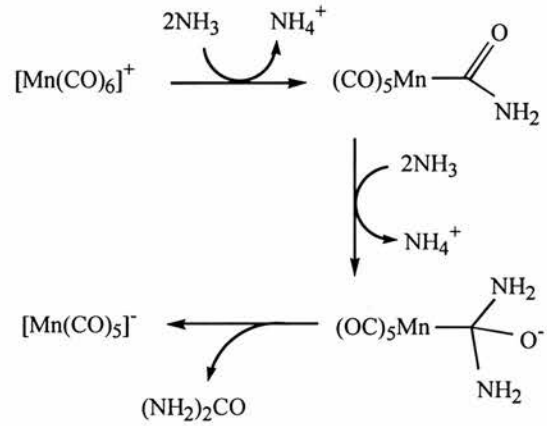

Overall;

$$Mn_2(CO)_{10} + CO + 2NH_3 \longrightarrow 2HMn(CO)_5 + CO(NH_2)_2$$

Figure 1.21 Stoichiometric urea production from $Mn_2(CO)_{10}$

1.3.6.2 Production of 1,3-dialkyl ureas from primary amines catalysed by $[Mn_2(CO)_{10}]$

Another possible pathway for the formation of urea is suggested in work performed involving the catalytic carbonylation of primary amines by $[Mn_2(CO)_{10}]$[72-74] which suggests that alkyl cyanate is the primary product. Reaction with a further mole of amine gives the substituted urea (figure 1.22).

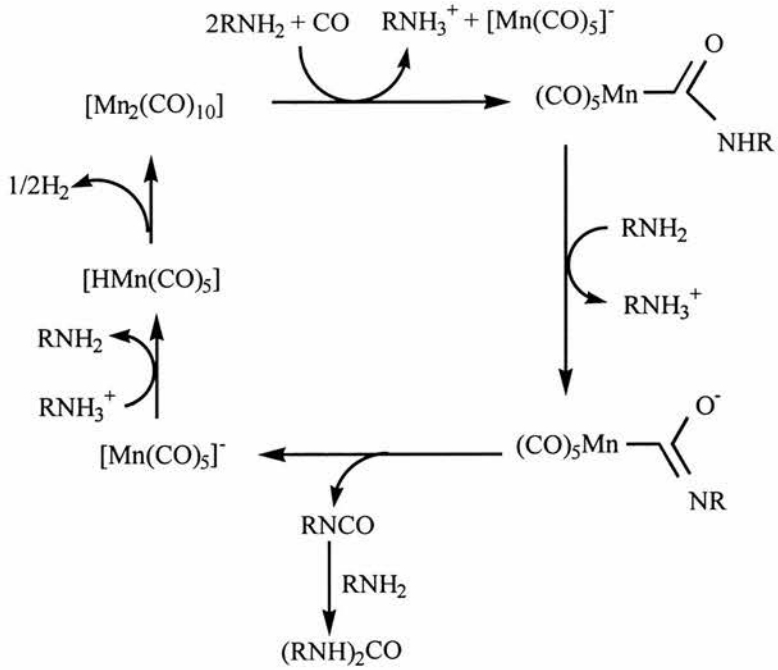

Figure 1.22 Catalytic production of 1,3-dialkulureas from primary amines using $[Mn_2(CO)_{10}]$ as catalyst

1.3.6.3 Carbonylation of primary amines to 1,3-disubstituted ureas catalysed by other metal carbonyls

Early reports of 1,3-disubstituted urea formation without detailed mechanistic information shows that carbonylation of primary amines by $Ni(CO)_4$[75-77] and $Co_2(CO)_8$[78] is also possible. For example, both species are capable of catalysing the carbonylation of aniline to formanilide and 1,3-diphenylurea. The reactions are performed under high temperatures and pressures (typically 200-280°C, 120-140 atm[75]) with the formamide being the primary product.

1.4 Reactions of transition metal complexes with ammonia

Reactions of ammonia with transition metal complexes can be envisaged to proceed in one of two ways, either oxidative addition across a metal centre, or nucleophilic attack at a coordinated CO group of a transition metal carbonyl complex.

It is important to review reactions of metal complexes with ammonia, in particular, oxidative addition, as the mechanism proposed by Taqui Khan and co-workers for catalysis of urea production from CO and NH_3 from $[Ru(HEDTA)CO]^-$ described in section 1.3.1 suggests that this occurs as the first step in the catalytic cycle.

1.4.1 Oxidative addition of ammonia across an active centre

Oxidative addition of N-H bonds is a potentially important step in the functionalisation of ammonia and other N-H containing compounds, however, there are very few genuine cases of oxidative addition of ammonia to a metal centre in solution[79-84]. There are examples of reactions between ammonia and some early transition metal complexes[85-88] (Ti, Zr, Hf) which cannot involve N-H oxidative addition since the metals are generally d^0. These reactions probably involve σ-bond metathesis with (rather than genuine oxidative addition of) ammonia resulting in the formation of imides or nitrides, and involve the simultaneous reductive loss of coordinated anions (e.g. loss of H_2 as shown in figure 1.23 (a)[86]). In the case for the reaction shown in figure 1.23 (b) between a complex of titanium and ammonia, CH_4 is lost rather than hydrogen[85]. The reactions are reported to occur readily at room temperature.

(a)

(b)

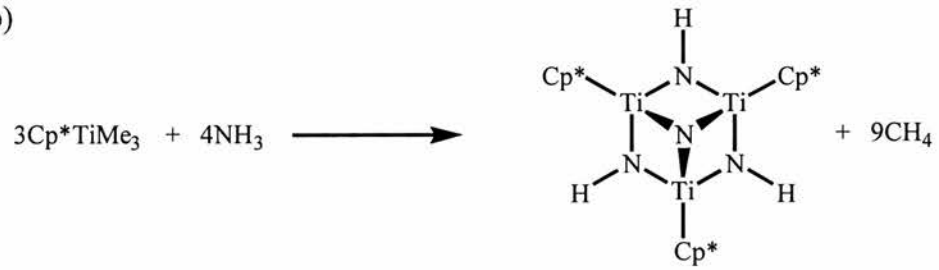

(Cp* = C_5Me_5, M = Hf, Zr)

Figure 1.23 Reactions of early transition metal complexes with ammonia

For the more reactive N-H bonds of imides and amides (pK_a typically 15-17), oxidative addition reactions are more common[89-96] than for amines (pK_a typically 32-35). The first observation of oxidative addition of ammonia to a mononuclear late transition metal complex was made in 1987 by Casalnuovo and co-workers[81] during studies on N-H activation which subsequently led to the catalytic stereoselective addition of aniline to norbornene[97]. In this case, it was found that $[Ir(PEt_3)_2(C_2H_4)_2Cl]$ would react with ammonia to produce several complexes with either Ir-NH_3 groups and bridging Ir-NH_2-Ir groups, or complexes in which only the bridging function is present (figure 1.24). The complexes with NH_3 as ligand were found to be unreactive to CO at "moderate temperatures and pressures", their relative stability attributed to the stabililty of the Ir-NH_2-Ir bridge. One of the complexes in which only bridging functions exist can be carbonylated at 50 psi, however, no subsequent reactions were examined.

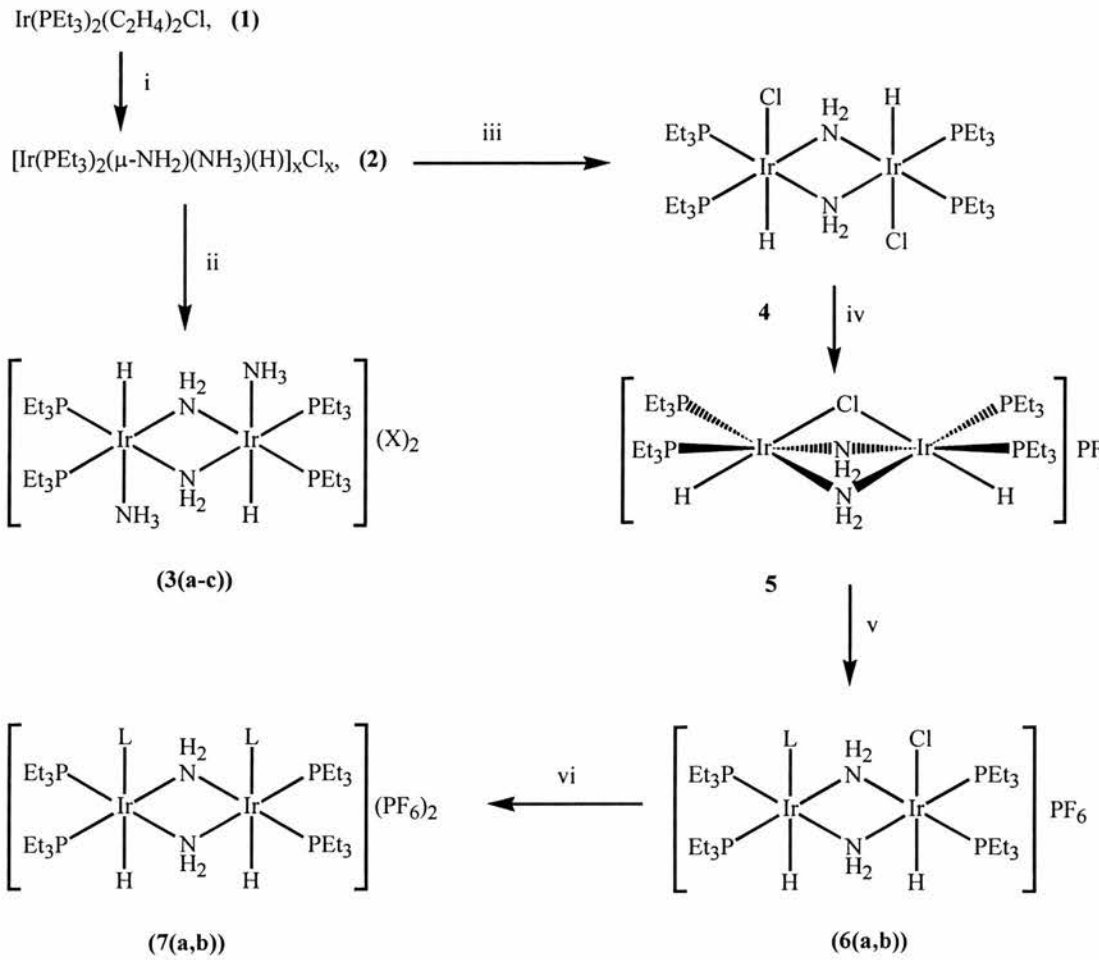

Figure 1.24 Reaction conditions: (i) $NH_{3\,(l)}$, 25°C, 24 h; (ii) $NaBPh_4$ or $TlPF_6$ in acetone (3**a**, X = BPh_4; **3b**, X = BF_4; **3c**, X = PF_6); (iii) 110°C, pyridine; (iv) $TlPF_6$, acetone; (v) L, acetone (**6a**, L = CO (50 psi); **6b**, L = ^{t}BuNC); (vi) $TlPF_6$ + L in acetone[97].

More recent reports[79,80] by Milstein and co-workers have elaborated further upon the N-H activation of ammonia by other complexes of Ir^I. Again, the mechanism involves co-ordination of ammonia to a low-valent $Ir^{(I)}$ olefin complex. Upon co-ordination, the metal centre becomes electron-rich enough to induce N-H cleavage of a subsequent incoming ammonia molecule.

A theoretical study into the activation of the N-H bond of ammonia by second row transition metal atoms[98] concluded that complexes of rhodium were the most likely of those metals on the right of the periodic table to induce N-H oxidative addition. Given the similarity between the energy barrier (calculated relative to ground state metal atoms and free NH_3 or CH_4) for ammonia insertion (7.1 kcal mol^{-1}) and that for

methane (6.8 kcal mol^{-1}) (see figure 1.25), it is interesting to note that C-H dissociation of alkanes has been observed for

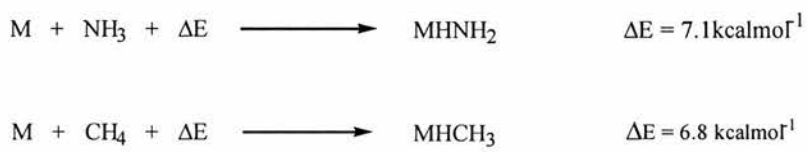

Figure 1.25 Theoretical barrier heights for the N-H and C-H insertion reactions of NH_3 and CH_4.

complexes of Rh^I with low activation barriers[99-101]. However, oxidative addition of CH_4 to transition metal complexes, as for NH_3, is similarly very rare[100,102-106] and this is attributed to the relatively low thermodynamic stability of the oxidative addition adduct $L_nM(H)(CH_3)$. The first authentic observations of alkane oxidative addition were made for photocatalytic complexes of iridium[105-108]. For example, photochemical activation of $[Cp^*Ir(PMe_3)H_2]$ results in loss of H_2 and the formation of $[Cp^*Ir(PMe_3)]$ which can react with alkanes in a fluorinated solvent as shown in figure 1.26.

The role of *hv* is to expel H_2 or CO to give a reactive intermediate which can insert readily into C-H bonds and this is typical of most reported instances of alkane insertion, the notable exception being the thermal activation of $[Cp^*Ir(PMe_3)(C_6H_{11})H]$ which loses cyclohexane at 150°C to oxidatively add CH_4 at a pressure of 20 bar.

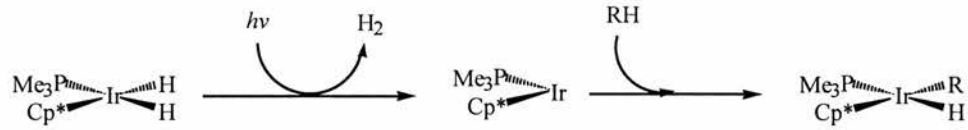

$Cp^* = C_5Me_5$

Figure 1.26 Oxidative addition of alkanes

Activation of C-H bonds for the selective functionalisation of hydrocarbons is also potentially a very important reaction from an industrial stand-point, for example, in the production of aldehydes by reaction with carbon monoxide, and whilst its

occurrence in the chemistry of complexes of the late transition metals is rare, it is not quite as rare as activation of the N-H bonds of ammonia.

By analogy with a complex which is known to be active for the photocatalytic oxidative addition of alkanes, it is possible to hypothesise about the potential reaction with ammonia instead of alkane. In the following example, benzene can be carbonylated to benzaldehyde, with a yield of 6520 % (calculated per mole of catalyst). The reaction proceeds under ambient conditions of temperature and pressure in the presence of $[RhCl(CO)(PMe_3)_2]$ under irradiation[99]. Photoassisted CO dissociation, followed by oxidative addition of the C-H bond, CO insertion to the carbon-metal bond and reductive elimination of an aldehyde was proposed as the reaction mechanism. If activation of ammonia were to take place at such a metal centre, then a possible mechanism for this reaction for the production of formamide is outlined in figure 1.27.

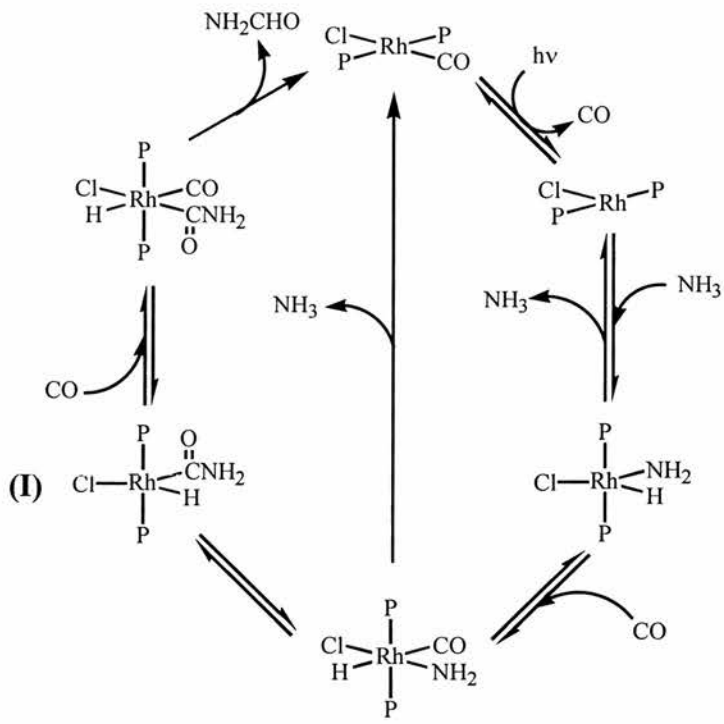

Figure 1.27 Possible mechanism for the photoassisted production of formamide from NH_3 and CO in the presence of $[RhCl(CO)(PMe_3)_2]$

However, calculations upon similar systems have shown that the oxygen atom of the coordinated amide (intermediate **(I)**) is likely to be very nucleophilic[109].

Protonation here would give a hydroxy aminocarbene which would then be susceptible to nucleophilic attack at carbon giving a coordinated hydroxydiamine group. ß-hydrogen abstraction from the OH group gives urea as shown in figure 1.28. The dihydride complex which results will probably be inert to further reaction, however, there is evidence (see chapter 6, section 6.2) that the isopropyl phosphine analogue $[RhH_2Cl(P^iPr_3)_2]$ reacts with ammonia. It is thought that the ammonia acts as a base removing HCl from the complex to give the 14-electron species $[RhH(P^iPr_3)_2]$ which is active enough to promote oxidative addition of ammonia. This complete cycle to produce urea would then involve two steps of oxidative addition of ammonia across different metal complexes. Given that ammonia has never been reported to oxidatively add across any complex of rhodium this mechanism is speculative at best!

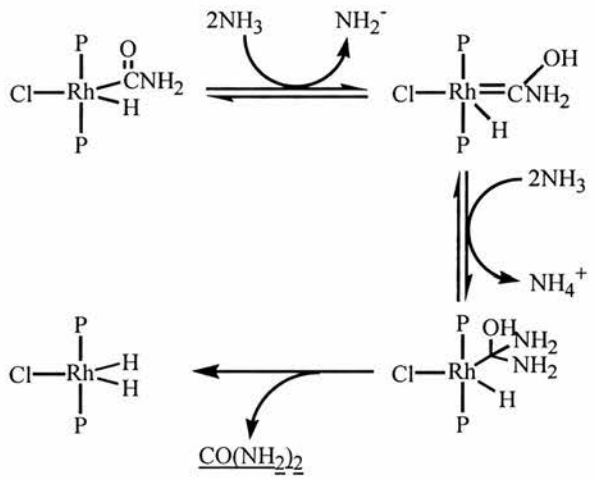

Figure 1.28. Propagation of scheme shown in figure 1.27 to accommodate for stoichiometric urea production.

1.4.2 Nucleophilic attack of ammonia upon coordinated CO[110]

Carbon monoxide in its free state is fairly unreactive, however, co-ordination-induced changes in the electronic distribution within the CO enhance its reactivity. For example, studies on the photoelectron spectra of metal carbonyls such as $Fe(CO)_5$ allows the conclusion that atomic charges on both metal and the CO carbon atoms are positive, whereas those for the O atoms of CO are negatively charged[111,112]. In contrast,

other calculations have shown that although CO in its free state has a very small dipole moment, the carbon atom may even possess a slightly negative charge[113]. This would explain the inert behaviour of CO towards nucleophiles under normal conditions. The susceptibility of a coordinated CO group to nucleophilic attack can be correlated to the extent of the elctron-withdrawing capacity of the L_nM fragment. Electron-donating ligands, or a net negative charge on the complex increase electron density on the metal which in turn increases the strength of the back-bonding to coordinated CO groups and the electrophilic nature of the C atoms of coordinated CO groups This explains why positively charged and neutral complexes are most commonly observed to react with nucleophiles.

Activation of metal carbonyls to the nucleophilic attack of amines and ammonia is a stoichiometric reaction that has been known for a long time and early reports[114-117] show that the reactions often occur under ambient conditions of temperature and CO pressure to give amides and formamide respectively. Although not directly implicated in the mechanisms of the reactions, it is likely that they proceed *via* a carbamoyl intermediate as shown in figure 1.29 which results from the nucleophilic attack of amine upon coordinated CO.

Carbamoyl (or carboxamido) functional groups have been known in organic chemistry for over a century and in inorganic chemistry for the past 35 years and have been proposed as intermediates in many stoichiometric and catalytic reactions[118,119].

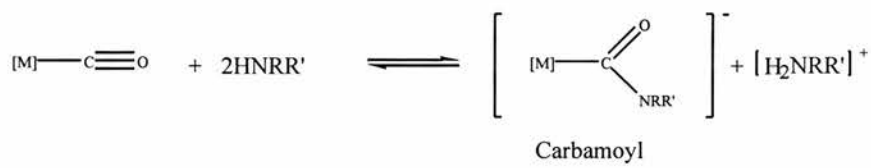

Figure 1.29 Formation of the carbamoyl moiety.

Usually, carbamoyl formation is rapid and occurs at room temperature The reaction with NH_3, primary and secondary alkylamines generally occurs readily, but aromatic amines do not undergo a similar reaction with any metal carbonyl complex as a result of low activity due to incorporation of the lone pair of non-bonding electrons on N into the delocalised π-electron system of the aromatic ring. Many cationic and some

neutral metal carbonyl complexes are known to be active, and it was found that the C-O stretching force constants are a good measure of the positive charge on the carbon atom of the CO group, and can be used to predict whether or not a nucleophilic reaction will occur[120] As a result of these studies, it has been concluded that as a general rule, CO ligands with a force constant greater than a certain value react to form exclusively carbamoyl complexes, whilst those within a certain range of values form an equililbrium mixture, and complexes with force constants below a critical value do not show evidence of carbamoyl formation[121].

1.5 References

1. Wohler, F., *Quart. J. Sci. Lit. Art,* Series 2, Part 1 (April - June), 1828, 491: Wohler, F., *Poggendorffs Ann.,* **12,** 1828, 253: Wohler, F., *Ann. Chim. Phys.,* **37,** 1828, 330.
2. Vale, C.P., Taylor, W.G.K., 'Aminoplastics', Iliffe, London, 1964.
3. Traube, W., *Annalen,* **432,** 1923, 226.
4. Othmer, K., *Encyclopedia of Chemical Technology,* Vol. 23, Wiley-Interscience, New York, 1983, 548: Hatch, L.F., *Petrol Refiner.,* **37,** 1958, 123.
5. Pratt, A., Kelly, Y., Private communication.
6. Roundhill, D.M., *Chem. Rev.,* **92,** 1992, 1.
7. Briner, E., *J. Chim. Phys.,* **4,** 1906, 267.
8. Taqui-Khan, M.M., Halligudi, S.B., Abdi, S.H.R., Shukla, S. *J. Mol. Catal.,*1988, **48,** 25.
9. Taqui-Khan, M.M. *Platinum Metals Rev.,* 1991, **35,** 70.
10. Indian Patent # 170438, 14 March 1989.
11. Taqui Khan, M.M., Halligudi, S.B., Abdi, S.H.R., *J. Mol. Catal.,* **48,** 1988, 325.
12. Iove, A., Torocheshnikov, N.S., Lyudkovskaya, M.A., Klevke, *Khim. Prom.,* 1964, 585; *Chem. Abstr.,* 1964, **61**, 12974c.
13. Iove, A., Torocheshnikov, N.S., Lyudkovskaya, M.A., Klevke, V.A., *Khim. Prom.,* 1964, 244; *Chem. Abstr.,* 1964, **61**, 5514f.
14. Iove, A., Torocheshnikov, N.S., Lyudkovskaya, M.A., Klevke, V. *Khim. Prom.,* 1965, **41,** 820; *Chem. Abstr.,* 1966, **64,** 19406a.
15. Takizawa, S., Kageyama, T., *Nippon Kagaku Zasshi,* 1966, **87,** 300; *Chem. Abstr.,* 1966, **65,** 15222f.
16. Gras, W., Stickrodt, W.J., Seipke, W., *Ger. Offen.,* 1963, 1158494; *Chem. Abstr.,* 1964, **61,** P11900g.
17. Stickrodt, W.J., Seipke, W., *Ger. Offen.,* 1964, 1163311; *Chem Abstr.,* 1964, **60,** P15744c..
18. Kutsher, G.S., Elliott, G.A., *U.S. Patent,* 1972, 3657339; *Chem. abstr.,* 1972, **77,** P4998u.
19. Inoue, S., *Chem. Abstr.,* 1988, **108,** 77611f.

20. Asashi Chem. Ind. Co., Chiyoda Chem. Eng. and Caster Co., *Brit. Pat.,*1972, 1275702; *Chem. Abstr.,* 1972, **77,** 151527t.
21. Herman, J.J., Lecloux, A., *Eur. Pat.,* 1986, 193982.
22 Kondo, K., Sonoda, N., Tsutsumi, S., *J. Chem. Soc., Chem. Comm.,* 1972, 307.
23. Sonodo, N., Yasuhara, T., Kondo, K., Ikeda, T., Tsutsumi, S., *J. Am. Chem. Soc.,* **93,** 1971, 6344.
24. Kambe, N., Kondo, K., Ishii, H., Sonoda, N., *Bull. Chem. Soc. Jpn.,* 1981, **54,** 1460.
25. Kambe, N., Kondo, K., Ishii, H., Sonoda, N., Murai, S., *Angew. Chem. Int. Ed. Engl.,* 1979, **18,** 547.
26. Robinson, P.L., Stainthorpe, K.R., *Nature,* **153,** 1944, 24.
27. Patterson, J.A., Atwell, H.V., *US Patent,* 2,993,931; *Chem. Abstr.,* **56,** 1962, 1392h.
28. Kamiguchi, T., *J. P.,* 1987, 6,216,456; *Chem. Abstr.,* **107,** 1987, 42087s.
29. Colquhoun, H.M., Thompson, D.J., Twigg, M.V., *Carbonylation: Direct Synthesis of Carbonyl compounds;* Plenum: New York, 1991.
30. Sheldon, R.A., *Chemicals from Sythesis Gas;* Dordrecht: Boston, MA, 1983.
31. Wender, I., Pino, P., *Organic Syntheses via Metal Carbonyls,* Wiley Interscience: New York, 1968.
32. McCusker, J.E., Abboud, K.A., McElwee-White, L., *Organometallics,* **16,** 1997, 3863.
33. Kondo, T., Kotachi, S., Tsuji, Y., Watanabe, Y., Mitsudo, T., *Organometallics,* **16,** 1997, 2562.
34. Halligudi, S.B., Bhatt, K.N., Khan, N.H., Kurashy, R.I., Venkatsubramanian, K., *Polyhedron,* **15,** 1996, 2093.
35. Jorgenson, A.L., Breedlove, B.K., Gladfelter, W.L., *Abst. Am. Chem. Soc.,* **210,** 173.
36. Giannoccaro, P., *J. Organomet. Chem.,* **470,** 1994, 249.
37. Mori, S., Matsuyoshi, H., Kudo, K., *Chem. Lett.,* 1991, 1397.
38. Giannocaro, P., Nobile, C.F., Mastrorilli, P., Ravasio, N., *J. Organomet. Chem.,* **419,** 1991, 251.

39. Srivastava, S.C., Shrimal, A.K., Srivastava, A., *J. Organomet. Chem.,* **414,** 1991, 65.
40. Bassoli, A., Rindone, B., Tollari, S., Chioccara, F., *J. Mol. Catal.,* **60,** 1990, 41.
41. Pri-Bar, I., Alper, H., *Can. J. Chem.,* **68,** 1990, 1544.
42. Giannoccaro, P., *J. Organomet. Chem.,* **336,** 1987, 271
43. Tsuji, Y., Takeuchi, R., Watanabe, Y., *J. Organomet. Chem.,* **290,** 1985, 249.
44. Dombek, B.D., Angelici, R.J., *J. Organomet. Chem.,* **134,** 1977, 203.
45. Calderazzo, F., *Inorg. Chem.,* **4,** 1965, 293.
46. Brackman, W., *Disc. Faraday Soc.,* 1968, **46,** 122
47. Brackman, W., British Patent #868460, 1961; *Chem. Abstr.,* **56,** 1962, P1434c.
48. Suss-Fink, G., Langenbahn, M., Jenke, T., *J. Organomet. Chem.,* **368,** 1989, 103.
49. Jenner, G., Bitsi, G., Schleiffer, E., *J. Mol. Catal.,* **39,** 1987, 233.
50. Bitsi, G., Jenner, G., *J. Organomet. Chem.,* **330,** 429.
51. Bitsi, G., Jenner, G., *Applied Cat.,* **32,** 1987, 293.
52. Tsuji, Y., Ohsumi, T., Kondo, T., Watanabe, Y., *J. Organomet. Chem.,* **309,** 1986, 333.
53. Martin, W.E., Farona, M.F., *J. Organomet. Chem.,* **206,** 1981, 393.
54. Dodd, J.A., Robert, R.L., U.S. Patent 4343655A, *Chem. Abstr.,* **97,** 1982, 164847k.
55. Sherwood, P.W., *J. Coat. Technol.,* **54,** 1982, 61.
56. Braunstein, P., *Chem. Rev.,* **89,** 1989, 1927.
57. Giannoccaro, P., *Inorg. Chim. Acta.,* **142,** 1988, 81.
58. Gargulak, J.D., Gladfelter, W.L., *Inorg. Chem.,* **33,** 1994, 253.
59. Voorhoeven, R.J.H., Trimble, L.E., *J. Catal.,* **53,** 1978, 251.
60. Radel, R.J., Kim, Y.K., *Statutory Invent. Regist. US 38,* 196, 754, 755; *Chem. Abstr.,* **109,** 1988, 75737g.
61. Voorhoeven, R.J.H., *Ger. Offen.,* 1978, 2, 809, 858; *Chem. Abstr.,* **89,** 1978, P214928.
62. Heker, C.W., Bell, T.A., *J. Catal.,* **88,** 1984, 289.
63. Tafesh, A.M., Weiguny, J., *Chem. Rev.,* **96,** 1996, 2035.
64. Lee, C.W., Lee, S.M., Oh, J.S., *Ind. Eng. Chem.Res.,* **30,** 1991, 1456.

65. Lee, S.M., Cho, N.S., Kim, K.D., Oh, J.S., Lee, C.W., Lee, J.S., *J. Mol. Catal.*, **73,** 1992, 43.

66. Goodall, B.L., *Eur. Patent* #319 111, 1989.

67. Lee, C.W., Lee, J.S., *J. Mol. Catal.*, **81,** 1993, 163.

68. Lee, C.W., Lee, S.M., Oh, J.S., Lee, J.S., *Catal. Lett.*, **19,** 1993, 217.

69. Ragaomo. F., Longo, T., Cenini, S., Demartin, F., *J. Chem. Soc., Dalton Trans.*, 1996, 3221.

70. Behrens, H., Wakamatsu, H., *Z. Anorg. Allg. chem.*, 1963, **320**, 30.

71. Behrens, H., Ruyter, E., Wakamatsu, H., *Z. Anorg. Allg. Chem.*, 1967, **349,** 241.

72. Dombek, B.D., Angelici, R.J., *J. Organomet. Chem.*, 1977, **134,** 203.

73. Calderazzo, F., *Inorg. Chem.*, 1965, **4,** 293.

74. Calderazzo, *U.S. Patent* #3316297, 1967.

75. Aliev, Y.Y., Romanova, I.B., *Neftekhimiya, Akad. Nauk Turkum. S.S.R.*, 1963, 204: *Chem. Abstr.*, **61,** 1964, 6913.

76. Reppe, W., *Annalen,* **582,** 1953, 1.

77. Reppe, W., Kroeper, H., *Annalen,* **582,** 1953, 38.

78. Sternberg, H.W., Wender, I., Friedel, R.A., Orchin, M., *J. Am. Chem. Soc.*, **75,** 1953, 3148.

79. Schulz, M., Milstein, D., *J Chem. Soc., Chem. Comm.*, 1993, 318.

80. Koelliker, R., Milstein, D., *Angew. Chem. Int. Ed. Engl.*, 1991, **30,** 707.

81. Casalnuovo, A.L., Calabrese, J.C., Milstein, D. *Inorg. Chem.*, 1987, **26,** 971.

82. Bercaw, J.E., Davies, D.L., Wolczanske, P.T., *Organometallics,* 1986, **5,** 443.

83. Suss-Fink, G.Z., *Naturforsch., B: Anorg. Chem., Org. Chem.*, 1980, **35B,** 454.

84. Bryan, E.G., Johnson, B.F.G., Lewis, J., *J. Chem. Soc., Dalton Trans.*, 1977, 1328.

85. Banaszak, M.M., Holl, P.T., Wolczanske, G.D., Van Duyne, *J. Am. Chem. Soc.*, 1990, **112,** 7989.

86. Roesky, H.W., Bai, Y., Noltemeyer, M., *Angew. Chem.*, 1989, **101,** 788; *Angew. Chem. Int. Ed. Engl.*, 1989, **28,** 754.

87. Hillhouse, G.L., Bercaw, J.E., *J. Am. Chem. Soc.*, 1984, **106,** 5472.

88. Armor, J.N., *Inorg. Chem.*, 1978, **17,** 213. Armor, J.N., *Inorg. Chem.*, 1978, **17,** 203.

89. Hadden, D., Roundhill, D.M., Fultz, W.C., Rheingold, A.L., *J. Am. Chem. Soc.,* **106,** 1984, 5014.

90. Goel, R.A., Srivastava, R.C., *J. Organomet. Chem.,* **244,** 1983, 303.

91. Yamamoto, T., Sano, K., Yamamoto, A., *Chem. Lett.,* 1982, 907.

92. Fornies, J., Green, M., Spencer, J.L., Stone, F.G.A., *J. Chem. Soc., Dalton Trans.,* 1977, 1006.

93. Rauchfuss, T.B., Roundhill, D.M., *J. Am. Chem. Soc.,* **96,** 3098.

94. Mague, J.T., *Inorg. Chem.,* **11,** 1972, 2558.

95. Roundhill, D.M., *Inorg. Chem.,* **9,** 1970, 254.

96. Nelson, J.H., Schmidt, D.L., Henry, R.A., Moore, D.W., Jonassen, H.B., *Inorg. Chem.,* **9,** 1970, 2678.

97. Casalnuovo, A.L., Calabrese, J.C., Milstein, D. *J. Am. Chem. Soc.,* 1988, **110,** 6738.

98. Blomberg, M.R.A., Siegbahn, P.E.M., Svensson, M., *Inorg. Chem.,* **32,** 1993, 4218.

99. Sakakura, T., Sodeyama, T., Sasaki, K., Wada, K., Tanaka, M., *J. Am. Chem. Soc.,* **112,** 1990, 7221.

100. Ghosh, C.K., Graham, W.A.G., *J. Am. Chem. Soc.,* **109,** 1987, 4726.

101. Jones, W.D., Feher, F.J., *J. Am. Chem. Soc.,* **104,** 1982, 4240.

102. Crabtree, R.H., *Chem. Rev.,* **95,** 1995, 987.

103. Jones, W.D., Maguire, J.A., *Organometallics,* **5,** 1986, 590.

104. Osman, R., Paltison, D.I., Perutz, R.N., Bianchini, C., Peruzzini, M., *J. Chem. Soc., Chem. Comm.,* 1994, 513.

105. Hoyano, J.K., McMaster, A.D., Graham, W.A.G., *J. Am. Chem. Soc.,* **105,** 1983, 7190.

106. Hoyano, J.K., Graham, W.A.G., *J. Am. Chem. Soc.,* **104,** 1982, 3723.

107. Janowicz, A.H., Bergman, R.G., *J. Am. Chem. Soc.,* **105,** 1983, 3929.

108. Janowicz, A.H., Bergman, R.G., *J. Am. Chem. Soc.,* **104,** 1982, 352.

109. Barratt, D.S., Glidewell, C., Cole-Hamilton, D.J., *J. Chem. Soc., Dalton Trans.,* 1988, 1079.

110. Ford, P.C., Rokicki, A., *Adv. Organomet. Chem.,* **28,** 1988, 139.

111. Beach, D.B., Smit, S.P., Jolly, W.L., *Organometallics,* **3,** 1984, 556.

112. Beach, D.B., Jolly, W.L., *Inorg. Chem.,* **22,** 1983, 2137.

113 Huheey, T.E., "Inorganic Chemistry," 2nd. Ed., p. 154, Harper, New York, 1978.

114. Hieber, W., Schuster, L., *Z. Anorg. Chem.,* 1956, **287**, 214.

115 Hieber, W., Hensinger, H., *J. Inorg. Nucl. Chem.,* 1957, **4**, 179.

116.. Bird, C.W., *Chem. Rev.,* 1962, **62**, 283.

117. Bird, C.W., "Transition Metal Intermediates in Organic Synthesis" Academic Press, New York, 1967.

118. Milstein, D., *Acc. Chem. Res.,* **21,** 1988, 428.

119. Angelici, R.J., *Acc. Chem. Res.,* **5,** 1972, 335.

120. Darensbourg, D.J., Darensbourg, M.Y., *Ibid.,* **9,** 1970, 1691.

121. Angelici, R.J., Blacik, L., *Inorg. Chem.,* **11,** 1972, 1754.

CHAPTER 2

Techniques for the analysis of urea

2.1 Introduction

Most literature methods for the separation and estimation of urea are concerned with its analysis in the blood or in urine. Urea is a product of nitrogen metabolism in mammals and accounts for 80-90% of nitrogen excretion in man (25-35 g daily). Without this method of transport of nitrogen from the body, we would certainly die. Less drastic is uraemia, a condition resulting from an increase in plasma urea concentration, the symptoms of which may be anorexia or lethargy resulting from an accumulation of toxins of which increased urea concentration provides an indication. Clinical methods of urea analysis provide the largest pool of data for its quantification but also, techniques for the analysis of impurities detrimental to its use as a fertiliser are very important to the industry in maximising efficiency in plant growth. What follows in this chapter is a summary of techniques which may be considered for urea analysis together with a literature review on each. In each case this is followed by our own observations on the utility of the technique and full experimental details of how we have operated the technique.

2.2 Chromatographic methods

"The essence of the chromatogram is the uniform percolation of a fluid through a column of more or less finely divided substance which selectively retards by whatever means, certain components of the fluid."

A.J.P. Martin

2.2.1 Gas chromatography (GC)

GC is a chromatographic method suitable for the separation of materials which are volatile without decomposition. Unfortunately (because it decomposes at temperatures where it is insufficiently volatile to be transported down the column (see section 1.1.2)), non-derivatised urea does not fall into this class of compounds. However, urea *has* been determined as derivatives in biological materials by gas chromatography as trifluoroacetyl urea[1,2], and in a recent report[3], gas chromatographic/mass spectrometric data was presented, and used for the determination of ^{13}C blood urea enrichment. In this particular case, the urea was converted to its dimethylaminomethylene derivative using dimethyl formamide dimethyl acetamide (DMFDMA), (see figure 2.1), with very good limits for the sensitivity of the technique. Separation of the urea prior to derivatisation was necessary for the analysis of blood urea, and glucose was removed by ion exchange prior to formation of the derivative and analysis by GC.

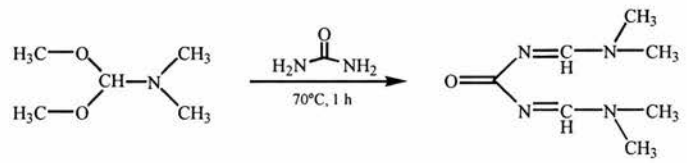

DMFDMA

Figure 2.1 Reaction of DMFDMA with urea

2.2.2 High performance liquid chromatography (HPLC)

HPLC is a method which is well suited to the analysis of compounds like urea which decompose at and above their melting point and require derivatisation for analysis by GC. Quantitative analysis for HPLC is possible by using UV spectrometry, mass spectrometry or refractive index detection. Where determination is attained using conductivity methods (as can be the case for ammonium or nitrate ions associated with fertiliser impurity), then hydrolysis of the urea with urease is necessary prior to analysis[4]. Mass spectroscopy, which does not rely upon the molecule having a chromophore would seem to be the best of these techniques of analysis.

Several publications[5-14] have concerned the determination of urea and related compounds by (HPLC), mostly involving the separation of simple molecules (such as biuret, triuret and methylenediurea[14], or urea and substituted ureas[11]) on reversed phase columns with polar mobile phases such as water, methanol, and acetonitrile. The technique is well suited to the analysis of many molecules for which GC is not a viable option. A conventional ion exchange chromatographic column in preference to ion chromatographic or reverse phase columns has been identified to be perhaps the most suitable type of stationary phase for the analysis of urea[10]. This would seem to be the case, however, separation of urea, glycolic and aminoxyacetic acid amides (which are polar metabolites of 2-acetyl-3-phenyl-tetrahydro-1,2,4-oxadiazin-5-one) is not possible on octadecyl-, cyanolsilyl- or amino-phase columns, but it was shown that separation can be achieved on silica with C_3-C_4 alcohol and water mixtures as the eluent[12].

Problems with analysis in HPLC generally arise as a result of the poor separability innate to the technique. It is clear from the above examples that intelligent choice of a stationary phase can help to overcome this problem although successful quantitative analysis is still dependent upon the chemical and polar nature of the other analytes from which separation is necessary. Likely products of the reaction to carbonylate ammonia (in the presence of an alcohol as solvent), as discussed later in this thesis, include urea, ammonium formate, alkyl formate, ammonium carbamate, isocyanate, formaldehyde, formamide and N-alkyl and N,N-dialkyl formamides as well as possibly substituted ureas and substituted amines. It would be perhaps optimistic to expect to be able to separate a few of these compounds let alone a combination of

perhaps half a dozen or more. Separation of amines and amides by reversed phase HPLC can result in severe peak tailing, is notoriously troublesome, and requires the use of specific column phases for adequate retention analysis. This is due to the presence of surface silanol groups which remain on the stationary phase after the derivatisation procedure. Endcapping with trimethyl siloxane groups helps to eliminate surface silanol groups, but is never completely successful.

2.2.3 Analysis by HPLC/UV/Vis.

Analysis by HPLC with detection by UV/Vis was performed using a separate system. Unbuffered HPLC grade water obtained from Fisons was filtered through a 0.45 μm cellulose filter and degassed by sonic vibration on a sonic bath before use, and after every subsequent period of ca. 48 hours. The columns used were initially the Hichrom RP18-10-3545, and later also the Spherisorb S10 ODS 2, both of which had dimensions 4.6 x 250 mm, with an average particle size of 10 μm. The flow rate was 1.0 cm^3/min., and the pressure was never allowed to exceed 4000 psi. A UV/Visible PU-8700 Series spectrophotometer was used as the detector, and the wavelength of detection for urea was set at 200 nm.

2.2.4 Results of HPLC analysis

HPLC was attempted using various reversed phase columns and several mobile phase systems. Urea was always eluted with little or no peak tailing, however, when analysing actual post-catalytic samples, there appeared to be many analytes which absorbed very strongly at 200 nm that were eluted simultaneously. Separation of these would have been very time-consuming and so other methods of analysis were sought.

2.3 HPLC coupled with electrospray interface for liquid chromatography/mass spectrometry (LC/MS)

2.3.1 Introduction

Historically, using previously available ionisation techniques (e.g. particle beam, thermospray), LC/MS has gained a reputation of being a difficult technique to use. Upon the introduction of atmospheric pressure ionisation techniques (electrospray and atmospheric pressure chemical ionisation (APcI)), this reputation has been quashed by allowing the easy coupling of liquid chromatography systems to mass spectrometers without problems traditionally encountered (blockages, vacuum problems, sensitivity and reproducibility).

The coupling of HPLC with mass spectroscopy using an electrospray interface is a technique pioneered some 10 years ago by Fenn and co-workers[15-17]. in which the extraordinary potential of electrospray ionisation (ESI) was demonstrated. Their experiments were based upon work performed by Dole and co-workers who attempted to generate, *in vacuo*, beams of macromolecules, more properly macroions[18-22]. Their idea was to electrospray a dilute solution of polystyrene molecules into nitrogen gas at atmospheric pressure. Several electrospray interface designs exist, and all depend on the ability to form a microfine spray from a needle maintained at a high voltage potential[23-27]. How that spray is formed and how the solvent is stripped from the spray are two of the parameters by which the various interfaces are distinguished. One theory is that when the solvent evaporates from the charged droplets, the charge density on the surface increases until the Rayleigh limit is reached at which point the Coulomb repulsion forces exceed the surface tension and the droplet subdivides (also referred to as coulombic explosion). The droplet subdivides further and further as the solvent evaporates until a state is reached in which each droplet contains only one macromolecule, and after further evaporation, only the macromolecule would remain with at least some of the charge remaining. This dispersion of macroions in the bath gas could then be expanded through a small supersonic jet into a vacuum chamber. A schematic representation of the electrospray apparatus can be observed in figure 2.2.

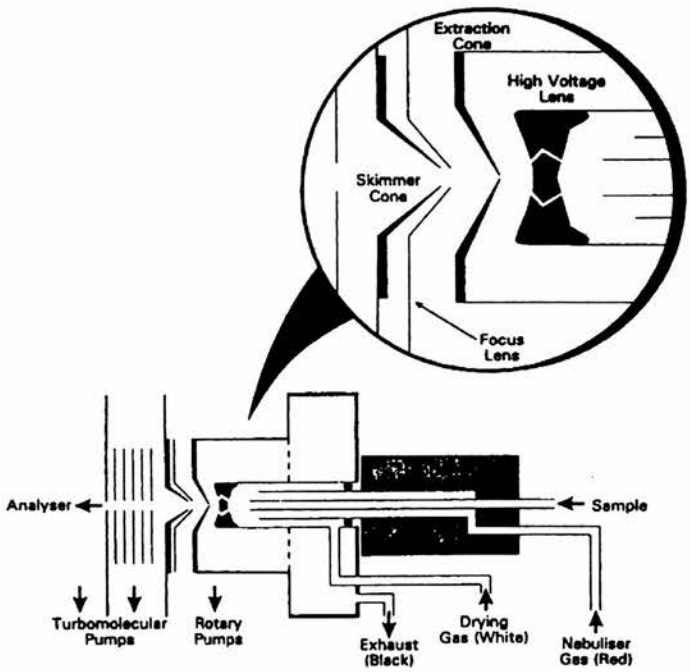

Figure 2.2 Schematic diagram of a coaxial high-flow pneumatically assisted electrospray source for VG Platform (Fisons, Biotech)

These early electrospray systems which relied upon a capillary at high voltage with no nebulizing gas could only tolerate very low flow rates (<5 μL min^{-1}). Upon the introduction of nitrogen as a nebulizing gas, higher flow rates could be accommodated (up to 40 μL min^{-1}). Recent advances resulting in the development of electrospray interfaces (megaflow) mean that flow rates up to 1.0 mL min^{-1} can be used even with a high aqueous content. Where possible, it is preferable to choose the dimensions of the LC column to facilitate analysis by electrospray ionisation at low flow rates. The main consideration for this is to decrease the need for excessive solvent use and very frequent source cleaning. Besides, in practice, it is generally found that the volume of sample entering the source is not an important consideration in limits of detection, rather, it is the actual concentration of sample which is most important. This is due to the greater efficiency of sample ionisation at lower flow rates.

2.3.2 Analysis by Liquid Chromatography/Mass Spectrometry

Chemicals

HPLC water and acetonitrile were obtained from Fisons Chemicals and were filtered through a 0.45μm nylon 66 membrane (obtained from Supelco). Degasification was attained by sonication for half an hour prior to use.

Liquid Chromatography/Mass Spectrometry

A JASCO model PU-980 intelligent HPLC pump was used to provide a flow of mobile phase. LC eluent conditions were always kept at 50:50 acetonitrile-water. The column was 250 mm by 1mm i.d., packed with 5-μm particles from Supelco with a proprietary functional group. A 2 μm nylon 66 filter frit was incorporated at the front of the column to guard against debris caused by pump or injection valve wear.

This LC system was connected to a VG platform ESP from Fisons (now Biomass) instruments (Manchester, UK.) equipped with microflow probe. A coaxial probe was employed. After separation by LC, the sample was introduced into the ESP source together with a nebulizing gas, which flows past the probe tip, producing an aerosol of sample, to maximise the efficiency of nebulization. A drying gas was added to ensure that sample which may have entered the gas line by capillary action was flushed out.

Data was processed using the Masslynx™ Mass Spectrometry Data System through Microsoft Windows installed in a Digital DEC PC 466.

Flow of mobile phase was varied between 10-20 μL/min, and it was not found that any decrease in sensitivity was noticed between the two rates.

Source cleaning procedure

If the source had not been cleaned for a period of several months, or if a significantly decreased ion current was apparent, then the source components were completely disassembled and cleaned as follows.

A 0.167 mm drill bit was pushed through the orifice in the centre of the sample cone to ensure that all particulate matter had been removed. The sample cone, skimmer, skimmer lens, blanking plug and counter electrode were cleaned with a swab wetted with concentrated formic acid which was also allowed to flow through any holes. Prior to reassembly, the sample cone, skimmer, skimmer lens, blanking plug and counter electrode were immersed in a 50:50 mixture of ethanol and water in a beaker and placed in an ultrasonic bath.

All repairs to joints were made by soldering, nylon gloves were always worn when handling source components as a precaution against contamination by fingerprinting which would have resulted in areas of unwanted charge during operation.

Sample Preparation

Aqueous solutions and aqueous acetonitrile solutions of urea, were prepared at various concentrations and filtered through 0.45μm frits to remove particulate matter prior to analysis.

A solution of poly(ethylene glycol) (PEG) in a 50:50 solution of CH_3CN - H_2O was filtered through a 0.45 μm filter prior to use. This solution was used as an ESP calibrant.

Table 2.1 Solvents suitable and unsuitable for electrospray atomisation[60]

Suitable	**Unsuitable**
Pyridine	Cyclohexane
Acetone	Hexane
Acetonitrile	Formamide
t-Butyl alcohol	Styrene
i-Propyl alcohol	Carbon disulphide
n-Propyl alcohol	Carbon tetrachloride
Ethanol	Ligroin
Water	Toluene
Methanol	Benzene
Tetrachloroethane	
1,2-Dichloroethane	
Dichloromethane	
Dimethyl Sulphoxide	
Dimethylformamide	
N-Methylformamide	
Hexamethylphosphorotriamide	
Chloroform	
Acetic acid	
Nitromethane	
Aniline	
Tetrahydrofuran	

The column employed for urea analysis (specified - 250mm by 1mm internal diameter) was an ABZ+Plus column, a speciality deactivated reversed phase column containing 5μm spherical silica particles, enabling the analysis of difficult compounds (acids, bases, zwitterions and very polar materials) with the use of simple mobile phases. This should reduce the significant peak tailing would results from the separation

of urea on an ordinary C-8 or C-18 column. Additionally, separation from carbamates and other likely products such as formamide should be attainable.

2.3.3 ESMS coupled with HPLC for the analysis of urea

ESMS parameters were optimised for the analysis of urea and are shown in Table 2. The main eluents of a trial run of a solution of authentic urea with concentration 1.78 mM in H_2O were analysed in the positive ion mode and were found at *m/z* 19, 42, and 61 corresponding to $[H_2O + H]^+$, $[CH_3CN + H]^+$, and $[CO(NH_2)_2 + H]^+$ with a 50:50 mixture of acetonitrile and water as the mobile phase. Some clusters of the type $[H(CH_3CN)(H_2O)_n]^+$ ($1<n<15$) were also observed as shown in the mass spectrum in figure 2.3. This particular spectrum was acquired in negative mode and so the clusters are of the type $[(OH)(CH_3CN)(H_2O)_n]^-$, however, similar patterns can also be observed in the positive mode.

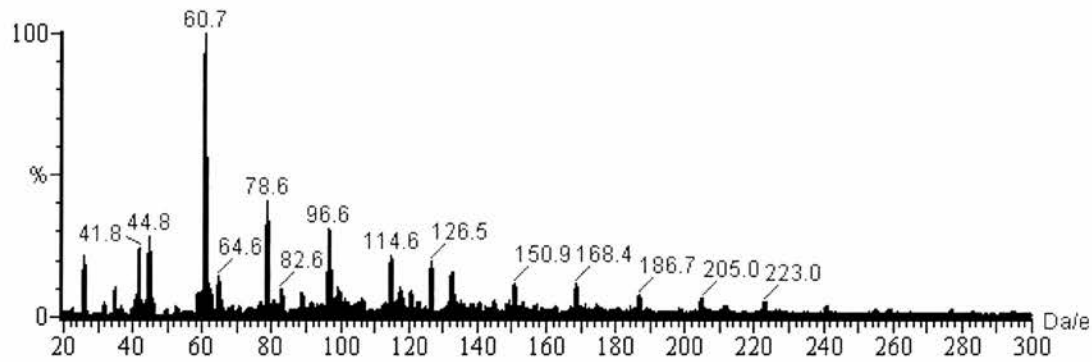

Figure 2.3 Observation of water clusters of the type $[(OH)(CH_3CN)(H_2O)_n]^-$

These species are well-documented[61-63] and clusters such as this have been the subject of elaborate publications; impressively, protonated clusters up to about m/z 1000 (n=55) have previously been identified[64].

Table 2.2 Optimisation of ESMS operating parameters used for analysis of urea

flow rate (μL/min)	20
drying gas flow rate (L/h)	300-330
ESP nebulizing gas flow (L/h)	12
ESP Capillary voltage (kV)	3.50
HV lens (kV)	0.40-0.50
Extraction voltage (V)	30-60
Focus voltage (V)	37-67
Source temperature (°C)	60-80
Low mass resolution (arbitrary)	12.5
High mass resolution (arbitrary)	12.5
Ion energy (V)	0.5-1.5

At a flow rate of 20 μL min^{-1}, urea is detected from the column during a period of 10-15 minutes after injection. Performing a mass chromatogram on the TIC (Total Ion Current) trace at a mass of 61.0 results in the observation of a chromatogram of compounds (in this case, only urea) eluted from the column in the mass range (60.5 - 61.5). The mass chromatogram and TIC can be observed in figure 2.4.

Extensive peak tailing is not observed, however, the total time of elution is long due in part to the low flow rate (20 μL min^{-1}) of mobile phase employed, and also, the volume of sample injected (10 μL) into the mobile phase. This is relatively large compared with the flow rate, and it takes 5 minutes for the sample to be discharged thoroughly from the column. Flow rates can be increased to compensate for the relatively high injection volume. Generally, it is acceptable to use flow rates up to 40 μL min^{-1} using a narrow bore column of 1 mm i.d.

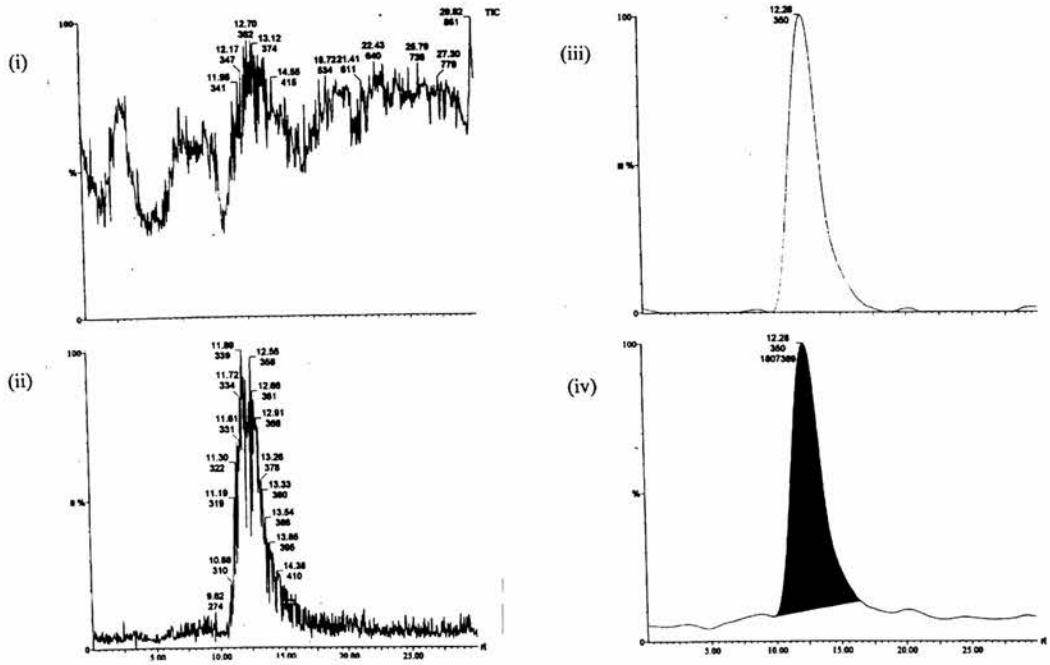

Figure 2.4 Elution of urea from HPLC column with MS detection (i) TIC trace (ii) Ion Current for m/z = 61 (iii) mass chromatogram for m/z = 61 (iv) integrated mass chromatogram for m/z = 61

It was found that the results obtained from experiments where the concentration of urea was varied were not suitable for quantitative analysis. This could be a result of small changes in pH from sample to sample. This is of primary importance when considering the analysis of urea from actual catalytic samples as a high pH associated with reactions performed in the presence of ammonia will suppress positive ion formation. Additionally, the same pH of solution would have to be used from sample to sample presenting not only problems of convenience, but also of practicality.

2.3.4 Analysis for actual reaction products by ESMS coupled with HPLC

ESMS analysis was performed upon neat filtered reaction solution. In the following example, urea was produced catalytically under actual experimental conditions described in section 3.2.6 and found (by ^{13}C NMR) to have a concentration of 0.11 M. Figure 2.5 shows the mass chromatograms obtained for this reaction solution which form the bulk of the total ion concentration (TIC) for masses of m/z = 74, m/z =

46 and m/z = 61 (protonated urea). The chromatograms have been obtained with a minor smoothing operation in order to show elution detail. The large contributions due to the presence of protonated formamide (m/z = 46) is to be expected, however, what is unexpected is the appreciable mass current observed at m/z = 74, corresponding to a species with atomic mass of 73. This species is thought to be N,N-dimethylformamide (by comparison with GCMS results).

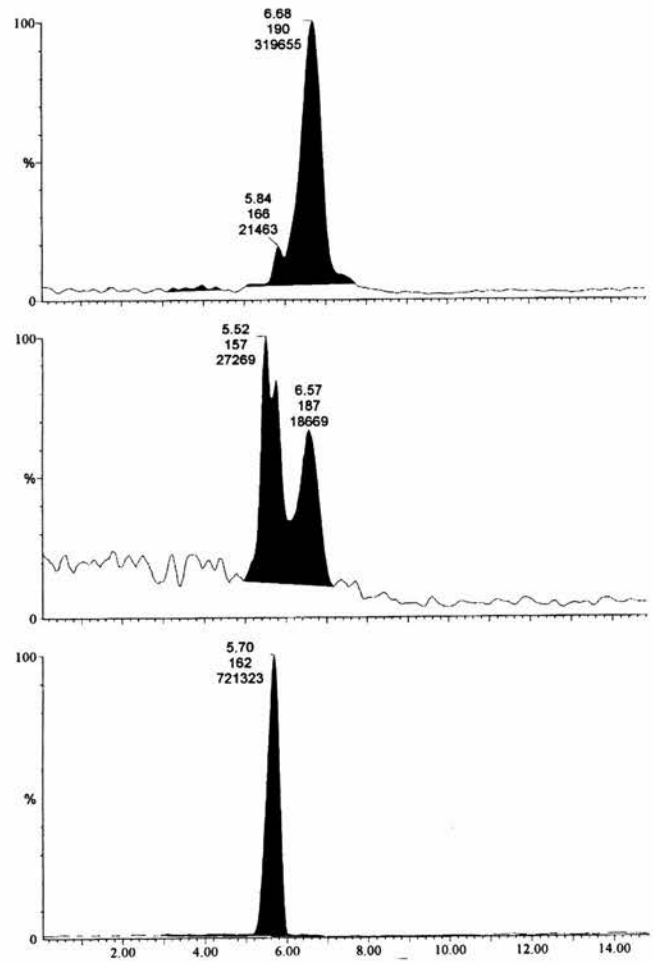

Figure 2.5 Elution of a genuine post-catalytic reaction sample from HPLC column. Top: m/z = 74; middle: m/z = 61; bottom: m/z = 46

2.4 Enzymatic Quantification of Urea[28-31]

The enzymatic estimation of urea involves determination of ammonia released by the action of urease on urea.

Urease (urea amidohydrolase, EC 3.5.1.5) is an example of a nickel metalloenzyme[32,33] and was first isolated from the bacterium *Micrococcus Urease* by Pasteur in 1876[34]. Andrews and co-workers have elaborated upon the nature of the interaction between urea and urease[35]. The hydrolytic conversion of urea to ammonia and CO_2 (via carbamic acid) is catalysed by urease (figure 2.6). Common methods of

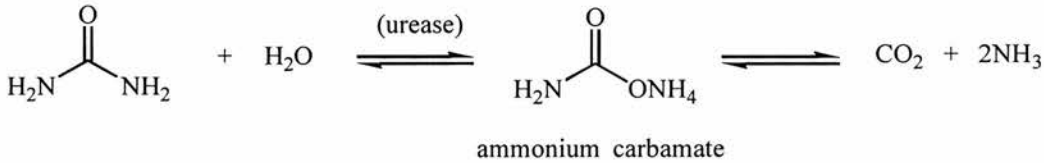

Figure 2.6 Hydrolytic action of urease on urea

determination of the ammonia evolved include the Bertholt reaction, methods coupled to other enzymes, and some dry chemistry techniques.

Specificity for urea is not complete as it also exhibits amido-hydrolysis towards semicarbazide, formamide, acetamide and N-hydroxyurea[35]. Interference from ammonia present in the solution from other sources is also an intrinsic problem.

2.4.1 Bertholt method

Bertholt discovered in 1859 that phenol reacts with ammonia in the presence of hypochlorite to produce a blue colour identified as a dissociated form of indophenol[36]. Nitroprusside catalyses this reaction under basic conditions and increases the colour intensity of the indophenol[37,38] (figure 2.7).

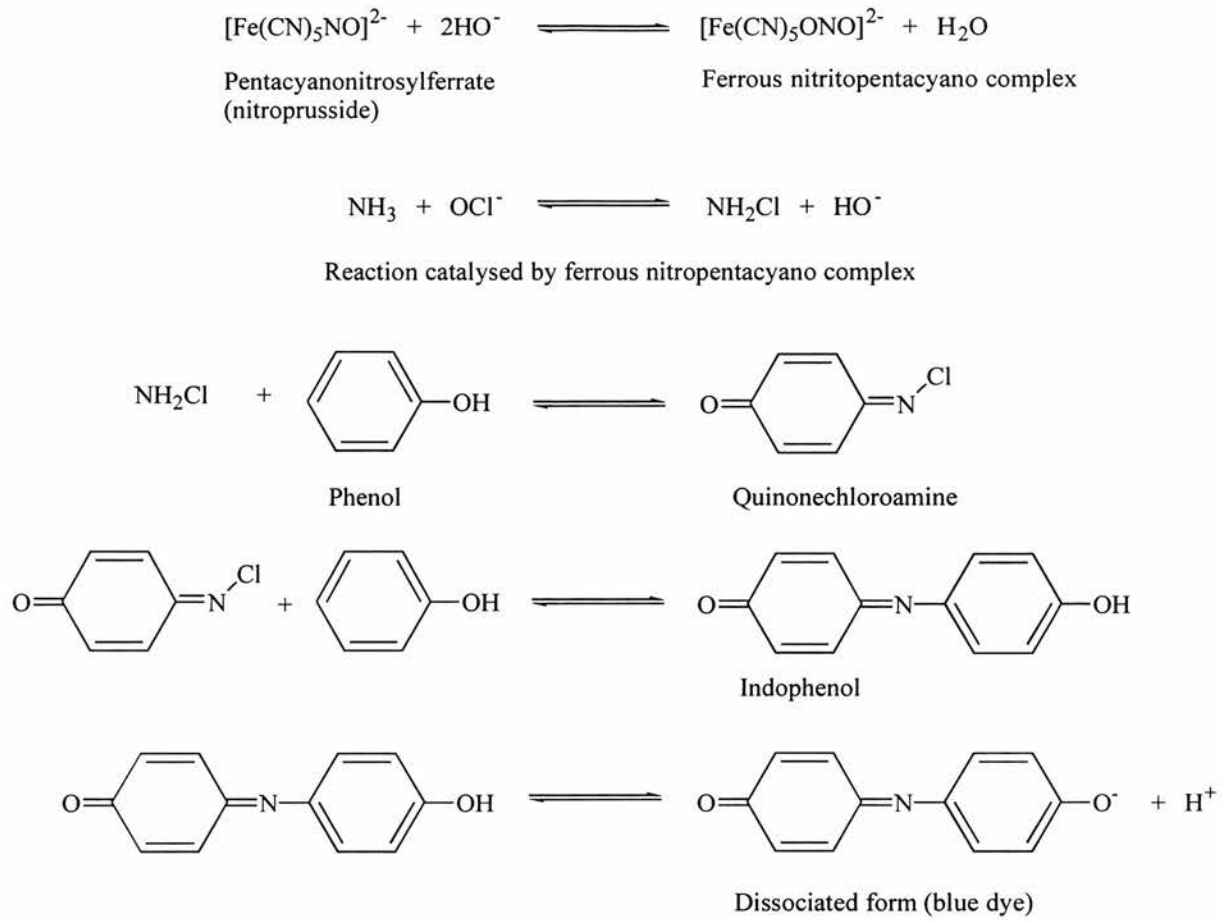

Figure 2.7 The Bertholt method for detection of ammonia produced after action of urease on urea

Phenol-nitroprusside solutions are stable under alkaline conditions for about 2 months[35] and colour development can be optimised at a temperature of 56°C. The colour is found to absorb increasingly in the region from 450 to 680 nm with a maximum absorption at 650 nm. Possible adaptations to the Bertholt reaction include using salicylate (which requires preparation in H_2SO_4 and HgO) instead of phenol. This results in the formation of a stable green coloured product. The salicylate method is favoured because the phenol reagent is less stable and more sensitive to deviations in pH[40,41].

2.5 Colorimetric Methods and Derivatisation

There are various colorimetric methods for the determination of urea[28-31], and of these, few are suitable because of instability or lack of sensitivity to low concentrations. However, the Fearon reaction of diacetyl monoxime[42] with urea is the most attractive of these (figure 2.8) . The mechanism of the reaction with urea under acidic conditions at elevated temperature (optimally 100-120°C) is highly complex and the result is the formation of an intensely coloured yellow product, (absorption peak 479 nm) proposed by some workers to be a carbonium ion[43]. The actual species which reacts to produce the chromogen is diacetyl (2,3 butanedione); diacetyl monoxime is used instead due to its greater stability.

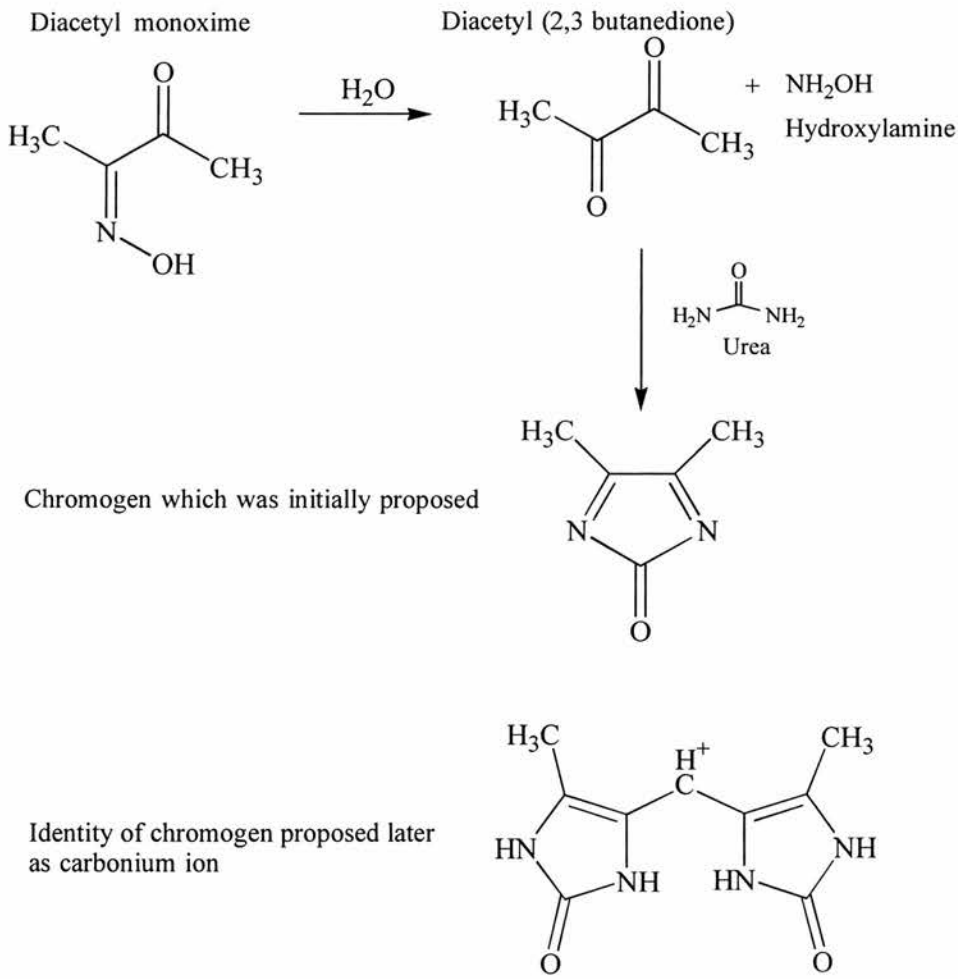

Figure 2.8. The proposed mechanisms of reaction of diacetyl monoxime with urea.

The hydroxylamine produced is thought to decrease the colour intensity of the chromogen[44], and is disposed of by reaction with oxidising agents such as strong acid[45] (e.g. a mixture of phosphoric acid with sulphuric acid). Diacetyl monoxime is stable for long periods in the dark and if kept refridgerated[29] which is why it is used in preference to diacetyl (2,3 butanedione[43]) which is less stable[46]. Potassium persulphate and ferric salts[30] have also been used as oxidising agents and ferric ions are thought to catalyse the reaction reducing the need to use such strongly acidic conditions. Analysers which employ the diacetyl monoxime method most often use thiosemicarbazide and ferric ions to intensify and stabilise the colour production, a method described by Marsh and co-workers[47].

Other carbamido compounds (e.g. citrulline and anatollin) as well as substituted ureas (many of which give a red colour[48] on reaction with diacetyl monoxime), amino acids and proteins are sensitive to this reaction, and so the specificity of this method may be in question[29,49]. There is no interference from ammonia, formamide or biuret, and the method can be automated. There are a few disadvantages to the method. The Beer-Lambert law is not obeyed, preparation of the complex must be carried out in a fume cupboard due to the noxious nature of the chemicals involved, and the intensity of the yellow product decreases as the chromogen decomposes over time after the reaction has been carried out. This means that if access to an automated analyser is not possible, then all samples must be analysed manually at roughly the same period of time after the reaction making quantitative analysis troublesome.

Diacetyl monoxime and the urease methods were applied in conjunction with each other in a report on the analysis of urea in sea water with accurate quantification and little interference from related compounds[50]. In a separate study[51], the reaction of benzoylacetyl monoxime[52,53] (see figure 2.9) to derivatise urea met with apparent good success in the quantification of urea in wine. Urea is thought to be responsible for the formation of ethyl carbamate (a carcinogen) by reaction with ethanol in wines[54] so it is important to maintain as low a urea concentration as possible in the wine manufacture. In this case, urea was isolated by ion exchange and then reacted with benzoylacetyl monoxime to yield a product with a chromophore which was analysed for absorbance at 540 nm.

Benzoylacetyl monoxime is closely related structurally to diacetyl monoxime, and the chromogen has a similar wavelength of absorbance, so they are probably of the same type. The product, however, is photosensitive and it has been shown to produce less colour with urea than diacetyl monoxime.

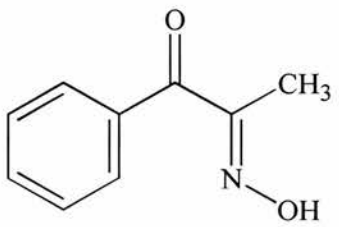

Figure 2.9 Benzoylacetyl monoxime

2.5.1 The determination of urea using diacetyl monoxime

Reagents Diacetyl monoxime (2.00g) was added to water (60 cm^3). Glacial acetic acid (2 cm^3) was added and the mixture was dissolved by gentle heating. The volume was made up to 100 cm^3 by addition of water. This solution was stored in the fridge after preparation between periods of usage.

Method To 100 μL of sample solution in a boiling tube 0.8 cm^3 diacetyl monoxime reagent, H_2SO_4 (3.2 cm^3) and water (4 cm^3) were added in succession. The boiling tube was placed in a boiling water bath for 30 min. Upon cooling, the observation of a yellow colour indicated the presence of the urea-diacetylmonoxime chromogen.

2.5.2 Reactions of sample solutions with diacetyl monoxime

Sample solutions reacted with diacetyl monoxime to produce a distinctive yellow colour, the absorbance peak of which corresponded exactly with that of the product from reaction with urea. It was found that colours faded rapidly after the colorimetric reaction (presumably due to decomposition of the resulting carbonium ion), making quantitative analysis of urea impractical, and only samples which were relatively strong in urea concentration kept their colour for periods of more than several days.

2.6 Analysis by nuclear magnetic resonance spectroscopy (NMR)

Urea only contains one carbon atom which is quaternary. Most quaternary carbon atoms are notorious for being slow to relax after excitation, and for especially weak samples signals may only be barely visible even after prolonged scanning. This problem can partially be overcome by prolonging the period between excitation and collection of emission data (the "relaxation delay") or by addition of a relaxation agent, normally a paramagnetic salt. ^{13}C nuclei can undergo relaxation through dipole-dipole interactions with unpaired electrons in spite of the distance between the orbit of the free electron and the ^{13}C nuclei. Chromium (III) triacetylacetonate is one such salt that can induce this transition, and dissolved oxygen as a result of its paramagnetism, can also produce the same effect.

Quantitative data can be obtained from ^{13}C NMR data by calibration with a foreign carbon-containing compound. Coupled with ^{13}C DEPT (distortionless enhancement by polarisation transfer)[55-59] analysis, ^{13}C NMR becomes a very powerful tool for the identification and quantification of urea (and other organic products) in reaction solutions.

2.6.1 ^{13}C NMR analysis

For long periods of scanning on a $^{13}C\{^{1}H\}$ nucleus, and for DEPT analysis, a Brucker 300 MHz NMR machine was used, and for shorter periods of scanning for proton and phosphorous nuclei, a Varian 300 MHz machine was employed. Unless described elsewhere, all samples for NMR were prepared in 5 mm tubes. A solution of 15.07 g (0.2509 mol) urea was dissolved in 250 cm^3 of distilled water. Different volumes of this solution were added to NMR tubes and made up to 500 μL with distilled water. D_2O (100 μL) was added as an NMR lock, and CH_3CN (50 μL) was added as internal standard. Each sample was scanned 400 times with a relaxation delay of 1.5 s. The intensity of the signal due to urea was divided by the intensity of the signal due to CH_3CN and expressed as an integral factor.

A typical group of spectra which could be obtained from such an experiment can be observed in figure 2.10.

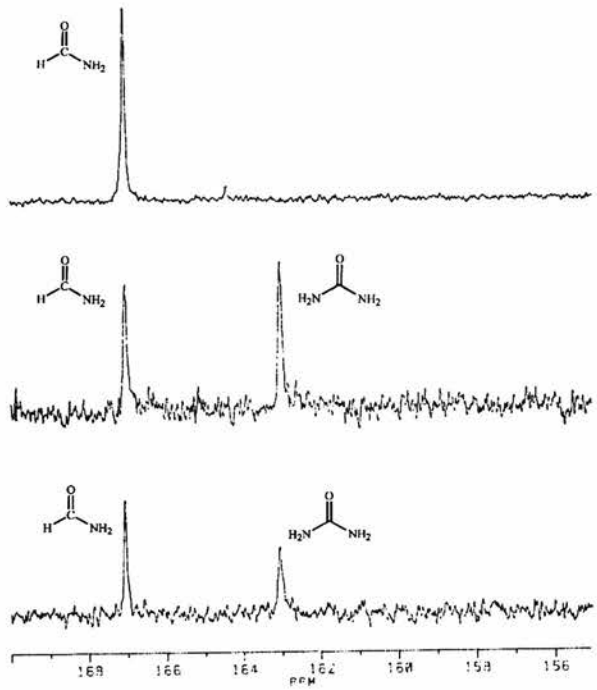

Figure 2.10 Typical spectra obtained after analysis of reduced sample (from top: ^{13}C DEPT spectra recorded over 25,000 scans, middle: ^{13}C NMR of sample spiked with authentic urea (exact overlap) after 432 scans, bottom: ^{13}C NMRof actual sample after 432 scans)

2.6.2 Quantification of urea by ^{13}C NMR

Data obtained showing the variation of integral factor with urea concentration can be observed in table 2.3. A plot of the integral factor versus concentration of urea gives a curve (figure 2.11) from which, if the integral factor for a sample is known, the urea concentration for that sample can be determined.

Table 2.3 Calibration data for the quantification of urea.

[a][$CO(NH_2)_2$]/ $moldm^{-3}$	Integral factor[b]	Number of scans[c]
1.0037	0.1322	400
0.9033	0.1296	400
0.8030	0.1019	400
0.7026	0.0922	400
0.6022	0.0819	400
0.5019	0.0457	400
0.4015	0.472	400
0.3011	0.0365	400
0.2007	0.0184	800
0.1004	0.0101	1200
0.0502	0.0599	30000

[a]Sample conditions: 500μL urea solution, 50 μL acetonitrile, 100μL D_2O lock.

[b]Intensity of signal observed for urea observed as a ratio of that observed for acetonitrile.

[c] Relaxation delay = 1.5 s. T = 25°C

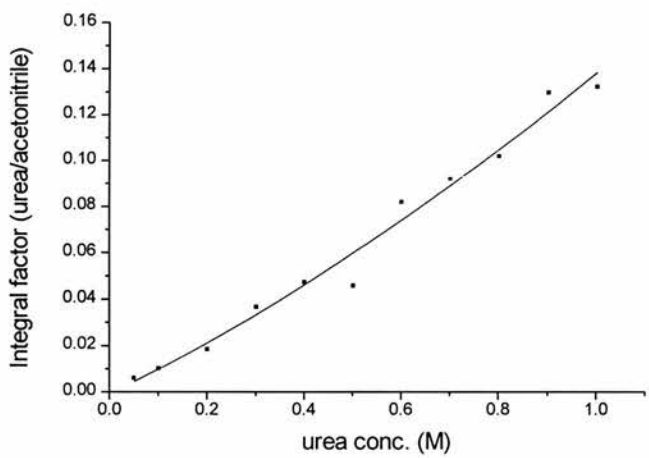

Figure 2.11 Variation of integral factor with concentration of urea

2.7 Conclusions

HPLC is not a technique well-suited to the analysis of urea in this case. Separation of compounds which are quite likely to be products in a reaction to carbonylate ammonia at elevated temperature and pressure would be extremely difficult, and (where UV/Vis absorption is the method of detection), the technique will be non-specific for urea. Detection by mass spectroscopy using an electrospray interface is also impractical due to the rigorous pH requirements of sample solutions.

Detection of urea by action of urease to release CO_2 and NH_3 and colorimetric reaction of NH_3 with a secondary reagent has obvious limitations. Firstly, the reaction solutions *contain* NH_3, and secondly, urease also produces NH_3 by action on formamide (a stoichiometric product of the reaction between CO and NH_3 at elevated temperature and pressure) both of which would produce incorrect analyses for urea content.

Good qualitative analysis for urea can be obtained by the reaction with diacetyl monoxime. Whilst the reaction is non-specific for urea, it is unlikely that other compounds in post-reaction mixtures other than substituted ureas (which would be detectable by GCMS) will interfere.

Quantitative data for urea analysis is available from ^{13}C NMR data using an internal calibrant (CH_3CN). Where the concentration of urea in a sample solution is unknown, the ^{13}C NMR can be acquired. The intensity of the signal due to urea can be compared with that of the calibrant and is expressed as a ratio. This ratio corresponds to a concentration of urea, the specific value of which can be read off a graph of integral factor versus urea concentration for authentic solutions of urea. The presence of urea can also be confirmed by spiking samples with authentic urea (exact overlap of signals), and by running ^{13}C DEPT analysis (complete suppression of urea signal).

2.8 References

1. Dickenman, R.C., Crafts, B.; Zak, B., *Am. J. Clin. Pathol.,* 1954, **24,** 981.
2. Timmermans, C.J., *Clin. Chim. Acta,* 1962, **7**, 887.
3. Beylot, M., France, D., Khalfallah, Y., Normand, S., Large, V., Brunengraber, H., *Biol. Mass Spec.,* 1994, **23,** 510.
4. Menconi, D.E., *Anal. Chem.,* **57,** 1985, 1790.
5. Tsuge, M., Senba, T., *Netsu Kokassei Jushi.,* 1981, **29,** 1132.
6. Grossenbacher, H., Cook, A.M., Hutter, R., *J. Chromatography,* 1985, **331,** 161.
7. Austin, E.R., Howard, R.G., Horn, R.C., *Anal. Chem.,* 1982, **54,** 1504.
8. Furukawa, M., Yokoyama, T., *J. Chromatography,* 1981, **208,** 424.
9. Qing Yang, Zen-Pei Sun, Da-Kui Ling, *J. Chromatography,* 1988, **447,** 208.
10. Shintani, H., *J. Liq. Chromatography,* 1994, **17,** 1737.
11. Kawase, J., Ueno, H., Nakae, A., Tsuji, K., *J. Chromatography,* 1982, **252,** 209.
12. Palfeledniczky, M.; Denes, G.; Ujszaszy, K. *Chromatographia,* 1987, **24,** 847.
13. Calleja, H., Courdy, C., Torres, L., *Analusis,* 1985, **13,** 166.
14. Muller, H., *Fresenius Zeit. analyt. chem.,* 1988, **332,** 464.
15. Yamashita, M., Fenn, J.B., *J. Phys. Chem.,* 1984, **88,** 4451; 1984, **88,** 4651.
16. Whitehouse, C.M., Dreyer, R.N., Yamashita, M., Fenn, J.B., *Anal. Chem.,* 1985, **57,** 675.
17. Wong, S.F., Menz, C.K., Fenn, J.B., *J. Phys. Chem,* 1988, **92,** 546.
18. Dole, M., Mack, L.L., Hines, R.L., Mobley, R.C., Ferguson, L.D., Alice, M.B., *J. Chem. Phys.,* 1968, **49,** 2240.
19. Mack, L.L., Kralik, P., Rheude, A., Dole, M., *J. Chem. Phys.,* 1970, **52,** 4977.
20. Clegg, G.A., Dole, M., *Biopolymers,* 1971, **10,** 821.
21. Teer, D., Dole, M., *J. Polymer Sci.,* 1975, **13,** 985.
22. Dole, M., Cox, H.L., Gieniec, J., *Adv. Chem. Ser.,* 1973, **125,** 73.
23. Bruins, A.D., Weidolf, L.O.G., Henion, J.D., *Anal. Chem.,* **59,** 1987, 2647.
24. Allen, M.A., Vestal, M.L., *J. Am. Soc., Mass Spectrom.,* **3,** 1992, 18.

25. Covey, T.R., Bonner, F.R., Shushan, B.I., Henion, J., *Rapid Comm. Mass Spectrom.,* **2,** 1988, 249.
26. Chowdbury, S.K., Katta, V., Chait, B.T., *Rapid Comm. Mass Spectrom.,* **4,** 1990, 81.
27. Smith, R.D., Loo, J.A., Edmonds, C.G., Barinaga, C.J., Udseth, H.R., *Anal. Chem.,* **62,** 882.
28. Butler, A.R., Walsh, D., *Trends Anal. Chem.,* 1982, **1,** 120.
29. Digiorgio, J. In. Henry, R.J., Cannon, D.C., Winkelman, J.W., (Eds.). "Clinical Chemistry: Principles and Techniques". Maryland: Harper and Row, 1974, 503.
30. Martinek, R.G., *J. Am. Med. Technol.,* **31,** 1969, 678.
31. Taylor, A.J., Vadgama, P., *Ann. Clin. Biochem.,* **29,** 1992, 245.
32. Dixon, N.E., Gazzola, C., Asher, C.J., Lee, D.S.W., Blakeley, R.L., Zerner, B., *Can. J. Biochem.,* **58,** 1980, 474.
33. Dixon, N.E., Gazzola, C., Watters, J.J., Blakeley, R.L., Zerner, B., *J. Am. Chem. Soc.,* **97,** 1975, 4130.
34. Pasteur, L., *Paris Acad. Sci. Compt. Rend.,* **83,** 1876, 10.
35. Andrews, R.K., Blakely, R.L., Zerner, B., *Adv. Inorg. Biochem.,* **6,** 1984, 245.
36. Berholt, M., *Rep. Chim. Appl., Soc. Chim. Paris,* **1,** 1859, 284.
37. Horn, D.B., Squire, C.R., *Clin. Chim. Acta,* **17,** 1967, 99.
38. Weichselbaum, T.E., Hagerty, J.C., Mark, H.B., *Anal. Chem.,* **41,** 848.
39. Varley, H., Gowelock, A.H., Bell, M., In: "Practical Clinical Biochemistry". 5th. Edn, Vol. 1: General topics and commoner tests. London: Heinemann, 1980, 451.
40. Gordon, S.A., Fleck, A., Bell, J., *Ann. Clin. Biochem.,* **15,** 1978, 270.
41. Searcy, R.L., Reardon, J., Foreman, J.A., *Am. J. Med. Technol.,* **33,** 1967, 15.
42. Fearon, W.R., *Biochem. J.,* 1939, **33,** 902.
43. Butler, A.R., Hussain, I., Leitch, E., *Clin. Chim. Acta,* 1981, **112,** 357.
44. Natelson, S., Scott, M.L., Beffa, C., *Am. J. Clin. Pathol.,* **21,** 1951, 63.
45. Kawerau, E., *Sci. Proc. Roy Dublin Soc.,* **42,** 1946, 63.
46. Friedman, H.S., *Anal. Chem.,* **25,** 1953, 662
47. Marsh, W.H., Fingerhut, B., Miller, H., *Clin. Chem.,* **11,** 1965, 624,
48. Ormsby, A.A., *J. Biol. Chem.,* **146,** 1942, 595.

49. McLaughlan, D.M. In. Gowenlock, A.H., McMurray, J.R., McLaughlan, D.M., (Eds.). "Varley's Practical Clinical Biochemistry", 6th. Edn. London: Heinemann, 1988, 350.
50. Price, N.M., Harrison, P.J., *Marine Biology,* 1987, **94,** 307.
51. Almy, J., Ough, C.S., *J. Agric. Food Chem.,* 1989, **37,** 968.
52. Dickenman, R.C., Crafts, B.; Zak, B., *Am. J. Clin. Pathol.,* 1954, **24,** 981.
53. Timmermans, C.J., *Clin. Chim. Acta,* 1962, **7**, 887.
54. Almy, J., Ough, C., *J. Agric. Food Chem.,* **37,** 1989, 968.
55. Bendall, M.R., Doddrell, D.M., Pegg, D.T., *J. Am. Chem. Soc.,* 1981, **103,** 4603.
56. Bendall, M.R., Doddrell, D.M., Pegg, D.T., *J. Magn. Reson.,* 1982, **48,** 302.
57. Schenker, K.V, von Philipsborn, W., *J. Magn. Reson.,* 1985, **61,** 294.
58. Pegg, D.T., Bendall, M.R., *J. Magn. Reson.,* 1984, **60,** 347.
59. Sorensen, O.W., *J. Magn. Reson.,* 1984, **57,** 506.
60. Hiraoka, K., Kudaka, I., *Rapid Comm. Mass Spec.,* 1990, **4,** 519.
61. Searcy, J.Q., Fenn, J.B., *J. Chem. Phys.,* 1974, **61,** 5282.
62. Yang, X., Castleman, A.W., *J. Am. Chem. Soc.,* 1989, **111,** 6845.
63. Wei, S., Shi, Z., Castleman, A.W., *J. Chem. Phys.,* 1991, **94,** 3268.
64. Chowdbury, S.K., Chait, B.T., *Anal. Chem.,* 1991, **63,** 1660.

CHAPTER 3

The carbonylation of ammonia to produce urea

3.1 Introduction

3.1.1 Oxidative addition as a possible method for ammonia activation

In chapter 1, work described by Taqui Khan and co-workers showing that the catalyst precursor $[Ru(EDTAH)Cl]^-$ is active for the production of urea from CO and ammonia under mild conditions of temperature and pressure was described. A mechanism involving oxidative addition of ammonia to the active species $[Ru(EDTAH)CO]^-$ was suggested as being the initial step in the reaction (figure 1.11, chapter 1). Referring back to section 1.4.1, we see that oxidative addition of ammonia across metal centres occurs only very rarely, and has only ever been actually observed for very electron-rich complexes of $Ir^{(I)}$, and to the zero-valent metal cluster $[Os_3(CO)_{12}]$. Reactions which probably involve σ-bond metathesis have been observed for transition metal complexes to the left of the periodic table. However, there is other evidence to suggest that a mechanism involving oxidative addition would be unlikely in this case. Firstly, the crystal structure[1] of the complex shows that the Ru-C bond of the carbonyl is long (1.843 Å), and the C-O bond is short (1.145 Å) as compared with other ruthenium (II) carbonyls[2,3]. This suggests that there is not a large electron density on the metal, and hence oxidative addition of ammonia seems highly unlikely. ν(CO) at 1940 cm^{-1} [4] does indicate a fairly high electron density, but not high enough to suggest oxidative addition of ammonia. In addition, oxidative addition would require deco-ordination of two further arms of the pentadentate EDTAH ligand. Deco-ordination of two arms of the HEDTA ligand is only entropically disfavoured if the two co-ordination sites thus formed are occupied by free ligands. The observation by ^1H NMR of oxidative addition of water to the complex to give metal hydrides[5] may suggest that such a reaction mechanism is possible, but, it is a far less rare phenomenon than for ammonia[6], and there are examples of it occurring for Pt[7,8], Rh[9,10] and Ir[11] to the right hand side of the periodic table, and also for metals to the left hand side of the periodic table[12-15]. In the case of $[Ru^{(II)}(EDTAH)CO]^-$, it almost certainly occurs by initial protonation, a reaction which is much less likely for ammonia because of its lower pKa (30 c.f. 14 for H_2O).

3.1.2 A possible alternative mechanism

Carbamoyl functional groups are extremely common both in organic and inorganic chemistry and are implicated in many catalytic and stoichiometric reactions. A brief review of such chemistry is described in section 1.4.2. Nucleophilic attack of ammonia on the coordinated CO group of an inorganic complex seems much more likely to occur than oxidative addition across its metal centre. This would generate the carbamoyl complex (I) as shown in the mechanism in figure 3.1. There is then a competition between two processes, either reductive elimination of formamide to give the starting complex or protonation on the oxygen atom (see section 1.4.1) of (I) to generate the carbene complex (II). As a result of protonation, the carbene complex should become quite electrophilic at carbon and susceptible to a second nucleophilic attack of ammonia generating the diamino(hydroxy)alkyl complex (III). β-hydrogen abstraction from this complex generates the hydride which can be protonated to form the dihydride which reductively eliminates hydrogen to complete the cycle.

Mechanistically, this alternative seems more plausible as only one site on the metal centre is required for reaction ensuring that the EDTAH remains pentadentate, and electronically, the mechanism does not include a ruthenium complex in the rather unusual +4 oxidation state either. Two steps in this mechanism are critical to potential catalysis to produce urea. The generation of the initial carbamoyl complex is essential, and subsequent protonation to yield the carbene complex is similarly crucial. Without protonation to give the carbene, it is unlikely that the carbon atom of the carbamoyl complex will be sufficiently electrophilic to be prone to any further nucleophilic attack by ammonia. Alternating steps involving nucleophilic attack and protonation place contradictory demands on different steps in the cycle, so the catalyst must have a delicate balance of electronic properties to prevent certain steps becoming too slow, or simply not occurring.

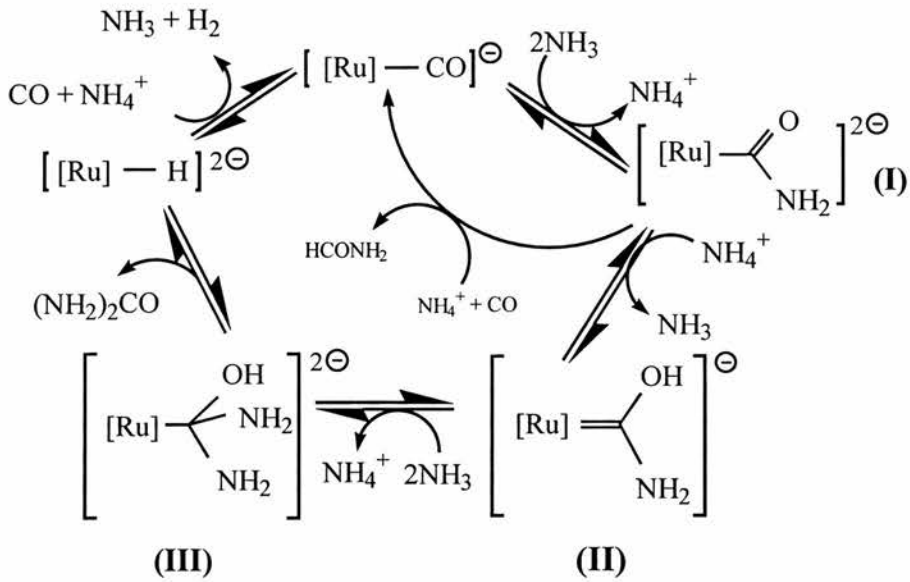

Figure 3.1 Mechanism of urea formation *via* a carbamoyl and a carbene complex

This is a possible simple mechanism which we propose may make metal carbonyl complexes in general active for the carbonylation of ammonia

3.1.3 The potential for WGSR catalysts active under basic conditions

Taqui Kahn and co-workers also claim water gas shift reaction activity for $[K(Ru^{(III)}(HEDTA)Cl).2H_2O]$, at 1 atm pressure, and 20°C[5] (very much milder conditions than for urea synthesis from aqueous ammonia). If the mechanism of nucleophilic attack described above is accurate, then it turns out, as we shall see later, that this mechanism is very similar to that of the WGSR catalysis by transition metal catalysts at elevated temperature and pressure in alkaline media. This led us to propose, therefore, that metal complexes which are precursors for the WGSR under basic conditions of pH[16] might also be active for the catalytic production of urea from CO and NH_3.

Cole-Hamilton and co-workers have also proposed a mechanism for the hydrogenation of carbon monoxide by iodide promoted ruthenium catalysts which involves successive attack of hydride and protons on coordinated CO[17] (figure 3.2). This mechanism also resembles that of figure 3.1, suggesting that catalysts for this reaction might also be suitable.

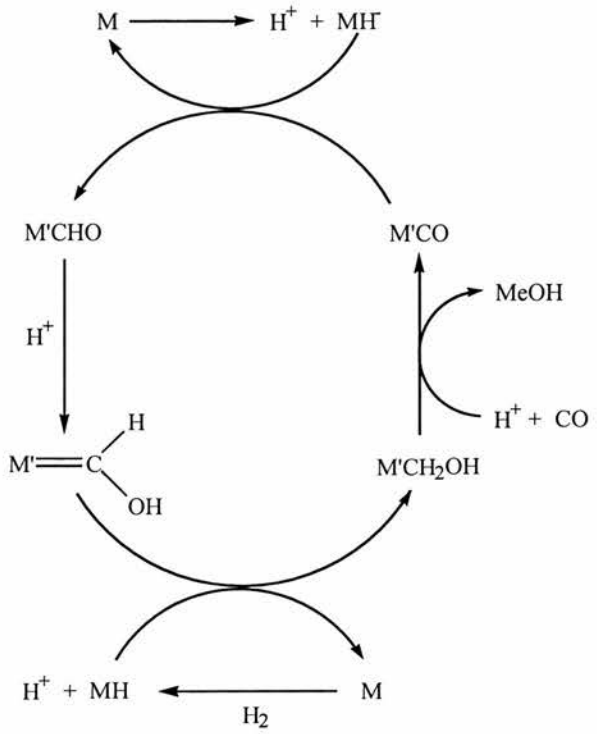

Figure 3.2 Hydrogenation of CO by complexes of ruthenium

3.1.3.1 The Water Gas Shift Reaction

The Water Gas Shift Reaction (WGSR) (figure 3.3) is commercially used for generation of pure H_2 for ammonia synthesis or for altering the H_2/CO ratio of synthesis gas for methanol manufacture. The WGSR is carried out with a heterogeneous catalyst at gas temperatures of 280-350°C using an iron-chromoxide catalyst[18]. For low temperature shift conversion, a copper oxide catalyst which requires sulphur-free feed gas is used. There has been much study of homogeneous systems with liquid water present with the aim of reducing the cost of production[19]. Although the reaction with liquid water is slightly endothermic, it is still highly favoured due to the large positive entropy change and negative change in free energy. It can thus potentially be carried out under much milder conditions of temperature and pressure.

$$CO_{(g)} + H_2O_{(g)} \rightleftharpoons CO_{2(g)} + H_{2(g)} \qquad \Delta H^\circ_{298} = -41.2\ kJmol^{-1}$$
$$\Delta G^\circ_{298} = -28.5\ kJmol^{-1}$$
$$\Delta S^\circ_{298} = -42.3\ Jmol^{-1}K^{-1}$$

$$CO_{(g)} + H_2O_{(l)} \rightleftharpoons CO_{2(g)} + H_{2(g)} \qquad \Delta H^\circ_{298} = +2.8\ kJmol^{-1}$$
$$\Delta G^\circ_{298} = -19.9\ kJmol^{-1}$$
$$\Delta S^\circ_{298} = +76.6\ Jmol^{-1}K^{-1}$$

Figure 3.3 Thermodynamics of the Water Gas Shift Reaction.

Modern studies of the WGSR are based on the work of Hieber and co-workers[20], who demonstrated that metal carbonyls are reduced by aqueous base to the corresponding anions or hydrides. Acidification of these solutions releases both CO_2 and H_2 by neutralisation of carbonate and subsequent reductive elimination of H_2 as shown in figure 3.4.

$$Fe(CO)_5 + 2OH^- \longrightarrow HFe(CO)_4^- + HCO_3^-$$
$$\downarrow H_2O,$$
$$Fe(CO)_4 + CO_2 + H_2$$

Figure 3.4 Mechanistic foundation of the WGSR under basic conditions

During the late seventies, increased interest in the homogeneous catalysis of the WGSR by complexes of ruthenium[21], rhodium[22,23], iron[24,25], and group 6 metal carbonyls[25,26] led to a reexamination of Reppe's observation that $Fe(CO)_5$ in the presence of base can catalyse this reaction[27]. These reports were the foundation of a proliferation of reports of the homogeneous catalysis of the WGSR during the eighties which were to highlight the very diverse range of metal complexes and conditions of pH under which the WGSR could be attained[16]. Research today is still concerned with the homogeneous WGSR, however, work is also focused on activities of metals and complexes absorbed onto surfaces, and their activities. As an example, it is known that gold deposition on

iron oxide surfaces enhances WGSR[28,29], and recently, gold deposited on TiO_2 was found to exhibit very high activities at low temperature for both the forward and reverse WGSR comparable with conventional catalysts[30].

The proposed mechanism of carbamoyl formation by the action of ammonia on coordinated CO is one feature which has parallels in most mechanisms for the WGSR conducted under alkaline conditions, and this similarity will become evident in the following section. Although there are examples of WGSR catalysts active under neutral, amine solutions, and acidic conditions[16], we shall concentrate on the WGSR under alkaline conditions because active species involved in these are likely to be closely related to those present during ammonia carbonylation. The mechanisms of reaction under alkaline conditions for these complexes all differ subtly, so using this strategy, not only do we screen these species for catalytic activity in the carbonylation of ammonia, but effectively, we also screen their mechanisms.

3.1.3.2 Iron pentacarbonyl

The homogeneous catalysis of the WGSR using basic solutions of $[Fe(CO)_5]$ was described by King and co-workers[24,25]. In the first of the two papers, it was shown that $[Fe(CO)_5]$ served as a catalyst for the WGSR in basic alcohol-water solutions. At a temperature of 161°C and with CO loading pressure of 14.6 bar; turnovers of nearly 20 mol H_2/mol $[Fe(CO)_5]$ /h were attained. The reaction was found to be zero order with respect to p_{CO}, and first order with respect to the base concentration. The attack of OH^- on $[Fe(CO)_5]$ was the rate determining step. Quantitative measurements have shown that a mechanism analogous to that in figure 3.5 is followed. This mechanism is typical of many but not all metal carbonyl WGSR catalysts and consists of four mains steps leading to the eventual closure of the cycle. (1) nucleophilic attack of ^-OH on coordinated CO; (2) decarboxylation by β-hydrogen abstraction; (3) protonation to give the dihydride; (4) reductive elimination of H_2 followed by carbonylation. Of these, it is normally step (1) or (3) which is rate-determining. High pressure *in situ* IR experiments showed that $[Fe(CO)_5]$ and $[HFe(CO)_4]^-$ were the only species present in solution during catalysis[31] and the observation of first order kinetics with respect to base concentration was attributed to the rate-limiting nucleophilic reaction of ^-OH on coordinated carbonyl.

In practice, the reaction solution is buffered by the stoichiometric production of formate from CO and ^{-}OH, and also by the presence of carbonate and bicarbonate. Increasing the pH to compensate for this proves futile as $[HFe(CO)_4]^-$ is too weak a base to be protonated under alkaline conditions, so the production of H_2 then becomes rate determining.

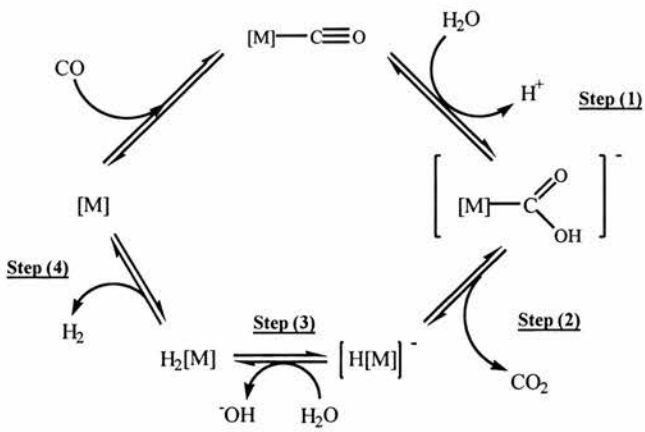

Figure 3.5 Water gas shift reaction mechanism common to most active metal carbonyls

3.1.3.3 Group 6 metal hexacarbonyls

Group 6 metal carbonyls $[M(CO)_6]$ have been shown to be catalyst precursors for the water gas shift reaction operating within a temperature range of 130 to 200°C in the presence of KOH and MeOH and at pressures ranging from ca. 7-40 bar[25,26]. It was shown that rates of WGSR catalysis were inversely proportional to p_{CO}. This observation suggests that a necessary first step in the mechanism is dissociation of CO to $[M(CO)_5]$ (figure 3.6). A likely second step was suggested to be co-ordination of formate ion (produced by the reaction of ^{-}OH with CO under alkaline conditions[32]).

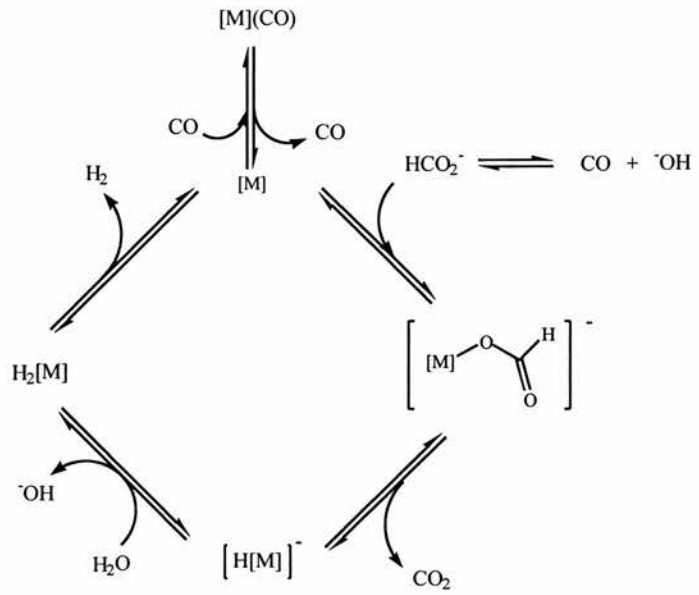

Figure 3.6 Likely mechanism of WGSR for $[M(CO)_6]$ (M = Cr, Mo, W.) by catalytic decomposition of formate ion. ([M] = $[M(CO)_5]$)

Co-ordination of formate to $[M(CO)_5]$ was confirmed as a possible step in the cycle by decarboxylating $[W(CO)_5(CO_2H)]^-$ by pyrolysis at 110°C[33]. Other steps in the cycle are very similar to those for the iron carbonyl system. The ammonia analogy to this mechanism would involve co-ordination of deprotonated formamide rather than formate to $[M(CO)_5]$ giving a metalloformamidate intermediate (see figure 3.7).

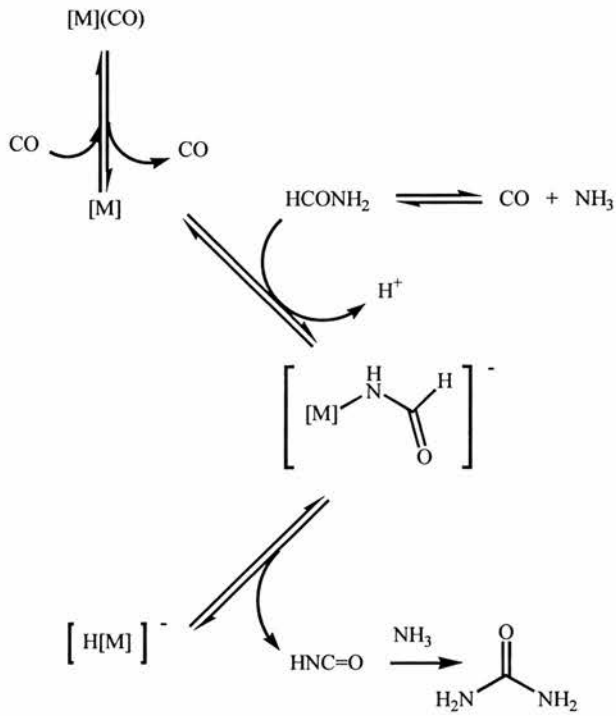

Figure 3.7 Activation of formamide by analogy with activation of formate for $[M(CO)_6]$

The much lower acidity of formamide compared to that of formic acid would explain the lack of activity of $[M(CO)_6]$ for urea production.

3.1.3.4 triruthenium dodecacarbonyl $[Ru_3(CO)_{12}]$

$[Ru_3(CO)_{12}]$ was the first WGSR catalyst described in the modern era of water gas shift catalysis[21] subsequent to the experiment performed by Hieber and co-workers on the iron carbonyl system in the 1950's[20]. The rates of turnover are very modest, however, the mechanism is different to those described above. First order kinetics are observed in both metal and p_{CO}. Although $[Ru_3(CO)_{12}]$ and $[H_4Ru_4(CO)_{12}]$ are found to have similar activities for the WGSR, and are known to exist in equilibrium with $[HRu_3(CO)_{11}]^-$ and $[H_3Ru_4(CO)_{12}]^-$, it was demonstrated that, by removing H_2 continuously with a palladium thimble, the equilibrium shown in figure 3.8 could be pushed to the right. Activity increased substantially suggesting that triruthenium

clusters (especially $[HRu_3(CO)_{11}]^-$) were largely responsible for catalysis[34]. This implies that $[H_3Ru_4(CO)_{12}]^-$ was playing only a minor role in the catalysis.

$$3[H_3Ru_4(CO)_{12}]^- + 9CO \rightleftharpoons 3[HRu_3(CO)_{11}]^- + Ru_3(CO)_{12} + 3H_2$$

Figure 3.8 Equilibrium of $[HRu_3(CO)_{11}]^-$ with $[H_3Ru_4(CO)_{12}]^-$ in the WGSR

Initial reports suggested that the mechanism shown in figure 3.5 may also be occurring in this case[35], however, the observation that p_{CO} is rate determining undermines this. $[Ru_3(CO)_{11}]$ is coordinately unsaturated, and reaction with CO would occur readily and would not be rate determining, so an alternative mechanism (see figure 3.9) must be considered. Although $[HRu_3(CO)_{11}]^-$ reacts with strong acid in the presence of CO to yield $[Ru_3(CO)_{12}]$[21], it is still a very weak base[36] and so protonation to give the dihydride under alkaline WGSR conditions is not likely to occur. An associative mechanism incorporating an electron-rich intermediate $[HRu_3(CO)_{12}]^-$ (resulting from the reaction of CO with $[HRu_3(CO)_{11}]^-$ (step (3))), which could function as a hydride transfer agent containing hydridic terminal hydrogen bound to either a metal[26,37,38] or a carbon atom of a formyl group[39] seems the most likely alternative (step (4)). Indeed, the reaction between $K[HRu_3(CO)_{11}]$ and CO at 1 bar in THF solution has been shown to produce KH and $[Ru_3(CO)_{12}]$[40].

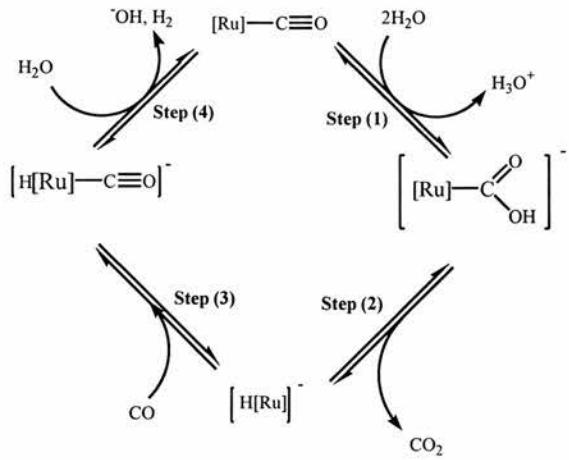

Figure 3.9 WGSR under basic conditions for $[Ru_3(CO)_{12}]$ ([Ru] = $Ru_3(CO)_{11}$)

3.1.3.5 Phosphine derivatised complexes of $[Ru_3(CO)_{12}]$

Phosphine-substituted clusters $[Ru_3(CO)_{10}(DPPE)]$ (DPPE = $Ph_2PCH_2CH_2PPh_2$) and $[Ru_3(CO)_8(DPPM)_2]$ (DPPM = $Ph_2PCH_2PPh_2$) were tested for WGSR activity and compared with $[Ru_3(CO)_{12}]$[34]. Inclusion of electron-donating ligands in the molecule should produce a more electron-rich intermediate upon reaction with CO in step (3) of the cycle in figure 3.9 which in turn reacts more rapidly with H_2O (step (4)) to give H_2 by protonation of the metal complex. Whilst this was shown to be the case for the mono-anions (see figure 3.10), only $[Ru_3(CO)_{10}(DPPE)]$ was shown to be more active overall than $[Ru_3(CO)_{12}]$ as a WGSR precursor and $[Ru_3(CO)_8(DPPM)_2]$ was found to be inactive. This was explained in terms of the extra electron density that DPPM donates being incorporated in the back-bonding from the metal to the remaining carbonyls decreasing their electrophilicity at carbon and rendering them less susceptible to nucleophilic attack by ^-OH. In this case, the back-bonding is so great that formation of the intermediate metallocarboxylic acid is not observed at all.

$$K[HRu_3(CO)_7(DPPM)_2] + CO + H_2O \longrightarrow [Ru_3(CO)_8(DPPM)_2] + H_2 + KOH \quad .....1$$

$$K[HRu_3(CO)_9(DPPE)] + CO + H_2O \longrightarrow [Ru_3(CO)_{10}(DPPE)] + H_2 + KOH \quad .....2$$

$$[HRu_3(CO)_{11}]^- + CO + H_2O \longrightarrow [Ru_3(CO)_{12}] + H_2 + KOH \quad .....3$$

Reactions 1 and 2 are found to occur at increased rates relative to 3

Figure 3.10 Protonation of diphosphino substituted tri ruthenium cluster anions

3.1.3.6 Alkyl phoshine complexes of rhodium (I)

Very elaborate work performed by Yoshida and co-workers showed that complexes of the type $[HRh(PR_3)_3]$ (R = Et, ^iPr, $(c\text{-}C_6H_{11})$) are active for the WGSR under conditions of neutral or slightly alkaline pH[9,10]. The systems were found to be catalytic under relatively mild conditions of temperature and work best in a co-ordinating solvent such as pyridine, an observation pertinent to the overall mechanism.

By careful isolation of reaction intermediates, oxidative addition of water was proven to be the first step of the mechanism to generate ·OH and coordinated hydride. The remainder of the catalytic cycle was found to be quite complicated and consists of several intricate steps, however, the general reactions important to elucidation of the WGSR can be observed in figure 3.11 which shows a simplified mechanism for the WGSR with $[HRh(P^iPr_3)_3]$ as precursor.

This is interesting from a mechanistic point of view. These are some of the few WGSR catalysts for which it is known that oxidative addition of water occurs readily at room temperature. It may then be possible that oxidative addition of NH_3 can occur, if not readily at room temperature, then under conditions of raised temperature and increased vapour pressure of NH_3. Observation of this would be unprecedented for a rhodium complex and would present us with a possible catalytic route to urea by analogy with the WGSR mechanism (e.g. see figure 1.28, chapter 1).

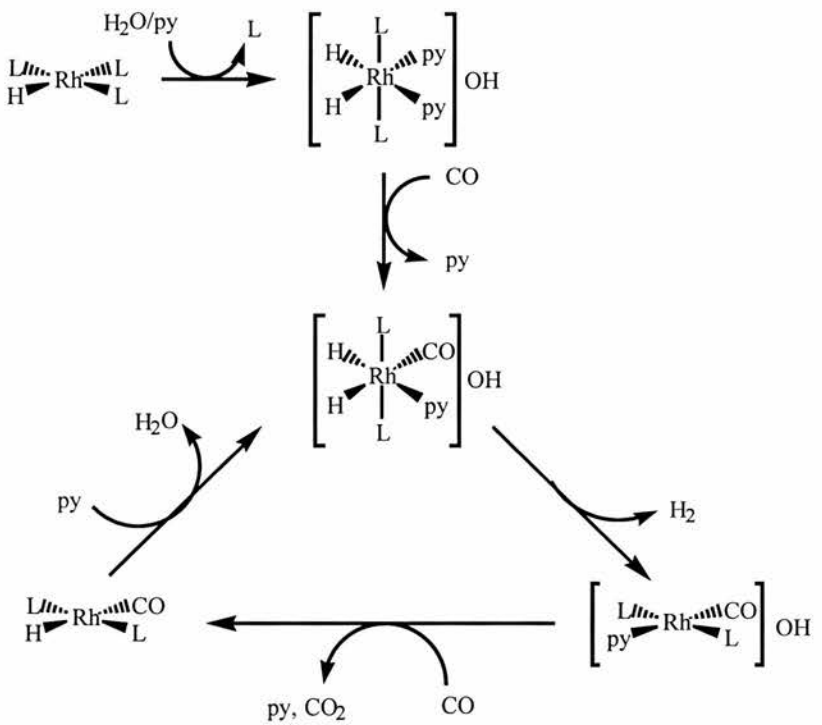

Figure 3.11 Simplified mechanism for WGSR catalysed by $[HRh(PR)_3]$. (L = R = P^iPr_3)[10].

3.2 Results and discussion

3.2.1 Reactions employing $K[Ru^{(III)}(EDTAH)Cl].2H_2O$ as catalyst precursor

The reaction between carbon monoxide, ammonia and the prepared ruthenium HEDTA complex $K[Ru(EDTAH)Cl].2H_2O$ at various concentrations of ammonia and catalyst complex was studied in aqueous solution at a loading pressure 30 bar CO and at a temperature of 80°C.

Three different sources of $K[Ru(EDTAH)Cl].2H_2O$ were used in these reactions, one prepared according to the below procedure (DCDB), another prepared according to the below procedure by a different internal worker (SM129), and a sample provided to us by Johnson Matthey plc, (JM 1266, Batch GRH/CO92/56).

Table 3.1 shows results obtained for this precursor under a variety of conditions of ammonia concentration.

Table 3.1 Results of reactions employing $K[Ru(EDTAH)Cl].2H_2O$ as catalyst precursor

Precursor[a]	T/°C	P_{CO}/bar	[catalyst] /mol $dm^{-3}.10^3$	$[NH_3]$ /mol dm^{-3}	time/h	products[b]
[1]	80	30	1.3	0.5	24	ammonium formate
[1]	80	30	2.3	0.5	20	ammonium formate, formamide
[1]	80	30	1.1	0.1	18	ammonium formate
[1]	80	30	1.5	0.11	5	ammonium formate
[JM]	80	30	1.7	1.1	5	ammonium formate
[2]	80	30	5.4	1.1	4	ammonium formate

[a] [1] = batch DCDB. JM = (JM 1266, Batch GRH/CO92/56), [2] = internal batch, SM129.

[b] Identified by ^{13}C NMR

Neither reaction of sample solutions with diacetyl monoxime, nor ^{13}C NMR experiments indicated the presence of any urea, but signals were observed which could be been attributed to ammonium formate (see figure 3.12), and formamide by virtue

both of their relative chemical shifts, and also by virtue of their ^{13}C DEPT 135 spectra. It is observed that ammonium formate is produced in a stoichiometric reaction between NH_3 and CO in aqueous solution in the absence of catalyst.

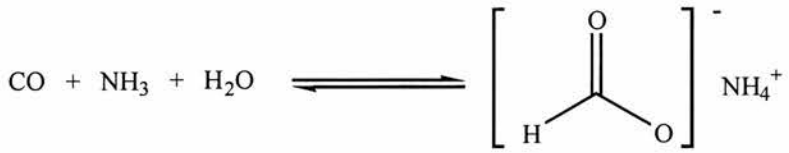

Figure 3.12 Stoichiometric formate production under basic conditions.

Taqui Khan and co-workers report yields of up to 16 mol urea/mol catalyst/hour, a turnover which is apparently independent of a wide range of working conditions stipulated both in the patent[41] and in the paper describing the carbonylation of ammonia[42]. Applying this theoretical yield to the scale we have been working, the final concentration of urea would be ca. 0.05 mol dm^{-3} (3 g dm^{-3}) which is certainly not beyond the range of detection by ^{13}C NMR. Upon concentration to a small volume, urea should appear as a prominent peak in the ^{13}C NMR of the mixture, however, this was not the case. It is usual to observe ammonium formate and formamide when the sample solution has been concentrated. Additionally, confirmation that the postulated catalytic species $[Ru^{(III)}(HEDTA)(CO)]^-$ is being produced *in situ* comes from ^{13}C NMR analysis of the concentrated sample (see figure 3.13).

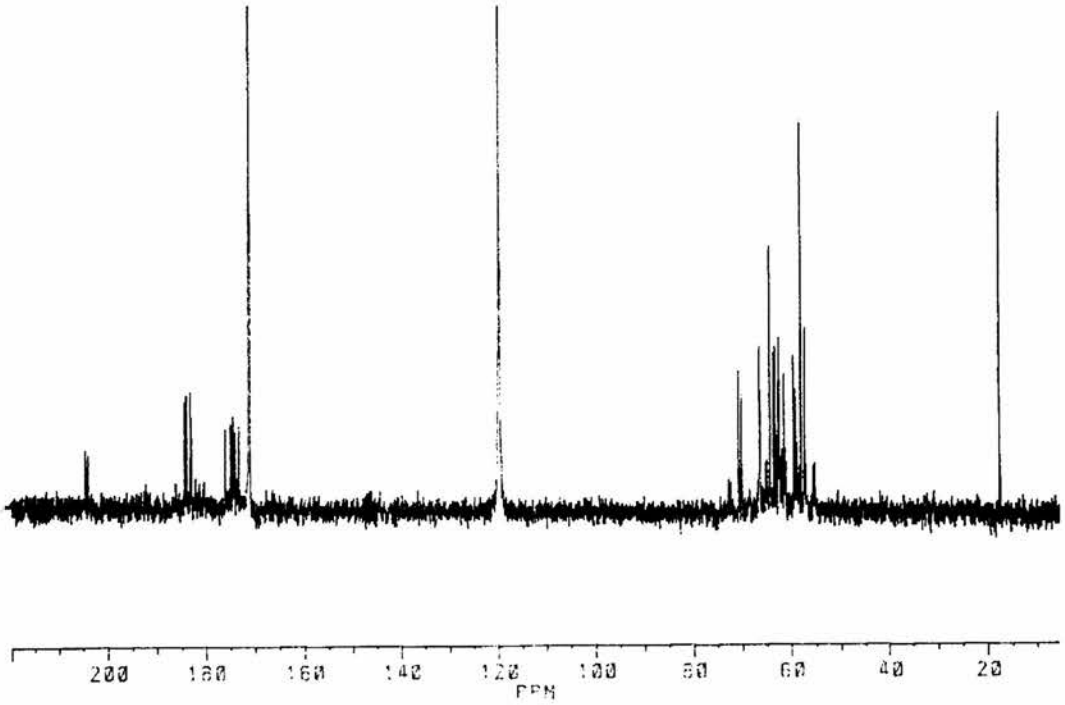

Figure 3.13 ^{13}C NMR of $[Ru^{(II)}(HEDTA)(CO)]^-$ produced from a catalytic reaction involving $[Ru^{(III)}(HEDTA)Cl]^-$.

Observation of permanent gases by GC reveals a turnover to H_2 corresponding to 0.5 mol per mol catalyst, a result which is independent of the duration of the experiment. It is unclear why this arises, but it may be as a result of WGSR activity in the aqueous solution.

Although it is hard to tell whether the production of formamide is catalytic (yields of formamide by the reaction of NH_3 and CO in the absence of catalyst are similar to yields in the presence of catalyst), its presence may indicate that the first step of nucleophilic attack of ammonia on the CO group of the complex postulated in the mechanism described in figure 3.1 may be occurring to give the carbamoyl complex (species (I) in figure 3.14). Protonation on the metal, followed by β-hydrogen abstraction then gives formamide, and regeneration of the starting catalytic species under CO pressure.

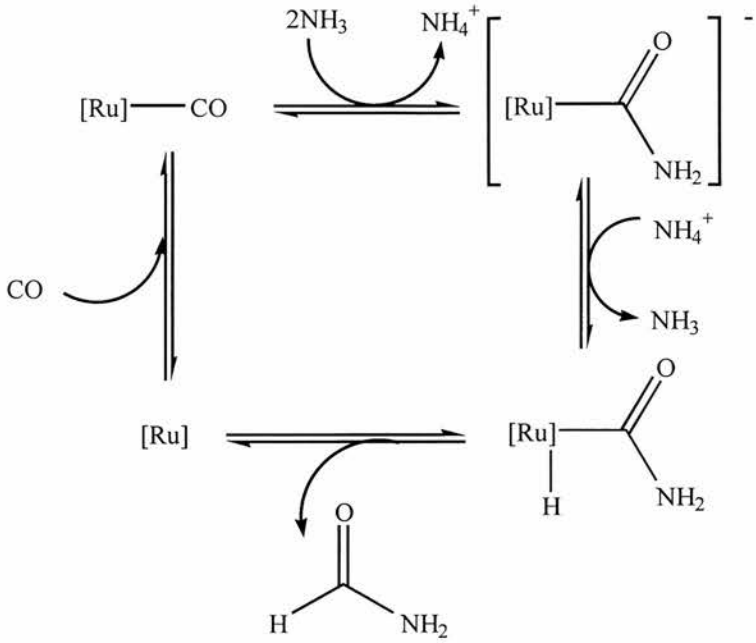

Figure 3.14 Possible mechanism for formamide production

This mechanism would perhaps indicate that the metal centre is too electron rich to allow the preferential protonation on the amide ligand. The metal centre must be electron deficient so as to enhance the electrophilic nature of the CO group and make it susceptible to nucleophilic attack by ammonia. It has been shown that $[RhH(PEt_3)_3]$ is readily protonated on the metal by weak acids such as water or ethanol, whilst $[Rh(COMe)(CO)_2(PEt_3)_2]$ protonates on the acyl oxygen atom oxygen atom using similarly weak acids[43]. It may be that the complex is not well enough balanced electronically to make it useful for urea production.

3.2.2 Reactions employing $K[Ru^{(II)}(EDTAH)CO].2H_2O$ as catalyst precursor

Given the apparent lack of success using $K[Ru^{(III)}(EDTAH)Cl].2H_2O$ as catalyst precursor, the actual proposed active carbonyl species was tried instead. Again, under the conditions described above, no urea was produced, only ammonium formate and formamide (seen by ^{13}C NMR after concentration).

3.2.3 Reactions with $[Fe(CO)_5]$ as catalyst precursor

Table 3.2 shows a summary of the various reaction conditions employed with $[Fe(CO)_5]$ as catalyst precursor. Given the WGSR activity for this species under alkaline conditions[24,25], reactions were performed using methanol as solvent. In all cases, formamide was observed as the major product of the reaction.

Table 3.2 Results of reactions employing $[Fe(CO)_5]$ as catalyst precursor

T/°C	P_{CO}/bar	$[Fe(CO)_5]$/ mol $dm^{-3}.10^3$	$[NH_3]$/ mol dm^{-3}	time/ h	products
120	20	4.8	5.7	20	formamide
140	20	4.8	5.7	20	formamide
160	10	4.8	6.1	6	formamide
160	20	4.8	6.1	6	formamide

Urea was not observed as a product in any of these reactions, even once the sample solutions had been evaporated to small volumes for the aquisition of ^{13}C NMR.

3.2.4 Reactions employing $[M(CO)_6]$ as catalyst precursor

The group 6 metal carbonyls are very efficient WGSR catalyst precursors under conditions of aqueous base[25,26]. The rate of the WGSR has been found to be inversely proportional to the CO pressure, an observation which suggests that loss of CO to give an active intermediate $[M(CO)_5]$ is an important pre-requisite for its activity. Several reactions were performed in the absence of H_2O under low pressures of CO (see table 3.3). Again, no urea was observed under the conditions studied. At these low pressures, loss of CO should be facile, however, assuming that the active species $[M(CO)_5]$ *is* formed under these conditions followed by nucleophilic attack of ammonia on coordinated CO, in analogy to the WGSR, then protonation is occurring on the metal in preference to the resulting carbamoyl complex. β-hydrogen abstraction from this complex then gives formamide as for $[Ru(HEDTA)(CO)]^-$.

Table 3.3 Results of reactions employing group (VI) metal carbonyls as catalyst precursor

catalyst precursor	T/°C	P_{CO}/bar	$[M(CO)_6]$/ mol $dm^{-3}.10^3$	$[NH_3]$/ mol dm^{-3}	time/ h	products
$W(CO)_6$	140	5	6.2	4.4	4	formamide
$W(CO)_6$	160	5	6.2	4.4	4	formamide
$Cr(CO)_6$	140	5	12.0	4.4	4	formamide
$Cr(CO)_6$	160	5	12.0	4.4	4	formamide

3.2.5 Reactions using alkyl phosphine complexes of rhodium (I)

The activity of $[RhH(PEt_3)_3]$ for ammonia carbonylation was tested under various conditions of temperature and pressure, and also with varying solvent systems (see table 3.4).

It was usual to observe the WGSR occurring under the reaction conditions which resulted in the production of ammonium carbonate and ammonium bicarbonate as the primary products of the reaction. Ammonium bicarbonate was isolated from one reaction (found: C 15.77, N 17.81, H 6.30 %. CH_5NO_3 requires C 15.19, N 17.77, H 6.33 %) as crystals on the inside of the glass liner of the autoclave. No urea was obtained from these reactions.

Reactions conducted under dry conditions using methanol as a solvent for ammonia resulted in the suppression of carbonate products of the reaction, however, the yield of formamide was not increased, and urea was still not observed. This would indicate that the oxidative addition step crucial to the function of $[RhH(PEt_3)_3]$ as a WGSR catalyst is not occurring for ammonia.

Table 3.4 Results of reactions employing $[RhH(PEt_3)_3]$ as catalyst precursor

T/°C	P_{CO}/ bar	$[RhH(PEt_3)_3]$/ mol $dm^{-3}.10^3$	$[NH_3]$/ mol dm^{-3}	time/h	products
100	20	16.0	3.3[a]	18	carbonates
100	40	16.0	2.0[a]	18	carbonates, ammonium formate
120	40	4.7	2.0[b]	18	carbonates, ammonium formate
120	40	4.7	2.0[b]	18	carbonates, ammonium formate
120	40	4.7	7.5[b]	18	carbonates, ammonium formate
80	40	4.7	7.5[b]	18	carbonates, ammonium formate, formamide,
120	40	9.4	0.2[b]	18	formamide, carbonates
50	40	9.4	2.0[b]	18	formamide, carbonates
80	40	9.4	7.5[b]	18	carbonates[c], ammonium formate, methyl formate

[a]Prepared as a solution of 2 parts $NH_{3(aq)}$, 1 part pyridine

[b]Prepared as a solution of 2 parts $NH_{3(aq)}$. 3 parts methanol

[c]ammonium carbonate isolated and identified by CHN and ^{13}C NMR

3.2.6 Production of urea catalysed by $[Ru_3(CO)_{12}]$

3.2.6.1 Initial results

As was the case for $[Fe(CO)_5]$ and $[M(CO)_6]$, reactions were performed in dry solvent-ammonia systems in order to study the behaviour of $[Ru_3(CO)_{12}]$ independently of the WGSR. Various conditions of pressure (2-50 bar) temperature (120-170°C) were employed in initial reactions, and the solvent system employed was methanol.

Table 3.5 shows results obtained during initial studies of $[Ru_3(CO)_{12}]$ as a catalyst for the carbonylation of ammonia to urea. Urea was identified as a product of

Table 3.5 Initial results obtained for urea catalysis by $[Ru_3(CO)_{12}]$ under a variety of conditions of temperature, pressure, time and ammonia concentrations with methanol as solvent.

$[Ru_3(CO)_{12}]$ (mM)	P(bar) (CO)	T(°C)	$[NH_3]$/M CH_3OH	time/h	Turnover h^{-1}	total	Diacetyl Monoxime
0	20	160	16.8	4	0	0	negative
2.99	50	160	16.8	24	0.57	13.7	positive
2.3	50	120	16.8	24	0	0	negative
4.01	10	160	16.8	4.5	1.6	7.2	positive
7.18	20	160	7.4	4	0	0	positive
4.59	20	160	7.2	4	2.5	10.0	-
4.59	20	150	7.2	4	3.2	12.8	-
4.27	20	140	7.4	18	1.5	27.0	positive
6.5	20	130	7.4	18	0.6	10.8	positive
4.54	15	160	7.2	4	6.2	24.9	-
3.85	10	160	7.4	24	1.16	27.8	positive
5.01	10	160	7.4	4	6.9	27.6	positive
5.2	20	170	6	18	0.5	9.0	positive
4.47	20	160	6	18	0	0	-
2.6	20	160	5.7	4.5	2.7	12.2	positive
4.45	20	150	6	18	0.8	14.4	positive
2.67	2	160	6	4	2.2	8.8	positive
11.7	16	160	4.6	3	2.2	6.6	positive

the reaction under most conditions tested. ^{13}C NMR together with ^{13}C DEPT measurements (complete suppression of urea), and spiking with authentic urea (exact overlap in the spectrum) (see figure 3.15) suggested that urea was a genuine product of the reaction. Confirmation of this came from reaction with diacetyl monoxime resulting

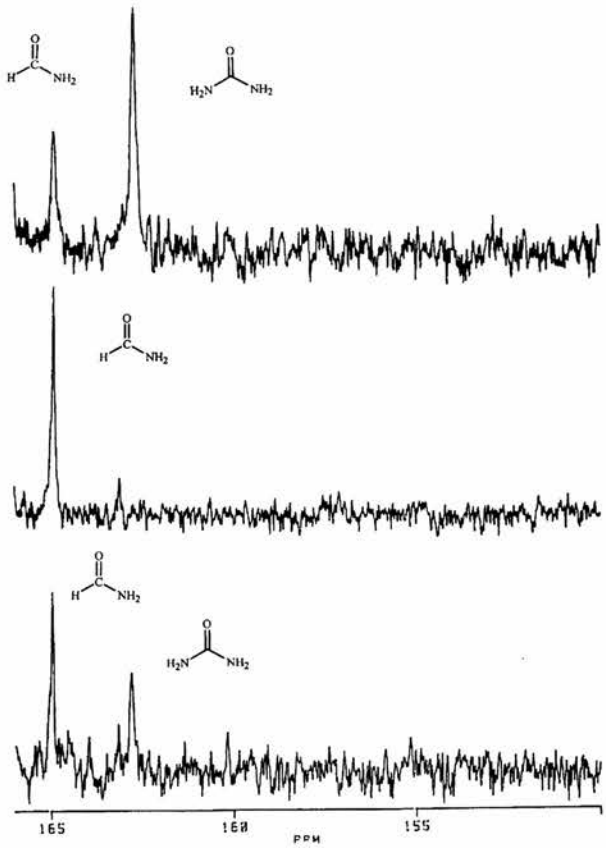

Figure 3.15 Typical ^{13}C NMR spectra obtained for a reduced sample of post-catalytic reaction solution (from top: sample spiked with authentic urea, middle: DEPT of sample, bottom: normal spectrum of reduced sample)

in the production of an intense yellow colour characteristic of urea. Table 3.5 is arranged into four blocks in order of ammonia concentration. The first point to note is that the concentration of ammonia in the reaction solution appears to be critical. Although not shown in this table, other results were obtained for much lower concentrations of ammonia where the urea obtained is undetectable by ^{13}C NMR. The reaction with diacetyl monoxime in these cases produces the yellow chromogen associated with urea, however, with much less intensity than most of the examples in this table. Methyl formate is probably the major product in the reactions performed at low concentrations of ammonia. We can observe that the samples with intermediate ammonia concentration (7.2 and 7.4 M) appear to be those which have the highest urea turnovers.

The starting pressure of CO in the reactions seems to be less critical, however, one trend which emerges upon examination is that as the pressure is reduced below 20 bar, the turnover of urea is not greatly affected. Indeed, it appears that as the pressure is reduced, the turnovers may actually increase. As the initial pressure of CO is increased above 20 bar, the yield of urea decreases

For these examples, it is difficult to say at what temperature the reaction is optimised for urea production, however, above 170°C, total decomposition of the catalyst system is observed, and below 130°C, the turnover of urea approaches zero.

From these results, it can be seen that the time of the reaction is very important with similar turnovers being produced within the first 3-4 hours of the reaction as are produced in 18 and 24 hours of reaction. This may be due to consumption of ammonia (in the form of formamide and other nitrogen containing products as well as urea) forcing the concentration of ammonia in the autoclave down to values where no urea production is possible (as seen from the reactions performed at relatively low concentrations of ammonia). Alternatively, the conversion of the active catalytic species to an inactive complex would also halt production of urea. The fact that the yield of urea at equilibrium is generally quite low can be attributed to the thermodynamics of the process (section 1.2.2). Referring to figure 1.10, it can be observed that low temperatures and high pressures should favour the formation of urea. What we observe is that the yield of urea increases up to 10-20 bar, but then decreases, whilst the yield decreases as the temperature is dropped below 150°C, probably because the reaction rate is decreased.

3.3.6.2 Optimisation of reaction conditions for urea production

Subsequent to these promising initial results, a more systematic approach was taken to the analysis of this system. Using the same batch of $[Ru_3(CO)_{12}]$ throughout, and keeping the concentration of ammonia in methanol constant, reactions were performed in which temperature, initial CO pressure, and the duration of the reaction were varied.

(i) Effect of temperature

Results for yields of urea for a system in which temperature was varied from 140-170°C can be observed in table 3.6, and in figure 3.16

A maximum turnover is achieved at 160°C. This is consistent with the results obtained in table 3.5, however, it is worth noting that the yields are not as high as those obtained initially.

Table 3.6 Variation of urea turnover with temperature

Temperature (°C)	Urea turnover (total)[a]	Urea turnover (h^{-1})
140	4.7	1.2
145	6.5	1.6
150	6.1	1.5
155	7.8	2.0
160	8.5	2.1
170	6.0	1.5

[a]Initial CO pressure = 15 bar, duration of reaction = 4 h, $[NH_3]$ = 7.2 M, $[Ru_3(CO)_{12}]$ = 3.91 mM.

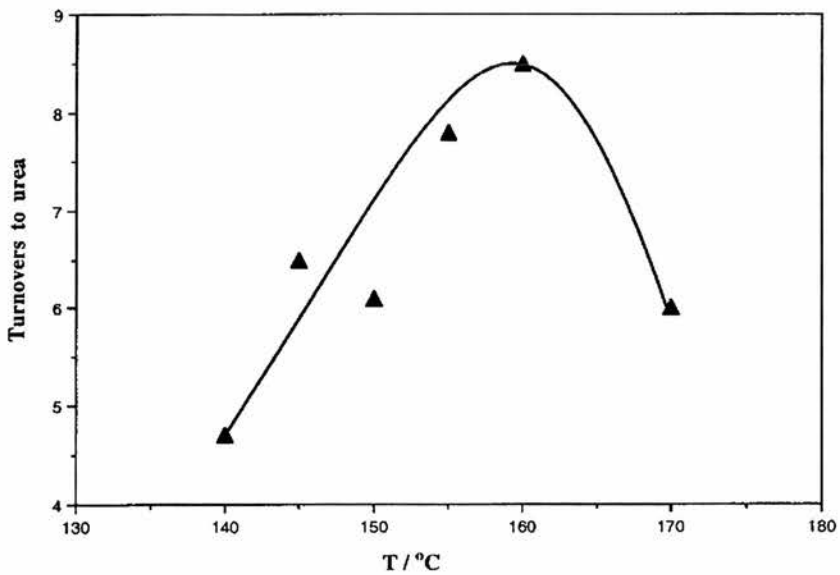

$[Ru_3(CO)_{12}]$ (3.91 mol dm^{-3}), $[NH_3]$ (7.2 mol dm^{-3}), methanol (5 cm^3), p_{CO} = 15 bar, t = 4h

Figure 3.16 A graph to show the variation of total turnover to urea with temperature

(ii) Effect of initial CO pressure

Initial CO pressures were varied from 2-40 bar, and the results of these reactions can be observed in table 3.7, and figure 3.17.

Above an initial CO pressure of 10 bar, the urea yield decreases noticeably - at 40 bar, it is less than ¼ that which is attained at 10 bar. However, below 10 bar, relative urea yield remains effectively unaltered even down to an initial CO pressure of 2 bar.

Table 3.7 Variation of urea turnover with pressure

Initial CO pressure (bar)	Urea turnover (total)[a]	Urea turnover (h^{-1})
2	12.9	3.2
5	13.2	3.3
10	12.3	3.1
15	8.5	2.1
20	6.5	1.6
30	5.7	1.4
40	2.6	0.7

[a]Temperature of reaction = 160°C, duration of reaction = 4 h, $[NH_3]$ = 7.4 M, $[Ru_3(CO)_{12}]$ = 4.16 mM.

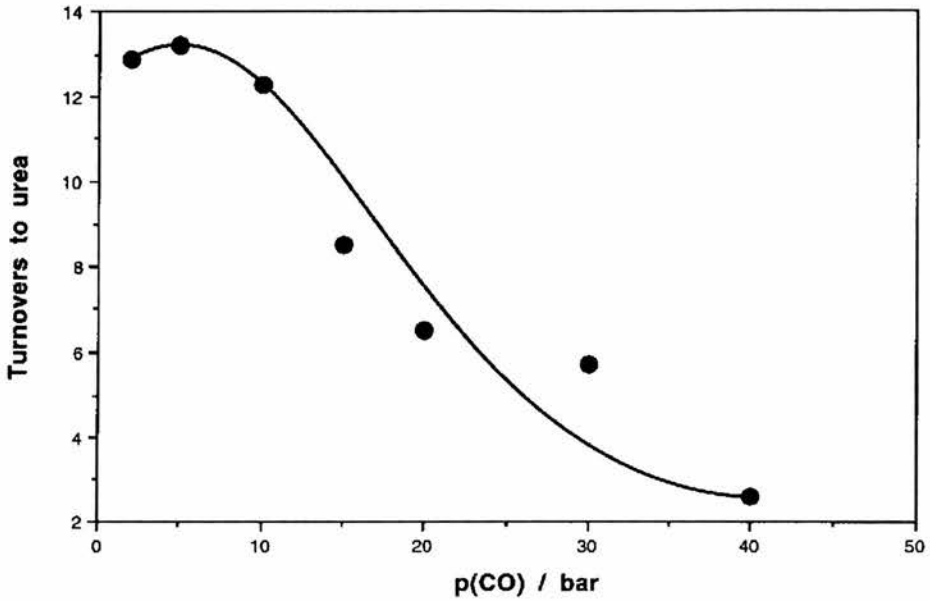

$[Ru_3(CO)_{12}]$ (4.16 mol dm^{-3}), $[NH_3]$ (7.4 mol dm^{-3}), methanol (5 cm^3), T = 160 °C, t = 4h

Figure 3.17 A graph to show the variation of total turnover to urea with CO charging pressure

(iii) Effect of reaction duration

Time of reaction was varied from ½ h to 4 h. The results of this experiment can be observed in table 3.8.

Table 3.8 Effect of urea turnover with reaction time

Reaction duration (h)	Urea turnover (total)[a]	Urea turnover (h^{-1})
0.5	7.1	14.3
1.0	10.0	10.0
1.5	10.0	6.6
2.0	18.9	9.4
3.0	14.3	4.8
4.0	12.3	3.1

[a]Initial CO pressure = 10 bar, reaction temperature = 160°C, $[NH_3]$ = 7.4 M, $[Ru_3(CO)_{12}]$ = 3.36 mM.

These results present us with evidence that a very active catalyst for the production of urea is at work in this system. It is unfortunate that it is only active at its optimum rate of turnover for less than an hour. This suggests either that a transient catalytic species is involved in the catalysis, or alternatively, that ammonia consumption, or subsequent reaction *in situ* of the urea formed is continuing.

A more meaningful way to look at these results is in terms of rate of urea turnover (figure 3.18). In this way, we can observe that the optimum rate of urea turnover occurs at a reaction time of ½ h, and the rate of turnover decreases as the reaction time is increased.

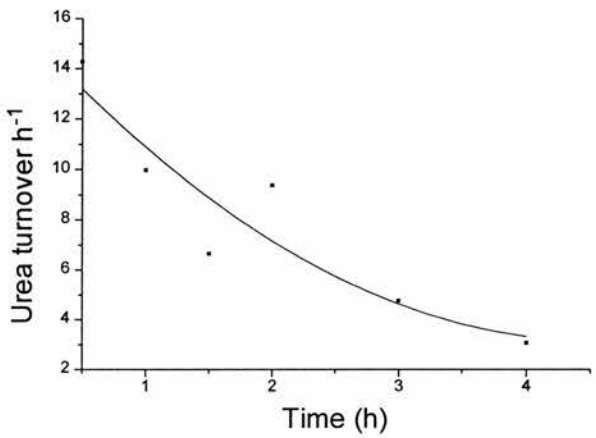

Figure 3.18 A graph to show how turnover to urea varies with reaction duration

3.2.7 Other products of the reaction catalysed by $[Ru_3(CO)_{12}]$ in methanolic ammonia

Other products of the reaction to produce urea catalysed by $[Ru_3(CO)_{12}]$ in methanolic ammonia which are detectable by GCMS include formamide, N-methyl formamide, N,N-dimethyl formamide, methyl formate and ammonium carbamate. ^{13}C NMR has revealed the presence of biuret in some reaction mixtures. Of these, only formamide and methyl formate are produced in significant quantities. All of these appear to be produced by reactions involving $[Ru_3(CO)_{12}]$ (comparing with ^{13}C NMR and GCMS results of a reaction performed in the absence of $[Ru_3(CO)_{12}]$), however, it is found that their presence is generally diminished in reactions performed under low pressures of CO and no attempt has been made to optimise reaction conditions for the production of any one of these species.

3.2.8 Different solvent systems; ethanol and propan-2-ol

3.2.8.1 Results obtained with low ammonia concentration

Ethanol and isopropanol are able to solvate $[Ru_3(CO)_{12}]$ more effectively than methanol, but they are poor solvents for ammonia. Initial experiments performed with ethanol as solvent had low concentrations of NH_3 (typically 2 mol dm^{-3}). Reactions were performed at temperatures between 120 and 170°C and CO loading pressures between 2 and 20 bar. Analysis of post-catalytic reaction solutions by GCMS showed that a peak which had been incorrectly assigned to urea by ^{13}C NMR during early investigation of this reaction was in fact attributable to ethyl formate. This result was confirmed by spiking with authentic urea, but it was also shown that when isopropanol was used as a solvent for ammonia instead of ethanol, the reaction yielded isopropyl formate as a product. GCMS results have also shown that methyl formate is a reaction product in the reaction to carbonylate ammonia, with methanolic ammonia as solvent.

The base-catalysed carbonylation of alcohols by alkali metals is known[44], and it is almost certain that this reaction is being observed in this case with methanol, ethanol and isopropanol as substrates. It is suggested that ammonia acts as the base to form an alkoxide and ammonium ion. The alkoxide ion can react with carbon monoxide to produce an alkoxy formyl ion which is then protonated by a molecule of alcohol to generate alkyl formate and alkoxy ion, as shown in figure 3.19.

$$RO:^- + CO \longrightarrow RCO_2^- \xrightarrow{ROH} HCO_2R + RO:^-$$

Figure 3.19 The base-catalysed carbonylation of alcohols

Other products of this reaction (with ethanol as solvent) as observed by GCMS show formamide, ethyl carbamate, ammonium carbamate, N-ethyl amines and N,N-diethylformamide to be major products. The ruthenium-catalysed formation of N-methyl formamides from synthesis gas and ammonia by $[Ru_3(CO)_{12}]$ with sulfolane as solvent has been observed before[45], the main products being formamaide, N-methylformamide, and N,N-dimethylformamide with formaldehyde, formed by CO

hydrogenation, postulated as intermediate. These solutions were found to yield such a small amount of urea that quantification by ^{13}C NMR was impossible, and only on reaction with diacetyl monoxime, a faint yellow colour was sometimes observed which faded rapidly over a short period of time. The turnover to urea in these cases is *not* catalytic.

3.2.8.2 Results obtained for higher ammonia concentrations in ethanol

On prolonged bubbling, it is possible to achieve a molarity of urea of up to ca. 6 mol dm^{-3}. This was not possible with propan-2-ol, given the reduced ability to solvate ammonia. Experiments were performed in stronger ethanolic ammonia. The results are summarised in table 3.9. Genuine catalysis of carbonylation of ammonia to urea is observed, and this is confirmed by spiking the sample with authentic urea, and by ^{13}C DEPT analysis. We can see that at 160°C, and a loading pressure of 10 bar CO, a superior turnover to urea is obtained than was observed for methanol under similar conditions. This may be a result of the superior ability of ethanol compared to methanol to solvate intermediate catalytic species.

These results also confirm our suggestion that the concentration of ammonia is critical in determining whether or not urea will be produced.

Table 3.9 Results of reactions performed in strong ethanolic ammonia

$[Ru_3(CO)_{12}]$/ mol.10^3	conc $[NH_3]$/ mol dm^{-3} [a]	T/°C	p_{CO} (loading)/ bar	Turnover (total)[b]
0.261	5.4	160	2	2.3
0.261	5.4	150	2	2.3
0.074	5.4	160	10	8
0.139	5.4*	160	5	4.3

[a] reaction vol. = 30 cm^3 except* = 40 cm^3, reaction duration = 1 h. [b] mols per mol $[Ru_3(CO)_{12}]$, by ^{13}C NMR

3.2.9 Colloidal experiments conducted in methanolic ammonia

Because we observed that high catalytic activity only occurred during the early stages of the catalytic reactions, and since metallic ruthenium was sometimes observed at the end of the reaction, it appeared possible that colloidal metal might be responsible for the catalytic activity but that this activity might terminate as the colloid agglomerated into macroscopic particles. In order to examine this hypothesis, reactions were carried out in the presence of carbowax and mercury.

It has been shown that protection of redox catalysts with a polymer such as carbowax 2000, can help to prevent colloidal agglomeration. This has the result of increasing their life time in solution, and periods of catalytic activity can be lengthened[46].

It has also been shown that Hg can act as a solvent for colloidal suspensions of platinum group metals precipitated from catalytic reaction solutions[47] providing some indication of whether or not a reaction is genuinely homogeneous, or whether it is being catalysed by a heterogeneous colloidal suspension.

It was therefore decided to conduct experiments in the presence of carbowax 1500. If a colloid were responsible for the catalytic activity, it would be stabilised by the polymer, markedly increasing their activity to carbonylate ammonia to urea. An experiment was also conducted in the presence of Hg which would dissolve the colloid resulting in dramatically reduced activity. The results of these experiments are summarised in table 3.10 together with a control reaction conducted in the presence of $[Ru_3(CO)_{12}]$, but without either additive. We can observe that no real change in catalytic activity results from having these species present in solution, so we can conclude from these experiments that the reaction to carbonylate ammonia to urea in methanolic ammonia is homogeneous and genuinely catalytic.

Table 3.10 Results obtained for colloidal experiments

Colloidal inhibitor	$[Ru_3(CO)_{12}]$ / mol.10^3	$[NH_3]$/ mol dm^{-3} [c]	T/°C	p_{CO} (loading)/ bar	t/ h	Total turnover[d]
none	0.160	4.4	160	5	1	4.4
Hg[a]	0.160	4.4	160	5	1	4.1
carbowax[b]	0.158	4.4	160	5	0.5	3.6

[a] 1.14 g [b] 0.5 g [c] Vol = 40 cm^3 [d] mol urea per mol $[Ru_3(CO)_{12}]$

3.2.10 Reactions performed in methanolic ammonia using tetranuclear ruthenium carbonyl cluster species

It has been shown that when $[H_4Ru_4(CO)_{12}]$ is used as a catalyst precursor for the WGSR, then after an initial "maturing" period of 24 h, a catalytically active system is obtained giving a solution which is spectroscopically indistinguishable from a catalytic system employing $[Ru_3(CO)_{12}]$ as precursor[22]. Further work upon this system has shown that the tetranuclear cluster anion $[H_3Ru_4(CO)_{12}]^-$ is in equilibrium with $[HRu_3(CO)_{11}]^-$ in the presence of H_2 and CO by the reaction shown in the schematic equations in figure 3.20[34]. We therefore decided to conduct two experiments using $[H_4Ru_4(CO)_{12}]$ (which is

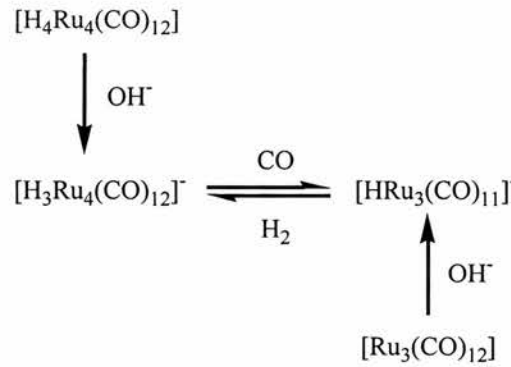

Figure 3.20 A schematic for the equilibrium of $[H_3Ru_4(CO)_{12}]^-$ and $[HRu_3(CO)_{11}]^-$ in the presence of CO and H_2

actually a 1:1 mixture of $[H_4Ru_4(CO)_{12}]$ and $[H_2Ru_4(CO)_{13}]$ as prepared) under conditions for which catalysis for the carbonylation of ammonia to urea in methanol

solution is normally observed. Results of these reactions are summarised in table 3.11. It is worth noting that not only was there no urea detectable as a product by ^{13}C NMR, but additionally, the yield of formamide was extremely low, similar to the amount expected from a reaction performed in the absence of catalyst.

Table 3.11 Reactions using tetranuclear clusters.

$[H_4Ru_4(CO)_{12}]$ / mol.10^3 [a]	conc $[NH_3]$/ mol dm^{-3} [b]	T/°C	p_{CO} (loading)/ bar	Turnover (total)[c]
0.269	4.4	160	2	0
0.269	4.4	160	5	0

[a] 50:50 mixture of $[H_4Ru_4(CO)_{12}]$ and $[H_2Ru_4(CO)_{13}]$. [b] Vol. = 30 cm^3, time = 2 h. [c] mols urea per mol $[Ru_3(CO)_{12}]$, by ^{13}C NMR

3.2.11 Reactions performed in the presence of hydrogen acceptors

There is a dual purpose to the strategy of using hydrogen acceptors in this reaction. Having identified H_2 to be a product of the reaction to carbonylate ammonia to urea, we see that an equilibrium akin to that shown in figure 3.20 becomes possible. Indeed, we have also shown by ^1H NMR that $[H_3Ru_4(CO)_{12}]^-$ and $[H_2Ru_4(CO)_{12}]^{2-}$ are probable products of this reaction, and that $[H_4Ru_4(CO)_{12}]$ as a precursor is *inactive* for urea production by itself under conditions for which $[Ru_3(CO)_{12}]$ is active. It would therefore be of value to study this reaction independently of these tetranuclear clusters. Secondly, we have proposed that ammonia is carbonylated to urea *non*-oxidatively by the reaction shown in figure 3.21. Removal of H_2 from this system would have the effect of pushing the equilibrium to the right, towards formation of urea.

The palladium thimble experiment of Shore and co-workers has already been described, and whilst this proved to be an excellent method for removing H_2, we have devised a simpler method. Inclusion of hydrogen acceptors, such as acetone or simple alkenes (e.g. *tert*-butylethylene ($(CH_3)_3CCHCH_2$)) in the reaction solutions will also have the effect of removing H_2. The results of these experiments can be observed in table 3.12.

$$2NH_3 + CO \rightleftharpoons CO(NH_2)_2 + H_2$$

Figure 3.21 Non-oxidative carbonylation of ammonia to urea

Table 3.12 Results of experiments performed in the presence of hydrogen acceptors

hydrogen acceptor[a]	$[Ru_3(CO)_{12}]$/ mol.10^3	$[NH_3]$/ mol dm^{-3} [b]	T/°C	p_{CO} (loading)/ bar	t/ h	Total turnover[c]
none	0.160	4.4	160	5	1	4.4
acetone	0.163	4.4	160	5	2	4.9
t-Butylethylene	0.163	4.4	160	5	2	4.6

[a] Vol. Employed = 500μL [b] Vol. = 30 cm^3 [c] mols urea per mol $[Ru_3(CO)_{12}]$, by ^{13}C NMR

We can see from these results that there is no real advantage in having a hydrogen acceptor present in the solution.

3.2.12 Reaction using $[HRu_3(CO)_{11}]^-$ as precursor

Evidence for the activity of $[HRu_3(CO)_{11}]^-$ as an intermediate in the reaction to catalyse ammonia to urea using $[Ru_3(CO)_{12}]$ as precursor was strengthened when it was demonstrated that it could be used as a precursor for this reaction. At a loading pressure of 5 bar CO, temperature of 160°C, a concentration of $[HRu_3(CO)_{11}][NEt_4]$ of 3.7 mmol dm^{-3}, and an ammonia concentration of 4.4 mol dm^{-3}, a total turnover to urea of 5.9 mol per mol $[HRu_3(CO)_{11}]^-$ over a period of 3 h was observed.

3.2.13 Acid enrichment experiments

Upon examination of the proposed mechanism for the catalytic production of urea (figure 3.1), we can see that the ultimate step to the process involves abstraction of one molecule of hydrogen to yield the starting catalytic complex; this abstraction results from protonation of the ruthenium hydride complex. Similarly, an intermediate process involves protonation of the oxygen atom of coordinated amide prior to the second nucleophilic attack by NH_3. Clearly, if we could bias the extent of protonation, by

increasing the proportion of ammonium ions in the solution, then this could possibly promote urea formation and hydrogen abstraction. Therefore, a reaction was conducted using ammonium chloride as a source of supplementary ammonium ions. $[Ru_3(CO)_{12}]$ (3 mM), methanolic ammonia ($[NH_3]$ 16.75 mol dm^{-3}), and ammonium chloride (1.0 mol dm^{-3}) were reacted under the following conditions over a period of 4 hours; p_{CO} (20 bar), temperature (160°C). The resultant reaction mixture was concentrated by evaporation *in vacuo,* and by virtue of its ^{13}C spectra was found to contain no urea.

Similarly, acidification of the system using water as the source of protons resulted in no marked enhancement of the $[Ru_3(CO)_{12}]$ system in the reaction to carbonylate ammonia to urea, however, an evolution of approximately 10 mol H_2 per mol $[Ru_3(CO)_{12}]$ per h in the first five hours of reaction was recorded at a loading pressure of 15 bar CO and a temperature of 160°C. Analysis by ^{13}C NMR revealed that urea was a product, with a total turnover of 10.2 mol per mol $[Ru_3(CO)_{12}]$. It is concluded, therefore, that the majority of hydrogen in this reaction is produced by the WGSR; an observation which is supported by the presence of carbonate and bicarbonate (produced by reaction of CO_2 with NH_3) in the ^{13}C NMR spectrum.

3.2.14 Reaction with formamide in the absence of catalyst

In order to confirm that the source of urea was not from stoichiometric reaction of ammonia with formamide, the following experiment was set up including formamide in the original reaction solution. 100μL (2.6 mmol) formamide was injected anaerobically into an autoclave containing 40 cm^3 of methanolic ammonia (10.6 mol dm^{-3} in ammonia). The vessel was charged to 5 bar CO and reacted at 150°C for a period of 2 h. After the autoclave had been cooled, analysis by ^{13}C NMR in the usual way revealed that formamide was the only carbonyl-containing compound which could be detected. This, together with the observation that NH_3 cannot be carbonylated to urea in methanolic or ethanolic ammonia in the absence of $[Ru_3(CO)_{12}]$ confirms that urea can be produced catalytically using $[Ru_3(CO)_{12}]$ as catalyst precursor in the presence of methanol or ethanol containing a high concentration of ammonia.

3.2.15 Reactions using phosphine derivatised complexes of $[Ru_3(CO)_{12}]$

The species $[Ru_3(CO)_{10}(DPPE)]$, $[Ru_3(CO)_{10}(DPPM)]$, $[Ru_3(CO)_8(DPPM)_2]$ and $[Ru_3(CO)_6(DPPM)_3]$ were screened for activity for the carbonylation of ammonia in methanolic and ethanolic solutions of ammonia. Under conditions required to attain activity for $[Ru_3(CO)_{12}]$, (160°C, 10 bar p_{CO}), catalyst degradation was evident in all cases except for that of $[Ru_3(CO)_6(DPPM)_3]$, however, even for this species it was found that the post-reaction samples contained no urea. Monitoring by GC during the course of the reactions established that even at lower temperatures, hydrogen production was negligible, and analysis by ^{13}C NMR at the end of the reactions allowed the conclusion that formamide was also not a major product of the reaction. It seems likely then that even for the more stable $[Ru_3(CO)_6(DPPM)_3]$, the initial step of carbamoyl formation is not occurring. This is in agreement with what is known for the WGSR using these species. When ligands which have a capacity for electron donation are added to $[Ru_3(CO)_{12}]$ to increase the rate of protonation to a hydride complex intermediate, then sometimes the fine electronic balance is upset to such an extent as to make another step in the cycle rate limiting. In this case, as for the WGSR, that step is nucleophilic attack which should result in the formation of a carbamoyl complex (a metallocarboxylic acid complex for the WGSR). The capacity for back-bonding to CO groups within the complex is increased making the carbon atoms of these CO groups less electrophilic, and less susceptible to attack by nucleophiles.

3.3 Conclusions

It has been found that urea is not a product of the carbonylation of ammonia under conditions described in the literature for reactions catalysed by $[Ru(HEDTA)Cl]^-$ or $[Ru(HEDTA)(CO)]^-$. Ammonium formate is the major product of these reactions under aqueous conditions and at various concentrations of ammonia, however, formamide is also observed under some circumstances by ^{13}C NMR spectroscopy.

$[Fe(CO)_5]$ and $[M(CO)_6]$ are also inactive for urea production in methanolic ammonia solutions. For $[Fe(CO)_5]$, this result probably arises as a result of the fine pH balance that has to be achieved to allow for steps of nucleophilic attack *and* protonation to occur concurrently within the same cycle. A strong pH dependence is also observed in the WGSR for $[Fe(CO)_5]$. In the case of $[M(CO)_6]$, where decomposition of formate (HCO_2^- (see figure 3.6)) has been proven as an important step in the cycle for the WGSR, the analogous step in the carbonylation of ammonia would be co-ordination of deprotonated formamide ($HCONH^-$ (see figure 3.22)) produced from stoichiometric reaction of NH_3 and CO. The concentration of formamide produced by this reaction is likely to be very small, but more importantly, the acidity of formamide is much lower than that of formic acid so that the required co-ordination as the anion ($HCONH^-$ is highly improbable. It is unlikely then that $[M(CO)_6]$ could function as a catalyst for ammonia carbonylation by this mechanism.

$[RhH(PEt_3)_3]$ has been found to be inactive for urea production in aqueous systems both in co-ordinating (pyridine) and non-co-ordinating (methanol) solvents. However, under conditions of varying ammonia concentration, WGSR activity was noted and ammonium carbonate isolated from post-reaction solutions. It is likely in this case then that oxidative addition of water is occurring preferentially to oxidative addition of ammonia. This is to be expected (see section 3.1.1), and is also supported by observation that oxidative addition of ammonia does not occur for this complex under ambient conditions of temperature and pressure (see section 6.2.3.1, chapter 6,).

$[Ru_3(CO)_{12}]$ *is* observed to function as a genuine homogeneous catalyst precursor for the carbonylation of ammonia in methanolic ammonia solutions. This activity is optimum at low pressures (2-10 bar p_{CO}) and relatively high temperatures (130-170°C). Ammonia concentration is critical; at low (< 4 mol dm^{-3}) concentrations,

urea is hardly observed as a product of the reaction at all (by reaction with diacetyl monoxime) ,and it is only when this concentration is increased that urea is seen.

The diphosphine-substituted clusters $[Ru_3(CO)_{10}(DPPE)]$, $[Ru_3(CO)_{10}(DPPM)]$, $[Ru_3(CO)_8(DPPM)_2]$ and $[Ru_3(CO)_6(DPPM)_3]$ are all inactive for the carbonylation of ammonia. This is due to both rapid degradation of catalyst, and also to increased electronegativity at the carbon atom of CO groups inhibiting formation of a carbamoyl complex by nucleophilic attack of NH_3.

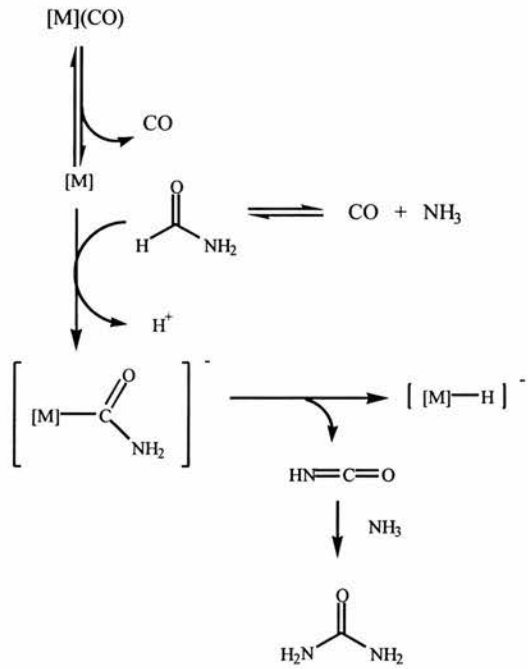

Figure 3.22 Steps necessary for activation of $[M(CO)_6]$ to formation of carbamoyl complex

3.4 Experimental

3.4.1 High pressure reactions

A typical procedure for carrying out a high pressure reaction is described as follows.

The catalyst precursor was weighed into a side-arm Schlenk tube and dissolved by magnetic stirring in the particular solvent of reaction, this was generally performed overnight. The resulting solution was transferred to the autoclave (see figure 3.23) under an argon atmosphere and charged to the desired pressure with carbon monoxide. The contents of the autoclave were agitated by magnetic stirring and the autoclave heated by steel heating bands, the temperature being maintained with heating controllers and thermocouples. After completion of the reaction, the autoclaves were slowly cooled and degassed (anaerobically if necessary). Heating the reaction vessel from room temperature to 160°C typically required 15-20 minutes.

Gas samples could periodically be removed through a port at the top of the reaction vessel for analysis with a Pye Unicam Series 204 chromatograph on a carbosphere 80/100 mesh column maintained at room temperature with Ar as a carrier gas.

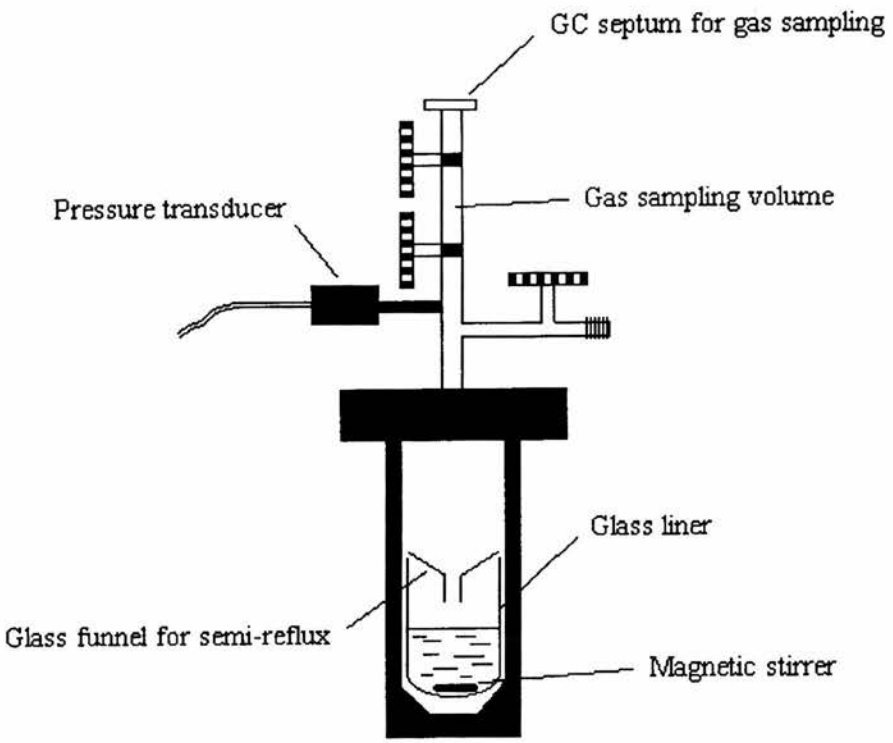

Figure 3.23 High pressure autoclaves adapted for H_2 analysis

Preparation of solvent/ammonia systems

Aqueous solutions of ammonia used in these experiments were prepared from a solution of 33 % w/w ammonia in water by dilution in distilled water to the desired concentration.

For the preparation of alcoholic solutions of ammonia, a known mass of alcoholic solvent was pre-weighed into a side-arm Schlenk and allowed to cool in icy water under Ar. NH_3 was bubbled slowly through the solution for several hours. Upon re-weighing, the mass of NH_3 absorbed, and hence the molarity of the solution in NH_3 could be evaluated.

Analysis by NMR

For $^{13}C\{^1H\}$ nuclei, and for ^{13}C DEPT analysis, a Brucker 300 MHz NMR machine was used, and for shorter periods of scanning for proton and $^{31}P\{^1H\}$ nuclei, a Varian 300 MHz machine was employed. Unless described elsewhere, all samples for

NMR were prepared in 5 mm tubes under atmospheres of dinitrogen, or argon where required. NMR solvents were degassed by several freeze-pump-thaw cycles, and dried over suitably sized activated molecular sieves.

Analysis of urea content

For the analysis of the urea content of a particular solution, the following general procedure was employed.

A known volume (which is a know percentage of the original reaction volume) of reaction mixture was taken from the cooled and degassed autoclave. This solution was then evaporated *in vacuo* to remove all of the volatile components. The residue was dissolved in a known small volume of H_2O (typically 1-2 cm^3). The resulting slurry was filtered through celite and a known volume of the filtrate (typically 500 μL) was transferred to an NMR tube. Also added to the NMR tube were known volumes of D_2O (NMR lock, typically 100μL) and acetonitrile (internal standard, typically 50 μL). A ^{13}C NMR spectrum was acquired over a known number of scans under a standard set of conditions, and the intensity of the signal corresponding to urea relative to that of CH_3CN was compared with those on a graph obtained for samples of authentic urea of known concentrations obtained after an equal number of scans measured under the same conditions (see section 2.6). From this graph, the concentration of urea in the NMR sample could be calculated, and from this, estimation of the concentration of urea in the original sample was possible. The turnover to urea was expressed either in terms of mols produced per mol of catalyst per hour, or total mols produced per mol of catalyst. ^{13}C NMR data could also be collected on raw samples without evaporation of solvent. A D_2O lock and CH_3CN internal standard were added, as normal.

3.4.2 Preparation of catalyst precursors

Chemicals

$RuCl_3.3H_2O$, Pt black, palladium on charcoal and $[Ru_3(CO)_{12}]$ were obtained from Johnson Matthey PLC and used as received, and residues were kept for return.

$RhCl_3.3H_2O$ was obtained from several commercial sources and used as received. All phospines were obtained either from Aldrich Chemical Co., or Strem Chemicals plc, and were used as received.. A sample of $K[Ru(HEDTA)Cl].2H_2O$ was provided by Johnson Matthey plc (JM 1266, Batch GRH/CO92/56) (found: C 24.07, H 3.33, N 5.57%. $C_{10}H_{17}ClN_2O_{10}KRu$ requires C 23.96, H 3.42, N 5.59%).

Preparations of all materials were carried out using standard Schlenk procedures[48]. Diethyl ether, THF, petroleum ether (40/60) and toluene were dried and distilled either over sodium benzophenone or calcium hydride in an atmosphere of dinitrogen or argon. Methanol and ethanol were dried and distilled over magnesium turnings activated with iodine.

Ammonia was generally not dried before use, however, where necessary, it could be dried by stirring over sodium until the appearance of a characteristic blue colour was noticed indicating dryness. Distillation at atmospheric pressure into a steel trap then provided a convenient store for dry ammonia.

$K[Ru^{(III)}(HEDTA)Cl].2H_2O$

$K_2[RuCl_5(H_2O)]$ was prepared by the method of Mercer and Buckley[49] in yields of up to 60%, and from this, following the method of Diamantis and Dubrawski[50] (a modification of a method by Ezerskaya and Solovykh[51]).

$RuCl_3.3H_2O$ (0.944 g) was dissolved in concentrated HCl (122 cm^3) and refluxed for 4 h. KCl (0.36 g) and Hg (12 cm^3) were added to the solution which was stirred under reflux for 30 min until a green solution formed, indicating the presence of $Ru^{(II)}$. Reduction *in vacuo* to ca. 15 cm^3 gave a red precipitate on opening to air. The precipitate was filtered onto celite, washed copiously with EtOH, and dried *in vacuo*. The solid was extracted from the celite with 6 mol dm^{-3} HCl. The extractions were reduced to a small volume on a heating bath, and cooling gave a red-brown precipitate ($K_2[RuCl_5(H_2O)]$, 0.4652 g, 35 %). $K_2[RuCl_5(H_2O)]$ was dissolved in a warmed solution of 0.001 M $HClO_4$ (10 cm^3) to which was added a hot solution of $Na_2(H_2EDTA)$ in 0.001 M $HClO_4$ (10 cm^3). The resulting yellow solution was refluxed for 90 min. Slow cooling gave a micro-crystalline yellow solid which was washed with cold water and ethanol.

(found: C 24.54, H 3.12, N 5.69 %. $C_{10}H_{17}ClN_2O_{10}KRu$ requires C 23.96, H 3.42, N 5.59 %)

$K[Ru^{(II)}(HEDTA)(CO)].2H_2O$

This compound was prepared by the method of Diamantis and Dubrawski[50].

CO/H_2 (1:1) was bubbled through an aqueous solution of $K[Ru^{(III)}(HEDTA)(Cl)].2H_2O$ (0.531 g in 20 cm^3 H_2O) containing palladium on carbon (5%) for 80 min. The resulting solution was filtered and concentrated. Precipitation with ethanol gave a pale yellow solid which was washed with ethanol. (0.255 g, 51%).
IR (nujol mull)1943 cm^{-1} (s), 1916 (s) (^{13}C stretch). Lit[50] 1940 cm^{-1} (s).
^{13}C NMR (D_2O) 202.6, 185.8, 183.6, 182.4, 173.9, 70.4, 65.6, 64.3, 63.0, 60,9, 59.0.
Lit[50] 202.8, 185.7, 184.1, 182.9, 170.7, 65.7, 64.8, 63.5, 61.3, 59.3, 57.9.
(found: C 24.90, H 2.81, N 5.56 %.$C_{10}H_{17}ClN_2O_{10}KRu$ requires C 23.96, H 3.42, N 5.59 %)

Preparation of $[RhH(PEt_3)_3]$[52]

$RhCl_3.3H_2O$ (1.14 g) was dissolved in THF (20 cm^3) with PEt_3 (1.8 cm^3) and a few drops of water and stirred for 20 hrs. The resulting suspension was evaporated to dryness *in vacuo.* Na/Hg amalgam (2%, 50 g), THF (20 cm^3), and PEt_3 (1.8 cm^3) were added to the residue, and the resulting suspension was stirred for a further 5 hrs. The mixture was filtered and evaporated to dryness *in vacuo*. The resulting solid was then dissolved in n-pentane and filtered several times before being reduced to a small volume and stored at -30°C. The green crystals obtained were collected and washed with cold n-pentane before drying *in vacuo*. Heating *in vacuo* at 65°C resulted in the production of a dark red oil (Yield 74%) which was made into a stock solution in petroleum ether (200 cm^3).

Preparation of $[Ru_3(CO)_{10}(DPPM)]$-[53]

A few drops of a concentrated solution of sodium diphenylketyl (in THF) were added, with rapid stirring, to a warmed (40°C) solution of $[Ru_3(CO)_{12}]$ (0.51 g, 0.80 mmol) and DPPM (0.31 g, 0.81 mmol) in THF (50 cm^3), and the resultant cherry-red solution was stirred at 40°C for 10 min. The solvent was removed *in vacuo*, and the residue was recrystallised from cold acetone/methanol. The crystals were recovered by filtration.

IR (acetone, cm^{-1}): 2079.6(s), 2063.3(m), 2020.0(s,sh), 2010.5(vs), 1997.0(vs,br), 1975(m,sh), 1955.4(s), 1922.4(vw) Lit[54] 2080(m), 2040(w), 2010(s), 1988(sh), 1960(m)

^{31}P NMR (CD_2Cl_2): 14.6 (s): Lit[53]: 13.6 (s)

^{1}H NMR (CD_2Cl_2): 4.13 (t, J=10.5 Hz) 7.4 (br, Ph)

Preparation of $[Ru_3(CO)_8(DPPM)_2]$ [55]

$[Ru_3(CO)_{12}]$ (0.48 g, 0.75 mmol) and DPPM (0.87 g, 2.26 mmol) were stirred together in toluene (40 cm^3) at 80°C for 8 h. The solvent was removed *in vacuo* at 40°C, and the residue was recrystallised from cold acetone/ethanol.

IR (acetone): 2039.1(m), 1998.5(w), 1994.7(vs), 1980.1(m,sh), 1932.5(vw), 1919.4(vw), 1887.6(vb,w): Lit (CsBr)[55] 2040 (s), 1955(br), 1890 (m)

^{31}P NMR (CD_2Cl_2): 19.36 (AA'BB' type spectrum ($[Ru_3(CO)_8(DPPM)_2]$)

(found: C 54.23, H 3.81%. $C_{58}H_{44}O_8P_4Ru_3$ requires C 53.79, H 3.42%.)

Preparation of $[Ru_3(CO)_6(DPPM)_3]$ [56]

$[Ru_3(CO)_{12}]$ (0.347 g, 0.54 mmol) and DPPM (0.625 g, 1.63 mmol) were refluxed in benzene (35 cm^3) for 8 h. The resulting solution was evaporated to dryness *in vacuo* and recrystallised from cold acetone/ethanol.

^{31}P NMR (CD_2Cl_2): 22.0 (s): Lit[56] 22.3

Preparation of $[Ru_3(CO)_{10}(DPPE)]$ [57]

A mixture of $[Ru_3(CO)_{12}]$ (0.300 g, 0.47 mmol) and DPPE (0.210 g, 0.53 mmol) in THF (20 cm^3) at a temperature of 40°C was treated with few drops of concentrated solution of sodium diphenylketyl (in THF) and stirred until the absence of bands at 2096 cm^{-1} and 2059 cm^{-1} was noted. The solvent was removed *in vacuo* and the red residue was recrystallised from cold acetone/methanol.

^{31}P NMR: 29.6 (s)

Preparation of $[HRu_3(CO)_{11}][Et_4N]$ [58]

$[Ru_3(CO)_{12}]$ (0.432 g, 0.677 mmol) was stirred for 20 min in a solution of THF (70 cm^3) containing $NaBH_4$ (0.14 g, 3.7 mmol). The reaction was filtered through celite and the filtrate evaporated to dryness *in vacuo*. The red residue was dissolved in methanol (25 cm^3), and after addition of Et_4NI (0.21 g, 0.81 mmol) in methanol (5 cm^3), the solution was concentrated to ca. 10 cm^3 *in vacuo*. Crystallisation at -30°C gave dark red crystals which were collected by filtration at -78°C.

IR (acetone): 2074(w), 2016(s), 1989(vs), 1953(m). Lit[59] 2072(w), 2011(s), 1983(s), 1949(sh), 1898(m), 1730(vw)

^1H NMR (d^6 acetone): -12.65 ppm. Lit[59] -12.9 ppm.

Preparation of $[H_4Ru_4(CO)_{12}]$ [60]

$[Ru_3(CO)_{12}]$ (0.617 g, 0.965 mmol) was dissolved in petrol ether (boiling fraction 100-120°C) (180 cm^3) and brought to reflux. H_2 was bubbled through the boiling solution *via* a cannular for a period of 1 h. The resulting yellow-orange solution was cooled and then concentrated to a small volume (ca. 5 cm^3) by distillation of the petrol ether at atmospheric pressure. The orange-yellow precipitate which resulted on cooling was collected by filtration and dried *in vacuo*. Recrystallisation from CH_2Cl_2/petrol ether (40-60°C boiling fraction) at -30°C gave a yellow powder which was collected by filtration at -78°C. Spectroscopic analysis reveals the presence of both $[H_4Ru_4(CO)_{12}]$ and $[H_2Ru_4(CO)_{13}]$ in a ratio of ca. 1:1.

I.R. (acetone): 2081(s), 2066(vs), 2062(s), 2030(m), 2025(s), 2011(w). Lit[60] 2081(s), 2067(vs), 2030(m), 2024(s), 2009(w)

^{1}H NMR (C_6D_6): -17.86 ppm ($[H_4Ru_4(CO)_{12}]$ integral ratio 2H), -18.69 ppm ($[H_2Ru_4(CO)_{13}]$ integral ratio 1H). Lit[60] -17.98 ppm

3.5 References

1. Taqui-Khan, M.M. *Platinum Metals Rev.,* 1991, **35,** 70.
2. Stainko, J.S., Chaipaymgpundu, S., *J. A. Chem. Soc.,* 1970, **92,** 5580.
3. Sundberg, R.S., Bryan, F.R., Taylor, I.F., Taube, H., *J. Am. Chem. Soc.,* 1974, **96,** 381.
4. Diamantis, A.A., Dubrawski, J.V. *Inorg. Chem.,* 1981, **20,** 1142.
5. Taqui-Khan, M.M., Halligudi, S.B., Shukla, S., *Angew. Chem., Int. Ed. Engl.,* 1988, **27,** 1734.
6. Siegbahn, P.E.M., Blomberg, M.R.A., Svensson, M., *J. Phys. Chem.,* **97,** 1993, 2564.
7. Fornies, J., Green, M., Spencer, J.L., Stone, F.G.A., *J. Chem. Soc., Dalton Trans.,* 1977, 1006.
8. Yoshida, T., Matsuda, T., Okano, T., Kitani, T., Otsuka, S., *J. Am. Chem. Soc.,* **101,** 1979, 2027.
9. Yoshida, T., Okano, T., Ueda, Y., Otsuka, S., *J. Am. Chem. Soc.,* **103,** 1981, 3411.
10. Yoshida, T., Okano, T., Otsuka, S., *J. Am. Chem. Soc.,* **102,** 1980, 5966.
11. Milstein, D., Calabrese, J.C., Williams, I.D., *J. Am. Chem. Soc.,* **108,** 1986, 6387.
12. Crabtree, R.H., In "Selective Hydrocarbon Activation: Principles and Progress". Eds; Davies, J.A., Watson, P.L., Greenberg, A., Liebman, J.F. VCH Publishers, New York, 1990; pp 1-18.
13. Yoon, M., Tyler, D.R., *J. Chem. Soc., Chem. Comm.,* 1997, 639.
14. Hillhouse, G.L., Bercaw, J.E., *J. Am. Chem. Soc.,* **106,** 1984, 5472.
15. Wilkinson, G., Birmingham, J.M., *J. Am. Chem. Soc.,* **76,** 1954, 4281.
16. Ford, P.C., Rokicki, A.J., *Adv. Organomet. Chem.,* **28,** 1988, 139.
17. Barratt, D.S., Cole-Hamilton, D.J., *J. Organomet. Chem.,* **306,** 1986, C41.
18. Rhodes, C., Hutchings, G.J., Ward, A.M., *Catal. Today,* **23,** 1995, 43.
19. Ishida, H., Koji, T., Morimoto, M., Tanaka, T., *Organometallics,* **5,** 1986, 724.
20. Heiber, W., Leutert, F., *Z. Anorg. Allg. Chem.,* **204,** 1932, 145.

21. Ungermann, C., Landis, V., Moya, S., Cohen, H, Walker, H., Pearson, R., Rinker, R., Ford, P.C., *J. Am. Chem. Soc.,* **101,** 1979, 5922.
22. Ford, P.C., Ungermann, C., Landis, V., Moya, S.A., Rinker, R.G., Laine, R.M., *ACS Adv. Chem. Ser.,* **173,** 1979, 81.
23. Ford, P.C., Rinker, R.G., Ungermann, C., Laine, R., Landis, V., Moya, S., *J. Am. Chem. Soc.,* **100,** 1978, 4595.
24. Frazier, C.C., Hanes, R.M., King, A.D., King, R.B., *Adv. Chem. Serv.,* 1979, **173,** 94.
25. King, A.D., King, R.B., Yang, D.B., *ACS Symp. Ser.* **152,** 1981, 107.
26. King, R.B., Frazier, C.C., Hanes, R.M., King, A.D., *J. Am. Chem. Soc.,* **100,** 1978, 2925.
27. Reppe, J.W., Reindl, E., *Leibigs Ann. Chem.,* **582,** 1953, 121.
28. Andreeva, D., Idakiev, V., Tabakova, T., Andreev, A., *J. Catal.,* **158,** 1996, 354.
29. Andreeva, D., Idakiev, V., Tabakova, T., Andreev, Giovanoli, R., *Appl. Catal.,* **134,** 1996, 275.
30. Sakurai, H., Ueda, A., Kobayashi, T., Haruta, M., *J. Chem. Soc., Chem. Comm.,* 1997, 271.
31. King, A.D., King, R.B., Yang, D.B., *J. Am. Chem. Soc.,* **102,** 1980, 1028.
32. Iwata, M., *Chem. Abstr.,* **70,** 1969, 76989.
33. Slegeir, W.A.R., Sapienza, R.S., Rayford, R., Lam, L., *Organometallics,* **1,** 1982, 1728.
34. Bricker, B.C., Nagel, C.C., Bhattacharyya, A.A., Shore, S.G., *J. Am. Chem. Soc.,* **107,** 1985, 377.
35. Ford, P.C., *Acc. Chem. Res.,* **14,** 1981, 31.
36 Keister, J.B., *J. Organomet. Chem.,* **190,** 1980, C36.
37. Dombek, B.D., Harrison, A.M., *J. Am. Chem. Soc.,* **105,** 1983, 2485.
38. Arndt, L., Delord, T., Darensbourg, M.Y., *J. Am. Chem. Soc.,* **106,** 1984, 456.
39. Fagan, P.J., Moloy, K.G., Marks, T.J., *J. Am. Chem. Soc.,* **103,** 1981, 6959 (and refs therein).
40. Bricker, J.C., Nagel, C.C., Shore, S.G., *J. Am. Chem. Soc.,* **104,** 1982, 1444.
41. Indian Patent # 170438, 14 March 1989.
42. Taqui Khan, M.M., Halligudi, S.B., Abdi, S.H.R., *J. Mol. Catal.,* **48,** 1988, 325.

43. Barrat, D.S., Glidewell, C., Cole-Hamilton, D.J., *J. Chem. Soc., Dalton Trans.,* 1988, 1079.

44. Tonner, S.P., Trimm, D.L., Wainwright, M.S., *J. Mol. Cat.,* 1983, **18,** 215.

45. Marsella, J.A., Pez, G.P., *J. Mol. Cat.,* 1986, **35,** 65.

46. Cole-Hamilton, D.J., Bruce, D.W., in 'Comprehensive Coordination Chemistry', ed. Wilkinson, G., Gillard, R.D., McCleverty, J.A., 1987, Pergamon Books Ltd., **6,** 488.

47. Anton, D.R., Crabtree, R.H., *Organometallics,* **2,** 1983, 855.

48. Shriver, D.F., "The Manipulation of Air Sensitive Compounds", McGraw-Hill, New York, 1969.

49. Mercer, E.E., Buckley, R.R. *Inorg. Chem.,* 1965, **4,** 1692.

50. Diamantis, A.A., Dubrawski, J.V. *Inorg. Chem.,* 1981, **20,** 1142.

51. Ezerskaya, N.A., Solovykh, T.P. *Zh. Neorg. Khim,* 1966, **11,** 1855.

52. Yoshida, T., Thorn, D.L., Okano, T., Otsuka, S., Ibers, J.A., *J. Am. Chem. Soc.,* 1980, **102,** 6451.

53. Foster, D.F., PhD. Thesis, 1985.

54. Cotton, F.A., Hanson, B.E., *Inorg. Chem.,* 1977, **16**, 3369.

55. Lavigne, G., Bonnet, J.J., *Inorg. Chem.,* **20,** 1981, 2713.

56. Cartwright, S., Clucas, J.A., Dawson, R.H., Foster, D.F., Harding, M.H., Smith, A.K.,*J. Organomet. Chem.,* 1986, **302** 403.

57. Bruce, M.L., Hambley, T.W., Nicholson, B.K., Snow, M.R., *J. Organomet. Chem.,* **235,** 1982, 83.

58. Inkrott, K.E., Shore, S.G., *J. Am. Chem. Soc.,* **100,** 1978, 3954.

59. Knight, J., Mays, M.J., *J. Chem. Soc., Dalton trans.,* 1972, 1022.

60. Knox, S.A.R., Koepke, J.W., Andrews, M.A., Kaesz, H.D., *J. Am. Chem. Soc.,* 1975, **97,** 3942.

CHAPTER 4

Attempted identification of active species, and mechanistic studies for the system employing $[Ru_3(CO)_{12}]$ as catalyst precursor

4.1. Introduction

We have shown that $[Ru_3(CO)_{12}]$ is an active precursor for the catalytic carbonylation of ammonia to urea. What is not evident from these observations is the actual identity of the catalytic species responsible for this reaction. It is important from a mechanistic perspective to try to identify this, and other species present in solution both prior to, during (by *in situ* analysis) and after reaction. This may also help us in understanding catalyst deactivation, which may be a problem in this system. For analysis of species before and after reaction, normal spectroscopic techniques are used such as IR, high-field ^1H NMR, and electrospray mass spectroscopy (ESMS, discussed in chapter 5). Chemical isolation can be useful and is normally achieved for negatively charged ruthenium clusters using a large counterion for ease of crystallisation, such as Ph_4As^+. The possible methods for *in situ* analysis include high temperature high pressure IR (HPIR), variable temperature, high pressure high field ^1H NMR (HPNMR), and hydrogen gas analysis by GC. In the studies to follow, HPIR utilises a Si rod mounted in such a way as to span the breadth of a Hastelloy autoclave. This provides a window of observation from ca. 1500 to 4000 cm^{-1} in the IR region of the electromagnetic spectrum, and is therefore particularly useful for the observation of metal-CO stretches. Knowledge of the charge on the complex can also be gained from such information; for example, considering only terminal carbonyl groups, neutral carbonyl cluster complexes commonly absorb in the region 2080-2000 cm^{-1}, for monoanions, this range is ca. 2050-1970 cm^{-1}, and for dianions, ca. 2030-1930 cm^{-1}. In negatively charged carbonyl complexes , the metal is able to back-bond more strongly to the CO groups than a neutral or positively charged complex. This decreases the strength of the bonding interaction in the CO group, which lengthens the bond and causes a relative decrease in the observed νCO.

When species which are present in post-catalytic and *in situ* reaction solutions have been identified, their relative activities can be compared by testing each species separately for activity. It is the nature of these cluster complexes that some of these species interconvert within solution. In these cases, it may then be necessary to devise an alternative strategy to study certain species independently from one another. For example, in the WGSR catalysed by $[Ru_3(CO)_{12}]$ in basic solution in which

$[HRu_3(CO)_{11}]^-$ and $[H_3Ru_4(CO)_{12}]^-$ (which is in equilibrium with $[HRu_3(CO)_{11}]^-$ and $[Ru_3(CO)_{12}]$ by the reaction shown in figure 4.1) were both implicated as possible active species, $[H_3Ru_4(CO)_{12}]^-$ was effectively removed from the system by removing H_2 with a palladium thimble[1]. This led to the discovery that $[H_3Ru_4(CO)_{12}]^-$ was playing only a minor role in the catalysis.

$$3[H_3Ru_4(CO)_{12}]^- + 9CO \rightleftharpoons 3[HRu_3(CO)_{11}]^- + Ru_3(CO)_{12} + 3H_2$$

Figure 4.1 Investigations of the WGSR in basic media.

Before we can begin a systematic analysis of possible clusters which may be present prior to, during, and after catalysis it is necessary to have some idea of the types of species we are looking for. The analogy between the carbonylation of ammonia and the WGSR catalysed by $[Ru_3(CO)_{12}]$ as precursor under basic conditions has been commented on in chapter 3, and since the postulated mechanisms have their similarities, it would not be surprising if several of the complexes present in both reactions were similar. Initial spectroscopic and kinetic studies upon the WGSR catalysed by $[Ru_3(CO)_{12}]$ under basic conditions showed that several trinuclear and tetranuclear carbonyl cluster complexes (principally $[H_3Ru_4(CO)_{12}]^-$ and $[HRu_3(CO)_{11}]^-$) were implicated in reaction[2]. These are listed in table 4.1 (together with some which are not implicated, but are related structurally and may be present under certain conditions of pH, and forcing conditions of temperature and pressure). The tetranuclear species $[H_2Ru_4(CO)_{12}]^{2-}$ has been proposed as a possible active intermediate in both the WGSR catalysed by $[Ru_3(CO)_{12}]$ as a precursor in the presence of 1,8-diazabicyclo[5.4.0]decene-7 (DBU)[3], and also in the reduction of benzaldehyde and nitrobenzene[4].

It is interesting to note that that $[Ru_3(CO)_{12}]$, $[H_3Ru_4(CO)_{12}]^-$ and $[HRu_3(CO)_{11}]^-$ have also been found to catalyse the carbonylation of cyclic amines, such as piperidine and morpholine to the corresponding formamides[5], so analogy with the WGSR under basic conditions already has its precedent for tri- and tetra-ruthenium carbonyl clusters in this reaction.

Table 4.1 Spectroscopic parameters for some common neutral and anionic tri- and tetra-ruthenium carbonyl clusters

Complex	ν(CO)/cm^{-1}	δ/ppm[a]	Solvent	Ref
$[Ru_3(CO)_{12}]$	2060(vs), 2030(s), 2010(m)[b]	-	-	6
$[HRu_3(CO)_{11}]^-$	2072(w), 2011(s), 1983(s),1949(sh), 1898(m),1730(vw)[c]	-12.9	-	7
$[Ru_3(CO)_{11}]^{2-}$	2012(m), 1980(m,sh), 1972(m,sh), 1952(s), 1935(s), 1887(m), 1755(w), 1675(w,br)[c]	-	-	8
$[H_2Ru_4(CO)_{13}]$	2080(vs), 2069(vs), 2055(vs), 2033(m), 2022(s), 2004(w), 1871(br)[d]	-18.6	$CDCl_3$	9
$[HRu_4(CO)_{13}]^-$	2018(s), 2001(s), 1975(m,sh), 1830(w,br)[e]	-15.54	CD_2Cl_2	10
$[Ru_4(CO)_{13}]^{2-}$	1954(s), 1915(m,sh), 1895(m), 1815(m), 1770(m), 1738(m,sh), 1718(s)[e]	-	-	10
$[H_4Ru_4(CO)_{12}]$	2081(s), 2067(vs), 2030(m), 2024(s), 2009(w)[c]	-17.98	$CDCl_3$	11
$[H_3Ru_4(CO)_{12}]^-$	2071(w), 2040(s), 2034(s), 2019(s), 2004(s), 1978(m),1950(w), 1932(m)[f]	-16.9	$(CD_3)_2(CO)$	12
$[H_2Ru_4(CO)_{12}]^{2-}$ (K_2 salt)	2028(w), 1998(s), 1960(vs), 1911(m), 1895(m,sh), 1817(w), 1770(w), 1742(m), 1719(m)[c]	-19.26	d^8-THF	13
$[H_2Ru_4(CO)_{12}]^{2-}$ $((Ph_3P)_2N)_2$ salt	2027(w), 1985(s), 1950(s), 1940(s), 1899(m), 1881(m), 1809(vw), 1763(m), 1753(m,sh)[c]	-	-	13
$[HRu_4(CO)_{12}]^{3-}$	1965(m,sh), 1942(s), 1880(w), 1730(vw,sh), 1710(w,br)[c]	-17.2	d^8-THF	8
$[Ru_4(CO)_{12}]^{4-}$	1980(s,sh), 1945(s), 1930(s), 1898(s), 1850(m,sh), 1745(m), 1710(m), 1660(w)[g]	-	-	8

[a]Relative to TMS [b]Cyclohexane [c]THF [d]*n*-heptane [e]dichloromethane [f]Acetone [g]acetonitrile

Some higher nuclearity clusters are listed in table 4.2. Thermal decompostion of $[Ru_3(CO)_{12}]$ gives $[Ru_6C(CO)_{17}]$[14] (initially thought to be $[Ru_6(CO)_{18}]$[15,16]). Reduction of $[Ru_3(CO)_{12}]$ by reaction in THF in the presence of $[Mn(CO)_5]^-$ gives the dianion

$[Ru_6(CO)_{18}]^{2-}$ which, after acidification gives $[HRu_6(CO)_{18}]^-$ (containing an intersitial hydrogen within the octahedral Ru_6 framework having δ = + 16.3 ppm[17]) and $[H_2Ru_6(CO)_{18}]$. Refluxing $[Ru_3(CO)_{12}]$ in a solution of diglyme for several hours in the presence of $[Mn(CO)_5]^-$ gives $[Ru_6C(CO)_{16}]^{2-}$ (which has also been shown to be produced as an inactive species in the hydrogenation of CO by ruthenium complexes with iodide promoters[18]) in high yield[19]. Stepwise protonation of $[Ru_6C(CO)_{16}]^{2-}$ at -30°C with H_2SO_4 in acetonitrile gives $[H_2Ru_6C(CO)_{16}]$[20]. The smaller carbido cluster $[Ru_5C(CO)_{15}]$ can be prepared by reaction of $[H_4Ru_4(CO)_{12}]$ under an ethane pressure of 10-12 bar at 130°C. This results in the production of a number of other complexes, also including $[Ru_6C(CO)_{17}]$[21].

Table 4.2 Some common high nuclearity ruthenium carbonyl clusters and spectroscopic parameters

Complex	**ν(CO)/cm^{-1}**	**δ/ppm[(a)]**	**Ref**
$[Ru_5C(CO)_{15}]$	2066(vs), 2034(s), 2016(m)[b]	-	21
$[Ru_6C(CO)_{17}]$	2064(s), 2049(s), 2007(w), 1993(w), 1958(w), 1854(w,br)[c]	-	22
$[H_2Ru_6(CO)_{18}]$	2060(s), 2054(s), 2008(m)[d]	-	23
$[HRu_6(CO)_{18}]^-$	2020(s), 1953(vw)[e]	+ 16.3	17
$[H_2Ru_6C(CO)_{16}]$	-	-15.71	20
$[Ru_6C(CO)_{16}]^{2-}$	2048(w), 2032(w), 1977(s), 1952(m,sh), 1918(m) 1820(m,sh), 1780(m)[e]	-	19

[a] Relative to TMS [b]cyclohexane [c]hexane [d]CCl_4 [e]CH_2Cl_2

Another class of ruthenium carbonyl cluster complexes are amides[24-26], the spectroscopic details of which are shown in table 4.3. These compounds can be prepared by reduction of $[HRu_3(CO)_{10}(\mu\text{-NO})]$ with molecular hydrogen in moist acetonitrile in low yield[24]. Alternatively, reduction of $[HRu_3(CO)_{10}(\mu\text{-NO})]$ with molecular hydrogen at 1000-2000 psig in heptane solution for 1-8 h results in the low yield of varying amounts of $[H_4Ru_4(CO)_{12}]$, $[H_2Ru_3(NH)(CO)_9]$ and $[HRu_4(NH_2)(CO)_{10}]$, which can be separated by liquid chromatography[25]. It is known, from work reported here, and also from personal correspondence[27] that ammonia can oxidatively add to

$[Ru_3(CO)_{12}]$ to produce both $[H_2Ru_3(NH)(CO)_9]$ and $[H_3Ru_4(NH_2)(CO)_{12}]$. To the best of our knowledge, there are no reports of identification and characterisation of the conjugate bases of these complexes (under the basic conditions of ammonia carbonylation, deprotonation is likely). This would make unequivocal assignment of these species difficult.

Table 4.3 Amide cluster carbonyl complexes.

Complex	**ν(CO)/cm^{-1} [(a)]**	**δ/ppm[b]**	**Solvent**	**Ref**
$[H_2Ru_3(NH)(CO)_9]$	2116(m), 2080(s), 2056(vs), 2046(s), 2012(s), 2002(s), 1989(m), 1975(vw), 1970(vw)	-17.49, 6.36	$CDCl_3$	25
$[H_3Ru_4(NH_2)(CO)_{12}]$	2103(vw), 2074(s), 2058(vs), 2020(sh), 2015(s), 2000(w)	-16.09, -1.08	$CDCl_3$	25
$[HRu_3(NH_2)(CO)_{10}]$	2103(w), 2067(s), 2052(s), 2026(s), 2012(s), 2005(s), 1996(w), 1987(w), 1969(vw)	2.74, 1.84, -13.88	$CDCl_3$	25

[a] hexane solution [b]Relative to TMS

4.2 Results and Discussion

4.2.1 Isolation of complexes pre- and post-reaction

Several reactions were conducted in an effort to isolate organometallic species which are present in solution at the end of reactions of carbonylation of ammonia in alcoholic solvents.

In the following reactions, the experimental of which are included with the results for clarity, isolation of reaction intermediates pre- and post-catalytic reaction in methanolic and ethanolic ammonia was attempted. The counterion used for this was Ph_4As^+ (a saturated solution of Ph_4AsCl in H_2O).

4.2.1.1 Preparation of samples derived from reactions conducted in methanolic ammonia

Sample **(I)**. A few crystals of $[Ru_3(CO)_{12}]$ were dissolved in methanolic ammonia (ca. 2 cm^3, 4.4 mol dm^{-3} in NH_3) under an atmosphere of Ar.

$[Ru_3(CO)_{12}]$ (0.648 g, 1.01 mmol) was dissolved in methanolic ammonia (60 cm^3, 4.4 mol dm^{-3} in NH_3) and stirred for 18 h under an atmosphere of Ar to give a red solution. Two 30 cm^3 portions were transferred *via* syringe into each of two steel autoclaves with internal volumes of 170 cm^3. Each autoclave was charged to a pressure of 2 bar CO and reacted with magnetic stirring at a temperature of 160°C for a period of 1 h. After cooling, the vessels were degassed and the contents of each transferred into the same side-arm Schlenk. This solution was treated with Ph_4AsCl (1.32 g, 3.1 mol equiv.) and filtered. The precipitated solid (sample **(II)**) was dissolved in acetone (20 cm^3). Further precipitation was induced by evaporation of the filtrate to ca 10 cm^3 *in vacuo*. The solid collected by filtration was also dissolved in acetone (20 cm^3), (sample **(III)**).

A small volume of the post-catalytic red solution (sample **(IV)**) had been transferred to a sample tube for analysis. This solution was analysed for urea content quantitatively by ^{13}C NMR and qualitatively by colorimetric reaction with diacetyl

monoxime and was found to contain urea corresponding to a total turnover of 2 mol urea per mol $[Ru_3(CO)_{12}]$ per hour.

4.2.1.2. Preparation of samples derived from reactions conducted in ethanolic ammonia

Sample **(V).** A few crystals of $[Ru_3(CO)_{12}]$ were dissolved in ethanolic ammonia (ca. 2 cm^3, 5.4 mol dm^{-3} in NH_3) under an atmosphere of Ar.

$[Ru_3(CO)_{12}]$ (0.487 g, 0.762 mmol) was dissolved in ethanolic ammonia (50 cm^3, 5.4 mol dm^{-3} in NH_3) by stirring overnight. The resulting red solution was transferred to an autoclave and charged with 2 bar of CO before heating to 160°C for a period of 1 h with magnetic stirring. The autoclave was cooled and degassed and the contents transferred to a side-arm Schlenk tube. Treatment with Ph_4AsCl (0.45 g, 1.14 mmol) in H_2O (ca. 2 cm^3) gave a yellow precipitate which was filtered and dissolved in acetone (ca. 20 cm^3, sample **(VI)**). The filtrate was also kept for analysis.

The raw solution retained after the reaction (sample **(VII)**) was analysed for urea content but was found to contain too small a quantity to be quantified by ^{13}C NMR.

For analysis of samples **(I)-(VII)** by ^1H NMR, the stock solutions (or raw sample solutions) were evaporated *in vacuo* to dryness and dissolved in d^6-acetone. IR analysis was performed on the prepared acetone stock solutions, or (in the case of raw sample solutions), the solutions were prepared by evaporation *in vacuo* to dryness followed by dissolving in acetone.

4.2.1.3 Results of chemical isolation experiments

Samples **(I)-(VII)** are samples of solutions from the reaction of $[Ru_3(CO)_{12}]$ in methanolic or ethanolic ammonia. ^1H NMR chemical shifts were noted for each species along with their IR absorption frequencies (table 4.4). We can see that prior to pressurisation with CO (Samples **(I)** and **(V)**), the primary species present in the solution is $[HRu_3(CO)_{11}]^-$. We have seen that this anion is implicated in the WGSR and is produced by the decarboxylation of a metallocarboxylic acid intermediate, however, it has also been prepared by the reaction of $[Ru_3(CO)_{12}]$ with reducing agents such as

$Na[BH_4]$[28] and KH[29]. In this case, the resulting salts can readily be converted back to $[Ru_3(CO)_{12}]$ under 1 atm CO at room temperature. For the analogous case, in the presence of ammonia, the anion is likely to be generated by initial nucleophilic attack of NH_3 on coordinated carbonyl, and, by analogy with the WGSR, by subsequent β-hydrogen abstraction of the resulting carbamoyl complex (see figure 4.2), to yield isocyanic acid and $[HRu_3(CO)_{11}]^-$.

Table 4.4 ^1H NMR and ν(CO) (cm^{-1}) for samples (I)-(VII)

Sample	**δ/ ppm[(a)]**	**ν(CO)[(b)]/ cm^{-1}**	**assignments**
(I)	-11.01(m), -12.65(s)[c]	2074(w), 2047(m), 2017(s), 1991(s), 1954(m)	$[HRu_3(CO)_{11}]^-$, [amide complex]$^-$
(II)	-19.01	2030(m), 1988(s), 1977(vs,br), 1955(vs), 1945(s,sh), 1920(m), 1906(s), 1888(m)	$[H_2Ru_4(CO)_{12}]^{2-}$ and another dianion
(III)	-16.88	2073(w), 2057(w), 2016(s), 1989(s) 1970(s,sh), 1952(vs), 1907(w)	$[H_3Ru_4(CO)_{12}]^-$
(IV)	-10.30(s), -10.47(m), -12.37(m), -19.04(m)	2073(w), 2050(m,sh), 2030(s,sh), 2016(s), 1988(s), 1977(s), 1951(s)	$[HRu_3(CO)_{11}]^-$, [amide complexes]$^-$, $[H_2Ru_4(CO)_{12}]^{2-}$
(V)	-10.47(w), -10.61(w), -12.39(s), -15.53(w)	2086(sh) 2075(sh) 2061(s), 2025(s,sh), 2015(vs), 1990(vs), 1953(s)	$[HRu_3(CO)_{11}]^-$, [amide complexes]$^-$
(VI)	-19.16	2030(m), 2016(w), 1989(vs), 1975(s,sh), 1956(vs), 1947(vs), 1905(s), 1887(m), 1880(m,sh)	$[H_2Ru_4(CO)_{12}]^{2-}$ and another dianion
(VII)	-10.43(w), -10.56(w), -12.53(s), -19.17(s)	2074(w), 2040(s,sh), 2016(vs), 2001(s), 1989(s), 1952(vs), 1930(s,sh)	$[HRu_3(CO)_{11}]^-$, [amide complexes]$^-$ $[H_2Ru_4(CO)_{12}]^{2-}$

[a] d^6 acetone, δ recorded relative to $(CH_3)_2CO$. Signs in parenthesis indicates relative strength of signal [b] Spectrum recorded in $(CH_3)_2CO$.

We also observe the presence of other resonances at slightly lower field (-10 - -11 ppm) in the ^1H NMR, most notably in the case where ethanol is solvent, and to a lesser extent where methanol is solvent. The IR of sample **(I)** shows mainly the presence of bands attributable to $[HRu_3(CO)_{11}]^-$, together with an unassigned signal at 2047 cm^{-1}, however, for sample **(V)**, the presence of several other stretches at 2086,

2061 and 2025 cm^{-1} and a signal which is stronger than that normally associated with $[HRu_3(CO)_{11}]^-$ at 1953 cm^{-1} provides evidence for the presence of at least one other species. IR evidence by itself suggests that a neutral species such as $[H_4Ru_4(CO)_{12}]$, or $[H_2Ru_3(CO)_{13}]$ may be responsible for these signals, however, these would be seen prominently in the ^1H NMR. We therefore propose that anionic amide carbonyl cluster complexes of ruthenium (such as the conjugate bases of the species in table 4.3) are also present in these pre-catalytic reaction solutions. This assignment is made mainly on the basis of evidence which will be presented in chapter 5, in discussion of the eletrospray mass spectra performed upon similar solutions.

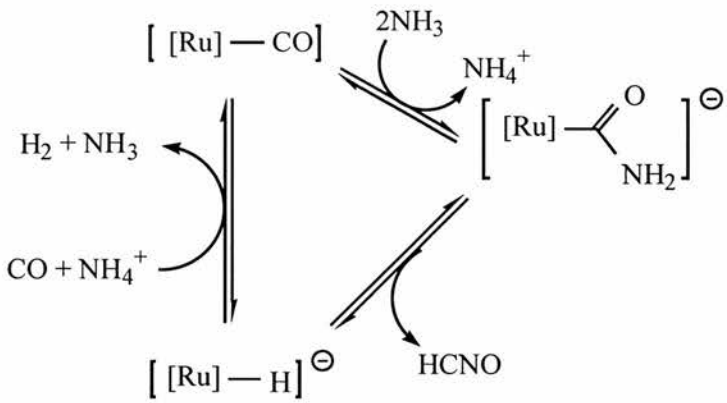

Figure 4.2 Initial production of $[HRu_3(CO)_{11}]^-$ in alcoholic ammonia solution

The salts which were precipitated from the solutions (sample **(II)** (methanol), sample **(VI)** (ethanol)) *appear* to contain only the dianionic cluster $[H_2Ru_4(CO)_{12}]^{2-}$ by ^1H NMR, however, the presence of several other stretches in the IR (especially at 1977 cm^{-1}) suggests that there is at least one other dianionic species present. This could be the conjugate base of $[HRu_3(CO)_{11}]^-$, ($[Ru_3(CO)_{11}]^{2-}$), but the IR does not fit accurately enough for this to be the case. We therefore propose (tentatively) that this other species is the higher nuclearity cluster dianion $[Ru_6C(CO)_{16}]^{2-}$.

It should be noted that the predominant species present at the end of the reaction (samples **(IV)** and **(VII)**) are those which were also present at the beginning of the reaction; $[HRu_3(CO)_{11}]^-$ and the postulated anionic amide carbonyl cluster complex.

4.2.1.4 Experiment conducted in methanolic ammonia under ambient conditions of temperature and CO pressure

In a separate experiment, $[Ru_3(CO)_{12}]$ (0.510 g, 0.80 mmol) was stirred under CO at atmospheric pressure and at room temperature in methanolic ammonia (30 cm^3 7.4 mol dm^{-3}). After several hours, the reaction mixture was evaporated to dryness *in vacuo* and some of the residue was dissolved in CD_2Cl_2. ^1H NMR revealed the presence of two hydride resonances (δ = -17.04 ppm, δ = -17.76 ppm; referenced to CH_2Cl_2), the larger of which (δ = -17.04 ppm) together with a broad low-field signal (+5.94 ppm) was assigned to $[H_2Ru_3(NH)(CO)_9]$. This assignment is also supported by IR analysis upon the evaporated residue in a nujol mull (ν(CO, cm^{-1}) = 2112(m), 2060(vs,br), 2016(vs,br)). Orange crystals were collected after recrystallisation from CH_2Cl_2. ^1H NMR (-17.76 ppm, referenced to CH_2Cl_2) and IR ((in CH_2Cl_2) ν(CO, cm^{-1}) = 2081(s), 2065(vs), 2029(m,sh), 2023(s), 2007(w,sh)) analysis performed upon these crystals unequivocally identified this species to be $[H_4Ru_4(CO)_{12}]$.

4.2.2 High Pressure Infra-Red (HPIR)

HPIR experiments were conducted on several systems. Two different solvents for ammonia were employed, methanol and 2-methoxyethanol. Different charging pressures were employed for the reactions in methanol. In each case, a summary of the reaction conditions is given together with an account of possible explanations of CO stretches. With the benefit of hind-sight, we will be able to compare these results with those in section 4.2.1.

4.2.2.1 Methanolic ammonia (p_{CO} = 5 bar, $[NH_3]$ = 7.4 mol dm^{-3})

$[Ru_3(CO)_{12}]$ (0.193 g, 0.3 mmol) was weighed into a side-arm Schlenk tube and dissolved in methanolic ammonia (10 cm^3, 7.4 mol dm^{-3} in NH_3). The red solution was transferred under Ar to the HPIR autoclave. This was charged to 5 bar CO and heated gradually to 160°C. Spectra recorded for this sample are summarised in table 4.5. Initially at 25°C and with only Ar pressure, the IR spectrum has been attributed to

Table 4.5

T/°C	ν(CO)/ cm^{-1}	assignment
25 (without CO charging)	2074(w), 2047(m), 2017(vs), 1991(s), 1967(w), 1954(m)	$[HRu_3(CO)_{11}]^-$ and possibly [amide complex]$^-$
25	2073(vw), 2047(w), 2017(vs), 1991(vs), 1967(w), 1955(m)	$[HRu_3(CO)_{11}]^-$ and possibly [amide complex]$^-$
60	2051(w), 2017(vs), 1991(vs), 1956(s)	$[HRu_3(CO)_{11}]^-$
85	2035(w), 2017(vs), 1992(vs), 1988(sh), 1966(w), 1957(m)	$[HRu_3(CO)_{11}]^-$
105	2035(m), 2017(s), 1992(s), 1989(s), 1966(m), 1957(s)	$[HRu_3(CO)_{11}]^-$ and dianionic species
125	2035(m), 2017(m), 2007(w,sh), 1992(m), 1988(m), 1956(s)	$[HRu_3(CO)_{11}]^-$ and dianionic species
145	2031(s), 1992(w), 1966(s,sh), 1954(vs), 1943(m)	$[HRu_3(CO)_{11}]^-$ (very weak) and dianionic species
160	2029(m), 1992(m), 1946(vs,br), 1720(vs,br)	dianionic species

$[HRu_3(CO)_{11}]^-$ on account of the remarkable likeness to an authentic sample (see figure 4.3), however, the bands at 2047 cm^{-1} and 1967 cm^{-1} cannot be assigned to any complex at present. It could be that they are due to deprotonation of an amide (such as one postulated in section 4.2.1) complex formed by oxidative addition of ammonia to $[Ru_3(CO)_{12}]$. This hypothesis is also supported by results obtained which are discussed in chapter 5. After pressurisation with CO at 25°C, there is no change in the IR stretches. On heating gradually to 105°C, we see that the band at 2047 cm^{-1} disappears and is replaced by a stretch at 2034 cm^{-1}. Additionally, a peak at 1989 cm^{-1} has become more prominent, the stretches which are attributable to $[HRu_3(CO)_{11}]^-$ have become weaker, and, by the time the temperature has reached 145°C, these bands have disappeared altogether. At this temperature, and at 160°C, the strongest bands in the spectrum are those at 2031 and 1955 cm^{-1}. These are in fact very similar to the frequencies which would be expected from the conjugate base of $[HRu_3(CO)_{11}]^-$, ($[Ru_3(CO)_{11}]^{2-}$), or another dianion such as $[Ru_4(CO)_{13}]^{2-}$, $[H_2Ru_4(CO)_{12}]^{2-}$, or even the higher nuclearity cluster $[Ru_6C(CO)_{16}]^{2-}$, proposed as having been observed during isolation of post-catalytic reaction species. Unequivocal identification of this species is not possible given the very broad and ill-defined spectrum at this temperature.

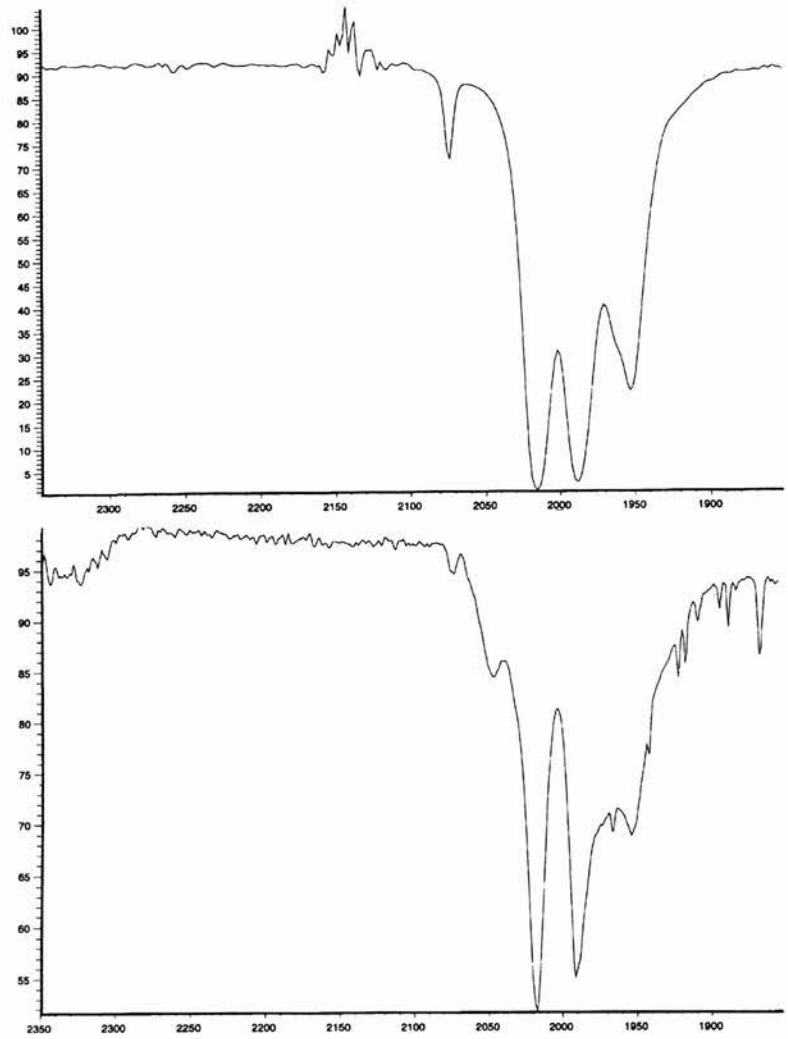

Figure 4.3 Comparison of I.R between HPIR expt and authentic $[HRu_3(CO)_{11}]^-$

4.2.2.2 Methanolic ammonia (p_{CO} = 15 bar, $[NH_3]$ = 1.6 mol dm^{-3})

$[Ru_3(CO)_{12}]$ (0.093 g, 0.15 mmol) was weighed into a side-arm Schlenk tube and dissolved overnight in methanolic ammonia (10 cm^3, 1.6 mol dm^{-3} in NH_3). The red solution was transferred under Ar to the HPIR autoclave. This was charged to 15 bar CO and heated gradually to 160°C. The spectra obtained for this sample are summarised in table 4.6. Initially, at 25°C after charging with CO, we see bands which are attributable to $[Ru_3(CO)_{12}]$ and $[HRu_3(CO)_{11}]^-$ which is to be expected by analogy with the WGSR. However, the presence of a band at extremely low frequency (for a neutral, or even most monoanionic species) is observed at 1934 cm^{-1}. At a temperature of 80°C, a similar spectrum is seen, however, a strong stretch at 1925 cm^{-1} is also present. We suggest it is possible that the signals at 1934 and 1925 cm^{-1} are due to the

presence of $[Ru_3(CO)_{11}]^{2-}$, and that the three species $[Ru_3(CO)_{12}]$, $[HRu_3(CO)_{11}]^-$ and $[Ru_3(CO)_{11}]^{2-}$ co-exist in equilibrium. As the temperature of the reaction is increased, there is no great change in the appearance of the spectra except that the bands that have been attributed to $[Ru_3(CO)_{11}]^{2-}$ have become stronger than those observed for species $[Ru_3(CO)_{12}]$ and $[HRu_3(CO)_{11}]^-$. The appearance of a stretch at 1720 cm^{-1} can be attributed to an organic carbonyl group, possibly methyl formate, or formamide.

These results are supported by ^1H NMR experiments performed upon the evaporated residue from the crude reaction solution (in CD_2Cl_2 referenced to CH_2Cl_2) which show that $[HRu_3(CO)_{11}]^-$ is the predominant species present (δ = -12.90 ppm), together with much smaller amounts of what could conceivably be $[H_3Ru_4(CO)_{12}]^-$ (δ = -17.12 ppm), however, the presence of a small broad signal at 6.2 ppm suggests that this could also be due to $[H_2Ru_3(NH)(CO)_9]$. Much smaller signals observed at -16.05 and -11.46 ppm have tentatively been assigned to $[H_3Ru_4(NH_2)(CO)_{12}]$ and its conjugate base $[H_2Ru_4(NH_2)(CO)_{12}]^-$. Urea was not observed to be a product of this reaction.

Table 4.6

T/°C	ν(CO)/ cm^{-1}	assignment
25	2055(s), 2030(m), 2026(m), 1986(vs), 1964(s,sh), 1934(m,sh)	$[Ru_3(CO)_{12}]$, $[HRu_3(CO)_{11}]^-$ and $[Ru_3(CO)_{12}]^{2-}$
80	2060(m), 2017(m,sh), 1986(vs), 1957(s), 1927(s)	$[Ru_3(CO)_{12}]$, $[HRu_3(CO)_{11}]^-$ and $[Ru_3(CO)_{12}]^{2-}$
100	2058(w), 2017(m), 1990(s), 1960(s), 1922(vs)	$[Ru_3(CO)_{12}]$, $[HRu_3(CO)_{11}]^-$ and $[Ru_3(CO)_{12}]^{2-}$
120	2058(m), 2017(s), 1991(vs), 1960(s), 1925(vs)	$[Ru_3(CO)_{12}]$, $[HRu_3(CO)_{11}]^-$ and $[Ru_3(CO)_{12}]^{2-}$
140	2058(m), 2020(s), 1991(vs), 1961(s), 1925(vs),	$[Ru_3(CO)_{12}]$, $[HRu_3(CO)_{11}]^-$ and $[Ru_3(CO)_{12}]^{2-}$
160	2058(m), 2017(s), 1990(vs), 1928(s)	$[Ru_3(CO)_{12}]$, $[HRu_3(CO)_{11}]^-$ and $[Ru_3(CO)_{12}]^{2-}$
80 (after cooling)	2058(m), 2020(s), 1991(vs), 1928(s), 1704(m)	$[Ru_3(CO)_{12}]$, $[HRu_3(CO)_{11}]^-$ and $[Ru_3(CO)_{12}]^{2-}$

4.2.2.3 Methanolic ammonia (p_{CO} = 16 bar, $[NH_3]$ = 4.6 mol dm^{-3})

$[Ru_3(CO)_{12}]$ (0.090 g, 0.14 mmol) was weighed into a side-arm Schlenk tube and dissolved overnight in methanolic ammonia (12 cm^3, 4.6 mol dm^{-3} in NH_3). The red solution was transferred under Ar to the HPIR autoclave. This was charged to 16 bar CO and heated gradually to 160°C. A summary of the spectra obtained during this heating process are summarised in table 4.7. These spectra have very similar stretching frequencies, and also similar strengths to those reported in section 4.2.2.2. This may be expected as the conditions are very similar except that the concentration of ammonia in this experiment is higher than that for the experiment reported in section 4.2.2.2. For this reason, the same assignments to catalytic species have been made, and the same conclusions are drawn.

Urea was identified as a product of this reaction by ^{13}C NMR, and was found to have a turnover frequency of approximately 0.53 per mol $[Ru_3(CO)_{12}]$ per h.

Table 4.7

T/°C	ν(CO)/ cm^{-1}	assignment
25	2060(m,sh) 2045(s,sh), 2040(s), 2020(m, sh), 1964(vs,br), 1924(s,sh)	$[Ru_3(CO)_{12}]$, $[HRu_3(CO)_{11}]^-$ and $[Ru_3(CO)_{12}]^{2-}$
80	2043(m), 2017(s), 1995(s,sh), 1957(s), 1919(vs)	$[Ru_3(CO)_{12}]$, $[HRu_3(CO)_{11}]^-$ and $[Ru_3(CO)_{12}]^{2-}$
100	2043(m,sh), 2020(s), 1990(s,sh), 1958(s), 1920(vs)	$[Ru_3(CO)_{12}]$, $[HRu_3(CO)_{11}]^-$ and $[Ru_3(CO)_{12}]^{2-}$
120	2043(m,sh), 2020(s), 1991(s,sh), 1958(s), 1920(vs)	$[Ru_3(CO)_{12}]$, $[HRu_3(CO)_{11}]^-$ and $[Ru_3(CO)_{12}]^{2-}$
140	2060(m,sh), 2020(s), 1990(s,sh), 1960(s), 1919(vs)	$[Ru_3(CO)_{12}]$, $[HRu_3(CO)_{11}]^-$ and $[Ru_3(CO)_{12}]^{2-}$
160	2060(m,sh), 2019(s), 1960(s), 1920(vs)	$[Ru_3(CO)_{12}]$, $[HRu_3(CO)_{11}]^-$ and $[Ru_3(CO)_{12}]^{2-}$

4.2.2.4 Ammonia/ 2-methoxyethanol solution (p_{CO} = 4.0 bar, $[NH_3]$ = 1.0 mol dm^{-3})

$[Ru_3(CO)_{12}]$ (0.112 g, 0.18 mmol) was weighed into a side-arm Schlenk tube and dissolved overnight in a solution of ammonia in 2-methoxyethanol (12 cm^3, ca.1.0 mol dm^{-3} in NH_3). The cherry-red solution was transferred under Ar to the HPIR autoclave and charged to 4 bar CO. The autoclave was gradually heated to 140°C. A summary of the spectra obtained during this heating process can be observed in table 4.8. The primary general observation from these experiments is that the appearance of the spectra do not change very much from one temperature to another, the major difference being that the stretch at ca. 1955 cm^{-1} becomes slightly more prominent throughout the course of heating to 140°C, and, on cooling back to room temperature, this stretch remains slightly stronger. We suggest that these observations are a result of an initial species (probably $[HRu_3(CO)_{11}]^-$) being deprotonated under forcing conditions of temperature to its conjugate base ($[Ru_3(CO)_{11}]^{2-}$). Since the spectra do not change significantly, all assignments are made to these two species. This hypothesis is supported once again by an ^1H NMR experiment performed upon the residue which had been dried *in vacuo* and redissolved in CD_2Cl_2. As was observed in experiment 4.b., hydride resonances could be seen (referenced to CH_2Cl_2) at δ = -12.90 ppm ($[HRu_3(CO)_{11}]^-$), together which a much smaller signal at δ = -17.12 ppm ($[H_2Ru_3(NH)(CO)_9]$ or $[H_3Ru_4(CO)_{12}]^-$) and very small resonances at δ = -16.06 ppm ($[H_3Ru_4(NH_2)(CO)_{12}]$, and δ = -11.46 ppm (the conjugate base of $[H_3Ru_4(NH_2)(CO)_{12}]$, $[H_2Ru_4(NH_2)(CO)_{12}]^-$). Urea could not be detected by ^{13}C NMR, and hydrogen analysis upon the gas at the end of the experiment after cooling suggested a total turnover of approximately 1 per mol $[Ru_3(CO)_{12}]$, however, this could be due to the WGSR.

Table 4.8

T/°C	ν(CO)/ cm^{-1}	assignment
25	2046(vw), 2013(vs), 1988(s), 1969(m,sh), 1952(m)	$[HRu_3(CO)_{11}]^-$,$[Ru_3(CO)_{11}]^{2-}$
80	2075(vw), 2046(w), 2017(vs), 1989(s), 1955(m,br)	$[HRu_3(CO)_{11}]^-$,$[Ru_3(CO)_{11}]^{2-}$
100	2075(vw), 2049(vw), 2017(vs), 1989(s), 1955(m,br)	$[HRu_3(CO)_{11}]^-$,$[Ru_3(CO)_{11}]^{2-}$
120	2075(vw), 2046(vw,sh), 2014(s), 1989(s), 1957(m, br)	$[HRu_3(CO)_{11}]^-$,$[Ru_3(CO)_{11}]^{2-}$
140	2075(vw), 2017(vs), 1986(s), 1957(m)	$[HRu_3(CO)_{11}]^-$,$[Ru_3(CO)_{11}]^{2-}$
80 (after cooling)	2075(w), 2045(w,sh), 2017(s), 2000(m,sh), 1988(s), 1955(w)	$[HRu_3(CO)_{11}]^-$,$[Ru_3(CO)_{11}]^{2-}$

4.3 Conclusions

HPIR analysis and ^1H NMR of isolated species has revealed that $[HRu_3(CO)_{11}]^-$ probably plays a major role in the catalytic reaction to carbonylate ammonia to urea under relatively low pressures (2-20 bar) and at mild temperatures (130-170°C) in methanolic or ethanolic solutions. This conclusion is supported by the observation that $[HRu_3(CO)_{11}][Et_4N]$ employed as catalyst precursor has significant ability to catalyse this reaction, comparable with the activity of $[Ru_3(CO)_{12}]$. The suggested presence of large concentrations of dianionic species present in reaction solutions (identified by HPIR) during heating, and especially prevalent at temperatures at which this system becomes active (120-160°C) probably have a debilitating impact upon the reaction. $[H_2Ru_4(CO)_{12}]^{2-}$ has been identified by ^1H NMR experiments conducted upon post-catalytic reaction solutions, and $[Ru_6C(CO)_{16}]^{2-}$ and $[Ru_3(CO)_{11}]^{2-}$ have been tentatively suggested as intermediates on the basis of HPIR results, and also IR upon post-catalytic reaction solutions. Although dianionic ruthenium cluster species have been implicated in catalysis of homogeneous reactions in the past[3,4], these reports have not been supported by hard mechanistic evidence that a mono-anionic complex is not actually responsible for the catalytic activity, however, in this case, it is extremely unlikely that the carbon atoms of carbonyl groups in a dianionic ruthenium cluster will be sufficiently electrophilic as to promote nucleophilic attack by ammonia.

We also believe it is possible (from reactions performed in methanol under ambient conditions of temperature and CO pressure, and in 2-methoxyethanol under elevated conditions of temperature and pressure) that products of oxidative addition of NH_3 to $[Ru_3(CO)_{12}]$ are present in reaction solutions as anions. The observation of these species is unprecedented until now.

We propose a mechanism for the carbonylation of ammonia to urea (figure 4.4) incorporating $[HRu_3(CO)_{11}]^-$ as the major active species.

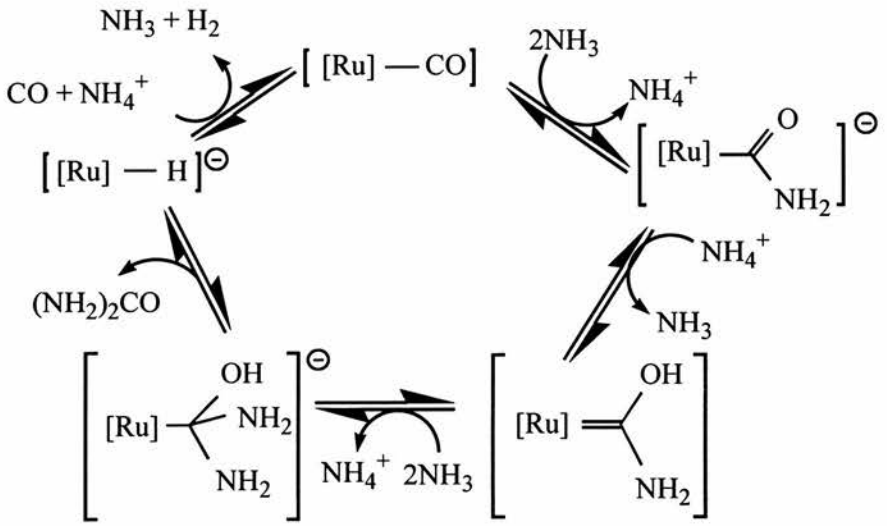

[Ru] = $[Ru_3(CO)_{11}]$

Figure 4.4 Proposed mechanism of carbonylation of ammonia to urea using $[Ru_3(CO)_{12}]$ as catalyst precursor

4.4 Experimental

4.4.1 High Pressure Infra Red reaction monitoring: General procedure

The HPIR cell used for the reactions described was a cylindrical internal reflectance cell (CIR) produced by SpectraTech. The rod material that was used was silicon with a cut off for IR transmission at 1500 cm^{-1}. The autoclave body was manufactured from Hastelloy C alloy. A diagramatic representation of the HPIR cell is shown in figure 4.5.

When the reaction solution had been transferred anaeorobically into the cell, the cell was closed and pressurised with CO at ca. 2 bar min^{-1}. Heating rods were inserted into the ports before the cell was mounted into the focusing mirror stage and the whole assembly was placed directly into the path of the IR beam. A thermocouple was placed into the thermocouple port and the cell heated to the required temperature. On completion of the reaction, the cell was allowed to cool to room temperature before slowly being vented to the atmosphere.

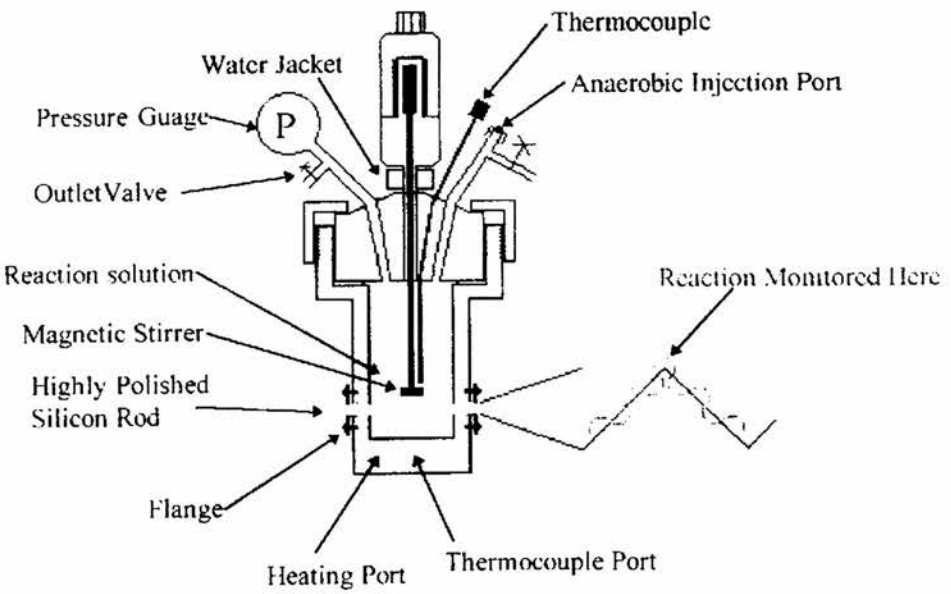

Figure 4.5 Schematic diagram of HPIR cell

The reaction is monitored by IR at the surface of the silicon rod as the IR beam is transmitted through the rod *via* internal reflection.

Apparatus

The employment of standard Schlenk procedures[30] was maintained throughout the preparation of samples and in the handling of post-catalytic reaction solutions.
^{1}H NMR and $^{31}P\{^{1}H\}$ NMR were recorded on a Varian Gemini 2000 machine, and $^{13}C\{^{1}H\}$ NMR were recorded on a Brucker AM 3000 spectrometer.
FTIR were recorded either on a Nicolet Protégé 460 Magna - IR Technology machine, or a PE 1710 IR Fourier Transform Spectrometer.

Chemicals

$[Ru_3(CO)_{12}]$ was obtained from Strem Chemical Co. and used as received. All other chemicals were obtained from commercial sources and used as received. Methanol and ethanol were dried over $Mg(OMe)_2$ and $Mg(OEt)_2$ respectively prior to use. Reaction grade acetone was obtained from Fisons Chemicals and distilled over CaH_2 prior to use. Methanol, 2-methoxyethanol and ethanol were dried and distilled over magnesium turnings activated with iodine.

Deuteroacetone was obtained from Aldrich Chemicals Ltd, and was degassed by a triple freeze-pump-thaw cycle and dried over 4A molecular seives prior to use.

For the preparation of solutions of ammonia in methanol and ethanol, a known mass of alcoholic solvent was pre-weighed into a side-arm Schlenk and allowed to cool in icy water under Ar. NH_3 was bubbled slowly through the solution for several hours. Upon re-weighing, the mass of NH_3 absorbed, and hence the molarity of the solution in NH_3 could be evaluated.

4.4 References

1. Bricker, J.C., Nagel, C.C., Bhattacharyya, A.A., Shore, S.G., *J. Am. Chem. Soc.,* **107,** 1985, 377.
2. Ungermann, C., landis, V., Moya, S., Cohen, H., Walker, H., Pearson, R., Rinker, R., Ford, P.C., *J. Am. Chem. Soc.,* **101,** 1979, 5922.
3. Wada, F., Shimuta, M., Goto, T., Ikeda, T., Kikukawa, K., Matsuda, T., *Chem. Lett.,* 1983, 1837.
4. Wada, F., Shimuta, M., matsuda, T., *Bull. Chem. Soc. Japan,* **62,** 1989, 2709.
5. Suss-Fink, G., Langenbahn, M., Jenke, T., *J. Organomet. Chem.,* **368,** 1989, 103.
6. Candlin, J.P., Shortland, A.C., *J. Organomet. Chem.,* 1969, **16,** 289.
7. Knight, J., Mays, M.J., *J. Chem. Soc., Dalton trans.,* 1972, 1022.
8. Bhattacharyya, A.A., Nagel, C.C., Shore, S.G., *Organometallics,* **2,** 1983, 1187.
9. Eady, C.R., Johnson, B.F.G., Lewis, J., *J. Chem. Soc., Dalton Trans.,* 1977, 477.
10. Nagel, C.C., Shore, S.G., *J. Chem. Soc., Chem. Comm.,* 1980, 530.
11 Knox, S.A.R., Koepke, J.W., Andrews, M.A., Kaesz, H.D., *J. Am. Chem. Soc.,* 1975, **97,** 3942.
12. Koepke, J.W., Johnson, J.R., Knox, S.A.R., Kaesz, H.D., *J. Am. Chem.Soc.,* 1975, **97**, 3947.
13. Inkrott, K.E., Shore, S.G., *Inorg. Chem.,* **18,** 1979, 2817.
14. Johnson, B.F.G., Johnston, R.D., Lewis, J., *J. Chem. Soc., Chem. Comm.,* 1967, 1057.
15. Piacenti, F., Bianchi, M., Benedetti, E., *J. Chem. Soc., Chem. Comm.,*1967, 775.
16. Sirigu, A., Bianchi, M., Benedetti, *J. Chem. Soc., Chem. Comm.,* 1969, 596.
17. Eady, C.R., Jackson, P.F., Johnson, B.F.G., Lewis, J., Malatesta, M.C., McPartlin, M., Nelson, J.H., *J. Chem. Soc., Dalton Trans.,* 1980, 383.
18. Dombek, B.D., *J. Organomet. Chem.,* 1983, **250,** 467.
19. Bradley, J.S., Ansell, G.B., Hill, E.W., *J. Organomet. Chem.,* **184,** 1980, C33.

20. Johnson, B.F.G., Lewis, J., Sankey, S.W., Wong, K., McPartlin, M., Nelson, W.J.H., *J. Organomet. Chem.,* **191,** 1980, C3.

21. Eady, C.R., Johnson, B.F.G., Lewis, J., Matheson, T., *J. Organomet. Chem.,* **73,** 1973, C82.

22. Johnson, B.F.G., Johnston, R.D., Lewis, J., *J. Chem. Soc., A,* 1968, 2865.

23. Churchill, M.R., Wormald, J., Knight, J., Mays, M.J., *J. Chem. Soc., Chem. Comm.,* 1970, 458.

24. Johnson, B.F.G., Lewis, J., Mace, J.M., *J. Chem. Comm.,* 1984, 186.

25. Smieja, J.A., Stevens, R.E., Fjare, D.E., Gladfelter, W.L., *Inorg. Chem.,* 1985, **24,** 3206.

26. Fjare, D.E., Keyes, D.G., Gladfelter, W.L., *J. Organomet. Chem.,* 1983, **250,** 383.

27. Johnson, B.F.G., Personal correspondence.

28. Johnson, B.F.G., Lewis, J., Raithby, P.R., Suss, G., *J. Chem. Soc., Dalton Trans.,* 1979, 1356.

29. Bricker, J.C., Nagel, C.C., Shore, S.G., *J. Am. Chem. Soc.,* **104,** 1982, 1444.

30. Shriver, D.F., "The Manipulation of Air Sensitive Compounds", McGraw-Hill, New York, 1969.

CHAPTER 5

Electrospray Mass Spectroscopy as a tool for the direct observation of anionic ruthenium clusters present in solution after catalysis of ammonia carbonylation to urea.

5.1 Introduction

5.1.1 An overview of ionisation techniques in mass spectroscopy

Classical techniques for achieving ionisation in mass spectroscopy such as electron impact (EI) and chemical ionisation (CI) involve vaporisation of the sample as a prerequisite. The ionisation mechanisms (direct interaction with high energy electrons (EI) or ions (CI)) generally lead to extensive fragmentation and a molecular ion is only rarely observed. The study of thermally unstable, involatile or large molecules is not possible using these techniques.

Softer ionisation techniques such as plasma desorption (PD), fast atom bombardment (FAB) and secondary ion mass spectrometry (SIMS) have been developed which give more structural information about large organic and organometallic molecules. These are examples of desorption techniques whereby ions are obtained directly from the condensed state (solid or liquid). In FAB mass spectroscopy (FABMS) the sample is mixed with an involatile matrix (e.g. glycerol). Desorption of molecules or ions (in the case of a pre-existing ionic sample) to the gas phase is achieved by bombarding the sample with high energy neutral atoms, typically argon. FABMS has received much attention over the years as a good method for analysis of diverse systems and has been used to good effect recently in the characterisation of a number of anionic ruthenium carbonyl cluster complexes[1]. Relatively intense parent species were observed for all species examined and sequential loss of CO was found to be the most predominant fragmentation process. However, this report seems to be one of the few cases of negative ion FABMS being used to probe anionic ruthenium carbonyl clusters, and historically identification is performed using classical spectroscopic techniques such as multinuclear NMR and IR.

Direct injection methods were essentially borne out of a necessity to develop ways of improving liquid chromatography mass spectroscopy (LCMS). The fundamental problem associated with LCMS in the past stems from the fact that the vacuum system of a regular mass spectrometer is unable to cope with the full solvent vapour of evaporated eluent resulting from the high flow rates of conventional liquid chromatography. Electrospray is now a common interface for LCMS and the

mechanism of this technique is described in some detail in section 2.2. Thermospray presents another commercially available solution to this problem. Sample solution containing a volatile electrolyte (e.g. $NH_4(CO_2CH_3)$) is injected through a heated capillary into an ion source evacuated with a pumping line opposite the capillary. The supersonic jet of droplets produced is subject to rapid evaporation during their period of travel through the heated source, and ions are ejected when the droplets become too small to contain their charge due to repulsive electrostatic forces. Most ions are produced in one of two ways, either *in situ*, by direct evaporation of solvent from a sample ion[2] (as in electrospray) or by gas phase reaction of a sample molecule (or ion) with an ion of electrolyte, itself ejected from a droplet. Ions are sampled through a conical exit aperture in the mass analyser. There is an analogy with CI in the second of these ionisation mechanisms, and ions can be generated under CI conditions by turning on an external filament when insufficient ions are produced under normal thermospray conditions. A schematic view of a thermospray LCMS interface is shown in figure 5.1.

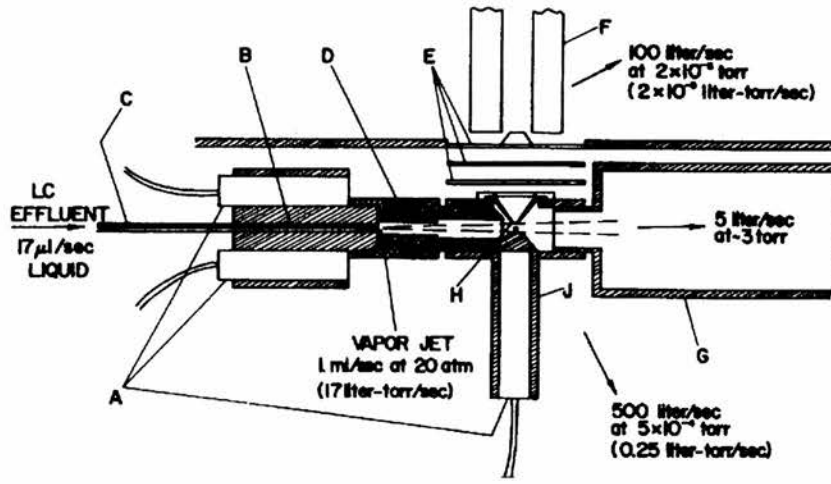

Figure 5.1 Schematic diagram of thermospray apparatus: (A) cartridge heater (B) copper block brazed to stainless steel capillary (C) stainless steel capillary (D) thick-walled copper tube (E) ion lenses (F) quadrupole mass filter (G) pump out line (H) ion exit aperture (J) source heater.

Thermospray is particularly useful for the characterisation of known compounds and the process can be easily used to obtain positive- or negative-ion mass spectra, but very little fragmentation is observed and it may be impossible to obtain any structural information about unknown compounds.

5.1.2 Electrospray mass spectroscopy

Whilst the area of electrospray mass spectroscopy (ESMS) has been growing rapidly for several years as an application for organic analysis (see section 2.2), its application and importance to inorganic and organometallic chemistry[3-22] has only recently been recognised[3,4]. Reports show that the technique is particularly useful for the study of inorganic species for which multinuclear NMR is unavailable[5-7], and it was also demonstrated, in the study of heterometal transition metal clusters that ESMS is extremely easy to use for compounds which would otherwise require analysis by single-crystal X-ray crystallography[5]. The systematic use of ESMS in the study of anionic and cationic metal carbonyl complexes has also received attention recently[5,7-9]. In all cases, observation of molecular ions is facile, usually dominating the mass spectra for species which are positively charged or not very rich in carbonyl groups, however, fragmentation can be achieved for carbonyl-rich anionic species. In another example, the solution dynamics of a copper (II) metallocrown ring have been studied using ESMS in conjunction with ^{1}H NMR[10], which shows the versatility of ESMS as a method of direct sample injection. This type of analysis would not be possible using desorption techniques.

ESMS is of particular interest as tuning can be optimised so as to cause minimal fragmentation of labile compounds, and, by altering the skimmer voltages, fragmentation can be specifically induced in a very controlled manner to provide details of structure within compounds which might be unobtainable by other methods. It is perhaps strange then that with such a wide scope for elegant analysis of charged inorganic or organometallic species present in solution that ESMS remains essentially untapped as possibly one of the best approaches to this type of analysis.

During our studies of ESMS as a probe for organic species present in post-catalytic solutions, spectra for the anions of ruthenium clusters were obtained in the

negative ion mode. It was realised that this provides a very useful method of analysis of organometallic species present in the solution after reaction without any need for chemical isolation. ^{1}H NMR and IR (both *in situ* and in analysis of isolated species) had been used previously, but ESMS provides unequivocal evidence for these complexes quickly and in a very facile manner.

5.2 Results and Discussion

5.2.1 Procedure of analysis of post-catalytic organometallic species by ESMS

All electrospray mass spectra were acquired in the negative ion mode. No organometallic species could be observed in the positive ion mode due to the basic nature of the solutions.

The ES mass spectra of the complex anions were recorded at different skimmer electrode voltages. Low skimmer voltages induce low amounts of fragmentation, and higher degrees of fragmentation can be achieved by using higher skimmer voltages. There are two skimmer cones, the extraction lens, and the focus lens. The focus lens potential was usually set to around 7 V more than the extraction lens potential although this was sometimes varied during tuning for optimum ion current. In the interest of consistency, and as a general rule, these voltages were the only variables during analysis. Table 5.1 shows the typical values of other settings for the electrospray source and mass spectrometer which were varied slightly at the off-set of tuning, then kept constant for the period of analysis which followed.

Table 5.1 Optimisation of tuning parameters used for the analysis of organometallics in post-reaction solutions

ESP Capillary voltage (kV)	2.5-3.2
HV lens (kV)	0.00-0.10
Source temperature (°C)	60
Low mass resolution (arbitrary)	10-12.5
High mass resolution (arbitrary)	10-12.5
Ion energy (V)	0.5-1.5

Most of the post-catalytic reaction mixtures which were found to be catalytic for urea production were a little too weak to obtain very good mass spectra. This problem was solved simply by increasing the concentration of catalyst used by ca. 10 times. Not only could good spectra be obtained for raw samples in these cases, but the anions

within the solution could be precipitated using Ph_4As^+ and isolated for more facile identification.

5.2.2 Results of ESMS analysis

5.2.2.1 Raw pre-catalytic sample solution with methanol as solvent

We have seen previously by ^1H NMR (refer to section 4.2.1) that the most common species in solution at the outset of a catalytic reaction is $[HRu_3(CO)_{11}]^-$ produced by the reaction of NH_3 with $[Ru_3(CO)_{12}]$ in analogy to the WGSR under basic conditions. This was confirmed by ESMS studies upon sample **(I)**. Figure 5.2 shows the mass spectra of this sample with varying skimmer electrode potentials. Figure 5.3 shows a graph of the calculated mass ion distribution compared with the actual distribution for the mass fragment $[HRu_3(CO)_{10}]^-$ which unequivocally identifies it as the mass fragment which is present.

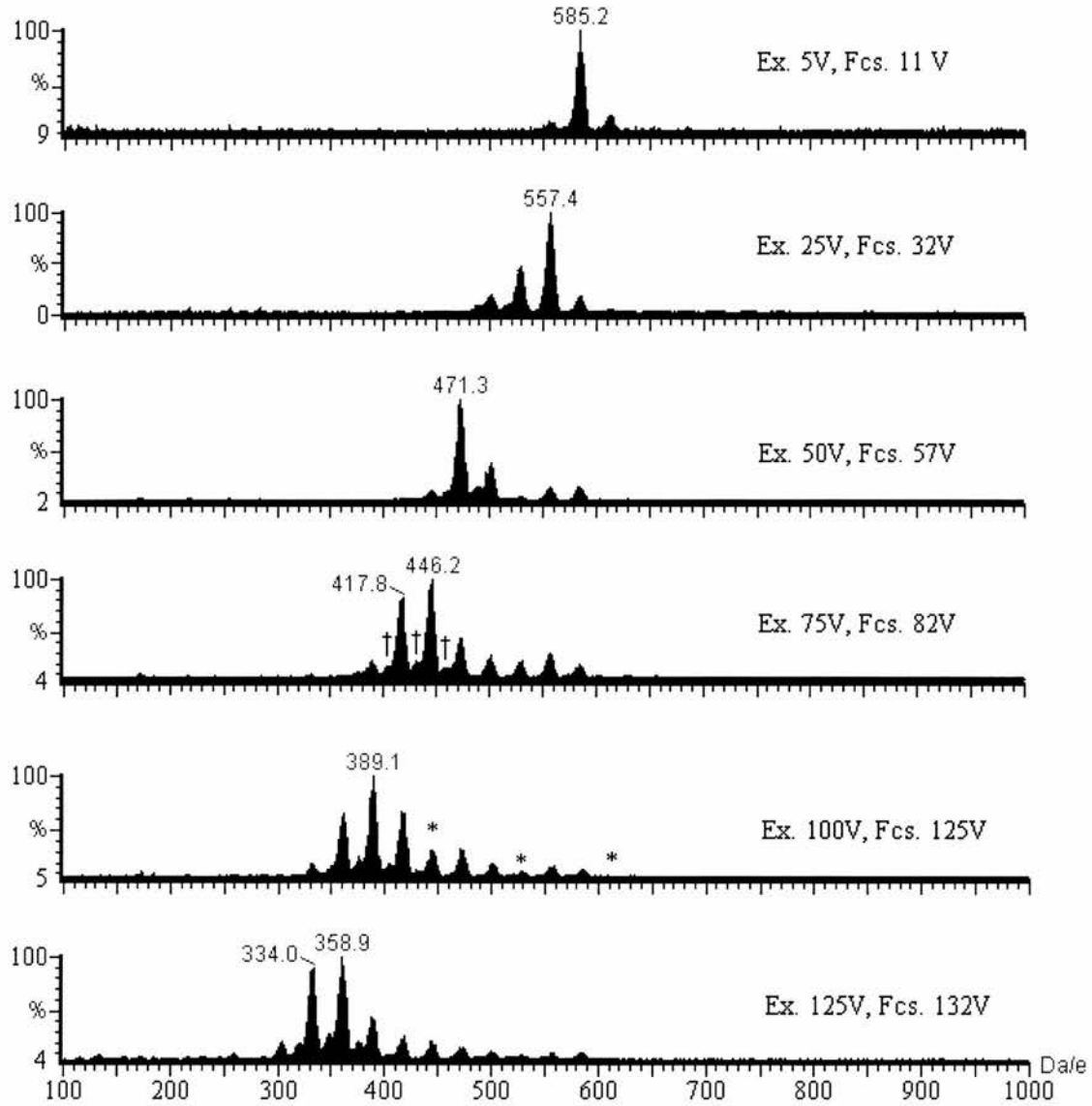

Figure 5.2 Variation of cluster distribution of $[HRu_3(CO)_{11}]^-$ with skimmer voltage (Ex. = extraction voltage, Fcs. = focus voltage)

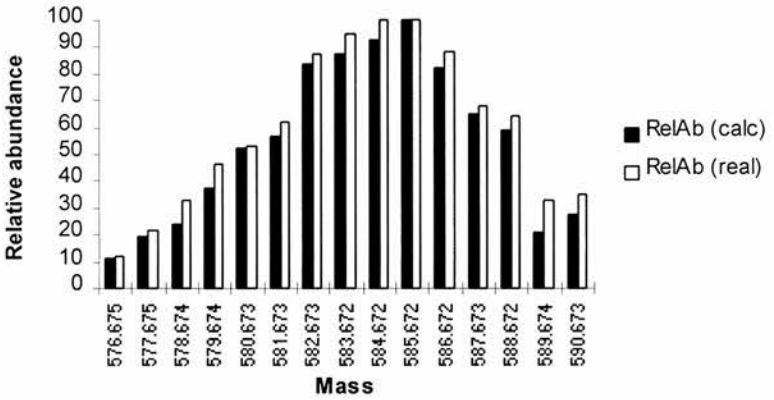

Figure 5.3 Calculated and observed isotopic mass distributions for the anionic fragment $[HRu_3(CO)_{10}]^-$.

Upon closer examination of all the spectra, it appears that the first CO group is lost from $[HRu_3(CO)_{11}]^-$ very easily indeed. The relatively high % abundance of $[HRu_3(CO)_{10}]^-$ (compared to its neighbouring fragments) suggests that this principal fragment is fairly stable. Fragments which appear to have relatively low abundance compared to their neighbours are best seen in the spectrum with extraction voltage = 100 V and are marked with an asterisk*. These fragments correspond to $[HRu_3(CO)_x]^-$ (x = 5, 8, 11). Using this argument, it could be inferred that these fragments possess somewhat less stability and that removal of a CO group is relatively easy for these ions than for their neighbours. A schematic diagram of the molecular structure of $[HRu_3(CO)_{11}]^-$ is shown in figure 5.4 (a). Crystal data for this compound[23], show that the Ru-C bonds on Ru_1 are on average longer (by ca. 0.01 Å) than the terminal Ru-C bonds attached to Ru_2 or Ru_3. This is because there are four terminal carbonyl groups on Ru_1, each competing for π-back donation of the available electron density whilst there are only three on Ru_2 and Ru_3. This means that the back bonding will be less, and hence the Ru-C bond will be weaker and longer for the carbonyls on Ru_1 than for those on Ru_2 and Ru_3. We can predict then that loss of CO from $[HRu_3(CO)_{11}]^-$ is most likely to occur from Ru_1 to generate the mass fragment shown in figure 5.4 (b)(i) which is observed predominantly at very low skimmer voltages. A further loss of two carbonyl groups, one from each of Ru_2 and Ru_3 (figure 5.4 (b)(ii)), generates $[HRu_3(CO)_8]^-$ which is analogous to $[HRu_3(CO)_{11}]^-$ in that there is one more CO group attached to Ru_1 than to

either Ru_2 or Ru_3. It should not be surprising therefore if the Ru_1-C bond lengths are long compared with those for $Ru_{(2\ or\ 3)}$-C and that the analogy with $[HRu_3(CO)_{11}]^-$ is propagated in the nature of its mass spectrum with facile loss of one CO group accounting for its relatively low abundance in the spectrum. The same argument can be applied for the mass fragment $[HRu_3(CO)_5]^-$ (figure 5.4 (b)(iii)) which contains four terminal CO groups, one on each of Ru_2 and Ru_3, and two on Ru_1.

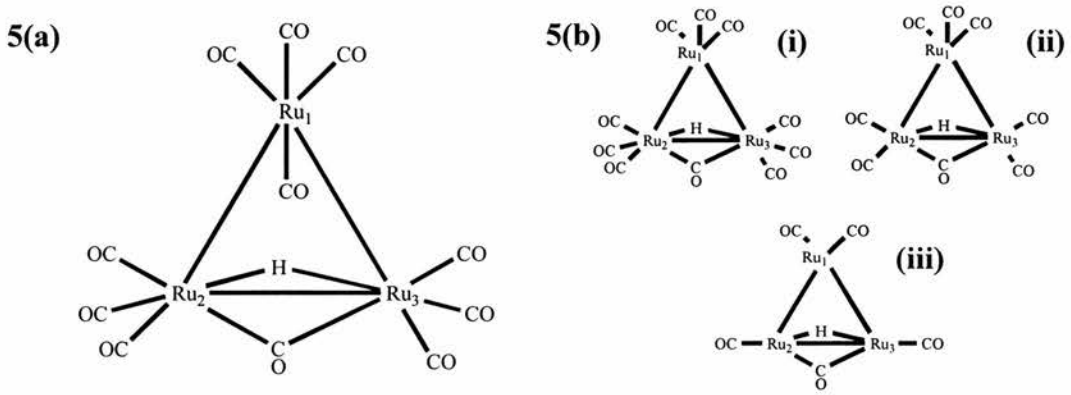

Figure 5.4 (a). A schematic representation of $[HRu_3(CO)_{11}]^-$; **5.4 (b)** ESMS mass fragments of $[HRu_3(CO)_{11}]^-$

No information was obtained from this experiment (or any subsequently) about the nature of the bonding in the triangulo Ru_3 cluster itself; the voltages which are required for this process to occur are probably beyond the limits of the instrumentation used.

It appears also from this analysis that loss of the bridging CO is difficult even at relatively high skimmer voltages. At the highest voltages studied, the peak corresponding to $[HRu_3]^-$ is small compared with that for $[HRu_3(CO)]^-$.

Also observed in figure 5.3, as well as mass distributions corresponding to fragments of $[HRu_3(CO)_{11}]^-$, are peaks which we believe to be due to monoanions of ruthenium amide carbonyl cluster complexes, such as those postulated in chapter 4. These ions are identified in figure 5.2 at an extraction voltage of 75 V, and are marked with a dagger (†). It is not possible to compare the actual mass ion distributions with the calculated distributions as the ion current is quite low. Additionally, the intensity of the signals due to fragments of $[HRu_3(CO)_{11}]^-$ are quite large, and have the effect of hiding

ion current signals of fragments of the postulated amide complexes. Although it is not possible to directly observe these complexes, their masses and ion distributions are in the region of 16-18 larger than those observed for $[HRu_3(CO)_{11}]^-$, so we feel confident that there is a case for these species being monoanions of ruthenium amide carbonyl clusters such as $[HRu_3(NH)(CO)_9]^-$ or $[H_2Ru_4(NH_2)(CO)_{12}]^-$. This hypothesis is supported by the observation of resonances in the high-field ^1H NMR spectra of solutions pre- and post-catalysis (section 4.2.1) which it is not possible to assign to known anionic ruthenium carbonyl cluster complexes.

5.2.2.2 Raw post-catalytic sample solution

We have already seen that the exact identification of species present after the catalytic reactions by classical spectroscopy such as IR and ^1H NMR is not facile and the results are often ambiguous due to the presence of a number of different anionic and neutral ruthenium carbonyl clusters. This becomes extremely problematic when dealing with clusters which do not contain hydride as a ligand and therefore rules out analysis by ^1H NMR spectroscopy. The value of ESMS is obvious in cases like this. Analysis of raw sample solutions allows direct observation of anionic species present at the end of catalysis.

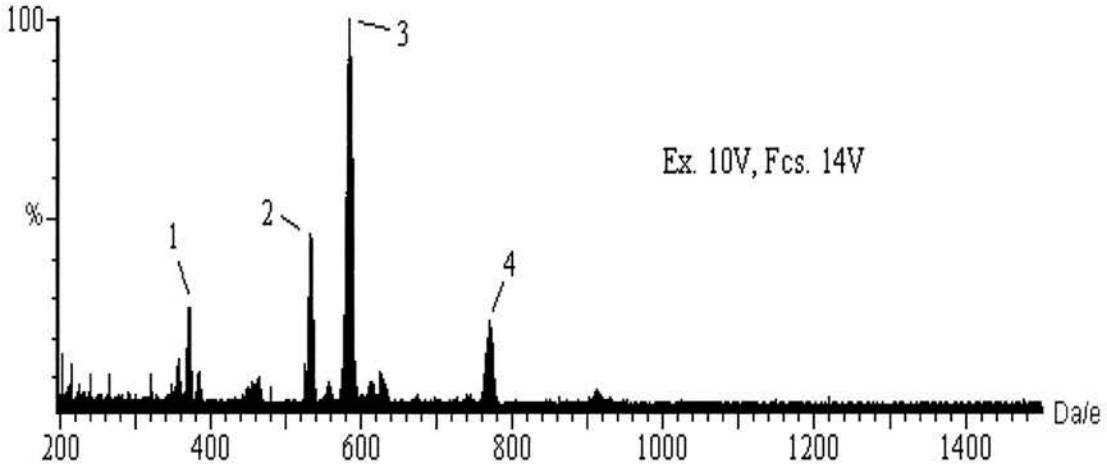

Figure 5.5 An electrospray mass spectrum of sample **(II)**. (1) = fragment of $[H_2Ru_4(CO)_{12}]^{2-}$, (2) = principal ion of $[Ru_6C(CO)_{16}]^{2-}$, (3) = fragment of $[HRu_3(CO)_{11}]^-$, (4) = principal ion of $[HRu_4(CO)_{13}]^-$

This versatility is illustrated in figure 5.5, an electrospray mass spectrum of sample **(II)**, a raw post-catalytic sample solution. This allows the rapid unequivocal identification of several anionic carbonyl cluster complexes to which tentative assignment had been given on the basis of ^1H NMR and IR. It is interesting to observe the dianionic species present. $[Ru_6C(CO)_{16}]^{2-}$ is made synthetically under reducing conditions by reflux of $[Ru_3(CO)_{12}]$ in diglyme in the presence of $[Mn(CO)_5]^-$ [24] and has been shown to be produced as an inactive species in the hydrogenation of CO by ruthenium complexes with iodide promoters[25]. $[H_2Ru_4(CO)_{12}]^{2-}$ is normally prepared by reaction of $[H_4Ru_4(CO)_{12}]$ with two equivalents of KH in THF[26]. The presence of $[Ru_6C(CO)_{16}]^{2-}$ and $[HRu_4(CO)_{13}]^-$ is again confirmed by comparing with calculated isotopic mass distributions of the parent ion (figure 5.6).

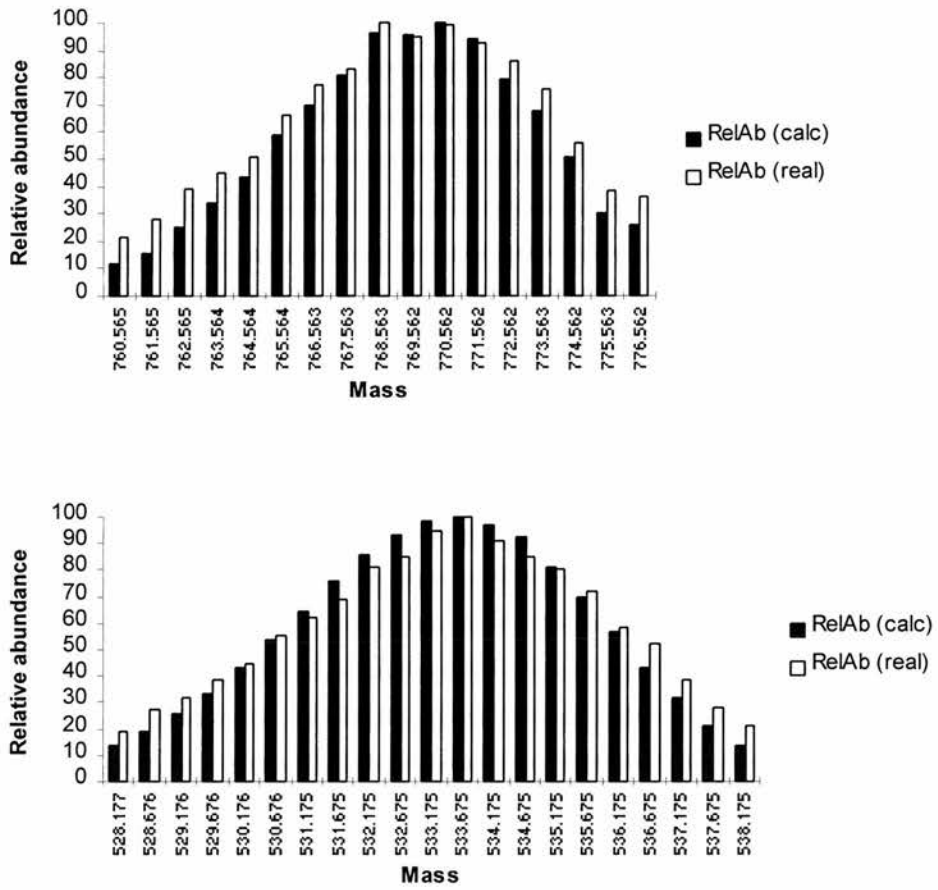

Figure 5.6 Comparison of real and calculated isotopic mass distributions for $[HRu_4(CO)_{13}]^-$ (top) and $[Ru_6C(CO)_{16}]^{2-}$ (bottom)

5.2.2.3 Ph_4As^+precipitated species

After reaction, some of the anionic ruthenium carbonyl clusters present in solution were precipitated with Ph_4As^+. This precipitate was dissolved in acetone (sample **(III)**). When ESMS was performed upon this sample (see figure 5.7), it was found that the predominant species present were $[Ru_6C(CO)_{16}]^{2-}$ (1), $[H_3Ru_4(CO)_{12}]^-$ (2), $[HRu_6C(CO)_{16}]^-$ (3), $[HRu_6(CO)_{18}]^-$ (assigned tentatively) (4), Ru_7 and Ru_8 carbonyl cluster complexes (5) and (6) which remain unidentified. Several anionic heptaruthenium and octaruthenium species are known[27], but on the basis of their isotopic mass distributions, (5) and (6) appear to be new. It was originally thought that these species could be salt-type monoanions with Ph_4As^+ (e.g. $[Ru_6C(CO)_{16}(Ph_4As)]^-$ or

$[Ru_6(CO)_{18}(Ph_4As]^-$), however, the isotopic mass distributions do not fit for these species either.

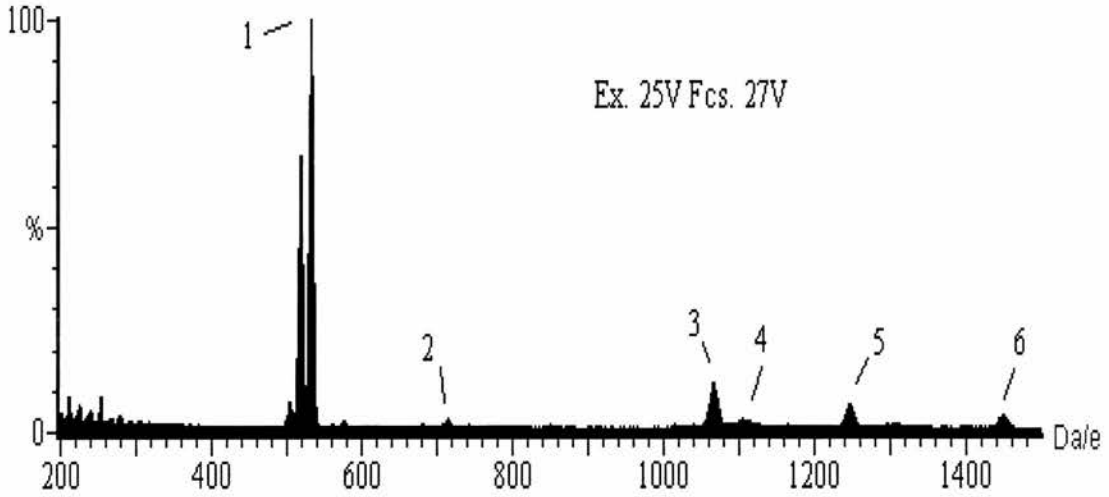

mass cluster	Mass fragment
1	$[Ru_6C(CO)_{16}]^{2-}$
2	$[H_3Ru_4(CO)_{12}]^-$
3	$[HRu_6C(CO)_{16}]^-$
4	$[HRu_6(CO)_{18}]^-$
5	Ru_7 unassigned
6	Ru_8 unassigned

Figure 5.7 Anionic ruthenium carbonyl cluster species precipitated with Ph_4As^+

The observation of $[HRu_6C(CO)_{16}]^-$ (figure 5.8 shows its real and calculated isotopic mass distribution) is slightly unexpected, however, it is reported as being produced in the stepwise protonation of $[Ru_6C(CO)_{16}]^{2-}$ by H_2SO_4 in acetonitrile[28], and in the reaction of $[HRu_6C(CO)_{15}]^-$ with carbon monoxide[29]. $[Ru_6C(CO)_{16}]^{2-}$ may be expected to behave as a strong base, however, the lack of evidence from ^1H NMR for the presence of $[HRu_6C(CO)_{16}]^-$ suggests that $[Ru_6C(CO)_{16}]^{2-}$ is being protonated *in situ* either in the source of the electrospray, or by reaction with H_2O in the mobile phase rather than existing as a genuine product of the catalytic reaction. This is also observed to occur when $[Ru_6C(CO)_{16}](PPN)_2$ is analysed by FABMS in the negative ion mode[1] where the predominant species observed is the protonated $[HRu_6C(CO)_{16}]^-$. The cluster

anion $[H_3Ru_4(CO)_{13}]^-$ is also not observed in the ^1H NMR, however, its deprotonated dianion $[H_2Ru_4(CO)_{13}]^-$is seen. This result suggests that protonation is also occurring *in situ* in this instance.

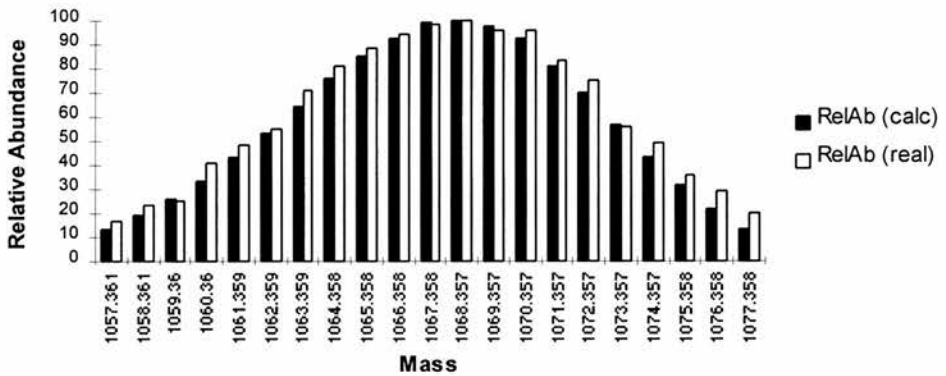

Figure 5.8 Calculated and observed isotopic mass distributions for $[HRu_6C(CO)_{16}]^-$

The variation of mass ion fragments with skimmer voltages can be observed in figure 5.9. As was observed previously, fragmentation increases as the skimmer potentials are increased, however, in this case, the fragmentation of $[Ru_6C(CO)_{16}]^{2-}$ (mass peak centred at 533.6 a.m.u.) occurs in a stepwise fashion (with loss of 14 mass units for each CO group (= 28/2)) until an extraction voltage of ca. 60 V is attained at which point further loss of CO groups from the anion is never attained. The ion peak which would be centred at 309 a.m.u. which would correspond to $[Ru_6C]^{2-}$ is not observed. In fact, the largest number of CO groups which have been observed to be lost from $[Ru_6C]^+$ is just seven. In stark contrast, the fragmentation of $[HRu_6C(CO)_{16}]^-$ is observed with a stepwise loss of 16 carbonyl groups until, at an extraction voltage of 120 V, an isotopic mass distribution is seen which fits the calculated distribution for $[HRu_6C]^-$. The crystal structure of $[HRu_6C(CO)_{16}]^-$ is known[29], however, the terminal CO ligands could not be located because of their low electron densities and the spectra are really too poor to tell us as much about the structure as we were able to elucidate for $[HRu_3(CO)_{11}]^-$.

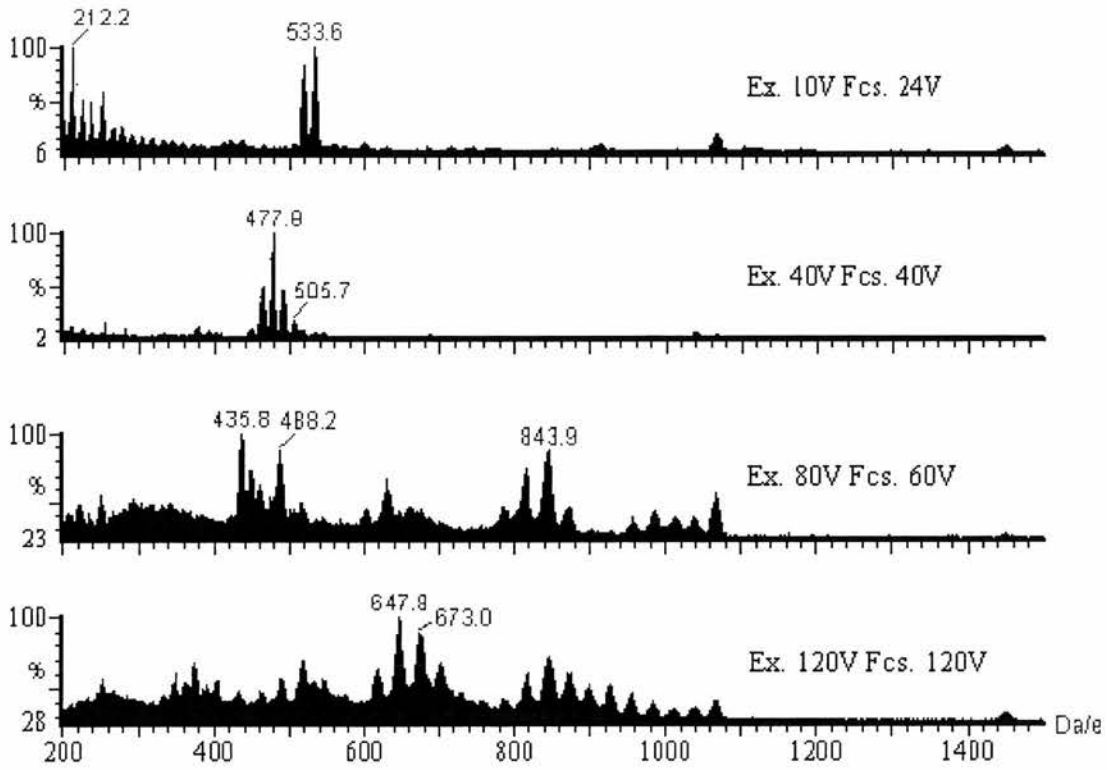

Figure 5.9 The fragmentation of sample **(III)** with applied skimmer voltage

5.2.2.4 Sample solutions obtained with ethanol as solvent

Sample **(IV)** is a solution of the products of the reaction between $[Ru_3(CO)_{12}]$ and ethanolic ammonia. ^1H NMR analysis upon this sample reveals that $[HRu_3(CO)_{11}]^-$ is the predominant product, a result which was confirmed by ESMS, the spectra of which were very similar to those obtained in figure 5.2. There is also evidence for the presence ruthenium amide carbonyl cluster complexes in this solution, however, as for sample **(I)**, their spectra are quite weak, especially when compared with the spectra for $[HRu_3(CO)_{11}]^-$.

A sample of raw post-reaction solution (sample **(V)**) shows that $[H_3Ru_4(CO)_{12}]^-$ and $[HRu_3(CO)_{11}]^-$ are present in the solution and these appear to be the species which are precipitated when Ph_4As^+ is added to the post-catalytic reaction solution as shown in figure 5.10. As the skimmer voltages are gradually increased from extraction and focus potentials of 3 V and 10 V to 150 V and 157 V respectively, gradual fragmentation of both parent species is observed until eventually, isotopic mass clusters due predominantly to $[Ru_3]^-$ and $[Ru_4]^-$ are seen.

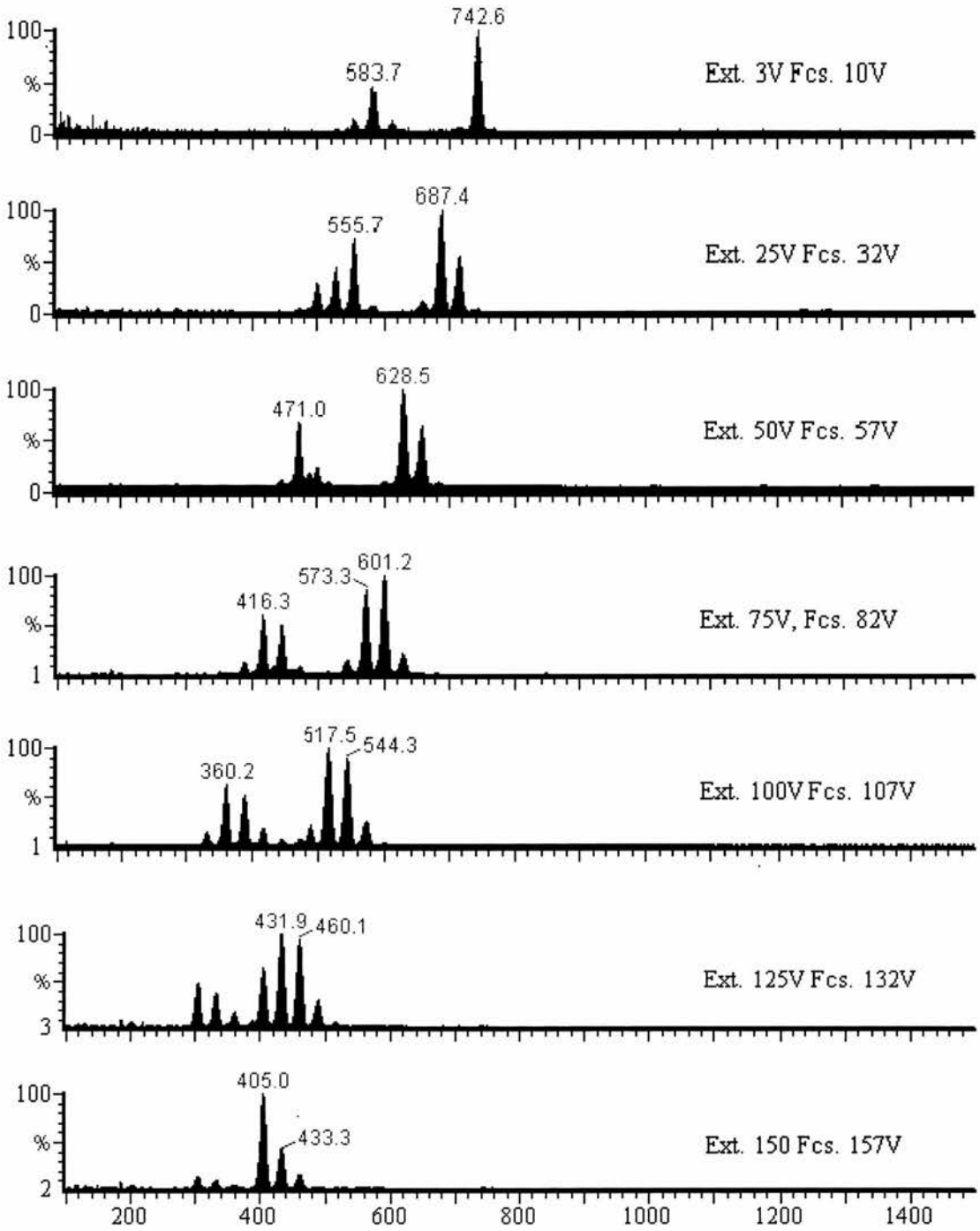

Figure 5.10 Controlled fragmentation of sample **(V)**, Ph_4As^+ precipitated cluster species

High-field ^1H NMR experiments conducted upon this sample solution reveal that $[H_3Ru_4(CO)_{12}]^-$ is not seen (a result also suggested by IR studies on the sample in solution), however, $[H_2Ru_4(CO)_{12}]^{2-}$ *is* observed in the ^1H NMR suggesting that the phenomenon observed for $[Ru_6C(CO)_{16}]^{2-}$ (section 5.2.2.3) is repeating itself. Somewhat

surprisingly, $[HRu_3(CO)_{11}]^-$ is not observed in the ^1H NMR either. It is thought that this is due to a combination of the increased sensitivity of the ESMS instrumentation for this anion relative to $[H_3Ru_4(CO)_{12}]^-$ and also that $[HRu_3(CO)_{12}]^-$ contains just over half as many hydrides per mol compared with $[H_2Ru_4(CO)_{12}]^{2-}$.

This conclusion is supported by ESMS studies performed upon sample **(VI)**, a solution of the filtrate remaining after collection of the Ph_4As^+ precipitated species. Mass spectra indicate the presence predominantly of $[HRu_3(CO)_{11}]^-$ together with a very small amount of $[H_3Ru_4(CO)_{12}]^-$, however, the ^1H NMR indicates that $[H_2Ru_4(CO)_{12}]^{2-}$ is the most abundant species in this solution.

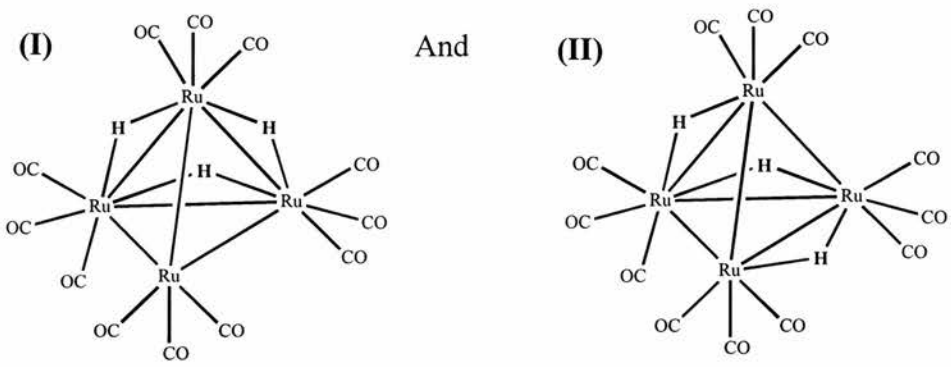

Figure 5.11 Schematic view of the X-ray crystal structures of the two isomers of $[H_3Ru_4(CO)_{12}]^-$.

It is worth noting that there appears to be no pattern of weak peaks observed for $[H_3Ru_4(CO)_{12}]^-$. This is in contrast to the electrospray mass spectrum $[HRu_3(CO)_{11}]^-$ (section 5.3.2.1). The pattern observed previously arose because of the non-symmetrical structure of $[HRu_3(CO)_{11}]^-$ which meant that some M-CO bonds were weaker than others, and therefore the corresponding mass fragment had a shorter lifetime inside the source of the mass spectrometer, and appeared weaker in the final spectrum. However, if we observe the X-ray crystal structure of $[H_3Ru_4(CO)_{12}]^-$ [30], which actually exists as two structural isomers (this is confirmed by low temperature ^1H NMR measurements[31]) (figure 5.11), which are far more symmetrical than $[HRu_3(CO)_{11}]^-$. We would expect then that the Ru-C bond lengths would be approximately equivalent, and of approximately equal strength, therefore no mass fragment would have relative

instability in the source of the mass spectrometer compared with its neighbours. Unfortunately, the original crystal structure report did not include information pertaining to Ru-C or C-O bond lengths, so the hypothesis has to be made without hard evidence of structure.

5.2.3.5 Comparison with FABMS

Table 5.2 shows a comparison between results of analysis by FABMS and ESMS with varying skimmer cone voltages for $[HRu_3(CO)_{11}]^-$. The table shows quite clearly the benefits to be gained from ESMS over FABMS. It is normal to be able to observe total loss of CO groups in a step-wise manner for ESMS by varying the skimmer voltages.

Table 5.2 A comparison between FABMS and ESMS for $[HRu_3(CO)_{11}]^-$

Fragment	FABMS[a]	Electrospray extraction voltage[b]					
		10	25	50	75	100	150
$[HRu_3(CO)_{11}]^-$	614(0)	0	0	0	0	0	0
$[HRu_3(CO)_{10}]^-$	586(100)	100	13	6	0	0	0
$[HRu_3(CO)_9]^-$	558(95)	28	100	12	7	0	0
$[HRu_3(CO)_8]^-$	530(39)	3	57	2	12	6	0
$[HRu_3(CO)_7]^-$	502(39)	0	40	18	14	18	0
$[HRu_3(CO)_6]^-$	474(38)	0	5	100	16	13	0
$[HRu_3(CO)_5]^-$	446(0)	0	0	19	77	34	3
$[HRu_3(CO)_4]^-$	418(0)	0	0	2	100	87	15
$[HRu_3(CO)_3]^-$	390(0)	0	0	0	27	100	28
$[HRu_3(CO)_2]^-$	362(0)	0	0	0	4	22	42
$[HRu_3(CO)]^-$	334(0)	0	0	0	0	2	80
$[HRu_3]^-$	306(56)	0	0	0	0	0	100

[a] Intensity in parenthesis

[b] Focus voltage = Extraction voltage + 7

5.3 Conclusions

ESMS has been shown to be an excellent technique for the identification of negatively charged ruthenium carbonyl cluster species present in solution after catalysis of the reaction between CO and NH_3 to produce urea. There are no real criteria for the sample solution to fulfill in order to be rendered suitable for analysis except that it must be clean and unlikely to precipitate during transport in the mobile phase. Observation of $[Ru_6C(CO)_{16}]^{2-}$ and other dianionic species at the end of the reaction performed in methanol is important and may be crucial in determining the current end-point of the catalytic activity. Table 5.3 shows other species present in post-catalytic solutions Identified by ESMS and a comparison with results of ^1H NMR

Table 5.3 ESMS results compared with ^1H NMR

Sample	Reaction solution	Major ESMS	^1H NMR[a]
(I)	Methanol (before reaction)	$[HRu_3(CO)_{11}]^-$ monoanionic amide complexes	$[HRu_3(CO)_{11}]^-$ monoanionic amide complexes
(II)	Methanol (after reaction)	$[HRu_3(CO)_{11}]^-$, $[HRu_4(CO)_{13}]^-$ $[Ru_6C(CO)_{16}]^{2-}$, $[H_2Ru_4(CO)_{12}]^{2-}$ monoanionic amide complexes	$[HRu_3(CO)_{11}]^-$, $[H_2Ru_4(CO)_{12}]^{2-}$ monoanionic amide complexes
(III)	Methanol (Ph_4As^+ precipitate in acetone)	$[Ru_6C(CO)_{16}]^{2-}$, $[H_3Ru_4(CO)_{12}]^-$ $[HRu_6C(CO)_{16}]^-$, $[HRu_6(CO)_{18}]$ also Ru_7 and Ru_8	$[H_2Ru_4(CO)_{12}]^{2-}$
(IV)	Ethanol (before reaction)	$[HRu_3(CO)_{11}]^-$ monoanionic amide complexes	$[HRu_3(CO)_{11}]^-$ monoanionic amide complexes
(V)	Ethanol (after reaction)	$[HRu_3(CO)_{11}]^-$, $[H_3Ru_4(CO)_{12}]^-$ monoanionic amide complexes	$[HRu_3(CO)_{11}]^-$, $[H_2Ru_4(CO)_{12}]^{2-}$ monoanionic amide complexes
(VI)	Ethanol (Ph_4As^+ precipitate in acetone)	$[HRu_3(CO)_{11}]^-$, $[H_3Ru_4(CO)_{12}]^-$	$[HRu_3(CO)_{11}]^-$, $[H_2Ru_4(CO)_{12}]^{2-}$

[a] Solvent = d^6 acetone

It is apparent from these results that the clusters $[H_2Ru_4(CO)_{12}]^{2-}$, and $[Ru_6C(CO)_{16}]^{2-}$ (also possibly $[Ru_6(CO)_{18}]^{2-}$) are protonated in solution , probably in the source of the ESMS by reaction with H_3O^+. The fact that this does not occur for $[H_2Ru_4(CO)_{12}]^{2-}$ in sample (II) is probably due to the high basicity of the raw sample solution after reaction.

Information about the molecular structure of $[HRu_3(CO)_{11}]^-$ was obtained from its electrospray mass spectra with varying skimmer voltages, the results of which compared well with what is already known and it has been shown that the it may be possible to determine the sructures of unknown organometallics using this technique if X-ray crystallography is not an option.

We have been able to postulate about the existence of monoanionic ruthenium amide carbonyl cluster complexes of the type $[HRu_3(NH)(CO)_9]^-$ and $[H_2Ru_4(NH_2)(CO)_{12}]^-$, based upon the observation of hydride signals in the high-field ^1H NMR which were unaccounted for. ESMS analysis conducted upon these solutions reveals the presence of complexes which *could* be due to these anions with m/z ca. 16-18 a.m.u larger than fragments observed for $[HRu_3(CO)_{11}]^-$.

We have seen the versatility of ESMS for the analysis of anionic ruthenium carbonyl cluster complexes compared with negative ion FABMS, using $[HRu_3(CO)_{11}][Et_4N]$ as substrate. A controlled fragmentation of the parent species is possible using ESMS.

5.4 Experimental

5.4.1 Electrospray

ESMS instrumentation

A JASCO model PU-980 intelligent HPLC pump was used to provide a flow of mobile phase. This system was connected to a VG platform ESP from Fisons instruments (Manchester, UK.) equipped with microflow probe. A coaxial probe was employed. Samples were introduced into the electrospray source *via* a 20 μL injection loop together with a nebulizing gas, which flows past the probe tip, producing an aerosol of sample. A drying gas was added to ensure that sample which may have entered the gas line by capillary action was flushed out.

The mobile phase employed was a 2:1 mixture of acetone:water or methanol:water and samples were either dissolved in glass-distilled acetone (from CaH_2) or, in the case of raw solutions, filtered and used without any further handling.

Data was processed using the Masslynx™ Mass Spectrometry Data System through Microsoft Windows installed in a Digital DEC PC 466.

Flow of mobile phase was varied between 10-20 μL/min, and it was not found that any decrease in sensitivity was noticed between the two rates.

Sample preparation

Sample solutions were anaerobically filtered through a 0.45 μm filter prior to analysis.

A solution of poly(ethylene glycol) (PEG) in a 50:50 solution of CH_3CN - H_2O was filtered through a 0.45 μm filter prior to use. This solution was used as a calibrant.

FABMS Instrumentation

Fast Atom Bombardment mass spectrometry was recorded on a VG Autospec (Fisons), and aquisition was performed in the negative mode with nitrobenzylalchohol as matrix.

Chemicals

The employment of standard Schlenk procedures[32] was maintained throughout the preparation of samples and in the handling of post-catalytic reaction solutions. HPLC water, acetonitrile and methanol were obtained from Fisons Chemicals and were filtered through a 0.45μm nylon 66 membrane (obtained from Supelco). $[Ru_3(CO)_{12}]$ was obtained from Strem Chemical Co. and used as received. Ph_4AsCl was obtained from Aldrich Chemiclas plc and used without purification. Methanol and ethanol were dried over $Mg(OMe)_2$ and $Mg(OEt)_2$ respectively prior to use. Reaction grade acetone was obtained from Fisons Chemicals and distilled over CaH_2 prior to use. Ammonia was dried over sodium and distilled under an Ar atmosphere into a steel cylinder. The metal carbonyl $Et_4N[HRu_3(CO)_{11}]$ was prepared by slight modification of the literature method[23].

5.4.2 Sample preparation

Solutions of ammonia in methanol and ethanol

A known mass of alcoholic solvent was pre-weighed into a side-arm Schlenk and allowed to cool in icy water under Ar. NH_3 was bubbled slowly through the solution for several hours. Upon re-weighing, the mass of NH_3 absorbed, and hence the molarity of the solution in NH_3 could be evaluated.

5.4.2.1 Samples derived from reactions conducted in methanolic ammonia

Sample **(I)**. A few crystals of $[Ru_3(CO)_{12}]$ were dissolved in methanolic ammonia (ca. 2 cm^3, 4.4 $moldm^{-3}$ in NH_3) under an atmosphere of Ar.

$[Ru_3(CO)_{12}]$ (0.648 g, 1.01 mmol) was dissolved in methanolic ammonia (60 cm^3, 4.4 $moldm^{-3}$ in NH_3) and stirred for 18 h under an atmosphere of Ar. Two 30 cm^3 portions were transferred *via* syringe into each of two steel autoclaves with internal volumes of 170 cm^3. Each autoclave was charged to a pressure of 2 bar CO and reacted with magnetic stirring at a temperature of 160°C for a period of 1 h. After cooling, the vessels were degassed and the contents of each transferred into the same side-arm Schlenk. A small volume of this red solution (sample **(II)**) was transferred to a sample tube for analysis. This solution was analysed for urea content quantitatively by ^{13}C NMR and qualitatively by colorimetric reaction with diacetyl monoxime and was found to contain urea corresponding to a total turnover of 2 mol urea per mol $[Ru_3(CO)_{12}]$ per hour. The remaining solution was treated with Ph_4AsCl (1.32 g, 3.1 mol equiv.) and filtered. The precipitated solid (sample **(III)**) was dissolved in acetone (20 cm^3). Further precipitation was induced by evaporation of the filtrate to ca 10 cm^3 *in vacuo*. The solid collected by filtration was also dissolved in acetone (20 cm^3).

5.4.2.2 Samples derived from reactions conducted in ethanolic ammonia

$[Ru_3(CO)_{12}]$ (0.487 g, 0.762 mmol) was dissolved in ethanolic ammonia (50 cm^3, 5.4 $moldm^{-3}$ in NH_3) by stirring overnight. A small aliquot of the resulting solution was taken for analysis (sample **(IV)**). The resulting solution was transferred to an autoclave and charged with 2 bar of CO before heating to 160°C for a period of 1 h with magnetic stirring. The autoclave was cooled and degassed and the contents transferred to a side-arm Schlenk tube (sample **(V)**). Treatment with Ph_4AsCl (0.45 g, 1.14 mmol) in H_2O (ca. 2 cm^3). The yellow precipitate was filtered and dissolved in acetone (ca. 20 cm^3, sample **(VI)**). The filtrate was also kept for analysis.

The raw solution retained after the reaction (sample **(IV)**) was analysed for urea content but was found to contain too small a quantity to be quantified by ^{13}C NMR.

5.5 References

1. Chihara, T., Yang, L.P., Esumi, Y., Wakatsuke, Y., *J. Mass Spec.,* **30.,** 1995, 684.
2. Irabarne, J.V., Dziedzic, P.J., Thompson, B.A., *Int. J. Mass Spcetrom. Ion. Phys.,* **50,** 1983, 331.
3. Stewart, I.I., Horlick, G., *Trac-trends Anal. Chem.,* **15,** 1996, 80.
4. Colton, R., D'Agostino, A., traeger, J.C., *Mass Spectrom. Rev.,* **14,** 1995, 79.
5. Ferrer, M., Reina, R., Rossell, O., Seco, M., Segales, G., *J. Organomet. Chem.,* 1996, **515,** 205.
6. Kane-Maguire, L.A.P., Kanitz, R., Sheil, M.M., *J. Organomet. Chem.,* 1995, **486,** 243.
7. Ahmed, I., Bond, A.M., Colton, R., Jurcevic, M., Traeger, J.C., Walter, J.N., *J. Organomet. Chem.,* 1993, **447,** 59.
8. Henderson, W., Nicholson, B.K., *J. Chem. Soc., Chem. Comm.,* 1995, 2531. 9. Henderson, W., McIndoe, J.S., Nicholson, B.K., Dyson, P.J., *J. Chem. Soc., Chem. Comm.,* 1996, 1183.
10. Gibney, B.R., Kessissoglou, D.P., Kampf, J.W., Pecoraro, V.L., *Inorg. Chem.,* **33,** 1994, 4840.
11. Henderson, W., Fawcett, J., Kemmit, D.W., McKenna, P., Russell, D.R., *Polyhedron,* **16,** 1997, 2455.
12. Colton, R., Traeger, J.C., Tedesco, V., *Inorg. Chim. Acta,* **210,** 1993, 193.
13. Colton, R.. Harrison, K.L., Mah, Y.A., Traeger, J.C., *Inorg. Chim. Acta,* **231,** 1995, 65.
14. Henderson, W., Taylor, M.J., *Polyhedron,* **15,** 1996, 1957.
15. Dakternieks, D., Zhu, H., Tiekink, E.R.T., Colton, R., *J. Organomet. Chem.,* **476,** 1994.
16. Canty, A.J., Colton, R., *Inorg. Chim. Acta,* **215,** 1994, 179.
17. Canty, A.J., Colton, R., Thomas, I.M., *J. Organomet. Chem.,* **455,** 1993, 283.
18. Colton, R., D'Agostino, A., Traeger, J.C., Klaui, *Inorg. Chim. Acta,* **233,** 1995, 51.
19. Zu, X., Nolan, S.P., Cole, R.B., *Anal, Chem.,* **66,** 1994, 119.

20. Henderson, W., Oliver, A.G., Downard, A.J., *Polyhedron,* **15,** 1996, 1165.

21. Canty, A.J., Colton, R., *Inorg. Chim. Acta,* **220,** 1994, 99.

22. Bennett, K.L., Carver, J.A., David, D.M., Kane-Maguire, L.A.P., Sheil, M.M., *J. Coord. Chem.,* **34,** 1995, 351.

23. Johnson, B.F.G., Lewis, J., Raithby, P.R., Suss, G., *J. Chem. Soc., Dalton Trans.,* 1979, 1356.

24. Bradley, J.S., Ansell, G.B., Hill, E.W., *J. Organomet. Chem.,* **184,** 1980, C33

25. Dombek, B.D., *J. Organomet. Chem.,* 1983, **250,** 467.

26. Inkrott, K.E., Shore, S.G., *J. Am. Chem. Soc.,* **100,** 1978, 3954.

27. Bruce, M.I., in *"Comprehensive Organometallic Chemistry,* Eds. Wilkinson, G., Stone, F.G.A., Abel, E.W., Pergammon, Oxford, 1982, pp 843-908 and refs. within.

28. Johnson, B.F.G., Lewis, J., Sankey, S.W., Wong, K., McPartlin, M., Nelson, W.J.H., *J. Organomet. Chem.,* **191,** 1980, C3.

29. Chihara, T., Yamazaki, H., *J. Organomet. Chem.,* **473,** 273.

30. Jackson, P.F., Johnson, B.F.G., Lewis, J., *J. Chem. Soc., Chem. Comm.,* 1978, 920.

31. Koepke, J.W., Johnson, J.R., Knox, S.A.R., Kaesz, H.D., *J. Am. Chem. Soc.,* **97,** 1975, 3947.

32. Shriver, D.F., "The Manipulation of Air Sensitive Compounds", McGraw-Hill, New York, 1969.

CHAPTER 6

Reactions of $RhCl_3.xH_2O$ with P^iPr_3 - The novel synthesis and crystal structure of a new polymorph of $[RhH_2Cl(P^iPr_3)_2]$ and the reproducible synthesis of $[RhH(P^iPr_3)_3]$.

Reactions of $[RhH(P^iPr_3)_3]$, $[RhH_2Cl(P^iPr_3)_2]$ and $[RhCl(CO)(PMe_3)_2]$ with NH_3

6.1 Introduction

Much time has been spent during our studies in the pursuit of a reproducible synthesis for $[RhH(P^iPr_3)_3]$, first described as being active for the WGSR by Otsuka and co-workers nearly two decades ago[1,2] (see also section 3.1.3.4). It has been found that $[RhH(P^iPr_3)_3]$ reacts oxidatively with water[3], ketones[4], and small chain alcohols[5,6]. It has also been shown to catalyse H/D exchange with aromatic hydrocarbons such as benzene[3].

The original method of synthesis involves the reaction of $RhCl_3.xH_2O$ with P^iPr_3 in THF[7] at ambient temperature. This is followed by reduction over sodium amalgam for 18 hours. The whole synthesis was carried out in an atmosphere of dinotrogen and in *dry* THF, which was suggested as the source of hydride. Work performed by Bruce[8] showed that $[RhHCl_2(P^iPr_3)_2]$, (spectroscopic analysis of which (ν_{Rh-H} (KBr) = 1940 cm^{-1}, ^1H NMR (CD_2Cl_2); δ = -31.25 (dt, $^1J_{Rh-H}$=32.6 Hz, $^2J_{H-Ph}$=12.48 Hz), ^{31}P NMR δ = 44 ppm (d, $^1J_{Rh-H}$=96.8 Hz)[8]) suggested a square pyramidal structure with an apical hydride and mutually *trans* phosphines, an assignment later confirmed by X-Ray analysis[9]) was the predominant intermediate after the initial reaction in THF. He also showed that H_2O, and not THF, was the source of hydride in this species by performing the reaction in the presence of D_2O to obtain $[RhDCl_2(P^iPr_3)_2]$. $[RhHCl_2(P^iPr_3)_2]$ has also been isolated in high yield and purity after reaction of $RhCl_3.xH_2O$ and P^iPr_3 by refluxing in propan-2-ol in the presence of H_2O[9,10]. After preparation of this intermediate, the next step in the synthesis of $[RhH(P^iPr_3)_3]$ presumably involves the reductive loss of Cl_2 by the action of Na upon $[RhHCl_2(P^iPr_3)_2]$ (see figure 6.1).

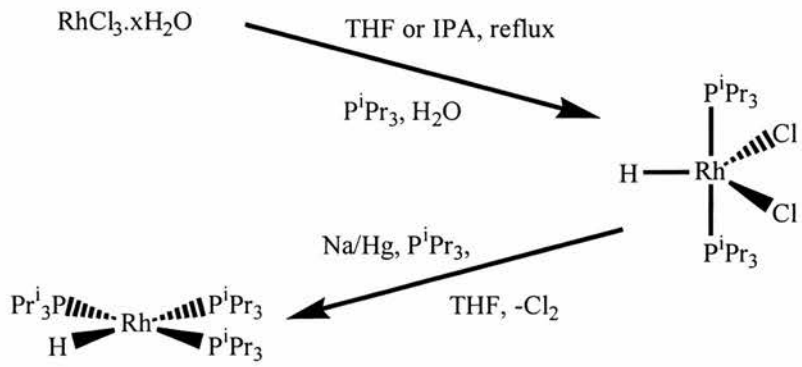

Figure 6.1 Likely mechanism for the formation of $[RhH(P^iPr_3)_3]$

As a continuation of the studies performed by Bruce upon these and related tri(*iso*-propyl)phosphine complexes of $Rh^{(I)}$, we are able to report here that $[RhH(P^iPr_3)_3]$ can be produced in relatively high yield by an alternative route.

Also presented are the results of work carried out in the attempted photoassisted oxidative addition of NH_3 to complexes of the type $[RhCl(CO)(PR_3)_2]$ (R = P^iPr, PMe), a reaction discussed in section 1.4.1, which have been shown to oxidatively add the C-H bonds of alkanes under similar conditions, and the attempted non-photoassisted activation of ammonia by oxidative addition to $[RhH(PR_3)_3]$ (R = ^{i}Pr, PEt). Theoretical thermodynamic calculations upon oxidative addition of ammonia to second row transition metal atoms have shown that of those to the right of the periodic table, Rh is the one which is most likely to undergo this kind of reaction[13]. It has also been demonstrated that the addition of ligands which can increase the electron density on the metal can reduce the barrier height for insertion by decreasing exchange energy loss in the reaction[14]. Given that complexes of the type $[RhH(PR_3)_3]$ (R = ^{i}Pr, PEt) have been observed to oxidatively add water, it was thought worthwhile to attempt reactions with ammonia.

6.2 Results and discussion

6.2.1 Reactions of [$RhCl_3.xH_2O$] and P^iPr_3

6.2.1.1 Synthesis of [$RhHCl_2(P^iPr_3)_2$]

In order to clarify earlier work, methods of preparation of [$RhHCl_2(P^iPr_3)_2$] were repeated. The best method of synthesis was found to be that involving reflux of $RhCl_3.xH_2O$ with excess P^iPr_3 in wet propan-2-ol over a period of 28 hours or more[11]. This leads to the formation of crystals of [$RhHCl_2(P^iPr_3)_2$] which are spectroscopically pure. On the other hand, reaction in THF in the presence of water and HCl also leads to formation of this complex, however, there is also a high yield of another unidentified compound for which ^{31}P NMR data suggest a complex of $Rh^{(I)}$ (^{31}P NMR (CD_2Cl_2) doublet, 69.6 ppm, J_{Rh-P} =119.8 Hz). The method of Bruce entails evaporation to dryness. This is, in practice very difficult to achieve, and it is found that even trace amounts of residual water greatly effect the course of subsequent reaction, as is discussed later.

It should be noted that Bruce details *two* methods of preparation of [$RhHCl_2(P^iPr_3)_2$] by reaction in THF, both of which require very similar stoichiometries, however, one method entails reflux overnight (which leads to the formation of an orange complex), whereas in the other method, the reaction occurs by simple stirring under ambient conditions (leading to the formation of a red complex). It has been found during spectroscopic analyses of the products from both of these reactions that, whilst the red compound obtained from reaction under ambient temperature, analyses correctly by ^1H NMR and ^{31}P NMR for [$RhHCl_2(P^iPr_3)_2$], the orange complex obtained from reaction under reflux normally has spectra with quite broad lines. In the ^{31}P NMR of the orange compound, the signal assigned to free phosphine (normally ca. 19.5 ppm) is normally displaced to lower field (ca. 30 ppm), and is broad. This compound is discussed in more detail in section 6.2.1.6.

6.2.1.2 Synthesis of $[RhH(P^iPr_3)_3]$, by reaction of $[RhHCl_2(P^iPr_3)_2]$ with sodium amalgam

As expected, production of $[RhH(P^iPr_3)_3]$, by reaction of $[RhHCl_2(P^iPr_3)_2]$ in THF solution over a sodium amalgam in the presence of excess P^iPr_3, can be realised, however, reproducibility is not good, and yields are rarely very high. It is found that the method of preparation of $[RhHCl_2(P^iPr_3)_2]$ which offers the optimum conversion to $[RhH(P^iPr_3)_3]$, is that of refluxing $RhCl_3.xH_2O$ with excess P^iPr_3 in propan-2-ol containing water. The direct preparation of $[RhH(P^iPr_3)_3]$ must be performed in an atmosphere of Ar. Reaction under an atmosphere of dinitrogen results in the formation of $[RhH(P^iPr_3)_2]$ (^{31}P NMR 66 ppm (d), 162 Hz; ^1H NMR -15.0 ppm (overlapping dt), J_{Rh-H} = 17.0 Hz, J_{P-H} = 20.8 Hz), and $[RhH(P^iPr_3)_2]_2(\mu\text{-}N_2)$ (^{31}P NMR d 67 ppm, 158 Hz; ^1H NMR -13.6 ppm (overlapping dt), J_{Rh-H} = 18.4 Hz, J_{P-H} = 18.2 Hz), however, $[RhH(P^iPr_3)_3]$ can be recovered from this solution by evaporation to dryness *in vacuo*, and recrystallisation from light petroleum ether in the presence of excess P^iPr_3.

There is some discrepancy between our results of spectroscopic parameters for $[RhH(P^iPr_3)_3]$, and those obtained independently from our studies. For instance, it is reported that the ^{31}P NMR spectrum consists of a doublet at 58.8 ppm[5] with J_{Rh-P} = 157 Hz or 32.2 ppm[15] with J_{Rh-P} = 157 Hz. We report that this value is 53.6 ppm in C_6D_6 with J_{Rh-P} = 157.3 Hz. Similarly, it has been reported that ν_{Rh-H} for $[RhH(P^iPr_3)_3]$ is 1975 cm^{-1}, and 1970 cm^{-1}, however, we find that this value is 1957 cm^{-1}. We feel confident that the species we have characterised spectroscopically *is* in fact $[RhH(P^iPr_3)_3]$. Proof of this comes from observation of the low temperature ^1H NMR in the section to follow, and also that the hydride signal disappears altogether when the spectrum is acquired in C_6D_6 or C_7D_8 indicating the H/D exchange reaction with aromatic hydrocarbon compounds which is known to be catalysed by this complex[3].

6.2.1.3 Low temperature ^1H NMR of $[RhH(P^iPr_3)_3]$

A solution of $[RhH(P^iPr_3)_3]$ in d^8 THF was used for this experiment with temperatures ranging from 313 to 203 K (see figure 6.2). The results are consistent with an AB_2MX type system. A similar AB_2X spin system is observed for the complex

$[NiH(PEt_3)_3]^+$ [16] also shown in figure 6.2. The system for the rhodium complex is more complicated as rhodium has a spin 1/2 whereas nickel has no spin, so all signals couple to rhodium as well as phosphorus.

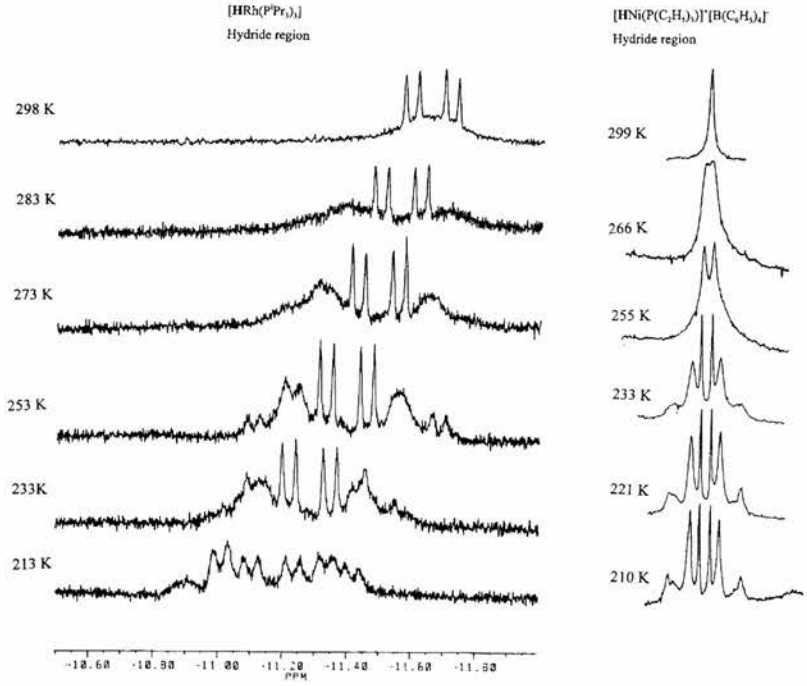

Figure 6.2 Low temperature ^1H NMR spectra of $[RhH(P^iPr_3)_3]$

6.2.1.4 Synthesis of $[RhH_2Cl(P^iPr_3)_2]$

Whilst attempting to synthesise $[RhH(P^iPr_3)_3]$, yellow plate crystals were isolated by crystallisation from light petroleum ether after reduction of $[RhHCl_2(P^iPr_3)_2]$ (made by the method of Bruce under ambient conditions of temperature) in sodium amalgam. It had previously been suggested[8] that this product was an oligomer of formula $[RhH(P^iPr_3)_2]_n$, however, we have identified this compound to be *cis*-$[RhH_2Cl(P^iPr_3)_2]$. Spectroscopic analysis (ν_{Rh-H} 2140 cm^{-1}; ^{31}P NMR (C_6D_6): 62.8 ($^1J_{Rh-H}$ =113.8 Hz; ^1H NMR (C_6D_6): -22.8 (overlapping dt, $^1J_{Rh-H}$ =26.4 Hz, $^2J_{H-Ph}$ =13.7 Hz)) supports this (see figure 6.3), and an X-Ray crystal structure confirms the assignment. It was proposed that this complex had been made accidentally, and rather fortuitously, by reduction of $[RhHCl_2(P^iPr_3)_2]$ under slightly wet conditions. Methods of preparation of $[RhHCl_2(P^iPr_3)_2]$ from THF entail work-up by removal of solvent (and residual water)

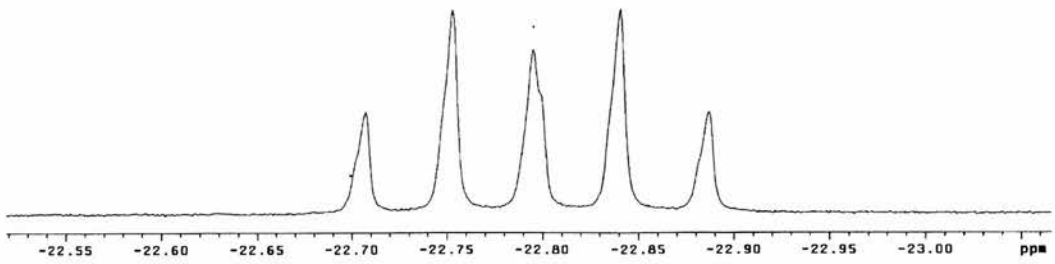

Figure 6.3 High field ^{1}H NMR of $[RhH_2Cl(P^iPr_3)_2]$ (C_6D_6)

in vacuo at 45°C after initial reaction. In practice, this can normally be readily achieved, after prolonged periods of pumping, however, if all water is not removed from the system, then formation of some $[RhH_2Cl(P^iPr_3)_2]$ is inevitable. There have been cases when conversion to this compound has been nearly quantitative. A probable mechanism for its formation is shown in figure 6.4 and involves reaction of water with sodium to

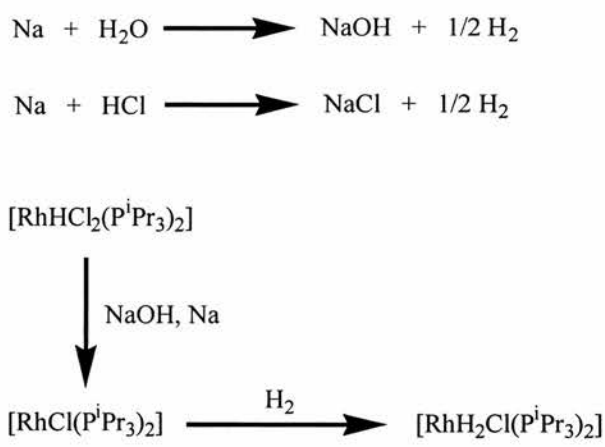

Figure 6.4 Likely mechanism for the formation of $[RhH_2Cl(P^iPr_3)_2]$ from $[RhHCl_2(P^iPr_3)_2]$

generate NaOH and H_2. The reaction of either NaOH or Na with $[RhHCl_2(P^iPr_3)_2]$ results in removal of HCl. Subsequent oxidative addition of H_2 to an intermediate proposed as $[RhCl(P^iPr_3)_2]$ results in formation of $[RhH_2Cl(P^iPr_3)_2]$. This mechanism is supported by a report that reaction of $[RhHCl_2(P^iPr_3)_2]$ with H_2 in a 50 % NaOH/

benzene system under conditions of phase transfer catalysis results in the rapid formation of $[RhH_2Cl(P^iPr_3)_2]$ in high yield[17]. This is indeed the case; however, having repeated the experiment, we have found that isolation of pure $[RhH_2Cl(P^iPr_3)_2]$ from the reaction solution has proved difficult, and it was found that during work-up, the dihydride initially formed disappears. We have been unable to identify or isolate subsequent products of this reaction. $[RhH_2Cl(P^iPr_3)_2]$ can also be prepared in 56% yield by reaction of $[RhCl(P^iPr_3)_2]$ with H_2 in a benzene solution[18], however, the overall yield of the reaction is quite low (around 25 %), as preparation of $[RhCl(P^iPr_3)_2]$ in 68 % yield involves reaction of $[RhCl(C_8H_{14})_2]$ (prepared in 74 % yield from the reaction of $RhCl_3$ with C_8H_{14} in propan-2-ol[19]) with excess P^iPr_3 in pentane solution. This method of preparation also supports our mechanism for the formation of $[RhH_2Cl(P^iPr_3)_2]$.

Since our initial isolations, we have found that a reproducible method of preparation of $[RhH_2Cl(P^iPr_3)_2]$ to a yield of up to 50 % involves reaction of $[RhHCl_2(P^iPr_3)_2]$ (prepared by prolonged reflux in propan-2-ol) over a sodium amalgam in the presence of THF, P^iPr_3 and H_2O. It appears, however, that there is a fine line between optimum conversion to, and the ultimate disappearance, of $[RhH_2Cl(P^iPr_3)_2]$ as observed during the phase transfer reaction. The solution turns yellow-brown after ca. 120 min stirring. Prolonged reaction results in the formation of a dark green solution from which $[RhH_2Cl(P^iPr_3)_2]$ cannot be isolated. A possible reason for this is that basic action of NaOH or Na upon $[RhH_2Cl(P^iPr_3)_2]$ results in the formation of $[RhH(P^iPr_3)_2]$ (a 14-electron complex proposed by Otsuka and co-workers[7]), which then reacts with P^iPr_3 to form $[RhH(P^iPr_3)_3]$. However, the solution is strongly basic, and it is likely that the electron-deficient $[RhH(P^iPr_3)_3]$ will be prone to attack by OH^-. Since isolation of complexes has proved difficult, this reaction is poorly understood, and we believe that a number of different products result.

6.2.1.5 Description of the structure of a new polymorph of *cis*-[$RhH_2Cl(P^iPr_3)_2$]

Previous elucidation by X-Ray diffraction of *cis*-[$RhH_2Cl(P^iPr_3)_2$] by Harlow and co-workers[9] described a triclinic crystal system having space group P1 containing two independent but similar molecules in the asymmetric unit. One of these possessed a pseudo-2-fold rotation axis passing through the Rh and Cl atoms, in the other molecule this axis was destroyed by the sufficiently different orientations of the two $^iPr_3$ groups. We found, surprisingly, that when we isolated the same compound under different conditions, it crystallised in a monoclinic crystal system with space group P2 1/n containing only one type of molecule, which has no pseudo-2-fold rotation axis (see figure 6.5 (see Appendix 1 for crystal structure report)). It was of interest to note that the H-Rh-H angle of 71° was slightly more obtuse and the Rh-H distances (1.45(4) Å, 1.51(3) Å) within the molecule were similarly, but to a lesser extent unequal, than was previously reported. However, it should be noted that the amount of 'T' square pyramidal geometry character in this molecule is slightly greater owing to the relatively acute Cl-Rh-Hx angle of 132°, and the rather more obtuse Cl-Rh-Hy angle of 155°. This results in a noticeable distortion of Hx away from the pseudo plane created by Cl-Rh-Hy, and towards one of the isopropyl groups. The H-H distance within the complex was found to be 1.74 Å.

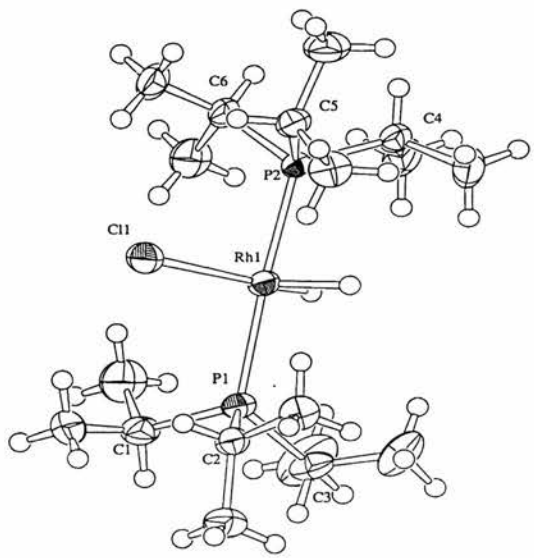

Figure 6.5 Molecular structure representation of [$RhH_2Cl(P^iPr_3)_2$]

It is interesting to note that the angle of P-Rh-P of 176.6° is very similar to that in both of the molecules in the triclinic system previously reported (compare 176.6° and 175.6°), and therefore it can be concluded that it is this slight distortion into a molecule with 'T'-type character which independently gives rise to the increase in bond lengths of Rh-Cl (compare 2.4275(9) Å to 2.413(1) Å, 2.422(1) Å), Rh-P (compare 2.3123(8) Å and 2.308(1) Å to 2.307(1) Å and 2.303(1) Å, 2.302(1) Å and 2.308(1) Å) and Rh-H bond lengths (compare 1.45(4) Å and 1.51(3) Å to 1.38 Å and 1.51 Å, 1.40 Å and 1.50 Å).

6.2.1.6 Synthesis of $[RhH(P^iPr_3)_3]$ by action of base on $[RhH_2Cl(P^iPr_3)_2]$

Werner and co-workers have reported recently that $[RhH(P^iPr_3)_3]$ can be formed from $[RhH_2Cl(P^iPr_3)_2]$[18]. They were then able to isolate pure $[RhH(P^iPr_3)_3]$ in high yield.

Their method involved reaction of $[RhH_2Cl(P^iPr_3)_2]$ in a toluene solution (in the presence of excess P^iPr_3) with ^{t}BuOK, and resulted in the formation of $[RhH(P^iPr_3)_3]$. Work-up involved extraction into petrol, reduction to an oil, dissolution in diethylether, and precipitating with cold methanol. A bright yellow precipitate was collected after the reaction. This method of synthesis is reproducible, and the product analyses for $[RhH(P^iPr_3)_3]$, found (by ^{31}P NMR) to be of greater purity than products obtained by the sodium amalgam reduction of $[RhHCl_2(P^iPr_3)_2]$. We had attempted this method of preparation using triethylamine as base, however, after reaction for several hours, only starting materials were recovered. Reductive elimination of HCl from $[RhH_2Cl(P^iPr_3)_2]$ only occurs in the presence of strong base, such as ^{t}BuOK, or NaOH.

$[RhH(CO)(P^iPr_3)_2]$ (a complex implicated as an intermediate in the WGSR catalysed by $[RhH(P^iPr_3)_3]$[1]) can also be synthesised by a modification of this preparation using $[RhH_2Cl(P^iPr_3)_2]$ as a starting material. Employing exactly the same procedure described above, $[RhH(P^iPr_3)_3]$ is precipitated from the solution with MeOH at room temperature, with which it reacts[1], to produce essentially pure $[RhH(CO)(P^iPr_3)_2]$.

6.2.1.7 Synthesis of $[RhHCl_3(P^iPr_3)_2](HP^iPr_3)$

It has been reported that reaction of $[RhHCl_2(P^iPr_3)_2]$ in the presence of excess phosphine under reflux in a THF solution leads to a new compound, thought to be of formula $[RhH_2Cl(P^iPr_3)_3]$[8]. We now report that this compound is, in fact $[RhHCl_3(P^iPr_3)_2][HP^iPr_3]$, an assignment supported by spectroscopic analysis (see figure 6.6) (ν_{Rh-H} 1943 cm^{-1}; ^{31}P NMR (CD_2Cl_2): 43.5 (d, $^1J_{Rh-H}$ =95.5 Hz), 32.7(s); ^1H NMR (CD_2Cl_2): -31.3 (very broad), + 8.1 (d, $^1J_{P-H}$ = 492 Hz), and confirmed by an X-Ray crystal structure elucidation. It seems very likely that this is also the orange product which results from the attempted preparation of $[RhHCl_2(P^iPr_3)_2]$ by reflux over prolonged periods of time in THF solution, a reaction described in section 6.2.1.1. It is also reported that when this compound is stirred over sodium amalgam in the absence of added P^iPr_3 in THF, that $[RhH_2Cl(P^iPr_3)_2]$ is the product which results[8], however, we have been unable to reproduce this synthesis.

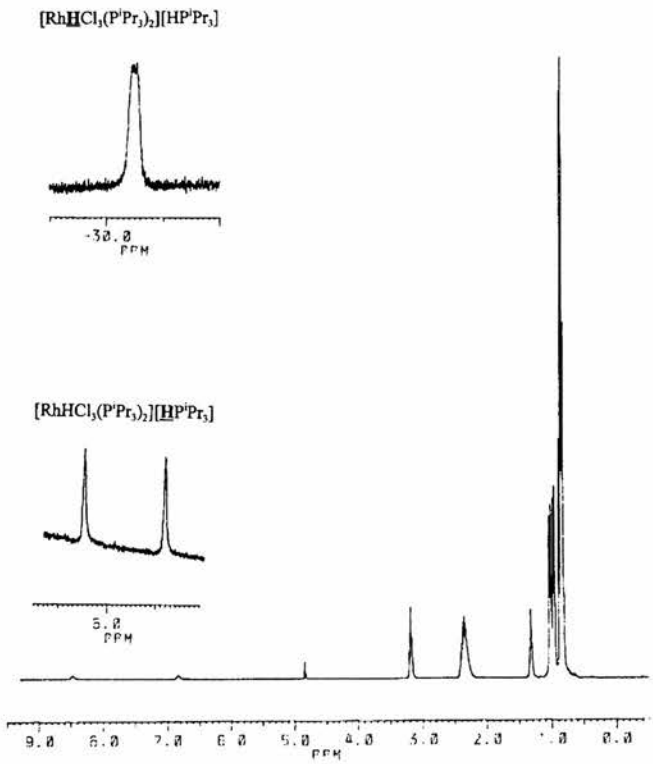

Figure 6.6 Low field ^1H NMR of $[RhHCl_3(P^iPr_3)_2][HP^iPr_3]$. Insets: Top left - high field hydride region: Bottom right - low field proton of $[\mathbf{H}P^iPr_3]^+$.

Variable temperature ^{31}P NMR (figure 6.7) and ^{1}H NMR (figure 6.8) show that the protonated phosphine $[HP^{i}Pr_3]^+$ does not exchange with the phosphine ligands on the $[RhHCl_3(P^{i}Pr_3)_2]^-$ complex itself, as the ^{31}P signal due to $[HP^{i}Pr_3]^+$ remains a singlet from 308 K down to 183 K. The doublet due to the co-ordinated phosphines of $[RhHCl_3(P^{i}Pr_3)_2]^-$ does change, however. At 308 K, this signal is very similar to that for $[RhHCl_2(P^{i}Pr_3)_2]$, with an almost identical coupling constant. On cooling to 263 K, this doublet starts to coalesce and its frequency shifts up-field. On cooling further to 203 K, it begins to couple to rhodium once again (δ = 31 ppm (d), $^{1}J_{Rh-P}$ = 96.8 Hz). In the ^{1}H NMR, at 308 K, there is a signal at -30.4 ppm (dt, $^{1}J_{Rh-H}$ = 12.8 Hz, $^{2}J_{P-H}$ = 31.1 Hz) which, supported by ^{31}P NMR evidence ((CD_2Cl_2) 43.5 (d, $^{1}J_{Rh-H}$ =113.8 Hz), 32.7(s)), we believe is due to the hydride on the neutral species $[RhHCl_2(P^{i}Pr_3)_2]$, and the singlet in the ^{31}P NMR is due to the chloride salt of $[HP^{i}Pr_3]^+$. It is only at temperatures below 263 K that this chloride starts to co-ordinate to the rhodium resulting in a coalescence of the ^{31}P NMR signal, and a shift in the position of the ^{1}H NMR signal from -30 to -21 ppm. At 203 K, then, the species which exists in solution is truly $[RhHCl_3(P^{i}Pr_3)_2][HP^{i}Pr_3]$, and as the temperature is raised, dissociation of $[HP^{i}Pr_3Cl]$ from $[RhHCl_3(P^{i}Pr_3)_2][HP^{i}Pr_3]$ starts to occur resulting in the observation of the two neutral species $[RhHCl_2(P^{i}Pr_3)_2]$, and $[HP^{i}Pr_3Cl]$.

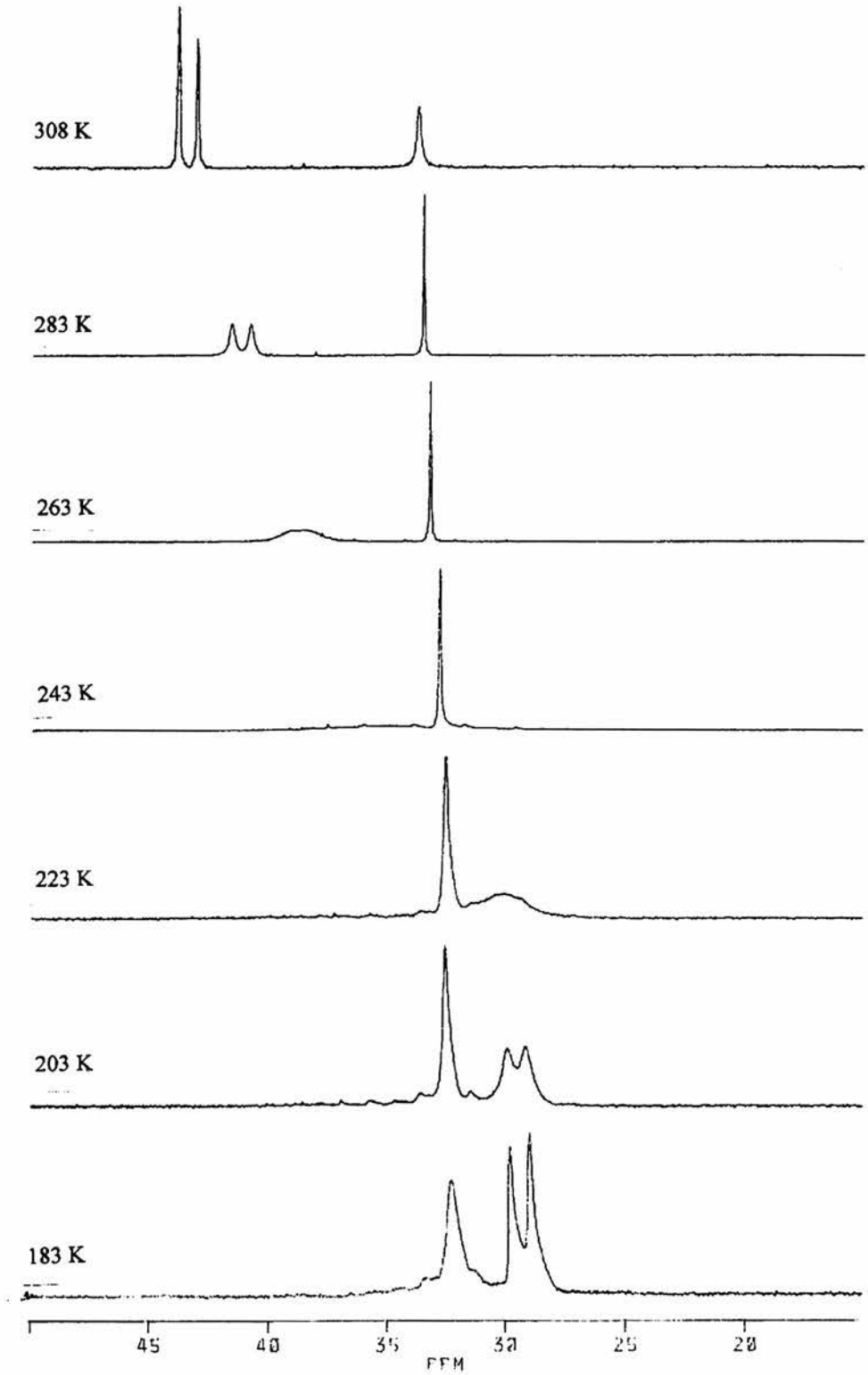

Figure 6.7 Variable temperature ^{31}P NMR $[RhHCl_3(P^iPr_3)_2](HP^iPr_3)$ (in CD_2Cl_2)

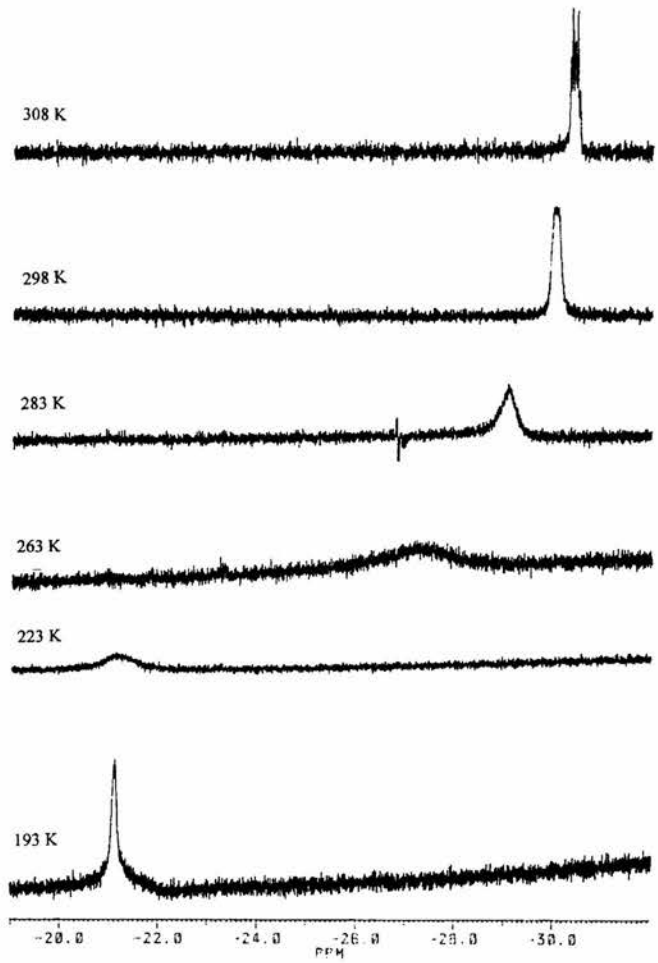

Figure 6.8 Variable temperature ^{1}H NMR of $[RhHCl_3(P^iPr_3)_2](HP^iPr_3)$ (in CD_2Cl_2)

6.2.1.8 Description of the structure of $[RhHCl_3(P^iPr_3)_2][HP^iPr_3]$

The availability of single crystals of $[RhHCl_3(P^iPr_3)_2][HP^iPr_3]$ allowed the opportunity for a single crystal X-ray diffraction study, in order to try and rationalise its spectroscopic characteristics, which were until then unexplained. A representation of the molecular structure of $[RhHCl_3(P^iPr_3)_2][HP^iPr_3]$ can be observed in figure 6.9, and structural parameters and experimental are contained in Appendix 2. The molecule exists in a P1 (#2) space group in a triclinic crystal system. Of note is the fact that the Rh-Cl(1) bond length *trans* to the hydride is much longer (0.21 Å) than the Rh-Cl(2,3) bond lengths *cis* to the hydride (which are similar to those observed for $[RhHCl_2(P^iPr_3)_2]$[9]). The Cl(2) - Cl(3) bond angle of 176.7° is similar to the angle of 180° observed in $[RhHCl_2(P^iPr_3)_2]$[9]. It seems possible, therefore, that in this salt, there is a high degree of hydrogen bonding interaction between free phosphonium cation and

$[RhHCl_2(P^iPr_3)_2]$. Indeed, the distance between Rh and P3 is just 3.88 Å. This is also supported by the low temperature NMR data discussed in the previous section which shows that, at low temperatures, the species which exists in solution is $[RhHCl_3(P^iPr_3)_2][HP^iPr_3]$, and, at higher temperatures, dissociation occurs resulting in the formation of $[RhHCl_2(P^iPr_3)_2]$ and $[HP^iPr_3Cl]$.

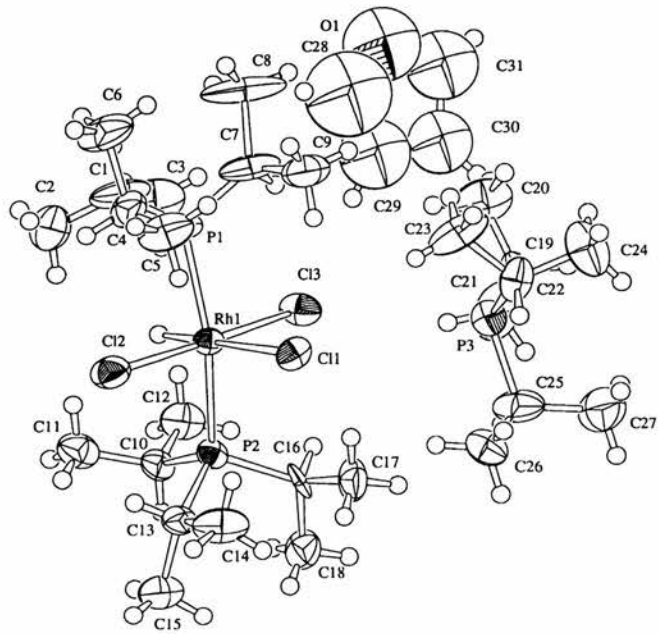

Figure 6.9 Molecular structure representation of $[RhHCl_3(P^iPr_3)_2](HP^iPr_3)$

Prior to this study, the complex had been formulated as $[RhHCl_2(P^iPr_3)_3]$ on the basis of its spectroscopic analysis, however, this seemed unlikely due to the steric bulk of the phosphine ligands and chlorides surrounding the Rh atom. CHN analysis suggested that if the complex was mononuclear, then it contained approximately 2.5 phophines, but it was difficult to obtain reliable data as the crystals were found to decompose quite rapidly in the absence of mother liquor. X-Ray crystal structure elucidation and variable temperature NMR analysis has confirmed the identity of this species as $[RhHCl_3(P^iPr_3)_2][HP^iPr_3]$ in the solid state, and at low temperatures in solution.

6.2.2 Reaction of $[RhH(P^iPr_3)_3]$ with NH_3

$[RhH(P^iPr_3)_3]$ is unstable in the solid state, decomposing over a period of days in a light-free, argon environment at -30°C. For this reason, the complex is stored as a concentrated solution at -30°C in light petroleum ether or THF under argon, and extracted for use when necessary.

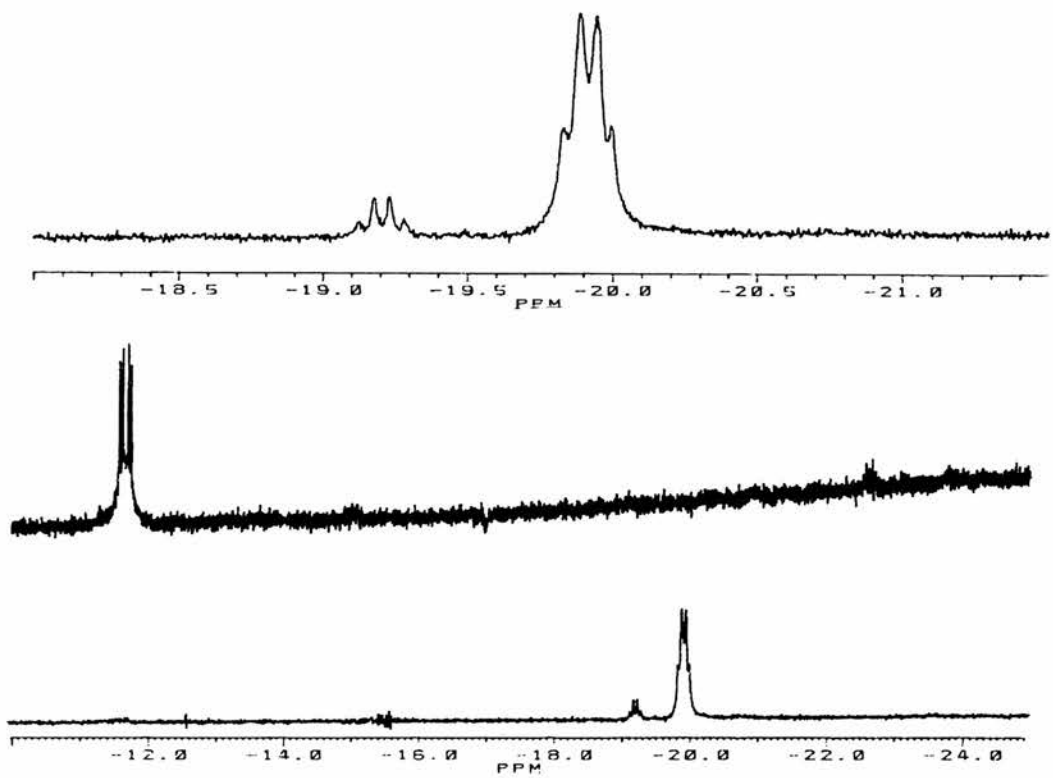

Figure 6.10 High field ^1H NMR spectra after (bottom), before (middle), and after (expanded) reaction of $[RhH(P^iPr_3)_3]$ with NH_3 (in d^8 THF).

Typical high-field ^1H NMR spectra (in d^8 THF) of $[RhH(P^iPr_3)_3]$ (referenced to THF) before, and after reaction with NH_3 (by stirring under under an atmosphere of NH_3 for a period of 24 h), can be observed in figure 6.10. We can see that the multiplet associated with $[RhH(P^iPr_3)_3]$ at ca. -11.5 ppm (middle spectrum) has been replaced with what appears to be two very broad doublets of triplets (bottom spectrum, and top (expanded) spectrum) at -19.2 ppm ($^1J_{Rh-H}$ = 16.5 Hz, $^2J_{P-H}$ = 14.8 Hz) and -19.9 ppm ($^1J_{Rh-H}$ = 17.2 Hz, $^2J_{P-H}$ = 15.1 Hz). This spectrum is independent of whether the reaction is performed in the presence of non-treated ammonia, or dry ammonia which eliminates H_2O present

as an impurity reacting preferentially with $[RhH(P^iPr_3)_3]$. The new resonances in the ^1H NMR are accompanied by a new doublet in the ^{31}P NMR at 57.3 ppm ($^1J_{Rh\text{-}P}$ = 113 Hz), indicating perhaps the formation of a new $Rh^{(III)}$ complex. It might be postulated that such a reaction would occur by oxidative addition of NH_3 to $[RhH(P^iPr_3)_3]$, as shown in figure 6.11. Similar results of ^1H and ^{31}P NMR evidence suggest that $[RhH_2Cl(P^iPr_3)_2]$

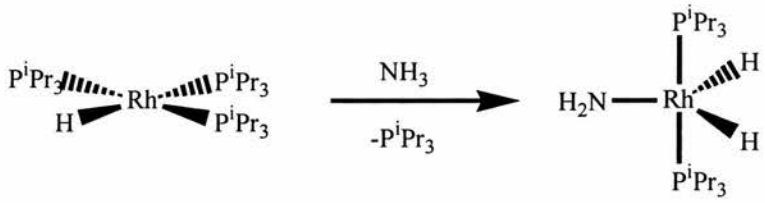

Figure 6.11 Possible mechanism for the reaction of $[RhH(P^iPr_3)_3]$ with NH_3

undergoes a similar kind of reaction with ammonia, probably *via* reductive elimination of HCl by the action of NH_3 to generate an intermediate 14-electron species, $[RhH(P^iPr_3)_2]$ which then reacts with NH_3 to form the same 5-coordinate $Rh^{(III)}$ complex postulated as the product of reaction between $[RhH(P^iPr_3)_3]$, and NH_3 (figure 6.12).

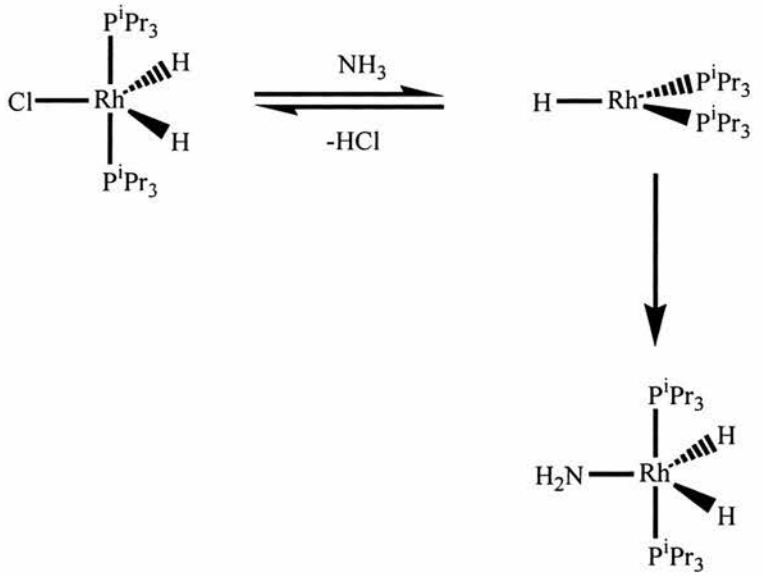

Figure 6.12 Possible mechanism for the reaction of $[RhH_2Cl(P^iPr_3)_2]$ with NH_3

It was found that under the same conditions, $[RhH(PEt_3)_3]$, which is analogous to $[RhH(P^iPr_3)_3]$, does not react with NH_3.

6.2.3 Photo-assisted reaction of $[RhCl(CO)(PMe_3)_2]$ with NH_3

Two different approaches were taken to the photo-assisted reaction of $[RhCl(CO)(PMe_3)_2]$ with NH_3. The substrate was either dissolved in perfluorinated solvent (C_6F_6), or in liquid NH_3. During initial studies upon the reaction in liquid NH_3, it was noticed that after several hours of photolysis, the yellow residues obtained after evaporation of NH_3 were highly insoluble in organic solvents. The reverse is certainly true for $[RhCl(CO)(PMe_3)_2]$ which is prepared in benzene and recrystallised from small-chain alcohols. Unfortunately, however, spectroscopically, this insoluble residue analyses for the starting material $[RhCl(CO)(PMe_3)_2]$. When the reaction is performed in perfluorobenzene, however, after bubbling with NH_3 for two hours with stirring, a yellow solid precipitates from the solution. After leaving for several hours, the yellow solid congeals to a red oil. Residual C_6F_6 can be removed by decantation, and the red oil is dried *in vacuo*. IR of this red oil in a KBr disc reveals the presence of new bands which could be due to hydride stretches at 2040(w,br), 1945(vs), and 1941(s), however, it is not possible to distinguish whether any new bands are present due to N-H stretches The carbonyl stretch at 1958 cm^{-1} associated with $[RhCl(CO)(PMe_3)_2]$ is still present, although greatly diminished. Unfortunately, due to the very low solubility of these species after reaction with NH_3, no NMR analysis was possible.

6.3 Conclusions

Making use of the fact that $[RhH_2Cl(P^iPr_3)_2]$ is a product of the reaction between $[RhHCl_2(P^iPr_3)_2]$ and H_2 under strongly basic conditions, we have been able to develop a high yield route to $[RhH(P^iPr_3)_3]$ *via* reaction of $[RhHCl_2(P^iPr_3)_2]$ in the presence of water with sodium amalgam.

The crystal structure of $[RhH_2Cl(P^iPr_3)_2]$ shows it to be a new polymorph of this compound.

The crystal structure of $[RhHCl_3(P^iPr_3)_2][HP^iPr_3]$ is in agreement with low temperature NMR evidence, however, in solution, at higher temperatures, there is evidence for the dissociation of $[RhHCl_3(P^iPr_3)_2][HP^iPr_3]$ to $[RhHCl_2(P^iPr_3)_2]$ and $[HP^iPr_3Cl]$.

$[RhH(P^iPr_3)_3]$ and $[RhH_2Cl(P^iPr_3)_2]$ are both found to react with dry NH_3 at ambient temperature and pressure in d^8 THF solutions. The exact nature of the products is not well understood, but it is suspected that they are the result of oxidative addition of NH_3 to the 14 electron intermediate $[RhH(P^iPr_3)_2]$ to give a 5-coordinate dihydrido amide complex.

$[RhCl(CO)(PMe_3)_2]$ reacts under conditions of photo-assistance with NH_3 in perfluorinated solvent. It is unclear as to the nature of the reaction due to the very poor solubility of the products in organic solvents, however, oxidative addition of NH_3 to the intermediate produced during photolysis, $[RhCl(PMe_3)_2]$, is thought be a possibility.

6.4 Experimental

General Procedures

The employment of standard Schlenk procedures[21] was maintained throughout the preparation of samples, with an atmosphere of argon dried over anhydrous Cr^{2+} on SiO_2. THF, diethyl ether, petroleum ether and toluene were dried and deoxygenated by distillation from sodium benzophenone ketyl. H_2O and D_2O were deoxygenated by a lengthy nitrogen or argon purge prior to use. Methanol and propan-2-ol were dried using $Mg(OMe)_2$ and deoxygenated by distillation. Deuterated solvents were degassed by a triple freeze-pump-thaw cycle.

For photolysis reactions, a 400 W mercury vapour lamp supplied by Applied Photophysics Ltd was used. This was cooled with a glass water jacket. In a typical reaction, a solution containing substrate and solvent in a Schlenk tube would be placed in close proximity to the lamp, and both would be wrapped together in tin foil to maximise light intensity. Where required in a gaseous state, ammonia was dried by distillation over sodium at atmospheric pressure and at -33°C into a stainless steel cylinder and used when necessary. Where ammonia was required as a solvent for a substrate, it could be vacuum distilled over sodium into a Schlenk tube and transferred *via* cannular as required.

Apparatus

^1H NMR and $^{31}P\{^1H\}$ NMR were recorded on a Varian Gemini 2000 machine, and $^{13}C\{^1H\}$ NMR were recorded on a Brucker AM 3000 spectrometer.

FTIR were recorded either on a Nicolet Protégé 460 Magna - IR Technology machine, or a PE 1710 IR Fourier Transform Spectrometer.

Chemicals

$RhCl_3.3H_2O$, $[RhCl(CO)_2]_2$, ^tBuOK, HCl, DCl and hexafluorbenzene were obtained from commercial sources and used as received. PEt_3 and PMe_3 were obtained

from Strem Chemicals plc and used without purification. P^iPr_3 was either purchased from Strem Chemicals plc or Aldrich Chemical Co., or prepared by reaction of PCl_3 with Grignard in THF[22].

Preparation of P^iPr_3

$MgBr^iPr_3$ (1.6 mol in THF (800 cm^3) was added dropwise to a stirring solution of PCl_3 (45 cm^3, 0.52 mol, slightly less than 1/3 mol equivalent) in THF (ca. 1 dm^3). Steady reflux was maintained without heating, and extra THF was added as necessary when agglomerations of salts precipitated from the solution. After addition, the solution was refluxed for 1 h. On cooling, the salts were dissolved by addition of H_2O, and the THF layer was separated by decantation. Evaporation to dryness *in vacuo* yielded a yellow oil which was vacuum distilled to give a clear liquid. Fractional distillation at 74-77°C, 16 mmHg gave a clear liquid.
^{31}P NMR ($CDCl_3$) 19.5 ppm. Lit[23] 19.3 ppm.

Preparation of $[RhH(PEt_3)_3]$ [15]

$RhCl_3.3H_2O$ (1.14 g) was dissolved in THF (20 cm^3) with PEt_3 (1.8 cm^3) and a few drops of water and stirred for 20 hrs. The resulting suspension was evaporated to dryness *in vacuo.* Na/Hg (2%, 50 g), THF (20 cm^3), and PEt_3 (1.8 cm^3) were added to the residue, and the resulting suspension was stirred for a further 5 hrs. The mixture was filtered and reduced to dryness *in vacuo*. The resulting solid was then dissolved in n-pentane and filtered several times before being evaporated to a small volume and stored at -30°C. The green crystals obtained were collected and washed with cold n-pentane before drying *in vacuo*. Heating *in vacuo* at 65°C resulted in the production of a dark red oil (Yield 74%) which was made into a stock solution in petroleum ether (200 cm^3).

Preparation of $[RhCl_2H(P^iPr_3)_2]$

Made by the method of Bruce in refluxing THF[8]

$RhCl_3.3H_2O$(1.04 g, 4.97 mmol) was dissolved in THF (50 cm^3), H_2O (10 cm^3), P^iPr_3 (2.5 cm^3, 12.5 mmol, (a 2.5 mol equivalent)), and HCl (a few drops) were added, and this mixture was refluxed with stirring for 18 h under Ar. The resulting red solution was dried *in vacuo* at a temperature of 45°C to remove residual water and washed copiously with diethylether (to remove phosphine oxide), light petroleum ether (to remove free phosphine), and water (to remove residual HCl). The remaining solid was again dried thoroughly *in vacuo*.

IR (KBr): 1939.1 cm-1Lit[8]1940 cm^{-1}

^{31}P NMR (CD_2Cl_2): $[RhCl_2H(P^iPr_3)_2]$, 43.6 (d, $^1J_{Rh-H}$ =96.5), 19.5 (s, P^iPr_3), 53.6 (s, P^iPr_3O); Lit[8]. (CD_2Cl_2): 44 (d $^1J_{Rh-H}$=96.8 Hz).

^1H NMR (CD_2Cl_2): -31.2 (dt, $^1J_{Rh-H}$ =32.3 Hz, $^2J_{H-Ph}$ =12.5 Hz) Lit[8]. (CD_2Cl_2): -31.3 (dt. $^1J_{Rh-H}$=32.6 Hz, $^2J_{H-Ph}$=12.48 Hz).

(found: C 41.52, H 8.54 %. $C_{18}H_{43}Cl_2P_2Rh$ requires C 43.65, H 8.75 %.).

Preparation of $[RhCl_2H(P^iPr_3)_2]$

Made by the method of Grushin and co-workers[11]

$RhCl_3.3H_2O$ (1.00 g, 4.78 mmol) was dissolved in propan-2-ol (60 cm^3) and H_2O (2.0 cm^3). P^iPr_3 (2.5 cm^3, 12.5 mmol, (a 2.5 mol equivalent)) were added to this solution which was then refluxed for 28 h under Ar. The resulting solution was left to cool slowly. The crystals were collected by filtration and washed with light petrol ether and diethylether. They were then dried *in vacuo* at 45°C to remove any residual water.

IR (KBr): 1939.1 cm^{-1} Lit[8] 1940 cm^{-1}

^{31}P NMR (CD_2Cl_2): 43.6 (d, $^1J_{Rh-H}$=94.6 Hz) Lit[8]. (CD_2Cl_2): 44 (d $^1J_{Rh-H}$ =96.8 Hz)

^1H NMR (CD_2Cl_2): -31.9 (dt. $^1J_{Rh-H}$ =32.7 Hz, $^2J_{H-Ph}$ =11.9 Hz). Lit[8]. (CD_2Cl_2): -31.3 (dt. $^1J_{Rh-H}$ =32.6 Hz, $^2J_{H-Ph}$ =12.48 Hz)

(found: C 43.59, H 9.03 %. $C_{18}H_{43}Cl_2P_2Rh$ requires C 43.65, H 8.75 %.)

Preparation of $[RhClH_2(P^iPr_3)_2]$

The method of preparation of $[RhCl_2H(P^iPr_3)_2]$ by Grushin and co-workers provides a route to the reproducible synthesis of $[RhClH_2(P^iPr_3)_2]$.

$[RhCl_2H(P^iPr_3)_2]$ (1.44 g, 2.90 mmol) was stirred in THF containing P^iPr_3 (0.4 cm^3) and H_2O (200 μL, 11 mmol) was decanted onto a sodium amalgam (0.2 g Na, 60 g Hg) and stirred slowly under Ar until the solution was yellow (ca. 2 h). The solution was decanted from the amalgam which was washed with THF (15 cm^3) and the washings added to the solution. The mixture was reduced to an oil *in vacuo* and extracted into light petroleum ether. This solution was reduced to a small volume *in vacuo* and stored at -30°C for a period of 72 h. Light yellow crystals grew which were contaminated with a darker material. This solid bulk was separated by filtration at -78°C and redissolved in light petroleum ether. This solution was reduced to a small volume *in vacuo* and stored at -30°C. Pale yellow crystals separated from the solution and were collected by filtration at -78°C.

IR (CH_2Cl_2): 2140 cm^{-1} Lit[8] 2140 cm^{-1}

^{31}P NMR (C_6D_6): 62.8 ($^1J_{Rh-H}$=113.8 Hz) Lit[8]: 67.9 (d $^1J_{Rh-H}$=115 Hz).

^1H NMR (C_6D_6): -22.8 (overlapping dt, $^1J_{Rh-H}$=26.4 Hz, $^2J_{H-Ph}$=13.7 Hz), 1.15 (q, J=7.1 Hz), 2.16 (m) Lit[18]: -22.70 (dt. $^1J_{Rh-H}$=26.5 Hz, $^2J_{H-Ph}$=13.3 Hz), 1.18 (dt), 2.20 (m)

Preparation of $[RhH(P^iPr_3)_3]$ [7]

The method of preparation of $[RhCl_2H(P^iPr_3)_2]$ by Grushin and co-workers described above provides the best precursor for this preparation.

THF (35 cm^3) and P^iPr_3 (1,5 cm^3, 8.0 mmol) were added to the orange crystals of $[RhCl_2H(P^iPr_3)_2]$ Subsequently, the suspension was treated with Na/Hg (1.0 g, 10 cm^3) and stirred for 18 h. The resulting solution was decanted from the amalgam which was also washed with THF, and the washings were added to the solution. The solvent was removed *in vacuo*, and the resulting yellow-brown tar was extracted into light petroleum ether and filtered through celite. The extractions were reduced to a small volume *in vacuo*, 15 drops of P^iPr_3 were added prior to storage at -30°C. After 24 h., yellow-brown crystals had grown. The solvent was decanted and the yellow crystals

were washed with cold light petroleum ether. The crystals were unstable to air, and unstable in the solid state under an atmosphere of argon. They were stored as a light petroleum ether solution from which volumes could be decanted and evaporated *in vacuo* as required.

IR (petrol): 1957 cm^{-1} Lit[7]: 1975 cm^{-1}

^{31}P NMR (C_6D_6): 53.6 (d, $^1J_{Rh-H}$=157.3 Hz) Lit[15]: 32.2 (d $^1J_{Rh-H}$=157 Hz), 19.7 (s, P^iPr_3).

^1H NMR (d^8 THF): -11.6, complex multiplet, AB_2XM type system. Lit[7]: -10.5, complex multiplet.

Preparation of $[RhH(P^iPr_3)_3]$

Made by the method of Werner and co-workers[20]

A solution of $[RhH_2Cl(P^iPr_3)_2]$ (0.52 mg, 1.13 mmol) and P^iPr_3 (2.0 cm^3, 10 mmol) in toluene (20 cm^3) was treated with ^{t}BuOK (13 g, 10 mmol) at 25°C and stirred for 10 min. The solvent was removed *in vacuo* and the orange residue was extracted with light petroleum ether (100 cm^3). The extractions were reduced *in vacuo* and the orange oil remaining was dissolved in diethylether (4.2 cm^3). The solution was cooled to -78°C and was slowly treated with similarly cooled dried methanol (90 cm^{3v}). The orange/yellow precipitate was filtered after 1 h. at -78°C, and was dried *in vacuo* to remove residual methanol. After 24 h. at ambient temperature and ambient conditions of light, degradation was noticed by colour change from yellow to dark orange, so the solid was stored in the freezer in tin foil.

IR (petrol): 1959.6 cm^{-1} Lit[7]: 1975 cm^{-1}

^{31}P NMR (C_6D_6): 53.6 ($^1J_{Rh-H}$ =157.3 Hz), Lit[15]: 32.2 (d $^1J_{Rh-H}$=157 Hz), 53.9 (s, P^iPr_3O), 19.8 (s, P^iPr_3).

^1H NMR (d^8 THF): -11.6, complex multiplet, AB_2XM type system Lit[7]: -10.5, complex multiplet.

Preparation of $[RhHCl_3(P^iPr_3)_2][HP^iPr_3].THF$

$[RhHCl_2(P^iPr_3)_2]$ (0.136 g, 0.28 mmol, prepared by the method of reflux in THF) was refluxed for 3 h with THF (4 cm^3) and P^iPr_3 (0.3 cm^3). On cooling slowly, orange

crystals of $[RhHCl_3(P^iPr_3)_2][HP^iPr_3]$. These were stored under the mother liquor to prevent decomposition.

IR (KBr) 1943 cm^{-1}

^{31}P NMR (CD_2Cl_2): 43.5 (d, $^1J_{Rh-H}$=113.8 Hz), 32.7(s).

^1H NMR (CD_2Cl_2): -31.3 (very broad), 8.1 (d, $^1J_{P-H}$ = 492 Hz),

(found: C 47.40, H 9.50 %. $C_{31}H_{68}Cl_3OP_3Rh$ requires C 49.98, H 9.08 %.)

Preparation of $[RhCl(CO)(PMe_3)_2]$ [12]

PMe_3 (0.31 cm^3, 3.0 mmol) in benzene (5.0 cm^3) was added drop-wise to a stirring solution of $[RhCl(CO)]_2$ (0.275 g, 0.71 mmol) in benzene (10 cm^3) at room temperature. Concentration to a small volume *in vacuo* gave a yellow precipitate which was separated by filtration and dissolved in ethanol (ca. 15 cm^3). This solution was filtered and reduced by evaporation of ethanol at 78°C until precipitation was noticed. Cooling slowly to room temperature gave yellow crystals which were collected by filtration, washed with cold ethanol and dried *in vacuo*. The mother liquor was stored at -30°C. Crystals were collected by decantation at -78°C and washed with cold hexane.

IR (KBr) 1958 cm^{-1}; Lit[24] (hexane) 1965 cm^{-1}

^{31}P NMR (C_6D_6) -10.1 ppm (d, $^1J_{Rh-H}$ = 114.6 Hz) Lit[12] -10.22 ppm (d, $^1J_{Rh-H}$ = 114.7 Hz)

(found: C 26.68, H 5.67 %. $C_{19}H_{42}ClOP_2Rh$ requires C 26.40, H 5.70 %.)

6.5 References

1. Yoshida, T., Okano, T., Otsuka, S., *J. Am. Chem. Soc.,* **102,** 1980, 5967.
2. Yoshida, T., Okano, T., Ueda, Y., Otsuka, S., *J. Am. Chem. Soc.,* **103,** 1981, 3411.
3. Yoshida, T., Okano, T., Saito, K., Otsuka, S., *Inorg. Chim. Acta.,* 1980, **44,** L135.
4. Okano, T., Yoshida, T., *Yuki Gosei Kagaku Kyokaish,* 1983, **41,** 359.
5. Morton, D., Cole-Hamilton, D.J., Utuk, I.D., Paneque-Sosa, M., Lopez-Poveda, M., *J. Chem. Soc., Dalton Trans.,* 1989, 489.
6. Delgado-Lieta, E., Luke, M.A., Jones, R.F., Cole-Hamilton, D.J., *Polyhedron,* 1982, **1,** 839.
7. Yoshida, T., Okano, T., Thorn, D.L., Tulip, T.H., Otsuka, S., Ibers, J.A., *J. Organomet. Chem.,* **181,** 1979, 183.
8. Bruce, D., PhD. Thesis, 1985.
9. Harlow, R.L., Thorn, D.L., Baker, R.L., Jones, N.L., *Inorg. Chem.,* 1992, **31,** 993.
10. Masters, C., Shaw, B.L., *J. Chem. Soc., A,* 1971, 3679.
11. Grushin, V.V., Alper, A., *Organometallics,* 1991, **10,** 1620.
12. Sakakura, T., Sodeyama, T., Sasaki, K., Wada, K., Tanaka, M., *J. Am. Chem. Soc.,* **112,** 1990, 7221.
13. Blomberg, M.R.A., Siegbahn, P.E.M., Svensson, M., *Inorg. Chem.,* **32,** 1993, 4218.
14. Blomberg, M.R.A., Siegbahn, P.E.M., Svensson, M., *J. Am. Chem. Soc.,* **115,** 1993, 4191.
15. Yoshida, T., Thorn, D.L., Okano, T., Otsuka, S., Ibers, J.A., *J. Am. Chem. Soc.,* **102,** 1980, 6451.
16. English, A.D., Meakin, P., Jesson, J.P., *J. Am. Chem. Soc.,* 1976, **98,** 422.
17. Grushin, V.V., Vymenits, A.B., Vol'pin, M.E., *J. Organomet. Chem.,* **382,** 1990, 185.
18. Werner, H., Wolf, J., Hohn, A., *J. Organomet. Chem.,* **287,** 1985, 395.
19. Van der Ent, A., Onderdelinden, A.L., *Inorg. Synth.,* **14,** 1973, 92.

20. Wolf, J., Nurnberg, O., Werner, H., *Chem. Ber.,* 1993, **126,** 1409.

21. Shriver, D.F., "The Manipulation of Air Sensitive Compounds", McGraw-Hill, New York, 1969.

22. Cowley, A.H., Mills, J.L., *J. Am. Chem. Soc.,* **91,** 1969, 2915.

23. Olah, G.A., McFarland, C.W., *J. Org. Chem.,* **34,** 1969.

24. Browning, J., Goggin, P.L., Goodfellow, R,J., Norton, M.G., Rattray, A.J.M., Taylor, B.F., Mink, J., *J. Chem. Soc., Dalton Trans.,* 1977, 2061.

APPENDIX 1

X-RAY CRYSTAL STRUCTURE PARAMETERS FOR $[RhH_2Cl(P^iPr_3)_2]$

X-ray Structure Report

Mon May 6 1996

Experimental

Data Collection

A green block crystal of $C_{18}H_{44}P_2RhCl$ having approximate dimensions of 0.30 x 0.30 x 0.40 mm was mounted on a glass fiber. All measurements were made on a Rigaku AFC7S diffractometer with graphite monochromated Mo-Kα radiation.

Cell constants and an orientation matrix for data collection , obtained from a least-squares refinement using the setting angles of 18 carefully centered reflections in the range $6.32 < 2\theta < 12.02°$ corresponded to a primitive monoclinic cell with dimensions:

a = 13.095(2) $\AA$

b = 12.614(4) $\AA$ $\quad \beta = 100.17(2)°$

c = 14.621(4) $\AA$

V = 2377(1) $\AA^3$

For Z = 4 and F.W. = 460.85, the calculated density is 1.29 g/cm^3. The systematic absences of:

h0l: h+l $\neq$ 2n

0k0: k $\neq$ 2n

uniquely determine the space group to be:

$P2_1/n$ (#14)

The data were collected at a temperature of 220 $\pm$ 1°C using the ω-2θ scan technique to a maximum 2θ value of 50.0°. Omega scans of several intense reflections, made prior to data collection, had an average width at half-height of 0.28° with a take-off angle of 6.0°. Scans of (1.78 + 0.35 tan θ)° were made at a speed of 16.0°/min (in omega). The weak reflections ($I < 15.0\sigma(I)$) were rescanned (maximum of 4 scans) and the counts were accumulated to ensure good counting statistics. Stationary background counts were recorded on each side of the reflection. The ratio of peak counting time to background counting time was 2:1. The diameter of the incident beam collimator was 1.0 mm and the crystal to detector distance was 235 mm, The computer-controlled slits were set to 9.0 mm (horizontal) and 13.0 mm (vertical).

Data Reduction

Of the 4539 reflections which were collected, 4339 were unique ($R_{int} = 0.018$). The intensities of three representative reflection were measured after every 150 reflections. No decay correction was applied.

The linear absorption coefficient, μ, for Mo-Kα radiation is 9.6 cm^{-1}. Azimuthal scans of several reflections indicated no need for an absorption correction. The data were corrected for Lorentz and polarization effects.

Structure Solution and Refinement

The structure was solved by direct methods[1] and expanded using Fourier techniques[2]. The non-hydrogen atoms were refined anisotropically. Some hydrogen atoms were refined isotropically, the rest were included in fixed positions. The final cycle of full-matrix least-squares refinement[3] was based on 3313 observed reflections ($I > 3.00\sigma(I)$) and 207 variable parameters and converged (largest parameter shift was 0.01 times its esd) with unweighted and weighted agreement factors of:

$$R = \Sigma||Fo| - |Fc||/\Sigma|Fo| = 0.025$$

$$R_w = \sqrt{(\Sigma w(|Fo| - |Fc|)^2/\Sigma wFo^2)}] = 0.023$$

The standard deviation of an observation of unit weight[4] was 1.92. The weighting scheme was based on counting statistics and included a factor (p = 0.002) to downweight the intense reflections. Plots of $\Sigma w(|Fo| - |Fc|)^2$ versus $|Fo|$, reflection order in data collection, sin θ/λ and various classes of indices showed no unusual trends. The maximum and minimum peaks on the final difference Fourier map corresponded to 0.35 and -0.49 $e^-/\AA^3$, respectively.

Neutral atom scattering factors were taken from Cromer and Waber[5] . Anomalous dispersion effects were included in Fcalc[6]; the values for Δf' and Δf" were those of Creagh and McAuley[7]. The values for the mass attenuation coefficients are those of Creagh and Hubbel[8]. All calculations were performed using the teXsan[9] crystallographic software package of Molecular Structure Corporation.

References

(1) SIR92: Altomare, A., Burla, M.C., Camalli, M., Cascarano, M., Giacovazzo, C., Guagliardi, A., Polidori, G. (1994). J. Appl. Cryst., in preparation.

(2) DIRDIF94: Beurskens, P.T., Admiraal, G., Beurskens, G., Bosman, W.P., de Gelder, R., Israel, R. and Smits, J.M.M. (1994). The DIRDIF-94 program system, Technical Report of the Crystallography Laboratory, University of Nijmegen, The Netherlands.

(3) Least-Squares:

Function minimized: $\Sigma w(|Fo| - |Fc|)^2$

where w = $\frac{1}{\sigma^2(Fo)} = \frac{4Fo^2}{\sigma^2(Fo^2)}$

$\sigma^2(Fo^2) = \frac{S^2(C+R^2B)+(pFo^2)^2}{Lp^2}$

S = Scan rate

C = Total integrated peak count

R = Ratio of scan time to background counting time

B = Total background count

Lp = Lorentz-polarization factor

p = p-factor

(4) Standard deviation of an observation of unit weight:

$$\sqrt{\Sigma w(|Fo| - |Fc|)^2/(No - Nv)}$$

where: No = number of observations

Nv = number of variables

(5) Cromer, D. T. & Waber, J. T.; "International Tables for X-ray Crystallography", Vol. IV, The Kynoch Press, Birmingham, England, Table 2.2 A (1974).

(6) Ibers, J. A. & Hamilton, W. C.; Acta Crystallogr., 17, 781 (1964).

(7) Creagh, D. C. & McAuley, W.J .; "International Tables for Crystallography", Vol C, (A.J.C. Wilson, ed.), Kluwer Academic Publishers, Boston, Table 4.2.6.8, pages 219-222 (1992).

(8) Creagh, D. C. & Hubbell, J.H..; "International Tables for Crystallography", Vol C, (A.J.C. Wilson, ed.), Kluwer Academic Publishers, Boston, Table 4.2.4.3, pages 200-206 (1992).

(9) teXsan: Crystal Structure Analysis Package, Molecular Structure Corporation (1985 & 1992).

EXPERIMENTAL DETAILS

A. Crystal Data

Empirical Formula	$C_{18}H_{44}P_2RhCl$
Formula Weight	460.85
Crystal Color, Habit	green, block
Crystal Dimensions	0.30 X 0.30 X 0.40 mm
Crystal System	monoclinic
Lattice Type	Primitive
No. of Reflections Used for Unit	
Cell Determination (2θ range)	18 (6.3 - 12.0°)
Omega Scan Peak Width	
at Half-height	0.28°
Lattice Parameters	a = 13.095(2)Å b = 12.614(4) Å c = 14.621(4) Å β = 100.17(2)°
	V = 2377(1) Å^3
Space Group	$P2_1/n$ (#14)
Z value	4
D_{calc}	1.288 g/cm^3
F_{000}	976.00
μ(MoKα)	9.61 cm^{-1}

B. Intensity Measurements

Diffractometer	Rigaku AFC7S

Radiation	MoKα (λ = 0.71069 Å) graphite monochromated
Attenuator	Zr foil (factor = 8.53)
Take-off Angle	6.0°
Detector Aperture	9.0 mm horizontal 13.0 mm vertical
Crystal to Detector Distance	235 mm
Temperature	220.0°C
Scan Type	ω-2θ
Scan Rate	16.0°/min (in ω) (up to 4 scans)
Scan Width	$(1.78 + 0.35 \tan \theta)°$
$2\theta_{max}$	50.0°
No. of Reflections Measured	Total: 4539 Unique: 4339 (R_{int} = 0.018)
Corrections	Lorentz-polarization

C. Structure Solution and Refinement

Structure Solution	Direct Methods (SIR92)
Refinement	Full-matrix least-squares
Function Minimized	$\Sigma w(\|Fo\| - \|Fc\|)^2$
Least Squares Weights	$\frac{1}{\sigma^2(Fo)} = \frac{4Fo^2}{\sigma^2(Fo^2)}$
p-factor	0.0020
Anomalous Dispersion	All non-hydrogen atoms
No. Observations (I>3.00σ(I))	3313
No. Variables	207
Reflection/Parameter Ratio	16.00
Residuals: R; Rw	0.025 ; 0.023
Goodness of Fit Indicator	1.92

Max Shift/Error in Final Cycle	0.01
Maximum peak in Final Diff. Map	0.35 $e^-/\AA^3$
Minimum peak in Final Diff. Map	-0.49 $e^-/\AA^3$

Table 1. Atomic coordinates and B_{iso}/B_{eq}

atom	x	y	z	B_{eq}
Rh(1)	0.22265(2)	0.18861(2)	0.98054(2)	2.218(5)
Cl(1)	0.15402(7)	0.31508(7)	0.86013(6)	3.56(2)
P(1)	0.22064(6)	0.05149(7)	0.87527(6)	2.39(2)
P(2)	0.22837(6)	0.31856(6)	1.09263(5)	2.16(2)
C(1)	0.3036(3)	0.0764(3)	0.7867(2)	3.43(9)
C(2)	0.0894(2)	0.0296(2)	0.8065(2)	2.56(7)
C(3)	0.2639(3)	-0.0826(3)	0.9203(2)	3.41(8)
C(4)	0.2601(3)	0.2797(2)	1.2165(2)	2.81(8)
C(5)	0.1050(2)	0.3931(2)	1.0813(2)	2.75(8)
C(6)	0.3296(2)	0.4209(2)	1.0865(2)	2.68(7)
C(7)	0.4009(3)	0.1373(3)	0.8313(3)	5.0(1)
C(8)	0.2496(3)	0.1387(3)	0.7020(2)	4.4(1)
C(9)	0.0799(3)	-0.0682(3)	0.7429(2)	3.58(9)
C(10)	0.0045(2)	0.0318(3)	0.8659(2)	3.30(8)
C(11)	0.3803(3)	-0.0895(3)	0.9540(3)	6.5(1)
C(12)	0.2072(3)	-0.1200(3)	0.9975(3)	5.4(1)
C(13)	0.3692(3)	0.2341(3)	1.2424(3)	4.16(9)
C(14)	0.1814(3)	0.2027(3)	1.2449(2)	4.26(10)
C(15)	0.0972(3)	0.4678(3)	1.1618(3)	4.13(10)
C(16)	0.0092(2)	0.3216(3)	1.0583(2)	3.61(9)
C(17)	0.2917(3)	0.5166(3)	1.0258(2)	3.81(9)
C(18)	0.4224(3)	0.3726(3)	1.0515(3)	4.14(10)
H(1)	0.3247	0.0099	0.7658	4.1154
H(2)	0.0763	0.0889	0.7660	3.0692

Table 1. Atomic coordinates and B_{iso}/B_{eq} (continued)

atom	x	y	z	B_{eq}
H(3)	0.2472	-0.1309	0.8701	4.0909
H(4)	0.2580	0.3423	1.2523	3.3780
H(5)	0.1032	0.4375	1.0286	3.3034
H(6)	0.3534	0.4461	1.1478	3.2156
H(7)	0.4357	0.0992	0.8837	6.0161
H(8)	0.4459	0.1453	0.7874	6.0161
H(9)	0.3815	0.2053	0.8505	6.0161
H(10)	0.2301	0.2065	0.7213	5.3311
H(11)	0.2958	0.1469	0.6591	5.3311
H(12)	0.1895	0.1013	0.6731	5.3311
H(13)	0.0139	-0.0682	0.7036	4.2977
H(14)	0.1328	-0.0663	0.7061	4.2977
H(15)	0.0872	-0.1307	0.7799	4.2977
H(16)	0.0112	0.0943	0.9027	3.9655
H(17)	-0.0616	0.0310	0.8267	3.9655
H(18)	0.0111	-0.0286	0.9053	3.9655
H(19)	0.3986	-0.1603	0.9717	7.7929
H(20)	0.4155	-0.0684	0.9055	7.7929
H(21)	0.3995	-0.0439	1.0060	7.7929
H(22)	0.2240	-0.0745	1.0497	6.4291
H(23)	0.1345	-0.1184	0.9756	6.4291
H(24)	0.2280	-0.1904	1.0149	6.4291
H(25)	0.3842	0.2211	1.3074	4.9872
H(26)	0.3733	0.1695	1.2099	4.9872

Table 1. Atomic coordinates and B_{iso}/B_{eq} (continued)

atom	x	y	z	B_{eq}
H(27)	0.4179	0.2833	1.2261	4.9872
H(28)	0.1139	0.2323	1.2299	5.1077
H(29)	0.1836	0.1377	1.2124	5.1077
H(30)	0.1979	0.1900	1.3098	5.1077
H(31)	0.1569	0.5118	1.1734	4.9584
H(32)	0.0369	0.5106	1.1463	4.9584
H(33)	0.0929	0.4275	1.2159	4.9584
H(34)	-0.0512	0.3642	1.0429	4.3284
H(35)	0.0159	0.2774	1.0071	4.3284
H(36)	0.0037	0.2788	1.1107	4.3284
H(37)	0.3464	0.5665	1.0285	4.5688
H(38)	0.2701	0.4940	0.9633	4.5688
H(39)	0.2349	0.5486	1.0476	4.5688
H(40)	0.4476	0.3137	1.0893	4.9686
H(41)	0.4015	0.3498	0.9890	4.9686
H(42)	0.4756	0.4243	1.0543	4.9686
H(43)	0.175(3)	0.133(3)	1.049(2)	6.7(10)
H(44)	0.307(3)	0.132(3)	1.046(2)	5.7(9)

$$B_{eq} = \frac{8}{3}\pi^2(U_{11}(aa^*)^2 + U_{22}(bb^*)^2 + U_{33}(cc^*)^2 + 2U_{12}aa^*bb^*\cos\gamma + 2U_{13}aa^*cc^*\cos\beta + 2U_{23}bb^*cc^*\cos\alpha)$$

Table 2. Anisotropic Displacement Parameters

atom	U_{11}	U_{22}	U_{33}	U_{12}	U_{13}	U_{23}
Rh(1)	0.0307(1)	0.0233(1)	0.0299(1)	-0.0019(1)	0.0043(1)	-0.0022(1)
Cl(1)	0.0636(6)	0.0367(5)	0.0333(5)	0.0073(5)	0.0042(4)	0.0014(4)
P(1)	0.0312(5)	0.0246(4)	0.0355(5)	-0.0011(4)	0.0072(4)	-0.0041(4)
P(2)	0.0321(4)	0.0224(4)	0.0270(4)	-0.0048(4)	0.0040(3)	-0.0001(4)
C(1)	0.049(2)	0.034(2)	0.055(2)	-0.003(2)	0.027(2)	-0.010(2)
C(2)	0.037(2)	0.027(2)	0.032(2)	-0.001(1)	0.003(1)	-0.001(1)
C(3)	0.047(2)	0.025(2)	0.054(2)	0.005(2)	-0.001(2)	-0.005(2)
C(4)	0.048(2)	0.028(2)	0.029(2)	-0.009(2)	0.002(2)	0.000(1)
C(5)	0.038(2)	0.028(2)	0.040(2)	-0.001(2)	0.009(2)	-0.001(2)
C(6)	0.040(2)	0.029(2)	0.032(2)	-0.012(2)	0.004(1)	0.000(1)
C(7)	0.048(2)	0.067(3)	0.082(3)	-0.016(2)	0.031(2)	-0.007(2)
C(8)	0.081(3)	0.050(2)	0.046(2)	-0.014(2)	0.032(2)	-0.005(2)
C(9)	0.047(2)	0.041(2)	0.047(2)	-0.006(2)	0.005(2)	-0.012(2)
C(10)	0.035(2)	0.044(2)	0.046(2)	-0.001(2)	0.004(2)	-0.001(2)
C(11)	0.048(3)	0.057(3)	0.136(4)	0.017(2)	0.001(3)	0.021(3)
C(12)	0.076(3)	0.038(2)	0.088(3)	0.003(2)	0.008(3)	0.023(2)
C(13)	0.061(3)	0.042(2)	0.048(2)	-0.009(2)	-0.011(2)	0.013(2)
C(14)	0.071(3)	0.050(2)	0.040(2)	-0.015(2)	0.009(2)	0.014(2)
C(15)	0.057(2)	0.039(2)	0.064(3)	0.003(2)	0.020(2)	-0.013(2)
C(16)	0.033(2)	0.049(2)	0.056(2)	0.001(2)	0.009(2)	-0.002(2)
C(17)	0.060(3)	0.039(2)	0.046(2)	-0.018(2)	0.008(2)	0.008(2)
C(18)	0.041(2)	0.056(3)	0.064(3)	-0.013(2)	0.017(2)	-0.001(2)

The general temperature factor expression:

$$\exp(-2\pi^2(a^{*2}U_{11}h^2 + b^{*2}U_{22}k^2 + c^{*2}U_{33}l^2 + 2a^*b^*U_{12}hk + 2a^*c^*U_{13}hl + 2b^*c^*U_{23}kl))$$

Table 3. Bond Lengths($\AA$)

atom	atom	distance	atom	atom	distance
Rh(1)	Cl(1)	2.4275(9)	Rh(1)	P(1)	2.3123(8)
Rh(1)	P(2)	2.3097(8)	P(1)	C(1)	1.859(3)
P(1)	C(2)	1.852(3)	P(1)	C(3)	1.866(3)
P(2)	C(4)	1.852(3)	P(2)	C(5)	1.852(3)
P(2)	C(6)	1.864(3)	C(1)	C(7)	1.532(5)
C(1)	C(8)	1.530(5)	C(2)	C(9)	1.536(4)
C(2)	C(10)	1.528(4)	C(3)	C(11)	1.519(5)
C(3)	C(12)	1.531(5)	C(4)	C(13)	1.525(5)
C(4)	C(14)	1.526(4)	C(5)	C(15)	1.525(4)
C(5)	C(16)	1.533(4)	C(6)	C(17)	1.528(4)
C(6)	C(18)	1.526(4)			

Table 4. Bond Lengths(Å)

atom	atom	distance	atom	atom	distance
Rh(1)	H(43)	1.45(4)	Rh(1)	H(44)	1.51(3)
C(1)	H(1)	0.95	C(2)	H(2)	0.95
C(3)	H(3)	0.95	C(4)	H(4)	0.95
C(5)	H(5)	0.95	C(6)	H(6)	0.95
C(7)	H(7)	0.95	C(7)	H(8)	0.95
C(7)	H(9)	0.95	C(8)	H(10)	0.95
C(8)	H(11)	0.95	C(8)	H(12)	0.95
C(9)	H(13)	0.95	C(9)	H(14)	0.95
C(9)	H(15)	0.95	C(10)	H(16)	0.95
C(10)	H(17)	0.95	C(10)	H(18)	0.95
C(11)	H(19)	0.95	C(11)	H(20)	0.95
C(11)	H(21)	0.95	C(12)	H(22)	0.95
C(12)	H(23)	0.95	C(12)	H(24)	0.95
C(13)	H(25)	0.95	C(13)	H(26)	0.95
C(13)	H(27)	0.95	C(14)	H(28)	0.95
C(14)	H(29)	0.95	C(14)	H(30)	0.95
C(15)	H(31)	0.95	C(15)	H(32)	0.95
C(15)	H(33)	0.95	C(16)	H(34)	0.95
C(16)	H(35)	0.95	C(16)	H(36)	0.95
C(17)	H(37)	0.95	C(17)	H(38)	0.95
C(17)	H(39)	0.95	C(18)	H(40)	0.95
C(18)	H(41)	0.95	C(18)	H(42)	0.95

Table 5. Bond Angles(°)

atom	atom	atom	angle	atom	atom	atom	angle
Cl(1)	Rh(1)	P(1)	92.84(3)	Cl(1)	Rh(1)	P(2)	90.55(3)
P(1)	Rh(1)	P(2)	176.60(3)	Rh(1)	P(1)	C(1)	113.5(1)
Rh(1)	P(1)	C(2)	111.9(1)	Rh(1)	P(1)	C(3)	118.4(1)
C(1)	P(1)	C(2)	104.3(2)	C(1)	P(1)	C(3)	102.7(2)
C(2)	P(1)	C(3)	104.6(1)	Rh(1)	P(2)	C(4)	118.7(1)
Rh(1)	P(2)	C(5)	112.3(1)	Rh(1)	P(2)	C(6)	113.1(1)
C(4)	P(2)	C(5)	105.3(1)	C(4)	P(2)	C(6)	101.1(1)
C(5)	P(2)	C(6)	105.1(1)	P(1)	C(1)	C(7)	109.4(2)
P(1)	C(1)	C(8)	114.0(2)	C(7)	C(1)	C(8)	108.5(3)
P(1)	C(2)	C(9)	114.6(2)	P(1)	C(2)	C(10)	112.7(2)
C(9)	C(2)	C(10)	111.7(3)	P(1)	C(3)	C(11)	113.0(3)
P(1)	C(3)	C(12)	112.5(2)	C(11)	C(3)	C(12)	109.4(3)
P(2)	C(4)	C(13)	112.4(2)	P(2)	C(4)	C(14)	112.9(2)
C(13)	C(4)	C(14)	109.9(3)	P(2)	C(5)	C(15)	114.9(2)
P(2)	C(5)	C(16)	112.8(2)	C(15)	C(5)	C(16)	111.7(3)
P(2)	C(6)	C(17)	114.4(2)	P(2)	C(6)	C(18)	110.7(2)
C(17)	C(6)	C(18)	108.5(3)				

Table 6. Bond Angles(°)

atom	atom	atom	angle	atom	atom	atom	angle
Cl(1)	Rh(1)	H(43)	132(1)	Cl(1)	Rh(1)	H(44)	155(1)
P(1)	Rh(1)	H(43)	98(1)	P(1)	Rh(1)	H(44)	89(1)
P(2)	Rh(1)	H(43)	79(1)	P(2)	Rh(1)	H(44)	87(1)
H(43)	Rh(1)	H(44)	71(1)	P(1)	C(1)	H(1)	108.2
C(7)	C(1)	H(1)	108.3	C(8)	C(1)	H(1)	108.2
P(1)	C(2)	H(2)	105.6	C(9)	C(2)	H(2)	105.6
C(10)	C(2)	H(2)	105.7	P(1)	C(3)	H(3)	107.2
C(11)	C(3)	H(3)	107.2	C(12)	C(3)	H(3)	107.2
P(2)	C(4)	H(4)	107.1	C(13)	C(4)	H(4)	107.1
C(14)	C(4)	H(4)	107.1	P(2)	C(5)	H(5)	105.5
C(15)	C(5)	H(5)	105.5	C(16)	C(5)	H(5)	105.5
P(2)	C(6)	H(6)	107.7	C(17)	C(6)	H(6)	107.7
C(18)	C(6)	H(6)	107.6	C(1)	C(7)	H(7)	109.5
C(1)	C(7)	H(8)	109.5	C(1)	C(7)	H(9)	109.5
H(7)	C(7)	H(8)	109.5	H(7)	C(7)	H(9)	109.5
H(8)	C(7)	H(9)	109.5	C(1)	C(8)	H(10)	109.4
C(1)	C(8)	H(11)	109.4	C(1)	C(8)	H(12)	109.5
H(10)	C(8)	H(11)	109.5	H(10)	C(8)	H(12)	109.5
H(11)	C(8)	H(12)	109.5	C(2)	C(9)	H(13)	109.5
C(2)	C(9)	H(14)	109.5	C(2)	C(9)	H(15)	109.4
H(13)	C(9)	H(14)	109.5	H(13)	C(9)	H(15)	109.5
H(14)	C(9)	H(15)	109.5	C(2)	C(10)	H(16)	109.5
C(2)	C(10)	H(17)	109.5	C(2)	C(10)	H(18)	109.5
H(16)	C(10)	H(17)	109.5	H(16)	C(10)	H(18)	109.5

Table 6. Bond Angles(°) (continued)

atom	atom	atom	angle	atom	atom	atom	angle
H(17)	C(10)	H(18)	109.5	C(3)	C(11)	H(19)	109.5
C(3)	C(11)	H(20)	109.5	C(3)	C(11)	H(21)	109.5
H(19)	C(11)	H(20)	109.5	H(19)	C(11)	H(21)	109.5
H(20)	C(11)	H(21)	109.4	C(3)	C(12)	H(22)	109.4
C(3)	C(12)	H(23)	109.4	C(3)	C(12)	H(24)	109.4
H(22)	C(12)	H(23)	109.5	H(22)	C(12)	H(24)	109.5
H(23)	C(12)	H(24)	109.5	C(4)	C(13)	H(25)	109.4
C(4)	C(13)	H(26)	109.4	C(4)	C(13)	H(27)	109.4
H(25)	C(13)	H(26)	109.5	H(25)	C(13)	H(27)	109.5
H(26)	C(13)	H(27)	109.5	C(4)	C(14)	H(28)	109.5
C(4)	C(14)	H(29)	109.4	C(4)	C(14)	H(30)	109.5
H(28)	C(14)	H(29)	109.5	H(28)	C(14)	H(30)	109.5
H(29)	C(14)	H(30)	109.5	C(5)	C(15)	H(31)	109.5
C(5)	C(15)	H(32)	109.5	C(5)	C(15)	H(33)	109.5
H(31)	C(15)	H(32)	109.5	H(31)	C(15)	H(33)	109.4
H(32)	C(15)	H(33)	109.5	C(5)	C(16)	H(34)	109.5
C(5)	C(16)	H(35)	109.5	C(5)	C(16)	H(36)	109.5
H(34)	C(16)	H(35)	109.5	H(34)	C(16)	H(36)	109.5
H(35)	C(16)	H(36)	109.5	C(6)	C(17)	H(37)	109.5
C(6)	C(17)	H(38)	109.5	C(6)	C(17)	H(39)	109.5
H(37)	C(17)	H(38)	109.5	H(37)	C(17)	H(39)	109.5
H(38)	C(17)	H(39)	109.5	C(6)	C(18)	H(40)	109.5
C(6)	C(18)	H(41)	109.5	C(6)	C(18)	H(42)	109.5
H(40)	C(18)	H(41)	109.5	H(40)	C(18)	H(42)	109.5

Table 6. Bond Angles(°) (continued)

atom	atom	atom	angle	atom	atom	atom	angle
H(41)	C(18)	H(42)	109.5				

Table 7. Torsion Angles(°)

atom	atom	atom	atom	angle	atom	atom	atom	atom	angle
Rh(1)	P(1)	C(1)	C(7)	35.7(3)	Rh(1)	P(1)	C(1)	C(8)	-86.0(3)
Rh(1)	P(1)	C(2)	C(9)	-173.5(2)	Rh(1)	P(1)	C(2)	C(10)	-44.2(2)
Rh(1)	P(1)	C(3)	C(11)	-71.9(3)	Rh(1)	P(1)	C(3)	C(12)	52.7(3)
Rh(1)	P(2)	C(4)	C(13)	63.4(2)	Rh(1)	P(2)	C(4)	C(14)	-61.6(3)
Rh(1)	P(2)	C(5)	C(15)	170.7(2)	Rh(1)	P(2)	C(5)	C(16)	41.1(3)
Rh(1)	P(2)	C(6)	C(17)	91.3(2)	Rh(1)	P(2)	C(6)	C(18)	-31.6(3)
Cl(1)	Rh(1)	P(1)	C(1)	60.7(1)	Cl(1)	Rh(1)	P(1)	C(2)	-57.1(1)
Cl(1)	Rh(1)	P(1)	C(3)	-178.8(1)	Cl(1)	Rh(1)	P(2)	C(4)	172.2(1)
Cl(1)	Rh(1)	P(2)	C(5)	49.0(1)	Cl(1)	Rh(1)	P(2)	C(6)	-69.8(1)
P(1)	Rh(1)	P(2)	C(4)	-6.8(6)	P(1)	Rh(1)	P(2)	C(5)	-130.1(5)
P(1)	Rh(1)	P(2)	C(6)	111.2(5)	P(2)	Rh(1)	P(1)	C(1)	-120.3(5)
P(2)	Rh(1)	P(1)	C(2)	122.0(5)	P(2)	Rh(1)	P(1)	C(3)	0.2(6)
C(1)	P(1)	C(2)	C(9)	63.4(3)	C(1)	P(1)	C(2)	C(10)	-167.3(2)
C(1)	P(1)	C(3)	C(11)	54.0(3)	C(1)	P(1)	C(3)	C(12)	178.6(3)
C(2)	P(1)	C(1)	C(7)	157.8(3)	C(2)	P(1)	C(1)	C(8)	36.1(3)
C(2)	P(1)	C(3)	C(11)	162.7(3)	C(2)	P(1)	C(3)	C(12)	-72.7(3)
C(3)	P(1)	C(1)	C(7)	-93.3(3)	C(3)	P(1)	C(1)	C(8)	145.0(3)
C(3)	P(1)	C(2)	C(9)	-44.1(3)	C(3)	P(1)	C(2)	C(10)	85.1(3)
C(4)	P(2)	C(5)	C(15)	40.2(3)	C(4)	P(2)	C(5)	C(16)	-89.4(2)
C(4)	P(2)	C(6)	C(17)	-140.8(2)	C(4)	P(2)	C(6)	C(18)	96.3(2)
C(5)	P(2)	C(4)	C(13)	-170.0(2)	C(5)	P(2)	C(4)	C(14)	65.0(3)
C(5)	P(2)	C(6)	C(17)	-31.5(3)	C(5)	P(2)	C(6)	C(18)	-154.4(2)
C(6)	P(2)	C(4)	C(13)	-60.8(3)	C(6)	P(2)	C(4)	C(14)	174.2(2)
C(6)	P(2)	C(5)	C(15)	-66.0(3)	C(6)	P(2)	C(5)	C(16)	164.4(2)

The ADC (atom designator code) specifies the position of an atom in a crystal. The 5-digit number shown in the table is a composite of three one-digit numbers and one two-digit number: TA (first digit) + TB (second digit) + TC (third digit) + SN (last two digits). TA, TB and TC are the crystal lattice translation digits along cell edges a, b and c. A translation digit of 5 indicates the origin unit cell. If TA = 4, this indicates a translation of one unit cell length along the a-axis in the negative direction. Each translation digit can range in value from 1 to 9 and thus ± 4 lattice translations from the origin (TA=5, TB=5, TC=5) can be represented.

The SN, or symmetry operator number, refers to the number of the symmetry operator used to generate the coordinates of the target atom. A list of symmetry operators relevant to this structure are given below.

For a given intermolecular contact, the first atom (origin atom) is located in the origin unit cell and its position can be generated using the identity operator (SN=1). Thus, the ADC for an origin atom is always 55501. The position of the second atom (target atom) can be generated using the ADC and the coordinates of the atom in the parameter table. For example, an ADC of 47502 refers to the target atom moved through symmetry operator two, then translated -1 cell translations along the a axis, +2 cell translations along the b axis, and 0 cell translations along the c axis.

An ADC of 1 indicates an intermolecular contact between two fragments (eg. cation and anion) that reside in the same asymmetric unit.

Symmetry Operators:

(1)	X,	Y,	Z	(2)	1/2-X,	1/2+Y,	1/2-Z
(3)	-X,	-Y,	-Z	(4)	1/2+X,	1/2-Y,	1/2+Z

APPENDIX 2

X-RAY CRYSTAL STRUCTURE PARAMETERS FOR $[RhHCl_3(P^iPr_3)_2][HP^iPr_3]$

X-ray Structure Report

Mon Oct 13 1997

Experimental

Data Collection

An orange block crystal of $RhCl_3P_3C_{31}H_{68}O$ having approximate dimensions of 0.40 x 0.25 x 0.20 mm was mounted on a glass fiber. All measurements were made on a Rigaku AFC7S diffractometer with graphite monochromated Mo-Kα radiation.

Cell constants and an orientation matrix for data collection , obtained from a least-squares refinement using the setting angles of 2 carefully centered reflections in the range $8.08 < 2\theta < 12.17°$ corresponded to atriclinic cell with dimensions:

a = 11.60(1) $\AA$	α = 95.55(5)°
b = 15.86(2) $\AA$	β = 93.33(5)°
c = 11.345(4) $\AA$	γ = 94.66(9)
V = 2066(2) $\AA^3$	

For Z = 2 and F.W. = 759.06, the calculated density is 1.22 g/cm^3. Based on a statistical analysis of intensity distribution, and the successful solution and refinement of the structure, the space group was determined to be:

$P\bar{1}$ (#2)

The data were collected at a temperature of 220 $\pm$ 1°C using the ω-2θ scan technique to a maximum 2θ value of 45.0°. Omega scans of several intense reflections, made prior to data collection, had an average width at half-height of 0.28° with a take-off angle of 6.0°. Scans of (1.52 + 0.35 tan θ)° were made at a speed of 16.0°/min (in omega). The weak reflections ($I < 15.0\sigma(I)$) were rescanned (maximum of 4 scans) and the counts were accumulated to ensure good counting statistics. Stationary background counts were recorded on each side of the reflection. The ratio of peak counting time to background counting time was 2:1. The diameter of the incident beam collimator was 1.0 mm and the crystal to detector distance was 235 mm, The computer-controlled slits were set to 9.0 mm (horizontal) and 13.0 mm (vertical).

Data Reduction

Of the 4588 reflections which were collected, 4264 were unique (R_{int} = 0.031). The intensities of three representative reflection were measured after every 150 reflections. No decay correction was applied.

The linear absorption coefficient, μ, for Mo-Kα radiation is 7.4 cm^{-1}. An empirical absorption correction based on azimuthal scans of several reflections was applied which resulted in transmission factors ranging from 0.86 to 1.00. The data were corrected for Lorentz and polarization effects.

Structure Solution and Refinement

The structure was solved by and expanded using Fourier techniques[2]. Some non-hydrogen atoms were refined anisotropically, while the rest were refined isotropically. Hydrogen atoms were included but not

refined. The final cycle of full-matrix least-squares refinement[3] was based on 3303 observed reflections ($I > 3.00\sigma(I)$) and 327 variable parameters and converged (largest parameter shift was 0.14 times its esd) with unweighted and weighted agreement factors of:

$$R = \Sigma||Fo| - |Fc||/\Sigma|Fo| = 0.099$$

$$R_w = \sqrt{(\Sigma w(|Fo| - |Fc|)^2/\Sigma wFo^2)} = 0.136$$

The standard deviation of an observation of unit weight[4] was 6.79. The weighting scheme was based on counting statistics and included a factor (p = 0.010) to downweight the intense reflections. Plots of $\Sigma w(|Fo| - |Fc|)^2$ versus $|Fo|$, reflection order in data collection, $\sin\theta/\lambda$ and various classes of indices showed no unusual trends. The maximum and minimum peaks on the final difference Fourier map corresponded to 2.45 and -1.81 $e^-/\AA^3$, respectively.

Neutral atom scattering factors were taken from Cromer and Waber[5] . Anomalous dispersion effects were included in Fcalc[6]; the values for Δf' and Δf" were those of Creagh and McAuley[7]. The values for the mass attenuation coefficients are those of Creagh and Hubbel[8]. All calculations were performed using the teXsan[9] crystallographic software package of Molecular Structure Corporation.

References

(1) ORIENT: Beurskens, P.T., Admiraal, G., Beurskens, G., Bosman, W.P., Garcia-Granda, S., Gould, R.O., Smits, J.M.M. and Smykalla, C. (1992). The DIRDIF program system, Technical Report of the Crystallography Laboratory, University of Nijmegen, The Netherlands.

(2) DIRDIF94: Beurskens, P.T., Admiraal, G., Beurskens, G., Bosman, W.P., de Gelder, R., Israel, R. and Smits, J.M.M. (1994). The DIRDIF-94 program system, Technical Report of the Crystallography Laboratory, University of Nijmegen, The Netherlands.

(3) Least-Squares:

Function minimized: $\Sigma w(|Fo| - |Fc|)^2$

where w = $\frac{1}{\sigma^2(Fo)} = \frac{4Fo^2}{\sigma^2(Fo^2)}$

$\sigma^2(Fo^2) = \frac{S^2(C+R^2B)+(pFo^2)^2}{Lp^2}$

S = Scan rate

C = Total integrated peak count

R = Ratio of scan time to background counting time

B = Total background count

Lp = Lorentz-polarization factor

p = p-factor

(4) Standard deviation of an observation of unit weight:

$$\sqrt{\Sigma w(|Fo| - |Fc|)^2/(No - Nv)}$$

where: No = number of observations

Nv = number of variables

(5) Cromer, D. T. & Waber, J. T.; "International Tables for X-ray Crystallography", Vol. IV, The Kynoch Press, Birmingham, England, Table 2.2 A (1974).

(6) Ibers, J. A. & Hamilton, W. C.; Acta Crystallogr., 17, 781 (1964).

(7) Creagh, D. C. & McAuley, W.J .; "International Tables for Crystallography", Vol C, (A.J.C. Wilson, ed.), Kluwer Academic Publishers, Boston, Table 4.2.6.8, pages 219-222 (1992).

(8) Creagh, D. C. & Hubbell, J.H..; "International Tables for Crystallography", Vol C, (A.J.C. Wilson, ed.), Kluwer Academic Publishers, Boston, Table 4.2.4.3, pages 200-206 (1992).

(9) teXsan: Crystal Structure Analysis Package, Molecular Structure Corporation (1985 & 1992).

EXPERIMENTAL DETAILS

A. Crystal Data

Empirical Formula	$RhCl_3P_3C_{31}H_{68}O$
Formula Weight	759.06
Crystal Color, Habit	orange, block
Crystal Dimensions	0.40 X 0.25 X 0.20 mm
Crystal System	triclinic
Lattice Type	Primitive
No. of Reflections Used for Unit	
Cell Determination (2θ range)	2 (8.1 - 12.2°)
Omega Scan Peak Width	
at Half-height	0.28°
Lattice Parameters	a = 11.60(1)Å b = 15.86(2) Å c = 11.345(4) Å α = 95.55(5)° β = 93.33(5)° γ = 94.66(9)°
	V = 2066(2) $Å^3$
Space Group	$P\bar{1}$ (#2)
Z value	2
D_{calc}	1.220 g/cm^3
F_{000}	806.00
μ(MoKα)	7.42 cm^{-1}

B. Intensity Measurements

Diffractometer	Rigaku AFC7S
Radiation	MoKα (λ = 0.71069 Å) graphite monochromated
Attenuator	Zr foil (factor = 8.53)
Take-off Angle	6.0°
Detector Aperture	9.0 mm horizontal 13.0 mm vertical
Crystal to Detector Distance	235 mm
Temperature	220.0°C
Scan Type	ω-2θ
Scan Rate	16.0°/min (in ω) (up to 4 scans)
Scan Width	$(1.52 + 0.35 \tan \theta)°$
$2\theta_{max}$	45.0°
No. of Reflections Measured	Total: 4588 Unique: 4264 (R_{int} = 0.031)
Corrections	Lorentz-polarization Absorption (trans. factors: 0.8553 - 1.0000)

C. Structure Solution and Refinement

Structure Solution	Direct Methods
Refinement	Full-matrix least-squares
Function Minimized	$\Sigma w(\|Fo\| - \|Fc\|)^2$
Least Squares Weights	$\frac{1}{\sigma^2(Fo)} = \frac{4Fo^2}{\sigma^2(Fo^2)}$
p-factor	0.0100
Anomalous Dispersion	All non-hydrogen atoms
No. Observations (I>3.00σ(I))	3303
No. Variables	327
Reflection/Parameter Ratio	10.10

Residuals: R; Rw	0.099 ; 0.136
Goodness of Fit Indicator	6.79
Max Shift/Error in Final Cycle	0.14
Maximum peak in Final Diff. Map	2.45 $e^-/\AA^3$
Minimum peak in Final Diff. Map	-1.81 $e^-/\AA^3$

Table 1. Atomic coordinates and B_{iso}/B_{eq}

atom	x	y	z	B_{eq}
Rh(1)	0.2233(2)	0.2515(1)	0.1817(2)	2.47(4)
Cl(1)	0.1306(5)	0.3707(3)	0.0809(5)	3.3(1)
Cl(2)	0.4126(5)	0.3142(4)	0.1653(5)	4.3(2)
Cl(3)	0.0390(5)	0.1827(4)	0.2043(5)	4.0(2)
P(1)	0.2249(6)	0.3173(4)	0.3780(5)	3.5(2)
P(2)	0.2446(5)	0.1574(3)	0.0109(5)	2.7(1)
P(3)	-0.2047(5)	0.3427(4)	0.0422(6)	3.4(2)
O(1)	-0.237(4)	0.143(3)	0.625(4)	18(1)
C(1)	0.286(3)	0.246(2)	0.487(2)	7.1(10)
C(2)	0.408(3)	0.233(2)	0.470(3)	7(1)
C(3)	0.210(3)	0.162(2)	0.479(2)	7.4(10)
C(4)	0.333(2)	0.415(2)	0.410(2)	4.7(7)
C(5)	0.308(3)	0.485(2)	0.331(2)	5.8(8)
C(6)	0.344(3)	0.456(2)	0.542(2)	7.0(9)
C(7)	0.097(3)	0.338(2)	0.435(2)	6.0(8)
C(8)	0.070(4)	0.346(2)	0.569(2)	10(1)
C(9)	0.031(3)	0.409(2)	0.378(2)	6.6(9)
C(10)	0.306(2)	0.059(1)	0.049(2)	3.2(6)
C(11)	0.429(2)	0.078(2)	0.112(2)	4.5(7)
C(12)	0.228(2)	0.008(1)	0.125(2)	4.8(7)
C(13)	0.343(2)	0.196(1)	-0.094(2)	3.3(6)
C(14)	0.304(3)	0.275(2)	-0.148(2)	5.6(8)
C(15)	0.388(2)	0.136(2)	-0.191(2)	4.8(7)
C(16)	0.105(2)	0.114(1)	-0.072(2)	2.9(6)

Table 1. Atomic coordinates and B_{iso}/B_{eq} (continued)

atom	x	y	z	B_{eq}
C(17)	0.040(2)	0.180(2)	-0.118(2)	4.6(7)
C(18)	0.111(2)	0.040(2)	-0.171(2)	4.8(7)
C(19)	-0.293(2)	0.276(1)	0.126(2)	3.9(6)
C(20)	-0.268(3)	0.300(2)	0.259(2)	7.1(10)
C(21)	-0.272(3)	0.180(2)	0.093(3)	7.0(9)
C(22)	-0.232(2)	0.454(1)	0.064(2)	4.1(7)
C(23)	-0.151(3)	0.502(2)	0.162(2)	6.5(8)
C(24)	-0.352(2)	0.469(2)	0.075(3)	6.4(9)
C(25)	-0.218(3)	0.304(2)	-0.115(2)	5.5(8)
C(26)	-0.133(2)	0.352(2)	-0.183(2)	5.7(8)
C(27)	-0.344(3)	0.306(2)	-0.167(3)	8(1)
C(28)	-0.159(7)	0.141(5)	0.559(8)	23(3)
C(29)	-0.186(5)	0.092(4)	0.455(5)	15(1)
C(30)	-0.301(5)	0.074(3)	0.444(4)	12(1)
C(31)	-0.337(5)	0.091(4)	0.570(5)	15(1)
H(1)	0.2828	0.2737	0.5649	8.5450
H(2)	0.4354	0.1978	0.5273	8.8698
H(3)	0.4528	0.2859	0.4791	8.8698
H(4)	0.4142	0.2055	0.3927	8.8698
H(5)	0.2384	0.1276	0.5377	8.9530
H(6)	0.1327	0.1725	0.4930	8.9530
H(7)	0.2128	0.1320	0.4027	8.9530
H(8)	0.4072	0.3971	0.3925	5.5931
H(9)	0.2355	0.5057	0.3490	6.9779

Table 1. Atomic coordinates and B_{iso}/B_{eq} (continued)

atom	x	y	z	B_{eq}
H(10)	0.3044	0.4626	0.2502	6.9779
H(11)	0.3674	0.5300	0.3455	6.9779
H(12)	0.3595	0.4136	0.5932	8.4539
H(13)	0.2726	0.4783	0.5603	8.4539
H(14)	0.4045	0.5000	0.5517	8.4539
H(15)	0.0491	0.2880	0.4054	7.2443
H(16)	0.1027	0.3015	0.6063	12.1620
H(17)	0.1034	0.3993	0.6059	12.1620
H(18)	-0.0111	0.3418	0.5749	12.1620
H(19)	0.0613	0.4638	0.4144	7.9367
H(20)	-0.0495	0.4014	0.3908	7.9367
H(21)	0.0408	0.4060	0.2954	7.9367
H(22)	0.3127	0.0241	-0.0230	3.8416
H(23)	0.4243	0.1120	0.1848	5.4490
H(24)	0.4604	0.0266	0.1261	5.4490
H(25)	0.4772	0.1084	0.0621	5.4490
H(26)	0.2217	0.0400	0.1990	5.8033
H(27)	0.2608	-0.0439	0.1382	5.8033
H(28)	0.1535	-0.0048	0.0853	5.8033
H(29)	0.4105	0.2170	-0.0459	3.9664
H(30)	0.2753	0.3122	-0.0875	6.7153
H(31)	0.2443	0.2585	-0.2085	6.7153
H(32)	0.3679	0.3036	-0.1803	6.7153
H(33)	0.4126	0.0870	-0.1580	5.7502

Table 1. Atomic coordinates and B_{iso}/B_{eq} (continued)

atom	x	y	z	B_{eq}
H(34)	0.4521	0.1643	-0.2243	5.7502
H(35)	0.3285	0.1190	-0.2517	5.7502
H(36)	0.0591	0.0905	-0.0143	3.4351
H(37)	0.0358	0.2249	-0.0562	5.4817
H(38)	-0.0356	0.1572	-0.1452	5.4817
H(39)	0.0788	0.2023	-0.1814	5.4817
H(40)	0.0351	0.0217	-0.2033	5.7036
H(41)	0.1454	-0.0055	-0.1383	5.7036
H(42)	0.1567	0.0599	-0.2312	5.7036
H(43)	-0.3716	0.2831	0.1062	4.6487
H(44)	-0.2994	0.3520	0.2815	8.5248
H(45)	-0.3030	0.2564	0.3010	8.5248
H(46)	-0.1868	0.3056	0.2777	8.5248
H(47)	-0.3124	0.1460	0.1446	8.4594
H(48)	-0.1914	0.1735	0.1026	8.4594
H(49)	-0.2993	0.1633	0.0135	8.4594
H(50)	-0.2108	0.4776	-0.0069	4.9140
H(51)	-0.1648	0.5602	0.1699	7.8282
H(52)	-0.1638	0.4785	0.2347	7.8282
H(53)	-0.0728	0.4965	0.1434	7.8282
H(54)	-0.3788	0.4470	0.1438	7.7191
H(55)	-0.3599	0.5288	0.0801	7.7191
H(56)	-0.3972	0.4423	0.0067	7.7191
H(57)	-0.2010	0.2462	-0.1218	6.6576

Table 1. Atomic coordinates and B_{iso}/B_{eq} (continued)

atom	x	y	z	B_{eq}
H(58)	-0.1489	0.4103	-0.1788	6.8508
H(59)	-0.0566	0.3485	-0.1497	6.8508
H(60)	-0.1388	0.3288	-0.2636	6.8508
H(61)	-0.3952	0.2731	-0.1237	9.6094
H(62)	-0.3640	0.3635	-0.1601	9.6094
H(63)	-0.3500	0.2842	-0.2478	9.6094
H(64)	-0.0819	0.1654	0.5809	27.8867
H(65)	-0.1346	0.0766	0.3965	18.2551
H(66)	-0.3493	0.0537	0.3749	14.9235
H(67)	-0.4067	0.0736	0.6047	18.7016
H(68)	0.2771	0.1824	0.2402	4.0000

$$B_{eq} = \frac{8}{3}\pi^2(U_{11}(aa^*)^2 + U_{22}(bb^*)^2 + U_{33}(cc^*)^2 + 2U_{12}aa^*bb^*\cos\gamma + 2U_{13}aa^*cc^*\cos\beta + 2U_{23}bb^*cc^*\cos\alpha)$$

Table 2. Anisotropic Displacement Parameters

atom	U_{11}	U_{22}	U_{33}	U_{12}	U_{13}	U_{23}
Rh(1)	0.037(1)	0.029(1)	0.0285(10)	0.0033(8)	0.0047(8)	0.0070(8)
Cl(1)	0.056(4)	0.032(3)	0.038(3)	0.007(3)	-0.003(3)	0.010(3)
Cl(2)	0.054(4)	0.062(4)	0.044(4)	-0.010(4)	0.004(3)	-0.006(3)
Cl(3)	0.059(4)	0.042(4)	0.050(4)	-0.009(3)	0.018(3)	0.000(3)
P(1)	0.063(5)	0.044(4)	0.029(3)	0.020(4)	0.008(3)	0.005(3)
P(2)	0.038(4)	0.030(3)	0.038(4)	0.011(3)	0.006(3)	0.006(3)
P(3)	0.043(4)	0.034(4)	0.053(4)	-0.002(3)	0.004(3)	0.005(3)
C(1)	0.17(4)	0.09(2)	0.02(1)	0.07(3)	0.01(2)	0.02(1)
C(2)	0.09(2)	0.13(3)	0.07(2)	0.05(2)	-0.01(2)	0.02(2)
C(3)	0.15(3)	0.08(2)	0.06(2)	0.01(2)	0.02(2)	0.04(2)
C(4)	0.04(2)	0.08(2)	0.05(2)	-0.02(1)	-0.01(1)	0.00(1)
C(5)	0.12(3)	0.04(2)	0.06(2)	-0.02(2)	0.00(2)	0.00(1)
C(6)	0.11(3)	0.10(2)	0.05(2)	-0.04(2)	0.00(2)	-0.02(2)
C(7)	0.15(3)	0.04(2)	0.03(1)	0.00(2)	0.01(2)	-0.02(1)
C(8)	0.29(5)	0.07(2)	0.03(2)	0.01(3)	0.05(2)	0.00(1)
C(9)	0.12(3)	0.10(2)	0.04(2)	0.06(2)	0.00(2)	0.00(2)
C(10)	0.04(2)	0.03(1)	0.05(1)	0.01(1)	0.01(1)	0.00(1)
C(11)	0.06(2)	0.05(2)	0.06(2)	0.02(1)	0.01(1)	0.01(1)
C(12)	0.08(2)	0.05(2)	0.06(2)	0.02(2)	0.01(2)	0.02(1)
C(13)	0.05(2)	0.04(1)	0.04(1)	0.02(1)	0.00(1)	0.00(1)
C(14)	0.12(3)	0.05(2)	0.05(2)	0.01(2)	0.03(2)	0.02(1)
C(15)	0.08(2)	0.06(2)	0.05(2)	0.02(2)	0.01(1)	0.00(1)
C(16)	0.01(1)	0.04(1)	0.06(2)	0.01(1)	0.02(1)	0.01(1)
C(17)	0.03(2)	0.06(2)	0.08(2)	0.00(1)	-0.01(1)	0.00(1)

Table 2. Anisotropic Displacement Parameters (continued)

atom	U_{11}	U_{22}	U_{33}	U_{12}	U_{13}	U_{23}
C(18)	0.05(2)	0.06(2)	0.07(2)	0.00(1)	-0.01(1)	-0.01(1)
C(19)	0.04(2)	0.05(2)	0.07(2)	0.02(1)	0.01(1)	0.01(1)
C(20)	0.14(3)	0.07(2)	0.07(2)	0.02(2)	0.01(2)	0.03(2)
C(21)	0.10(3)	0.03(2)	0.12(3)	0.01(2)	-0.04(2)	0.01(2)
C(22)	0.05(2)	0.04(2)	0.07(2)	0.00(1)	-0.01(1)	0.02(1)
C(23)	0.15(3)	0.05(2)	0.05(2)	-0.03(2)	-0.02(2)	0.01(1)
C(24)	0.06(2)	0.04(2)	0.14(3)	0.01(2)	0.01(2)	0.01(2)
C(25)	0.09(2)	0.06(2)	0.05(2)	0.00(2)	0.01(2)	-0.02(1)
C(26)	0.05(2)	0.11(2)	0.06(2)	0.01(2)	0.02(2)	0.01(2)
C(27)	0.07(2)	0.15(3)	0.08(2)	-0.03(2)	0.00(2)	0.00(2)

The general temperature factor expression:

$$\exp(-2\pi^2(a^{*2}U_{11}h^2 + b^{*2}U_{22}k^2 + c^{*2}U_{33}l^2 + 2a^*b^*U_{12}hk + 2a^*c^*U_{13}hl + 2b^*c^*U_{23}kl))$$

Table 3. Bond Lengths($\AA$)

atom	atom	distance	atom	atom	distance
Rh(1)	Cl(1)	2.578(6)	Rh(1)	Cl(2)	2.362(7)
Rh(1)	Cl(3)	2.360(7)	Rh(1)	P(1)	2.365(6)
Rh(1)	P(2)	2.366(6)	P(1)	C(1)	1.90(3)
P(1)	C(4)	1.90(2)	P(1)	C(7)	1.70(3)
P(2)	C(10)	1.85(2)	P(2)	C(13)	1.81(2)
P(2)	C(16)	1.87(2)	P(3)	C(19)	1.79(2)
P(3)	C(22)	1.82(2)	P(3)	C(25)	1.82(2)
O(1)	C(28)	1.21(8)	O(1)	C(31)	1.45(6)
C(1)	C(2)	1.46(4)	C(1)	C(3)	1.53(4)
C(4)	C(5)	1.53(3)	C(4)	C(6)	1.56(3)
C(7)	C(8)	1.56(3)	C(7)	C(9)	1.59(3)
C(10)	C(11)	1.55(3)	C(10)	C(12)	1.52(3)
C(13)	C(14)	1.53(3)	C(13)	C(15)	1.53(3)
C(16)	C(17)	1.47(3)	C(16)	C(18)	1.54(3)
C(19)	C(20)	1.52(3)	C(19)	C(21)	1.57(3)
C(22)	C(23)	1.52(3)	C(22)	C(24)	1.45(3)
C(25)	C(26)	1.50(3)	C(25)	C(27)	1.54(4)
C(28)	C(29)	1.36(8)	C(29)	C(30)	1.34(6)
C(30)	C(31)	1.52(6)			

Table 4. Bond Lengths($\AA$)

atom	atom	distance	atom	atom	distance
C(1)	H(1)	0.95	C(2)	H(2)	0.95
C(2)	H(3)	0.95	C(2)	H(4)	0.95
C(3)	H(5)	0.95	C(3)	H(6)	0.95
C(3)	H(7)	0.95	C(4)	H(8)	0.95
C(5)	H(9)	0.95	C(5)	H(10)	0.95
C(5)	H(11)	0.95	C(6)	H(12)	0.95
C(6)	H(13)	0.95	C(6)	H(14)	0.95
C(7)	H(15)	0.95	C(8)	H(16)	0.95
C(8)	H(17)	0.95	C(8)	H(18)	0.95
C(9)	H(19)	0.95	C(9)	H(20)	0.95
C(9)	H(21)	0.95	C(10)	H(22)	0.95
C(11)	H(23)	0.95	C(11)	H(24)	0.95
C(11)	H(25)	0.95	C(12)	H(26)	0.95
C(12)	H(27)	0.95	C(12)	H(28)	0.95
C(13)	H(29)	0.95	C(14)	H(30)	0.95
C(14)	H(31)	0.95	C(14)	H(32)	0.95
C(15)	H(33)	0.95	C(15)	H(34)	0.95
C(15)	H(35)	0.95	C(16)	H(36)	0.95
C(17)	H(37)	0.95	C(17)	H(38)	0.95
C(17)	H(39)	0.95	C(18)	H(40)	0.95
C(18)	H(41)	0.95	C(18)	H(42)	0.95
C(19)	H(43)	0.95	C(20)	H(44)	0.95
C(20)	H(45)	0.95	C(20)	H(46)	0.95
C(21)	H(47)	0.95	C(21)	H(48)	0.95

Table 4. Bond Lengths($\AA$) (continued)

atom	atom	distance	atom	atom	distance
C(21)	H(49)	0.95	C(22)	H(50)	0.95
C(23)	H(51)	0.95	C(23)	H(52)	0.95
C(23)	H(53)	0.95	C(24)	H(54)	0.95
C(24)	H(55)	0.95	C(24)	H(56)	0.95
C(25)	H(57)	0.95	C(26)	H(58)	0.95
C(26)	H(59)	0.95	C(26)	H(60)	0.95
C(27)	H(61)	0.95	C(27)	H(62)	0.95
C(27)	H(63)	0.95	C(28)	H(64)	0.95
C(29)	H(65)	0.95	C(30)	H(66)	0.95
C(31)	H(67)	0.95			

Table 5. Bond Angles(°)

atom	atom	atom	angle	atom	atom	atom	angle
Cl(1)	Rh(1)	Cl(2)	92.3(2)	Cl(1)	Rh(1)	Cl(3)	91.1(2)
Cl(1)	Rh(1)	P(1)	96.2(2)	Cl(1)	Rh(1)	P(2)	99.0(2)
Cl(2)	Rh(1)	Cl(3)	176.7(2)	Cl(2)	Rh(1)	P(1)	90.0(2)
Cl(2)	Rh(1)	P(2)	89.2(2)	Cl(3)	Rh(1)	P(1)	89.4(2)
Cl(3)	Rh(1)	P(2)	90.5(2)	P(1)	Rh(1)	P(2)	164.8(2)
Rh(1)	P(1)	C(1)	110.3(8)	Rh(1)	P(1)	C(4)	113.7(8)
Rh(1)	P(1)	C(7)	118.9(9)	C(1)	P(1)	C(4)	99(1)
C(1)	P(1)	C(7)	101(1)	C(4)	P(1)	C(7)	109(1)
Rh(1)	P(2)	C(10)	111.9(7)	Rh(1)	P(2)	C(13)	116.3(7)
Rh(1)	P(2)	C(16)	114.5(7)	C(10)	P(2)	C(13)	102.9(10)
C(10)	P(2)	C(16)	101.1(10)	C(13)	P(2)	C(16)	108.6(10)
C(19)	P(3)	C(22)	113(1)	C(19)	P(3)	C(25)	111(1)
C(22)	P(3)	C(25)	110(1)	C(28)	O(1)	C(31)	109(6)
P(1)	C(1)	C(2)	112(2)	P(1)	C(1)	C(3)	109(2)
C(2)	C(1)	C(3)	111(2)	P(1)	C(4)	C(5)	112(1)
P(1)	C(4)	C(6)	115(1)	C(5)	C(4)	C(6)	107(2)
P(1)	C(7)	C(8)	127(2)	P(1)	C(7)	C(9)	115(1)
C(8)	C(7)	C(9)	105(2)	P(2)	C(10)	C(11)	110(1)
P(2)	C(10)	C(12)	112(1)	C(11)	C(10)	C(12)	110(1)
P(2)	C(13)	C(14)	112(1)	P(2)	C(13)	C(15)	121(1)
C(14)	C(13)	C(15)	109(1)	P(2)	C(16)	C(17)	112(1)
P(2)	C(16)	C(18)	117(1)	C(17)	C(16)	C(18)	109(1)
P(3)	C(19)	C(20)	111(1)	P(3)	C(19)	C(21)	110(1)
C(20)	C(19)	C(21)	109(2)	P(3)	C(22)	C(23)	111(1)

Table 5. Bond Angles(°) (continued)

atom	atom	atom	angle	atom	atom	atom	angle
P(3)	C(22)	C(24)	114(1)	C(23)	C(22)	C(24)	113(2)
P(3)	C(25)	C(26)	111(1)	P(3)	C(25)	C(27)	110(1)
C(26)	C(25)	C(27)	111(2)	O(1)	C(28)	C(29)	114(7)
C(28)	C(29)	C(30)	108(6)	C(29)	C(30)	C(31)	103(4)
O(1)	C(31)	C(30)	100(4)				

Table 6. Bond Angles(°)

atom	atom	atom	angle	atom	atom	atom	angle
P(1)	C(1)	H(1)	107.6	C(2)	C(1)	H(1)	107.5
C(3)	C(1)	H(1)	107.6	C(1)	C(2)	H(2)	109.5
C(1)	C(2)	H(3)	109.6	C(1)	C(2)	H(4)	109.5
H(2)	C(2)	H(3)	109.5	H(2)	C(2)	H(4)	109.4
H(3)	C(2)	H(4)	109.5	C(1)	C(3)	H(5)	109.6
C(1)	C(3)	H(6)	109.5	C(1)	C(3)	H(7)	109.6
H(5)	C(3)	H(6)	109.4	H(5)	C(3)	H(7)	109.4
H(6)	C(3)	H(7)	109.3	P(1)	C(4)	H(8)	107.2
C(5)	C(4)	H(8)	107.2	C(6)	C(4)	H(8)	107.2
C(4)	C(5)	H(9)	109.5	C(4)	C(5)	H(10)	109.5
C(4)	C(5)	H(11)	109.5	H(9)	C(5)	H(10)	109.4
H(9)	C(5)	H(11)	109.4	H(10)	C(5)	H(11)	109.5
C(4)	C(6)	H(12)	109.5	C(4)	C(6)	H(13)	109.4
C(4)	C(6)	H(14)	109.5	H(12)	C(6)	H(13)	109.4
H(12)	C(6)	H(14)	109.5	H(13)	C(6)	H(14)	109.4
P(1)	C(7)	H(15)	101.5	C(8)	C(7)	H(15)	101.4
C(9)	C(7)	H(15)	101.4	C(7)	C(8)	H(16)	109.4
C(7)	C(8)	H(17)	109.4	C(7)	C(8)	H(18)	109.5
H(16)	C(8)	H(17)	109.5	H(16)	C(8)	H(18)	109.5
H(17)	C(8)	H(18)	109.5	C(7)	C(9)	H(19)	109.5
C(7)	C(9)	H(20)	109.5	C(7)	C(9)	H(21)	109.5
H(19)	C(9)	H(20)	109.4	H(19)	C(9)	H(21)	109.4
H(20)	C(9)	H(21)	109.5	P(2)	C(10)	H(22)	107.6
C(11)	C(10)	H(22)	107.6	C(12)	C(10)	H(22)	107.6

Table 6. Bond Angles(°) (continued)

atom	atom	atom	angle	atom	atom	atom	angle
C(10)	C(11)	H(23)	109.5	C(10)	C(11)	H(24)	109.5
C(10)	C(11)	H(25)	109.5	H(23)	C(11)	H(24)	109.5
H(23)	C(11)	H(25)	109.4	H(24)	C(11)	H(25)	109.5
C(10)	C(12)	H(26)	109.5	C(10)	C(12)	H(27)	109.5
C(10)	C(12)	H(28)	109.4	H(26)	C(12)	H(27)	109.5
H(26)	C(12)	H(28)	109.4	H(27)	C(12)	H(28)	109.5
P(2)	C(13)	H(29)	103.5	C(14)	C(13)	H(29)	103.5
C(15)	C(13)	H(29)	103.5	C(13)	C(14)	H(30)	109.5
C(13)	C(14)	H(31)	109.5	C(13)	C(14)	H(32)	109.5
H(30)	C(14)	H(31)	109.5	H(30)	C(14)	H(32)	109.4
H(31)	C(14)	H(32)	109.5	C(13)	C(15)	H(33)	109.5
C(13)	C(15)	H(34)	109.5	C(13)	C(15)	H(35)	109.4
H(33)	C(15)	H(34)	109.5	H(33)	C(15)	H(35)	109.5
H(34)	C(15)	H(35)	109.5	P(2)	C(16)	H(36)	105.5
C(17)	C(16)	H(36)	105.5	C(18)	C(16)	H(36)	105.5
C(16)	C(17)	H(37)	109.5	C(16)	C(17)	H(38)	109.5
C(16)	C(17)	H(39)	109.4	H(37)	C(17)	H(38)	109.5
H(37)	C(17)	H(39)	109.5	H(38)	C(17)	H(39)	109.4
C(16)	C(18)	H(40)	109.4	C(16)	C(18)	H(41)	109.5
C(16)	C(18)	H(42)	109.5	H(40)	C(18)	H(41)	109.4
H(40)	C(18)	H(42)	109.5	H(41)	C(18)	H(42)	109.5
P(3)	C(19)	H(43)	108.4	C(20)	C(19)	H(43)	108.4
C(21)	C(19)	H(43)	108.4	C(19)	C(20)	H(44)	109.4
C(19)	C(20)	H(45)	109.5	C(19)	C(20)	H(46)	109.5

Table 6. Bond Angles(°) (continued)

atom	atom	atom	angle	atom	atom	atom	angle
H(44)	C(20)	H(45)	109.4	H(44)	C(20)	H(46)	109.4
H(45)	C(20)	H(46)	109.5	C(19)	C(21)	H(47)	109.4
C(19)	C(21)	H(48)	109.5	C(19)	C(21)	H(49)	109.4
H(47)	C(21)	H(48)	109.5	H(47)	C(21)	H(49)	109.4
H(48)	C(21)	H(49)	109.5	P(3)	C(22)	H(50)	105.5
C(23)	C(22)	H(50)	105.4	C(24)	C(22)	H(50)	105.5
C(22)	C(23)	H(51)	109.4	C(22)	C(23)	H(52)	109.4
C(22)	C(23)	H(53)	109.5	H(51)	C(23)	H(52)	109.4
H(51)	C(23)	H(53)	109.5	H(52)	C(23)	H(53)	109.6
C(22)	C(24)	H(54)	109.5	C(22)	C(24)	H(55)	109.4
C(22)	C(24)	H(56)	109.4	H(54)	C(24)	H(55)	109.5
H(54)	C(24)	H(56)	109.5	H(55)	C(24)	H(56)	109.5
P(3)	C(25)	H(57)	107.7	C(26)	C(25)	H(57)	107.7
C(27)	C(25)	H(57)	107.6	C(25)	C(26)	H(58)	109.5
C(25)	C(26)	H(59)	109.5	C(25)	C(26)	H(60)	109.5
H(58)	C(26)	H(59)	109.5	H(58)	C(26)	H(60)	109.4
H(59)	C(26)	H(60)	109.5	C(25)	C(27)	H(61)	109.5
C(25)	C(27)	H(62)	109.5	C(25)	C(27)	H(63)	109.5
H(61)	C(27)	H(62)	109.5	H(61)	C(27)	H(63)	109.4
H(62)	C(27)	H(63)	109.5	O(1)	C(28)	H(64)	123.3
C(29)	C(28)	H(64)	122.3	C(28)	C(29)	H(65)	126.3
C(30)	C(29)	H(65)	125.4	C(29)	C(30)	H(66)	128.7
C(31)	C(30)	H(66)	127.7	O(1)	C(31)	H(67)	128.9
C(30)	C(31)	H(67)	130.3				

Table 7. Torsion Angles(°)

atom	atom	atom	atom	angle	atom	atom	atom	atom	angle
Rh(1)	P(1)	C(1)	C(2)	63(2)	Rh(1)	P(1)	C(1)	C(3)	-61(2)
Rh(1)	P(1)	C(4)	C(5)	61(1)	Rh(1)	P(1)	C(4)	C(6)	-175(1)
Rh(1)	P(1)	C(7)	C(8)	153(1)	Rh(1)	P(1)	C(7)	C(9)	-68(2)
Rh(1)	P(2)	C(10)	C(11)	-62(1)	Rh(1)	P(2)	C(10)	C(12)	62(1)
Rh(1)	P(2)	C(13)	C(14)	-62(1)	Rh(1)	P(2)	C(13)	C(15)	164(1)
Rh(1)	P(2)	C(16)	C(17)	62(1)	Rh(1)	P(2)	C(16)	C(18)	-169(1)
Cl(1)	Rh(1)	P(1)	C(1)	178(1)	Cl(1)	Rh(1)	P(1)	C(4)	-70.2(9)
Cl(1)	Rh(1)	P(1)	C(7)	61(1)	Cl(1)	Rh(1)	P(2)	C(10)	-177.8(8)
Cl(1)	Rh(1)	P(2)	C(13)	64.5(8)	Cl(1)	Rh(1)	P(2)	C(16)	-63.5(8)
Cl(2)	Rh(1)	P(1)	C(1)	-89(1)	Cl(2)	Rh(1)	P(1)	C(4)	22.1(9)
Cl(2)	Rh(1)	P(1)	C(7)	153(1)	Cl(2)	Rh(1)	P(2)	C(10)	90.1(8)
Cl(2)	Rh(1)	P(2)	C(13)	-27.7(8)	Cl(2)	Rh(1)	P(2)	C(16)	-155.7(8)
Cl(3)	Rh(1)	P(1)	C(1)	87(1)	Cl(3)	Rh(1)	P(1)	C(4)	-161.2(9)
Cl(3)	Rh(1)	P(1)	C(7)	-29(1)	Cl(3)	Rh(1)	P(2)	C(10)	-86.6(8)
Cl(3)	Rh(1)	P(2)	C(13)	155.6(8)	Cl(3)	Rh(1)	P(2)	C(16)	27.6(8)
P(1)	Rh(1)	P(2)	C(10)	2(1)	P(1)	Rh(1)	P(2)	C(13)	-114(1)
P(1)	Rh(1)	P(2)	C(16)	117(1)	P(2)	Rh(1)	P(1)	C(1)	-2(1)
P(2)	Rh(1)	P(1)	C(4)	109(1)	P(2)	Rh(1)	P(1)	C(7)	-119(1)
O(1)	C(28)	C(29)	C(30)	12(10)	O(1)	C(31)	C(30)	C(29)	17(5)
C(1)	P(1)	C(4)	C(5)	178(1)	C(1)	P(1)	C(4)	C(6)	-58(2)
C(1)	P(1)	C(7)	C(8)	32(2)	C(1)	P(1)	C(7)	C(9)	169(2)
C(2)	C(1)	P(1)	C(4)	-55(2)	C(2)	C(1)	P(1)	C(7)	-168(2)
C(3)	C(1)	P(1)	C(4)	179(2)	C(3)	C(1)	P(1)	C(7)	66(2)
C(4)	P(1)	C(7)	C(8)	-72(2)	C(4)	P(1)	C(7)	C(9)	64(2)

Table 7. Torsion Angles(°) (continued)

atom	atom	atom	atom	angle	atom	atom	atom	atom	angle
C(5)	C(4)	P(1)	C(7)	-74(2)	C(6)	C(4)	P(1)	C(7)	48(2)
C(10)	P(2)	C(13)	C(14)	175(1)	C(10)	P(2)	C(13)	C(15)	41(2)
C(10)	P(2)	C(16)	C(17)	-177(1)	C(10)	P(2)	C(16)	C(18)	-49(1)
C(11)	C(10)	P(2)	C(13)	63(1)	C(11)	C(10)	P(2)	C(16)	175(1)
C(12)	C(10)	P(2)	C(13)	-172(1)	C(12)	C(10)	P(2)	C(16)	-60(1)
C(13)	P(2)	C(16)	C(17)	-69(1)	C(13)	P(2)	C(16)	C(18)	58(1)
C(14)	C(13)	P(2)	C(16)	68(1)	C(15)	C(13)	P(2)	C(16)	-64(2)
C(19)	P(3)	C(22)	C(23)	92(2)	C(19)	P(3)	C(22)	C(24)	-38(2)
C(19)	P(3)	C(25)	C(26)	-172(1)	C(19)	P(3)	C(25)	C(27)	62(2)
C(20)	C(19)	P(3)	C(22)	-62(2)	C(20)	C(19)	P(3)	C(25)	171(1)
C(21)	C(19)	P(3)	C(22)	174(1)	C(21)	C(19)	P(3)	C(25)	48(2)
C(22)	P(3)	C(25)	C(26)	60(2)	C(22)	P(3)	C(25)	C(27)	-64(2)
C(23)	C(22)	P(3)	C(25)	-141(1)	C(24)	C(22)	P(3)	C(25)	87(2)
C(28)	O(1)	C(31)	C(30)	-11(7)	C(28)	C(29)	C(30)	C(31)	-18(7)
C(29)	C(28)	O(1)	C(31)	0(10)					

The ADC (atom designator code) specifies the position of an atom in a crystal. The 5-digit number shown in the table is a composite of three one-digit numbers and one two-digit number: TA (first digit) + TB (second digit) + TC (third digit) + SN (last two digits). TA, TB and TC are the crystal lattice translation digits along cell edges a, b and c. A translation digit of 5 indicates the origin unit cell. If TA = 4, this indicates a translation of one unit cell length along the a-axis in the negative direction. Each translation digit can range in value from 1 to 9 and thus ± 4 lattice translations from the origin (TA=5, TB=5, TC=5) can be represented.

The SN, or symmetry operator number, refers to the number of the symmetry operator used to generate the coordinates of the target atom. A list of symmetry operators relevant to this structure are given below.

For a given intermolecular contact, the first atom (origin atom) is located in the origin unit cell and its position can be generated using the identity operator (SN=1). Thus, the ADC for an origin atom is always 55501. The position of the second atom (target atom) can be generated using the ADC and the coordinates of the atom in the parameter table. For example, an ADC of 47502 refers to the target atom moved through symmetry operator two, then translated -1 cell translations along the a axis, +2 cell translations along the b axis, and 0 cell translations along the c axis.

An ADC of 1 indicates an intermolecular contact between two fragments (eg. cation and anion) that reside in the same asymmetric unit.

Symmetry Operators:

(1)	X,	Y,	Z		(2)	-X,	-Y,	-Z